Spotlight on Fungal Rhodopsins:
A Microscopic and Electrophysiological Study

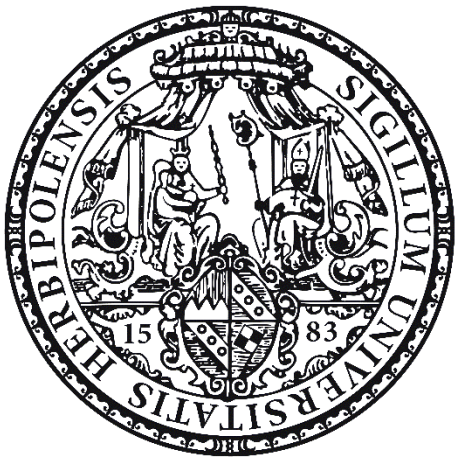

Doctoral thesis

for a doctoral degree

at the Institute of Biotechnology and Biophysics,

Biocenter, Julius Maximilian University Wuerzburg

Authored by

Sabine Panzer

Kitzingen

Wuerzburg, 2022

Submitted on: ……..……..

Members of the Thesis Committee:

Chairperson: ……..

Primary Supervisor: PD Dr. Ulrich Terpitz

Second Supervisor: Prof. Dr. Alfred Batschauer

Date of Public Defence: ……..…

Date of Receipt of Certificates: ……

“(Fortunately) One cannot predict the future”

Botond Roska, 2015

List of Publications

Publications related to this work:

Panzer S*., Zhang C*., Konte T., Bräuer C., Diemar A., Yogendran P., Yu-Strzelczyk J., Nagel G., Gao S., Terpitz U. (2021) `Modified Rhodopsins from *Aureobasidium pullulans* Excel With Very High Proton Transport Rates` *Frontiers in Molecular Biosciences*, 8, 941. Doi 10.3389/fmolb.2021.750528

Sputh S., Panzer S., Stigloher C., Terpitz U. (2021) `Superaufgelöste Mikroskopie: Pilze unter Beobachtung` *BIOspektrum* 27 (4): 380-382. doi 10.1007/s12268-021-1592-6

Götz R., Panzer S., Trinks N., Eilts J., Wagener J., Turrà D., Di Pietro A., Sauer M., Terpitz, U. (2020) `Expansion microscopy for cell biology analysis in fungi` *Frontiers in Microbiology*, 11, 574. doi 10.3389/fmicb.2020.00574

Panzer, S., Brych, A., Batschauer, A., & Terpitz, U. (2019) `Opsin 1 and Opsin 2 of the Corn Smut Fungus *Ustilago maydis* Are Green Light-Driven Proton Pumps` *Frontiers in Microbiology* 10: 735. doi 10.3389/fmicb.2019.00735

*These authors share first authorship

Other publications:

Lu J., Dreyer I., Dickinson M.S., Panzer S., Jaslan D., Navarro-Retamal C., Geiger D., Terpitz U., Becker D., Stroud R.M., Marten I., Hedrich R. (2021) `*Vicia faba* TPC1, a genetically encoded variant of the vacuole Two Pore Channel 1, is hyperexcitable` *bioRxiv preprint* doi 10.1101/2021.12.22.473873

Brych A., Haas F. B., Parzefall K., Panzer S., Schermuly J., Altmüller J., Engelsdorf T., Terpitz U., Rensing S. A., Kiontke S., Batschauer A. (2021) `Coregulation of gene expression by White collar 1 and phytochrome in *Ustilago maydis*` *Fungal Genetics and Biology* 152: 103570. doi 10.1016/j.fgb.2021.103570

Martens J., Panzer S., van den Wijngaard J.P.H.M., Siebes M., Schreiber L.M. (2019) `Influence of contrast agent dispersion on bolus-based MRI myocardial perfusion measurements: A computational fluid dynamics study` *Magnetic Resonance in Medicine*. doi 10.1002/mrm.28125

Barrera V., Fliss B., Panzer S., Bolliger S. A. (2019) `Gunshot residue on dark materials: a comparison between infrared photography and the use of an alternative light source` *International journal of legal medicine* 133(4), 1115-1120. doi 10.1007/s00414-018-1965-7

Sterzik V., Hinderberger P., Panzer S., Bohnert M. (2018) `Visualizing old biological traces on different materials without using chemicals` *International journal of legal medicine* 132(1), 35-41. doi 10.1007/s00414-017-1678-3

Sterzik V., Panzer S., Apfelbacher M., Bohnert M. (2016) `Searching for biological traces on different materials using a forensic light source and infrared photography` *International journal of legal medicine* 130(3), 599-605. doi 10.1007/s00414-015-1283-2

Abstract

Microbial rhodopsins are abundant membrane proteins often capable of ion transport and are found in all three domains of life. Thus, many fungi, especially phyto-associated or phyto-pathogenic ones, contain these green-light-sensing photoreceptors. Proteins that perceive other wavelengths are often well characterized in terms of their impact on fungal biology whereas little is known about the function of fungal rhodopsins. In this work, five fungal rhodopsins, UmOps1 and UmOps2 from the corn smut *Ustilago maydis* as well as ApOps1, ApOps2 and ApOps3 from the black yeast *Aureobasidium pullulans*, were characterized electrophysiologically using mammalian expression systems and the patch-clamp technique to explore their ion transport properties. The latter three were modified using a membrane trafficking cassette, termed "2.0" that consists of the lucy rho motif, two Kir2.1 Golgi apparatus trafficking signals and a Kir2.1 endoplasmic reticulum export signal, what resulted in better plasma membrane localization. Rhodopsin mutants were created to identify amino acid residues that are key players in the ion transport process. Current enhancement in the presence of weak organic acids, that was already described before for the fungal rhodopsin CarO from *Fusarium fujikuroi* (García-Martínez *et al.*, 2015; Adam *et al.*, 2018), was investigated for the *U. maydis* rhodopsins as well as for ApOps2 by supplementing acetate in the patch-clamp electrolyte solutions. All five rhodopsins were found to be proton pumps unidirectionally transporting protons out of the cytosol upon green-light exposure with every rhodopsin exhibiting special features or unique characteristics in terms of the photocurrents. To name just a few, UmOps1, for example, showed a striking pH-dependency with massive enhancement of pump currents in the presence of extracellular acidic pH. Moreover, especially ApOps2 and ApOps3 showed very high current densities, however, the ones of ApOps3 were impaired when exchanging intracellular sodium to cesium. Concerning the mutations, it was found, that the electron releasing group in UmOps1 seems to be involved in the striking pH effect and that the mutation of the proton donor site resulted in almost unfunctional proteins. Moreover, a conserved arginine inside ApOps2 was mutated to turn the proton pump into a channel. Regarding the effect of weak organic acids, acetate was able to induce enhanced pump currents in UmOps1 and ApOps2, but not in UmOps2. Due to the capability of current production upon light illumination, microbial rhodopsins are used in the research field of optogenetics that aims to control neuronal activity by light. ApOps2 was used to test its functionality in differentiated NG108-15 cells addressing the question whether it is a promising candidate that can be used as an optogenetic tool. Indeed, this rhodopsin could be functionally expressed in this experimental system. Furthermore, microscopic studies were done to elucidate the localization of selected rhodopsins in fungal cells. Therefore, conventional (confocal laser scanning or structured illumination microscopy) as well as novel super-resolution techniques (expansion or correlated light and electron microscopy) were used. This was done on *U. maydis* sporidia, the yeast-like form of this fungus, via eGFP-tagged UmOps1 or UmOps2 expressing strains. Moreover, CarO-eYFP expressing *F. fujikuroi* was imaged microscopically to confirm the plasma membrane and tonoplast localization (García-Martínez *et al.*, 2015) with the help of counterstaining experiments. UmOps1 was found to reside in the plasma membrane, UmOps2 localized to the tonoplast and CarO was indeed found in both of these localizations. This work gains further insight into rhodopsin functions and paves the way for further research in terms of the biological role of rhodopsins in fungal life cycles.

Zusammenfassung

Mikrobielle Rhodopsine sind häufig vorkommende Membranproteine, welche oft fähig sind, Ionen zu transportieren. Sie kommen in allen drei Domänen vor. So weisen auch Pilze – vor allem pflanzenassoziierte oder pflanzenpathogene – diese Grünlichtrezeptoren auf. Proteine, die andere Wellenlängen empfangen können, sind bereits häufig gut in Bezug auf ihren Einfluss auf die Pilzbiologie untersucht, wohingegen nur wenig über die Funktion der pilzlichen Rhodopsine bekannt ist. Hier wurden fünf Rhodopsine, UmOps1 und UmOps2 des Maisbeulenbrandes *Ustilago maydis*, sowie ApOps1, ApOps2 und ApOps3 des schwarzen Hefepilzes *Aureobasidium pullulans* bezüglich ihrer Ionentransport-Eigenschaften mit Hilfe von Säugerzelllinien und der Patch-Clamp Technik untersucht. Die drei letzteren wurden mit der „2.0"-Modifikation ausgestattet, bestehend aus dem lucy rho Motif, zwei Kir2.1 Golgiapparat Transfer- und einem Kir2.1 Endoplasmatischen Retikulum-Export-Signal, was zu einer besseren Plasmamembran-Lokalisierung der Proteine führte. Es wurden weiterhin Rhodopsin-Mutanten hergestellt um Aminosäuren zu identifizieren, welche im Ionentransport Schlüsselfunktionen einnehmen. Des Weiteren wurde der Effekt von schwachen organischen Säuren auf den Ionentransport der *U. maydis* Rhodopsine und auf ApOps2 mittels Supplementation der Patch-Clamp-Elektrolyten mit Acetat untersucht. Dieser Effekt wurde bereits früher für CarO aus *Fusarium fujikuroi* nachgewiesen (García-Martínez *et al.*, 2015; Adam *et al.*, 2018) und bezeichnet eine Erhöhung der lichtinduzierten Ströme durch die extrazelluläre Anwesenheit schwacher organischer Säuren. Alle fünf untersuchten Rhodopsine wurden als Grünlicht getriebene Pump-Rhodopsine identifiziert, welche Protonen unidirektional aus dem Zytosol transportieren. Hierbei zeigten die lichtinduzierten Ströme jedes Rhodopsins spezielle Eigenschaften und Merkmale. Unter anderem zeigte UmOps1 eine unerwartete pH-Abhängigkeit indem die Pumpströme bei extrazellulärem sauren pH massiv erhöht wurden. Des Weiteren zeigten sowohl ApOps2 als auch ApOps3 sehr hohe Stromdichten, wobei jedoch die von ApOps3 rapide abnahm, sobald intrazelluläres Natrium durch Caesium ersetzt wurde. Bezüglich der Rhodopsin-Mutanten konnte gezeigt werden, dass die Proton-Releasing-Group von UmOps1 wahrscheinlich in die erstaunliche pH-Abhängigkeit involviert ist und dass die Mutation des Proton-Donors zu meist nicht funktionalen Proteinen führt. Ein konserviertes Arginin in ApOps2 wurde mutiert um das Pump-Rhodopsin in einen Kanal umzuwandeln. Der Schwache-Organische-Säure-Effekt konnte für UmOps1 und ApOps2, nicht aber für UmOps2 nachgewiesen werden. Wegen ihrer Ionentransport-Eigenschaften werden mikrobielle Rhodopsine in der Optogenetik eingesetzt um neuronale Zellen mittels Lichts zu steuern. Hier wurde ApOps2 benutzt um dessen Funktionalität in ausdifferenzierten NG108-15 Zellen zu testen und ob dieses Rhodopsin ein vielversprechender Kandidat für optogenetische Anwendungen wäre. In der Tat gelang es, ApOps2 funktional in diesem Testsystem zu exprimieren. Des Weiteren wurde die Lokalisation von UmOps1 und UmOps2 in Sporidien (hefeähnliche Form von *U. maydis*) mittels eGFP-Label untersucht, sowie die Plasmamembran- und Tonoplast-Lokalisierung von CarO-eYFP in *F. fujikuroi* (García-Martínez *et al.*, 2015) mittels Gegenfärbungen bestätigt. Hierfür wurden konventionelle (konfokale Laserraster-, sowie strukturierte Beleuchtungsmikroskopie) und auch neuartige hochaufgelöste Mikroskopie-Methoden (Expansions- und korrelative Licht- und Elektronenmikroskopie) verwendet. Es konnten hier weitere Einblicke in die Funktionen pilzlicher Rhodopsine gewonnen werden, welche den Weg für weitere Forschung in Bezug auf den Einfluss dieser Proteine auf das Leben der Pilze ebnen.

Contents

1 Introduction

Fungi are ubiquitous organisms that inhabit a huge range of different niches: They live in very different climate zones, where they can be found on surfaces or in waters. Moreover, they have the ability to colonize other living beings in a pathogenic or non-pathogenic way. Fungi affect our daily lives while acting as pathogen for plants, animals and humans causing various diseases on the one hand. On the other hand, many benefits can be obtained from these tiny organisms in terms of industrial and biotechnological relevance. Secondary metabolisms like antibiotics gained huge importance in medicine, yeast or penicillium strains are used in fermentation processes or food industry, respectively and a wide range of fungal enzymes replace harsh chemicals. Fungi are also able to withstand very challenging environments; they then are called extremophils. For example, halotolerant or halophilic fungi can live under high salt concentrations; thermophilic or psychrophilic fungi resist very high or low temperature and alkalotolerants are able to compensate alkaline environments. Even in high radiation or radioactive contamination areas and in space, some fungi are able to grow. (Baxter and Illston, 1980; Gunde-Cimerman *et al.*, 2000; Zhdanova *et al.*, 2000; Zalar *et al.*, 2005, 2011; Horneck, Klaus and Mancinelli, 2010; Zajc *et al.*, 2012; Zajc, Džeroski, *et al.*, 2014; Zajc, Kogej, *et al.*, 2014; Cortesão *et al.*, 2021; Odoh *et al.*, 2021)

In many terrestrial environments, solar radiation is an omnipresent factor that fungi can exploit or have to deal with. Evolution brought up different photoreceptors that detect distinct spectral ranges of the sunlight ranging from UV- to far-red light so that the fungi can perceive environmental changes and react to them by adaptation of growth, development, reproduction or cellular processes. Blue light is detected by receptors consisting of Flavin as chromophore like photolyases and cryptochromes or Light-Oxygen-Voltage (LOV) domain or Blue Light Using Flavin (BLUF) containing proteins. An important example for photoreceptors containing LOV domains are the White Collar proteins (White Collar-1, WC-1; White Collar-2, WC-2) that form together the White Collar Complex (WCC), which was extensively studied in *Neurospora crassa* and was shown to be a key player in circadian clock and is involved in gene expression regulation (Ballario *et al.*, 1996; Linden and Macino, 1997; He *et al.*, 2002). Homologues of this protein can be found among many other representatives of the fungal kingdom. Red light is absorbed by biliverdin-binding phytochromes which were firstly described in plants (Smith, 2000; Rockwell, Su and Lagarias, 2006; Inoue, Nishihama and Kohchi, 2017). Green light is detected by rhodopsins containing the carotenoid retinal as chromophore; these proteins are less studied compared to blue and red-light receptors so far. (Corrochano, 2019; Yu and Fischer, 2019)

Fungal rhodopsins belong to the type 1 rhodopsins, which are designated as microbial rhodopsins and show structure homology to the animal (type 2) rhodopsins that are G-protein coupled receptors (GPCRs). A huge variety of type 1 rhodopsins were identified in the genomes of many organisms from bacteria over archaea to eukaryotic organisms by the help of improved genome screening methods, since Oesterhelt and Stockenius discovered Bacteriorhodopsin (BR) as the first and up to now best-studied microbial rhodopsin in 1971 in the purple membrane of *Halobacterium salinarum*, that acts as an outward directed proton pump (Oesterhelt and Stoeckenius, 1971; Brown, 2014; Ernst *et al.*, 2014). In general, microbial rhodopsins are transmembrane proteins consisting

of 7 alpha helices that have bound the retinal to a conserved lysine residue. Upon illumination, the ground-state all-*trans* retinal (ATR) photoisomerizes to its 13-*cis* form what triggers the respective function (Ernst *et al.*, 2014). Microbial rhodopsins can act as photo sensors, ion channels or ion pumps. For example, also in *Halobacterium salinarum* two photo sensors, sensory rhodopsin I (SRI) and sensory rhodopsin II (SRII) as well as an inward chloride pump (Halorhodopsin, HR) were discovered (Matsuno-Yagi and Mukohata, 1980; Bogomolni and Spudich, 1982; Schobert and Lanyi, 1982; Spudich *et al.*, 1986). The green algae *Chlamydomonas reinhardtii* expresses a cation and an inward rectifying proton channel (Channelrhodopsin 1 and Channelrhodopsin 2; ChR1 and ChR2), the marine bacterium *Krokinobacter eikastus* contains an outward sodium pump (*Krokinobacter eikastus* rhodopsin 2, KR2), the halophilic bacterium *Salinibacter ruber* expresses the proton pump Xanthorhodopsin (XR), in *Guillardia theta* anion channels were found, the marine bacterium *Parvularcula oceani* consists of the inward proton pump PoXeR (*Parvularcula oceani* xenorhodopsin) and the arctic alga *Coccomyxa subellipsoidea* contains the proton-pump CsR (Nagel *et al.*, 2002, 2003; Balashov *et al.*, 2005; Inoue *et al.*, 2013, 2016; Govorunova *et al.*, 2015; Kato *et al.*, 2015; Vogt *et al.*, 2015). These examples give just a small overview of the wide range of different rhodopsin functions.

Although many microbial rhodopsins were electrophysiologically and biologically characterized especially during the last years, the function of only few fungal representatives is known. Nop-1 acts as a photosensor and is involved in the pathogenicity and reproduction of *Neurospora crassa*; LR (in literature also termed Mac) from *Leptosphaeria maculans* as well as CarO from *Fusarium fujikuroi* are both proton pumps exhibiting a fast photocycle, with the latter one being involved in spore germination retardation (Bieszke, Braun, *et al.*, 1999; Bieszke, Spudich, *et al.*, 1999; Bergo *et al.*, 2002; Prado *et al.*, 2004; Waschuk *et al.*, 2005; García-Martínez *et al.*, 2015; Wang *et al.*, 2018). The rhodopsins of *Phaeosphaeria nodorum* (PhaeoRD1 and PhaeoRD2) show fast photocycling activity (Fan *et al.*, 2011). *Sclerotia sclerotium* rhodopsin Sop-1 was shown to play a role in the virulence of that fungus and rhodopsin BeGC1 from *Blastocladiella emersonii* activates a guanylyl cyclase (Avelar *et al.*, 2014; Gao *et al.*, 2015; Lyu *et al.*, 2016) with the latter one being only distantly related to the fungal rhosdopsins. Two rhodopsins of *Ustilago maydis* (UmOps1 and UmOps2) could recently be described to act as outward directed proton pumps, moreover the opsins from *Alternaria alternata* were shown to exhibit ion transport function and are involved in germination and spore production processes (Panzer, 2017; Pinecker, 2020). In general, fungal rhodopsins can be divided into three subgroups, at least among the Ascomycota: NR (*N. crassa* rhodopsin nop-1)-like rhodopsins, which exhibit slow photocycles or photosensory function, LR-like and CarO-like rhodopsins, both with fast photocycles and possible proton pump activitiy (Brown and Jung, 2006). However, LR- and NR-like rhodopsins seem to be closer related to each other than to the CarO-like ones and build together the Nop-1-clade (Adam *et al.*, 2018; Wang *et al.*, 2018).

Despite rhodopsins are designated as green light sensing proteins, microbial rhodopsins can be activated by light of the entire visible spectral range depending on the amino acid environment of the chromophore concerning polarity, charge and aromatic residues as well as hydrogen bonding effects (Ernst *et al.*, 2014). Chr2 for example is maximally activated upon blue, HR by yellow light (Bogomolni, Taylor and Stoeckenius, 1984; Nagel *et al.*, 2003). However, the fungal rhodopsins electrophysiologically characterized so far show their maximum activity under green light

conditions and this is the case especially for plant-associated fungi, what makes sense, since green light dominates the phyllosphere (Bergo *et al.*, 2002; Waschuk *et al.*, 2005; García-Martínez *et al.*, 2015; Panzer, 2015, 2017). Vice versa, indeed, many rhodopsin-carrying fungi show plant-association (Adam *et al.*, 2018). Another special feature detected in two fungal rhodopsins which are assigned to the CarO-like rhodopsins, CarO itself and UmOps1, were shown to react to the extracellular presence of weak organic acids (WOA) like acetate or indole acetic acid (IAA) with enhancement in proton pump activity (García-Martínez *et al.*, 2015; Panzer, 2017; Adam *et al.*, 2018). Since IAA is a plant hormone, this could be a hint of a possible interaction or signaling pathway between plants and these fungi.

Nowadays, many attempts were done to exploit the function of microbial rhodopsins. For example, these proteins are employed in bioelectronics, where they are act as bio-nanomaterial (Mahyad, Janfaza and Hosseini, 2015; Li *et al.*, 2018). Moreover, the huge research field of optogenetics makes use of microbial rhodopsins to activate or inhibit neuronal activity by light (Adamantidis *et al.*, 2015; Deisseroth, 2015; Duebel, Marazova and Sahel, 2015; Govorunova and Koppel, 2016; Kojima, Shibukawa and Sudo, 2020). Recently, a breakthrough could be achieved by enabling a blind person regaining vision at least partially by receiving optogenetic therapy using ChrimsonR, a derivate of the channelrhodopsin from *Chlamydomonas noctigama* (Sahel *et al.*, 2021). Further optogenetic tools are among others ChR2, NpHR (inward chloride channel (halorhodopsin) from *Natronomonas pharaonis*) and Arch-3 (*Halorubrum sodomens*e) or their derivates, but also the fungal rhodopsin LR gained importance in this research field (Chow *et al.*, 2010; Flytzanis *et al.*, 2014; Duebel, Marazova and Sahel, 2015; Govorunova and Koppel, 2016).

To gain more insights into fungal rhodopsins, it is important to characterize more of these proteins in terms of their function. In this work, the patch-clamp technique was used to electrophysiologically investigate 3 rhodopsins from the ubiquitous halotolerant fungus *Aureobasidium pullulans* (ApOps1, ApOps2 and ApOps3) as further representatives of Ascomycete rhodopsins regarding their ion transport properties and – in case of ApOps2 - the possibility of application in optogenetics. Moreover, UmOps1 and UmOps2 from the plant pathogen *U. maydis* were further characterized - by using previous results as a basis - as basidiomycetal rhodopsins with regard to their proton pump function, which could already be shown before (Panzer, 2017). Moreover, UmOps1 mutants were created to specify key amino acid residues necessary for special characteristics of this rhodopsin. The boosting effect of acetate was tested in UmOps1 as well as in ApOps2 under physiological conditions. Besides electrophysiology, microscopic experiments were performed with *U. maydis* sporidia expressing UmOps1 or UmOps2, respectively, tagged with enhanced green fluorescent protein (eGFP) to gain information about their native localization in the fungus. In addition, *F. fujikuroi* spores and hyphae were microscopically investigated to confirm the localization of enhanced yellow fluorescent protein (eYFP)-tagged CarO specified before (García-Martínez *et al.*, 2015). For these studies, the well-established fluorescence-based microscopic methods confocal laser scanning microscopy (CLSM) and structured illumination microscopy (SIM) were used. The novel super-resolution techniques expansion microscopy (ExM) and correlative light and electron microscopy (CLEM) were tested on *U. maydis* sporidia. Both methods gained attention in recent years besides a range of other super-resolution techniques, which all provide higher resolutions compared to conventional CLSM and SIM. In general, super-

resolution microscopy is the method of choice when it comes to imaging of fungi since gaining insights in subcellular structures of those tiny organisms is challenging due to their small size.

This work provides further insights into the function, reaction to extracellular stimuli as well as the subcellular localization of selected fungal rhodopsins and paves the way for learning more about the biological role of these proteins and their application in diverse research fields.

2 Theory and Focus

2.1 Fungi

2.1.1 Ustilago maydis

U. maydis as causing agent of the corn smut is a prominent representative of the order of smut fungi (Ustilaginales, phylum Basidiomycota). Its natural host is *Zea mays* (and the native form Teosinte *Zea mexicana*) but it also has the capacity to infect other plant species (León-Ramírez *et al.*, 2004). The life cycle of *U. maydis* is dimorphic consisting of a yeast-like and a hyphal state with the infectious form being obligate biotrophic (Banuett, 1992). Infected plants develop huge tumors, which are a traditional delicacy in Mexico known as Huitlacoche (Valverde *et al.*, 1995). These so-called galls can develop on leaves, fruits, stems and flowers (Figure 1A-D) due to massive teliospore formation inside. When they rupture, the teliospores (Figure 1E) are spread and germinate if circumstances are convenient. The metabasidium (also termed promycelium) forms while meiosis occurs and releases haploid basidiospores (in this work termed sporidia, Figure 1F) via budding and postmeiotic mitosis (O'Donnell and McLaughlin, 1984). These sporidia themselves can either reproduce asexually by budding or mate sexually by the formation of conjugation tubes followed by plasmogamy between two sporidia of different mating types (Kronstad and Leong, 1989; Banuett, 1992; Bölker, Urban and Kahmann, 1992; Gillissen *et al.*, 1992; Snetselaar, 1993). With sexual reproduction, the fungus gains the ability to infect the plant. Hyphae grow by inserting septae, which separate the apical zone containing the two still separate nuclei from the other compartments at the basal zone, which are lacking a cytosol (Lehmler *et al.*, 1997). By receiving surface signals from the plant, the fungus induces appressoria formation and is able to penetrate plant cells via these specialized infection structures (Mendoza-Mendoza *et al.*, 2009). Once inside the plant, mitosis occurs and dicaryotic hyphae begin to grow intracellularly and later also inside the apoplast (Snetselaar and Mims, 1994). The extensive growth of the hyphae inside the plant leads to the formation of the characteristic tumors. The hyphae are embedded in a mucous matrix and fragmentate while the nuclei undergo karyogamy (Ehrlich, 1958; Banuett and Herskowitz, 1996). From these fragments the black teliospores are formed. A detailed review on the life-cycle of *U. maydis* is given by Vollmeister *et al.* (Vollmeister *et al.*, 2012).

U. maydis is a well-investigated model organism in biology especially concerning plant-microbe interactions and its genome was encoded in 2006 (Martínez-Espinoza, García-Pedrajas and Gold, 2002; Kämper *et al.*, 2006; Steinberg and Perez-Martin, 2008). However, for a long time, very little was known about the photobiology of this fungus. Quite recently, research in this topic forged ahead and interesting results were gained. The *U. maydis* genome encodes for a set of different putative photoreceptors covering the perception of a range of wavelengths (Kämper *et al.*, 2006; Estrada *et al.*, 2009; Brych *et al.*, 2016).

Four members of the cryptochrome/photolyase family (CPF), namely Cry1, Cry2, Phr1 and Phr2 were found to bind mainly the flavin adenine dinucleotide (FAD) and are responsible for different DNA-repair mechanisms and in addition - in case of Phr1 and Phr2 - in UV-tolerance. The WC-1

homolog Wco1 binds flavins as chromophore and is a very important blue-light perceiving transcription factor. Together with another homolog Wco2, it forms the WCC that is localized to the nucleus controlling the expression of a huge subset of genes including among others also the four CPF photoreceptors. An additional Wco1 homolog was identified containing no chromophore binding site, however a light-dependent function in basidiocarp-formation could be observed. Furthermore, *U. maydis* consists of a phytochrome, Phy1, that perceives red/far-red light via the chromophore biliverdin and is involved in gene expression regulation, also in cooperation with the WCC, despite being expressed only in the cytoplasm. Another photoreceptor identified in *U. maydis* is Blf1, a BLUF-domain containing protein whose function was not yet characterized in detail. (Brych *et al.*, 2016, 2021; Sánchez-Arreguin *et al.*, 2020)

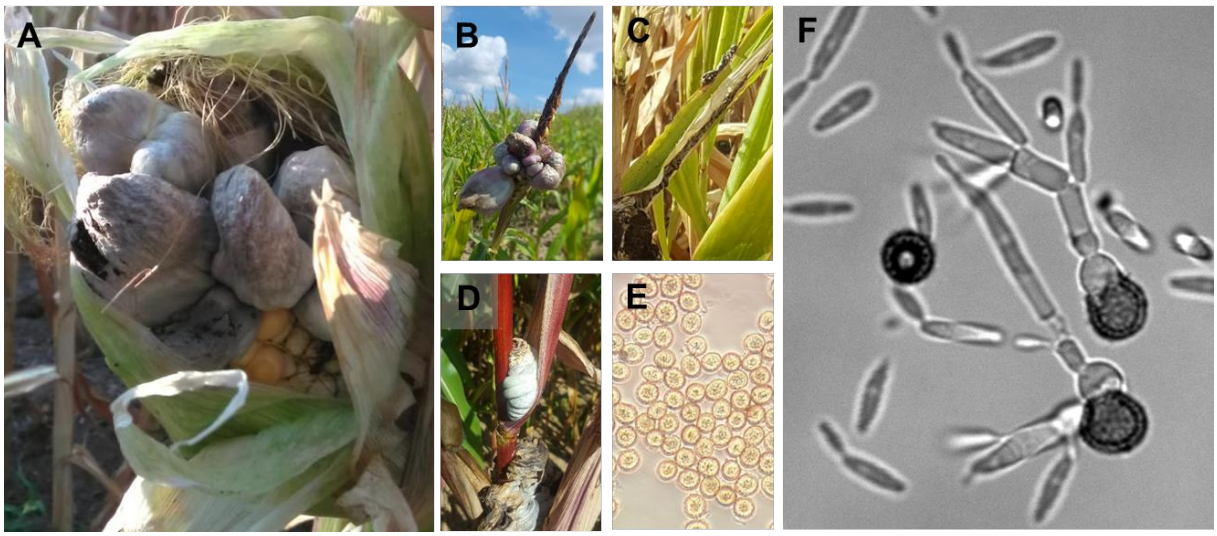

Figure 1: Appearance of *U. maydis* on Corn Plants. Different stages in the *U. maydis* life cycle are depicted. Tumors filled with black teliospores can appear on corn cobs (**A**), flowers (**B**), leaves (**C**) and stems (**D**). The thick-walled teliospores (**E**) germinate under appropriate conditions and produce a metabasidium which releases haploid basidiospores, termed sporidia (**F**).

Three genes coding for opsins were found in the *U. maydis* genome (Estrada *et al.*, 2009; Brych *et al.*, 2016), termed here UmOps1 (UMAG_02629), UmOps2 (UMAG_00371), and UmOps3 (UMAG_04125). In addition, it could be shown that *U. maydis* expresses a functional carotene cleavage oxygenase, Cco1, that takes the final step in the production of retinal from β-carotene, with retinal constituting the rhodopsin chromophore. The genes coding for UmOps1 as well as for UmOps2 were shown to be upregulated upon illumination at acidic pH already in 2009 (Estrada *et al.*, 2009). This result was confirmed and investigated in more detail later: UmOps1 transcript levels were 1000-fold induced upon blue-light illumination and Wco1 was shown to be a major expression regulator of the UmOps1 gene (Brych *et al.*, 2016; Panzer *et al.*, 2019). For UmOps2 the situation was more complex since besides Wco1, additional photoreceptors seem to be involved in regulation and the transcript levels were higher compared to UmOps1 already in darkness (Panzer *et al.*, 2019). In contrast to UmOps1 and UmOps2, UmOps3 could not be detected under experimental conditions (Estrada *et al.*, 2009; Brych *et al.*, 2016), but was found to be expressed *in*

planta shortly after infection acting as a heat shock protein that is connected with the virulence of *U. maydis* (Ghosh, 2014; Lanver *et al.*, 2018). Since only UmOps1 and UmOps2 are expressed in axenic cultures, this work focusses on the microscopic and electrophysiological investigation of these two rhodopsins. Preliminary studies could show that both, UmOps1 and UmOps2, are green light-driven outward proton pumps with UmOps1 showing a boost in pumping activity under extracellular acidic conditions as well as in additional presence of WOA (acetate; IAA; indole propionic acid, IPA) (Panzer, 2017).

This work aims to complete the previous dataset in terms of rhodopsin function of UmOps1 and UmOps2 via patch-clamp experiments. Additional measurements were done concerning pH- and voltage dependency, identification of transported ion species and characteristics that are exhibited in presence of acetate under physiological conditions. Moreover, two mutants were functionally tested concerning the importance of the proton donor site as well as the proton releasing group. Microscopic experiments were done on UmOps2-eGFP expressing sporidia to identify the localization of UmOps2 that could be already observed before, but not assigned to a specific subcellular compartment yet (Panzer, 2017). This kind of experiments were also done for UmOps1-eGFP expressing sporidia. Moreover, novel super-resolution techniques, ExM and CLEM, were tested.

2.1.2 Aureobasidium pullulans

A. pullulans is a saprophytic melanin-containing black yeast that belongs to the order of Dothideales (phylum Ascomycota). This fungus consists of many species and varieties and the taxonomic classification has always been challenging. In former times, *A. pullulans* was often used synonymous for *Pullularia pullulans*, but this may not be completely sustainable due to differences in reproductive structures (Kocková-Kratochvílová, Černáková and Sláviková, 1980). Even nowadays with the help of state-of-the-art sequencing techniques, new insights are achieved and the taxonomic integration is shifted. Recently, four variants of *A. pullulans* were investigated and redefined as separate species: *A. pullulans*, *A. subglaciale*, *A. namibiae* and *A. melanogenum* (Gostinčar *et al.*, 2014). *A. pullulans* is an extremophilic fungus, that inhabits a wide range of different –including stressful- niches. Habitats can be rocks, plants and houses as well as tropical regions and ice glaciers (Webb and Mundt, 1978; Verhoeff *et al.*, 1992; Urzì *et al.*, 1999; Andrews, Spear and Nordheim, 2002; Dimakopoulou *et al.*, 2008; Zalar *et al.*, 2008, 2011; Humphries *et al.*, 2017; Prasongsuk *et al.*, 2018). Even in salterns this halotolerant fungus can be found, however with a slowed down growth (Gunde-Cimerman *et al.*, 2000; Kogej *et al.*, 2005; Zajc *et al.*, 2012). The dominant reproduction form of this fungus is vegetative growth (Ramos and García Acha, 1975; Kocková-Kratochvílová, Černáková and Sláviková, 1980), however, mating type loci necessary for sexual reproduction are also present in the genome (Gostinčar *et al.*, 2014). *A. pullulans* gained importance in biotechnology for its production of pullulan (poly-α-1,6-maltotriose) from which among others edible films are made (Leathers, 2003; Cheng, Demirci and Catchmark, 2011) as well as for the production of β-glucan, what might be of medical interest due to its interaction with antibodies (Tada *et al.*, 2009; Muramatsu *et al.*, 2012). Moreover, *A. pullulans* can be used as a biocontrol agent (Sharma, Singh and Singh, 2009). On the other hand, this fungus also has the ability to act as an opportunistic human pathogen (Chan *et al.*, 2011).

In contrast to *U. maydis*, very little is known about the photobiology in *A. pullulans* although light effects on growth and melanin production were detected as early as in the 1960s (Lingappa, Sussman and Bernstein, 1963). Only recently, it could be shown, that *A. pullulans* contains a set of genes that code for key players involved in circadian rhythm, whose homologs were well investigated in *N. crassa*. Among those genes are the blue light-receptors WC-1, WC-2 and Vivid (VVD) which interact with a set of other proteins and indeed, *A. pullulans* is able to adapt colony growth to light-dark cycles (Franco *et al.*, 2017). Moreover, in the genome of *A. pullulans* three genes coding for opsins were found which consist of the conserved lysine residue necessary for retinal-binding, termed ApOps1 (gb|KEQ89910.1), ApOps2 (gb|KEQ89333.1) and ApOps3 (gb|KEQ87154.1) (Panzer *et al.*, 2021). Previously, first experiments revealed that ApOps1 as well as ApOps2 are capable of ion – most likely proton - pumping with maximal activity under green light-illumination (Panzer, 2015; Bräuer, 2018; Yogendran, 2018).

In this work, all three *A. pullulans* rhodopsins were electrophysiologically characterized regarding the optimal activation wavelength, the pH- and voltage dependency as well as the ion species that is transported. Therefore, constructs that were modified to yield better membrane trafficking by tagging them with the "2.0"-motif (Zhou *et al.*, 2021) were produced by members of the Georg Nagel group (Physiological Institute, Department of Neurophysiology, University of Wuerzburg, Wuerzburg, Germany). The 2.0-motif consists of Lucy-Rho (lr), a cleavable N-terminal signal peptide, two Kir2.1 Golgi apparatus trafficking signals (TT) and the Kir2.1 endoplasmic reticulum export signal (E) so that the constructs are as follows: lr-rhodopsin-TT-eYFP-E. These improved constructs were investigated with the patch-clamp technique. Furthermore, a channel-mutant of ApOps2 2.0 (ApOps2 2.0(F79A,R112H)), also kindly provided by members of the Georg Nagel group, was investigated in terms of pH- and voltage dependency. Moreover, the effect of acetate on the rhodopsin activity under physiological conditions as well as the possibility to use this rhodopsin as optogenetic tool was investigated for the original ApOps2 and partly for ApOps2 2.0 construct. First, the transport capacities were investigated for all three *A. pullulans* rhodopsins in comparison with ChR2, LR and eArch3.0, then ApOps2 was expressed and functionally tested in differentiated Neuroblastoma/Glioma (NG) 108-15 cells.

2.1.3 Fusarium fujikuroi

F. fujikuroi (formerly the teleomorph was known as *Gibberella fujikuroi*) is a rice pathogen of the order of Hypocreales (phylum Ascomycota). It causes the Bakanae disease attended with shoot elongation, etiolation and chlorosis caused by the hormone gibberellic acid what is produced by this fungus. Another symptom can also be complete stagnation of growth. (Ou, 1985; Adam *et al.*, 2018; Sunani *et al.*, 2020) *F. fujikuroi* can reproduce asexually via conidia, sexual reproduction is maintained by mating of – hyphae with + hyphae forming a gametangium from which dikaryotic hyphae grow. These hyphae form perithecia with asci, where karyogamy and then meiosis occurs.

The carotenoid synthesis and retinal providing pathway are well understood in this fungus. Beginning with Geranylgeranylpyrophosphate, β-carotene is formed via several intermediate states and finally cleaved into two retinal molecules. All of those steps are mediated by enzymes arranged in the so-called car gene cluster. (Avalos *et al.*, 2017) The accumulation of carotenoids was shown

to be blue light-regulated involving a flavin binding cryptochrome as well as the White Collar homolog WcoA (Castrillo and Avalos, 2015; Castrillo *et al.*, 2015; Avalos *et al.*, 2017). The latter one was recently shown to be a master regulator of gene expression also in a light independent manner (Pardo-Medina *et al.*, 2020).

The *F. fujikuroi* genome codes for two opsins, CarO and OpsA (Prado *et al.*, 2004; Estrada and Avalos, 2009). *CarO* is localized within the *car* gene cluster and is upregulated upon light exposure. Another gene of the *car* gene cluster, *carS* is involved in regulation of carotenoid accumulation as well as *carO* expression. In the *F. fujikuroi carS* mutant strain, carotene is accumulated and CarO is expressed already in the dark (Avalos *et al.*, 2017). CarO was shown to act as an outward-directed proton pump, activated by green light and responding to extracellular WOAs with enhancement of pump current. It localizes to the plasma membrane as well as to the tonoplast. Furthermore, CarO is involved in the inhibition of conidia germination and in the regulation of plant infection. In contrast, OpsA yielded no photocurrents and no phenotypes in infected plants under experimental conditions (Brunk, 2014; García-Martínez *et al.*, 2015; Adam *et al.*, 2018; Sputh, 2020), but it was shown to be highly upregulated *in planta* (Niehaus *et al.*, 2017).

In this study, CarO localization was tested again on CarO-eYFP expressing conidia and hyphae using conventional super-resolution microscopy (CLSM and SIM) to confirm previous localization studies (García-Martínez *et al.*, 2015; Sputh, 2020) with the help of plasma membrane-, tonoplast- and vacuole marking dyes. Moreover results obtained from CLEM experiments on CarO-eYFP expressing hyphae (Sputh, 2020) will be used as comparison to experiments carried out with UmOps1- or UmOps2-eGFP expressing sporidia to test further the application of this microscopic technique in fungi.

2.2 Microbial Rhodopsins

2.2.1 Structure and Function of Microbial Rhodopsins

Microbial rhodopsins exhibiting various functions are found in all domains of life: bacteria, archaea and eukaryotes (Spudich, 2006; Klare, Chizhov and Engelhard, 2008; Brown, 2014; Béjà and Lanyi, 2014; Ernst *et al.*, 2014). Recent research proposes that light-harvesting via retinal occurred very early in evolution (DasSarma and Schwieterman, 2021) and in addition, the similar overall structure of microbial rhodopsins indicates that these proteins play an important role in light perception and exploitation. The general tertiary structure is a 7-transmembrane-helix motif (helices A-G) connected by three extra- and three intracellular loops (ECL1-3, ICL1-3). The retinal chromophore (ATR in the ground state) binds to a conserved lysine residue in helix G via Schiff base. Upon illumination, the ATR photoisomerizes to its 13-*cis* form. This process is followed by conformational rearrangements throughout the whole protein what triggers the appropriate function. Then, the chromophore and thus the whole protein relax back to the ground state and can again be activated. This whole process that is passed through upon light exposure, is called photocycle and it reveals various intermediate states and exhibits very unique and specific characteristics in the individual rhodopsins depending on amino acid sequence and structural features. (Ernst *et al.*, 2014)

In recent years, several crystal structures of bacterial and archaeal rhodopsins were resolved, but just two are available from eukaryotes. One of them is CsR from *C. subellipsoidea*, the second one just very recently became available and is the first and only structure of a fungal rhodopsin resolved so far, namely LR from *L. maculans* (Fudim *et al.*, 2019; Zabelskii *et al.*, 2021). To visualize the general overall structure similarity of microbial rhodopsins by simultaneously highlighting differences, the structures of XR (*Salinibacter ruber*, Eubacteria), BR (*H. salinarum*, Archaea), CsR (*C. subellipsoidea*, Eukaryota, Plantae, Chlorophyta) and LR (*L. maculans*, Eukaryota, Fungi, Ascomycota) are depicted (Figure 2) (Lanyi and Schobert, 2003; Luecke *et al.*, 2008; Fudim *et al.*, 2019; Zabelskii *et al.*, 2021). Sequences were searched with the help of National Center for Biotechnology Information (NCBI) protein search (NCBI Resource Coordinators, 2016), the models were created using Swissmodel (Biasini *et al.*, 2014) (BR: 1py6.1.A.; XR: 3ddl.1.A; CsR: 6gyh.1.A; LR: 7bmh.1.A) and processed using Pymol Molecular Graphics System 1.8.2.1. All of the four rhodopsins show proton pump function (Lozier, Bogomolni and Stoeckenius, 1975; Balashov *et al.*, 2005; Waschuk *et al.*, 2005; Vogt *et al.*, 2015). The key amino acids necessary for that process in BR as well as their counterparts in the other rhodopsins are highlighted to emphasize the conservation but also slight deviations of those residues (see also Table 1 and Supplementary Figure 1). Most relevant residues are the lysine residue binding ATR via the protonated Schiff base (BR K216), the primary proton acceptor (BR D85), the proton donor (BR D96), the proton releasing group (BR E194, BR E204, BR D212) and some mediators (BR R82, BR T89). Equally important for the transport process are water molecules at specific positions providing hydrogen bonds and therefore stabilization of particular states (Ernst *et al.*, 2014). The proton transport process will be described shortly by reference to archaeal rhodopsin BR, since this is the best-studied microbial rhodopsin up to now.

The photocycle of BR passes through different intermediates termed BR, K, L, M, N and O state. The ground state with retinal in its all-*trans* conformation is represented by the BR state. Here, the Schiff base is protonated due to its high acid dissociation constant (pKa), moreover it is hydrogen bonded to a water molecule (W402). The proton acceptor BR D85 is also hydrogen bonded to W402, but in addition to W401. These interactions prevent proton uptake from the extracellular side, since they cause a low pKa of BR D85. Another water molecule (W400) forms hydrogen bonds to W401, BR R82 and BR D212. Upon light illumination ATR photoisomerizes to its 13-*cis* conformation forming the K intermediate which turns into the L intermediate while the Schiff base is twisted to the cytoplasmic side. Rearrangements of water molecules and amino acids lead to the transfer of the proton from the Schiff base to BR D85 (see (1) in Figure 2) due to pKa value changes (L-M state transition). BR R82 twists toward the extracellular side caused by the loss of hydrogen bonding. There it interacts electrostatically with the electron releasing group what provokes a proton to be released in the M state to the extracellular side (see (2) in Figure 2). In M-N transition, the Schiff base is reprotonated by the proton donor BR D96 mediated by water molecules (see (3) in Figure 2). 13-*cis* retinal reisomerizes to ATR and BR D96 receives a proton from the intracellular side in the O intermediate (see (4) in Figure 2). To finally reach the ground state BR, the proton releasing group is reprotonated by BR D85 (see (5) in Figure 2). (Khorana *et al.*, 1979; Lanyi and Luecke, 2001; Lanyi and Schobert, 2003; Lanyi, 2006; Kikukawa *et al.*, 2012; Nango *et al.*, 2016)

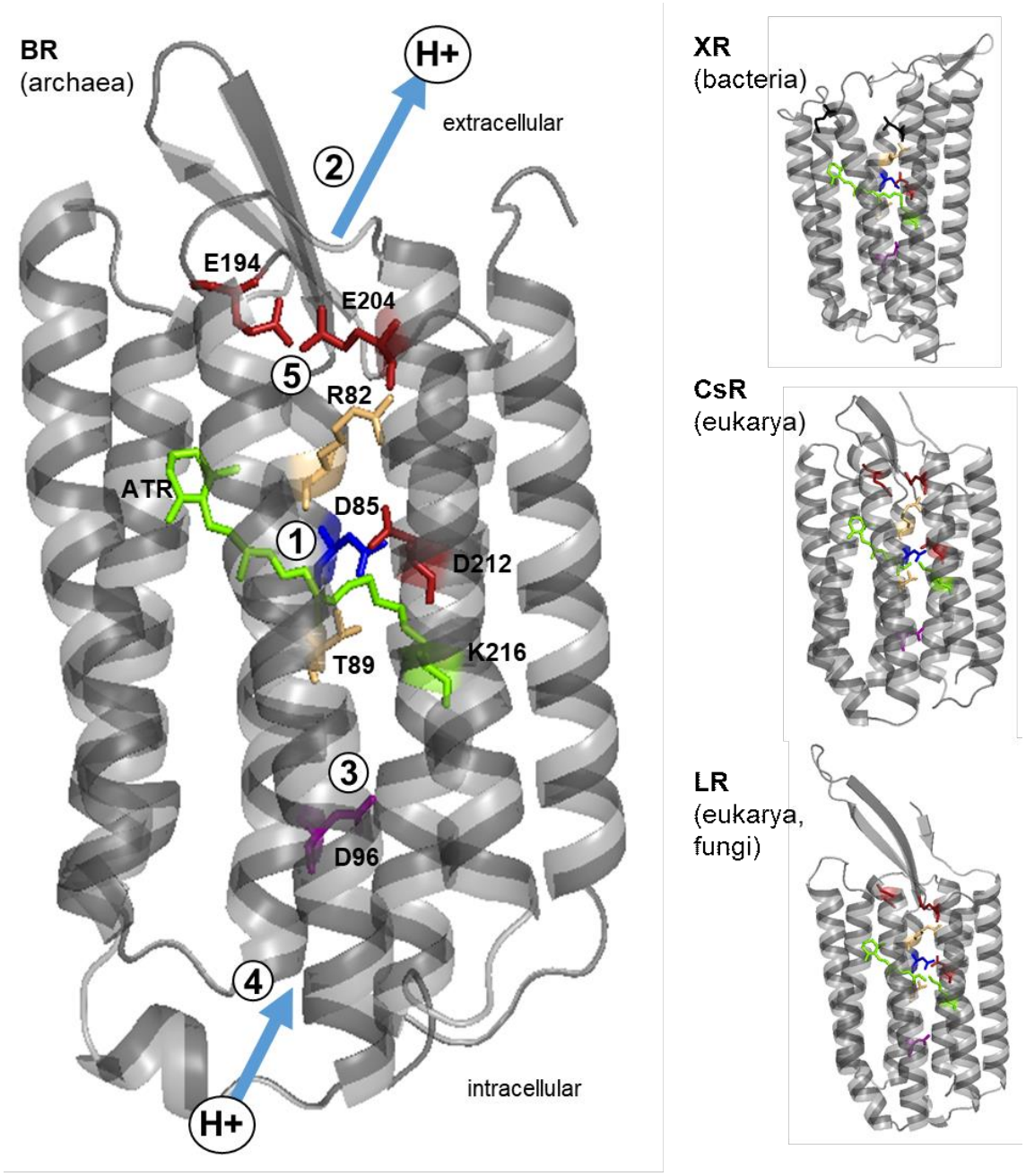

Figure 2: Crystal Structure Models of Bacteriorhodopsin (BR; *H. salinarum*, Archaea), Xanthorhodopsin (XR, *S. ruber*, Bacteria), *C. subellipsoidea* Rhodopsin (CsR, Eukaryota, Plantae) and Leptosphaeria Rhodopsin (LR, *L. maculans*, Eukaryota, Fungi). Highlighted are the chromophore ATR as well as amino acids important for the proton pump function in BR and their counterparts in the other rhodopsins. Archaeal and eukaryotic structures show higher similarity compared to bacterial rhodopsins. Numbers depict single steps of the photo cycle upon light illumination (for explanation see text). Models were created using Swissmodel based on structural information (BR: 1py6.1.A; XR: 3ddl.1.A; CsR: 6gyh.1.A; LR: 7bmh.1.A) and processed with Pymol Molecular Graphics System 1.8.2.1. (Lanyi and Schobert, 2003; Luecke *et al.*, 2008; Fudim *et al.*, 2019; Zabelskii *et al.*, 2021)

The important amino acids are conserved among three of the depicted rhodopsins, BR, CsR and LR with slight variation in the proton releasing group of LR (D in position BR E194). The situation for XR is different: Here, the lysine (BR K216), the proton acceptor (BR D85), mediators (BR R82 and BR T89) and one residue of the proton releasing group (BR D212) are conserved, whereas the proton donor (BR D96) shows a glutamate. In addition, the proton releasing group has a different structure in bacterial rhodopsins revealing no separation of the extracellular bulk to the protein interior on the extracellular side (Zabelskii *et al.*, 2021) and therefore lacking the conserved glutamates that are present in BR (BR E194, BR E204). The higher similarity of the eukaryotic microbial rhodopsins to the archaeal ones underlines the closer relationship between eukaryotes and archaea compared to eubacteria. A striking feature of the first fungal rhodopsin resolved so far, is the long ECL1 that together with the N-Terminus forms an antiparallel 3-stranded β-sheet that is involved in stabilization and membrane orientation of the rhodopsin (Zabelskii *et al.*, 2021).

2.2.2 Fungal Rhodopsins

Fungal rhodopsins as a subgroup of microbial rhodopsins can be further classified into clades like already mentioned. For Ascomycetes, these are the Nop-1- and the CarO-like rhodopsin clade (Adam *et al.*, 2018). The Nop-1-clade can further be subgrouped into LR-like rhodopsins which show a fast photocycle and proton-pump function and the NR-like rhodopsins that show only sensory activity due to their slow photocycle. CarO-like rhodopsins exhibit also fast photocycles with pump activity. Another classification describes four subgroups of opsins, Nop-1-like, CarO-like, orp-1-like and hsp30-like (Wang *et al.*, 2018) opsins with the latter two lacking the conserved retinal-binding lysine residue. This classification also is only applicable for Ascomycetes while the situation in Basidiomycetes seems to be more complex and challenging and opsins cannot be so clearly divided into specific subgroups (Adam *et al.*, 2018; Wang *et al.*, 2018; Panzer *et al.*, 2019). However, the rhodopsins of *U. maydis* could be assigned to the CarO-like rhodopsins in terms of UmOps1 and UmOps3, whereas UmOps2 belongs to the LR-like rhodopsins. In case of *A. pullulans*, ApOps3 is LR-like and ApOps1 as well as ApOps2 are CarO-like rhodopsins (Adam *et al.*, 2018).

Rhodopsin genes are found in a lot of plant-associated fungi and fungal rhodopsins characterized so far are green light-driven proton pumps. The exploitation of the wavelength dominating in the plant environment could make sense for fungi to save other energy sources like adenosine triphosphate (ATP). Moreover, many rhodopsins of plant-associated fungi can be assigned to the CarO-like rhodopsin clade and a characteristic feature of CarO itself as well as for UmOps1 is the reaction to the plant hormone IAA (Panzer, 2017; Adam *et al.*, 2018). This may indicate a possible role of these rhodopsins as a signaling or communication site in plant-fungus interaction.

To visualize the rhodopsins characterized in this work, sequences were searched by the help of NCBI (NCBI Resource Coordinators, 2016) protein search and the models were created with Swissmodel (Biasini *et al.*, 2014). Since no crystal structures are available for these proteins, CsR (6gyh.1.A) as well as LR (7bmh.1.A) for comparison were chosen as templates (Figure 3) (Fudim *et al.*, 2019; Zabelskii *et al.*, 2021). Solid QMEANDisCo values are given as quality scores (Studer *et al.*, 2020). Moreover, multiple sequence alignment was done using PSI/TM-Coffee (Chang *et al.*,

2012) to show conservation and slight differences of amino acid residues which are important for proton transport in BR and their counterparts in the other rhodopsins (Table 1 and Supplementary Figure 1).

The modelled structures show relatively high structure and residue quality estimates that are similar for all models, with CsR-based models yielding higher values for UmOps1 and ApOps1. LR-based models yielded higher values for UmOps2 and ApOps3. ApOps2 showed equal QMEANDisCo values for both templates. When CsR is used as a template, the models do not show a very pronounced ECL1 whereas all LR-based models do so. Notably ApOps3 is the only model showing the 3-stranded beta sheet characteristic for LR consisting of ECL1 and the N-terminus what resulted in the highest quality estimate of all model structures. However, the situation concerning the ECL1 in reality can only be estimated here, since the structures are based on templates and therefore, template specific features may bias the models.

Table 1: Conserved Amino Acid Residues Necessary for Proton Transport in BR and their Counterparts in Other Rhodopsins. Listed are important amino acid residues of the fungal rhodopsins CarO (*F. fujikuroi*), UmOps1, UmOps2 (*U. maydis*), ApOps1, ApOps2, ApOps3 (*A. pullulans*) and LR (*L. maculans*) as well as of the algal rhodopsin CsR (*C. subellipsoidea*) and the bacterial rhodopsin XR (*S. ruber*) in comparison with the well-studied archaeal rhodopsin BR. The lysine residue necessary for retinal binding (BR K216) and the aspartate that acts as primary proton acceptor (BR D85) as well as the mediator residues arginine (BR R82) and threonine (BR T89) are conserved in all depicted rhodopsins. The proton donor aspartate (BR D96) is changed to a glutamate in UmOps1 and in XR. Concerning the proton releasing group, in XR only one aspartate (BR D212) is conserved, while in the other rhodopsins an aspartate and a glutamate (BR D212 and BR E204) are conserved while the third component (BR E194) either is glutamate or aspartate. The closer relationship of eukaryotic rhodopsins to archaeal ones compared to bacterial rhodopsins is clearly visible.

Rhodopsin	Retinal Binding Site	Proton Acceptor	Proton Donor	Proton Releasing Group			Mediators	
BR	K216	D85	D96	E194	E204	D212	R82	T89
CarO	K246	D117	D128	E224	E234	D242	R114	T121
UmOps1	K247	D118	E129	D225	E235	D243	R115	T122
UmOps2	K245	D115	D126	E223	E233	D241	R112	T119
ApOps1	K244	D115	D126	E222	E232	D240	R112	T119
ApOps2	K244	D115	D126	E222	E232	D240	R112	T119
ApOps3	K254	D123	D134	D232	E242	D250	R120	T127
LR	K270	D139	D150	D248	E258	D266	R136	T143
CsR	K215	D86	D97	E193	E203	D211	R83	T90
XR	K240	D96	E107	M211	L228	D236	R93	T100

Regarding the key amino acids necessary for proton transport in BR, all rhodopsins shown here possess conserved counterparts with slight variations. In all five fungal rhodopsins that are characterized in this work, the lysine residue binding the chromophore (BR K216) as well as the primary proton acceptor (BR D85), the arginine and threonine mediator residues (BR R82 and BR T89) and a glutamate and an aspartate of the proton releasing group (BR E204 and BR D212) are conserved. The third important residue of the proton releasing group (BR E194) shows a

glutamate in UmOps2, ApOps1 and ApOps2, but an aspartate in UmOps1 and in ApOps3. The proton donor site (BR D96) presents also aspartates in UmOps2, ApOps1, ApOps2 as well as ApOps3, only UmOps1 has a glutamate at that position. For the sake of completeness, in the multiple sequence alignment (Table 1), also CarO (*F. fujikuroi*) was considered showing that the depicted amino acid residues are conserved in comparison with BR.

Despite their overall similarity, every rhodopsin modelled here shows its special characteristics and differs slightly in structural features and the amino acid residue counterparts necessary for proton transport in BR. However, all of them present the key residues and should exhibit ion transport activity upon illumination what was indeed already shown before at least for UmOps1, UmOps2, ApOps1 and ApOps2 (Panzer, 2015, 2017; Bräuer, 2018; Yogendran, 2018; Panzer *et al.*, 2019).

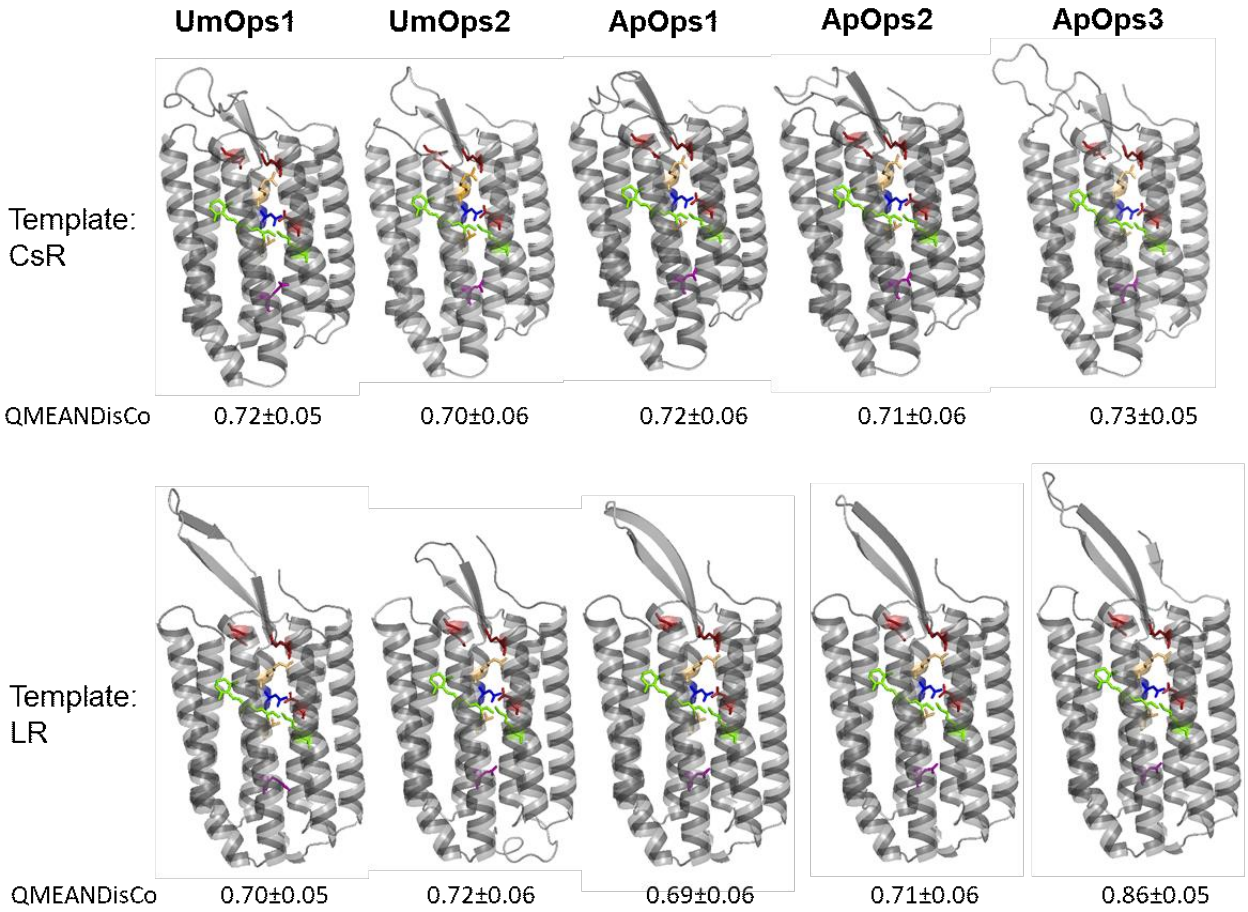

Figure 3: Template-based Structure Models of UmOps1 and UmOps2 (*U. maydis*) as well as ApOps1, ApOps2 and ApOps3 (*A. pullulans*). Highlighted are the counterpart residues of amino acids important for the proton pump function in BR (light green: chromophore binding lysine + ATR; blue: primary proton acceptor; yellow: mediators; purple: proton donor; red: proton releasing group). Models were created using Swissmodel based on structural information of CsR (6gyh.1.A) or LR (7bmh.1.A), respectively, and processed with Pymol Molecular Graphics System 1.8.2.1. QMEANDisCo values are given as structure- and residue-based quality estimates.

2.3 Fluorescence Microscopy

2.3.1 Basic Principle of Fluorescence and its Application in Microscopy

Molecules which are able to show fluorescence are called fluorophores. These molecules spontaneously emit light after being irradiated with a specific wavelength (excitation wavelength). The physical principle behind that can be explained with the help of the Jablonski diagram (Figure 4A). The horizontal lines show electronic and vibrational states and the spin multiplicities (singlet "S" and triplet "T" states) of electrons, the arrows indicate their transitions between the states. When a fluorophore is irradiated with the excitation wavelength, photons are absorbed within femtoseconds. That leads to the rise of electrons from the singlet ground state S_0 to a higher singlet state ($S_{1...n}$). Inside a specific singlet state, an electron can occupy different vibrational states. The loss of energy can occur in various ways. Vibrational relaxation is the drop of electrons from a higher to a lower vibrational state inside a distinct electronic state. When internal conversion occurs, electrons transit between two electronic states. They drop from a higher to a lower electronic state, while occupying a high vibrational state in the latter one. There, again vibrational relaxation takes place to reach the lowest vibrational state in that distinct electronic state. The two mentioned transitions are non-radiative, the energy is released in form of heat. When an electron drops from the lowest vibrational state of S_1 back to any vibrational state of S_0, radiation occurs in a nanosecond timescale. This process is called fluorescence. Due to vibrational relaxation that is also involved in the process, the emitted radiation has less energy than the one which excited the system. That means, the emitted light shows a higher wavelength compared to the absorbed radiation. This phenomenon is called the Stokes shift and enables fluorescence microscopy. For electrons it is also possible to undergo intersystem crossing involving spin reversal to transit from S_1 to the triplet electronic state T_1. According to the selection rules of quantum mechanics, intersystem crossings are forbidden transitions and therefore occur in a much slower time scale (up to 100 s) compared to fluorescence. When dropping back to S_0 from the lowest vibrational state of T_1 phosphorescence or non-radiative relaxation can occur. (Lichtman and Conchello, 2005; Sauer, Hofkens and Enderlein, 2010)

Nowadays, fluorescence microscopy is a common tool used by researchers to localize cellular compounds in living or fixated cells. Cellular structures are labelled with fluorescent dyes directly, with the help of antibodies or via gene fusion constructs containing fluorescent proteins (FP's). As mentioned above, the Stokes shift plays an important role in detecting fluorescence. The emitted light can be separated from the excitation light with the help of dichroic mirrors, so that the fluorescence signals can be observed without disturbing signals deriving from the light source. The basic principle of fluorescence microscopy is illustrated in Figure 4B. Light is emitted by a light source, purified by an excitation filter and then reaches the dichroic mirror. The excitation light is reflected there and reaches the sample, where it causes the fluorophores to emit fluorescence. This emission light showing a higher wavelength, again hits the dichroic mirror but can pass and fall onto the detector. If necessary, an additional emission filter can be placed in front of the detector to purify the emission light. Although this technique brought huge advantages for biological laboratories, no higher resolutions can be achieved compared to bright field microscopy. The Abbe limit comes into play for light diffracting structures and is defined as the smallest distance (d) of

two lines of a grid at which they can be resolved as two distinct objects. This is dependent on the wavelength (λ) and the numeric aperture (NA) of the objective and condenser (see equation 1) (Abbe, 1873).

$$d = \frac{\lambda}{NA_{objective} + NA_{condenser}} \quad (1)$$

For self-luminous structures, e.g., fluorophores, the Rayleigh criterion takes effect. The minimum distance of two point-like sources of light, at which they can be resolved as two separate points, is when the point spread function maximum of the first source falls into the first minimum of the point spread function of the second source (equation 2) (Rayleigh, 1903).

$$d = \frac{0.61 * \lambda}{NA_{objective}} \quad (2)$$

Over time, researchers had the aim to overcome those limits in resolution and developed a bunch of microscopic techniques to yield higher resolutions specific for different sample types and applications. Those techniques are called super-resolution techniques. Of course, electron microscopy (EM) offers resolutions down to 1 nm or even lower, but this method requires extensive sample preparation and is a very invasive technique, where live cell imaging is not possible. Conventional super-resolution fluorescence techniques are for example CLSM or SIM

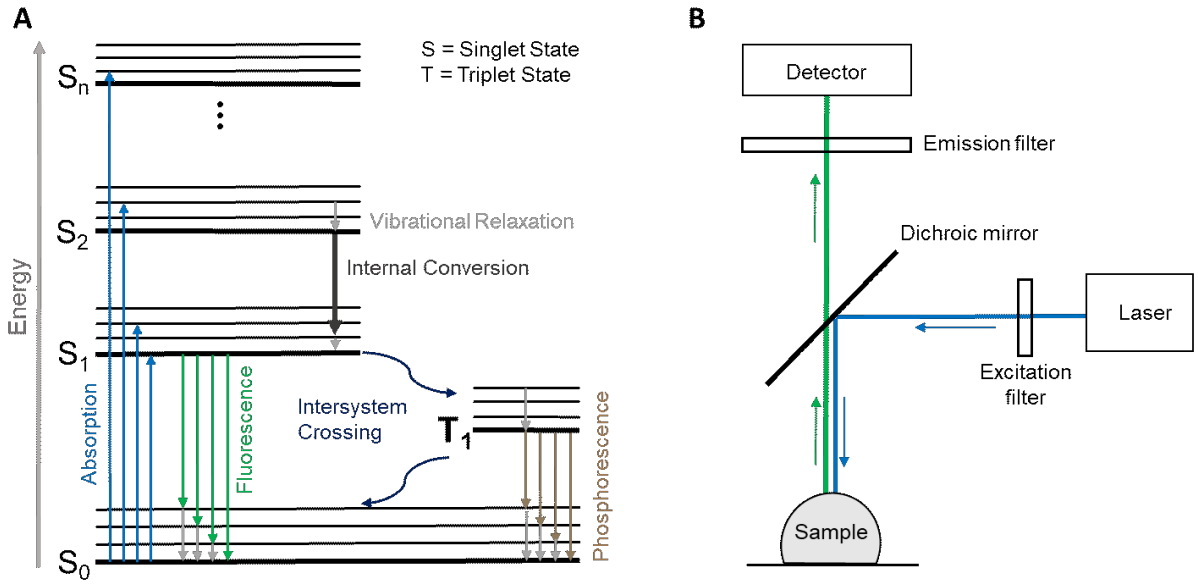

Figure 4: Basic Principle of Fluorescence and Fluorescence Microscopy. A: The Jablonski diagram illustrates the different electronic and vibrational states as well as spin multiplicities that can be occupied by electrons after irradiation. Moreover, the transitions between these states are depicted. **B:** Basic principle and beam path of fluorescence microscopy. The Stokes shift enables imaging of the emitted fluorescence by the help of a dichroic mirror (for further explanation see text). Adapted from (Panzer, 2017)

which could increase the resolution by √2 or 2, respectively (Gustafsson, 2000; Sauer, Hofkens and Enderlein, 2010). To gain even higher resolutions in the fluorescence microscopy sector (down to 10 nm), stimulated emission depletion (STED) and single molecule localization microscopic (SMLM) methods like stochastic optical reconstruction microscopy (STORM), photoactivated localization microscopy (PALM) and direct stochastic optical reconstruction microscopy (dSTORM) were developed among others (Hell and Wichmann, 1994; Betzig *et al.*, 2006; Rust, Bates and Zhuang, 2006; van de Linde *et al.*, 2011). Different methods were combined to take advantages from both techniques, for example SIM and localization microscopy (Rossberger *et al.*, 2013) or even electron and fluorescence microscopy. The latter one is called CLEM and aims to show fluorescence signals in the background of cellular compounds visible in electron micrographs (Müller-Reichert *et al.*, 2007; Markert *et al.*, 2016). Another novel technique is ExM. Here, not the optical system is adjusted but the sample itself is physically expanded, so one can implement this technique by using conventional fluorescence microscopes (Chen, Tillberg and Boyden, 2015). In this work, CLSM, SIM as well as CLEM and ExM were used to gain insights into fungal cell structure and rhodopsin localizations.

2.3.2 Well-established Super-resolution Microscopy – CLSM and SIM

CLSM allows imaging of living or fixated cells by recording flat planes of the fluorescent samples. This is done by integrating a pinhole into the beam path (Figure 5A). The sample is illuminated and emits fluorescence via fluorophores, so is doing the focal point, i.e., in the structure of interest. By using a lens system, a confocal point is created, that lies exactly where the pinhole is located. By adjusting the pinhole diameter, more or less light from points outside the focal plane can be excluded from reaching the detector. In such a manner, the sample can be scanned with the laser creating a full image of focal points. The smaller the pinhole diameter, the flatter the plane that is

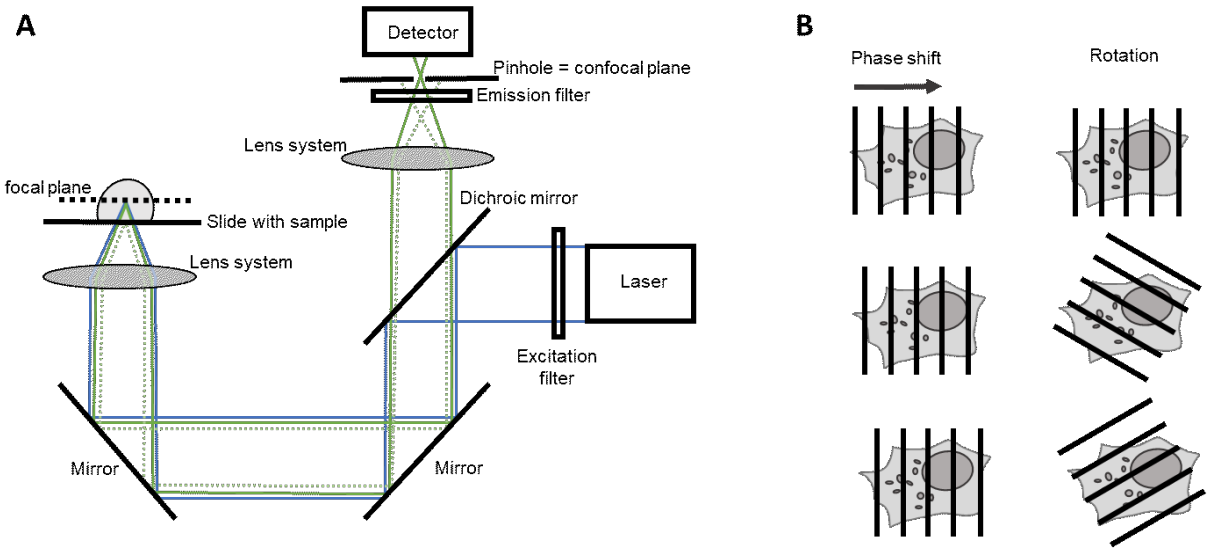

Figure 5: Basic Principle of CLSM and SIM. A: Beam path of a CLSM with integrated pinhole for exclusion of light that does not derive from focal points. Adapted from (Panzer, 2017) **B:** Principle of phase shift and rotation of the grid integrated in a SIM to achieve a Moiré pattern from which a final image with about doubled resolution can be processed.

detected and the sharper the image that is taken. However, when the diameter is chosen too small, very little light will reach the detector and the image quality will not be sufficient, so one hast to adjust the pinhole diameter in dependence on wavelength and fluorescence intensity. In general, the resolution can be increased to about √2 with this technique. (Sauer, Hofkens and Enderlein, 2010)

Another conventional super-resolution technique that can be used to record live as well as fixated samples is SIM. Basically, SIM is a wide field technique, which reaches about double the resolution of wide field microscopy by integrating a grid into the beam path that can be shifted and rotated (Figure 5B). Overlaying the structural information of the sample with this grid gives rise to a so-called Moiré pattern. Usually, 3 or 5 phase shifts and rotations are applied resulting in 9 or 25 single images, respectively. This recorded subset is then computationally processed and a final image is reconstructed showing lateral resolutions of around 100-150 nm depending on grid frequency and orientations. (Gustafsson, 2000; Demmerle *et al.*, 2017; Heintzmann and Huser, 2017)

2.3.3 Novel Microscopic Approaches – ExM and CLEM

ExM

Many super-resolution techniques are based on the adaptation of the optical elements of the setup or exploit the photophysical properties of special dyes to reach sub diffraction resolution. In contrast, for ExM, the sample itself is physically expanded with the help of a swellable polymer so that imaging can be performed on conventional fluorescence microscopic setups (Chen, Tillberg and Boyden, 2015). During the last years, this approach has been used in very different research fields, for example bacteria and plants were investigated, subcellular structures were imaged with ultrastructure ExM (U-ExM) or tissue slices were visualized using expansion pathology (Gambarotto *et al.*, 2019; Kao and Nodine, 2019; Kunz *et al.*, 2019; Wassie, Zhao and Boyden, 2019; Bucur *et al.*, 2020). The general process is as follows (Figure 6): For ExM, the sample has to be fixated, no live-cell imaging is possible. The structure of interest is labelled with an amine or acrydite containing fluorescent dye, then the sample is embedded into a polyacrylamide gel where the linkage of the dye to it can be achieved for example with glutaraldehyde (GA). After that, the sample is treated with Proteinase K to completely homogenize cellular components, while all structures and also the labels stay at their places because of the incorporation into the gel. In a next step, the gel is expanded isotropically together with the homogenized structures and the fluorescent labels, so that one can image the sample with a conventional fluorescence microscope but reach increased resolution. (Chozinski *et al.*, 2016; Faulkner, Thomas and Neely, 2020) Another possibility is the post-labelling strategy, that means labelling of the structure of interest after the expansion step, e.g., via the magnified analysis of the proteome (MAP) approach (Ku *et al.*, 2016). Moreover, post labelling was combined with SMLM techniques to yield even clearer and more detailed images of the ultrastructure of cellular components (Zwettler *et al.*, 2020). The typical expansion factor of ExM is 4-fold, but also 10-fold and even 20-fold expansion was reached using iterative expansion (Chang *et al.*, 2017; Truckenbrodt *et al.*, 2019). In addition, it is possible to adjust the expansion factor between 2 and 8 with the help of a technique called ZOOM (Park *et al.*, 2019).

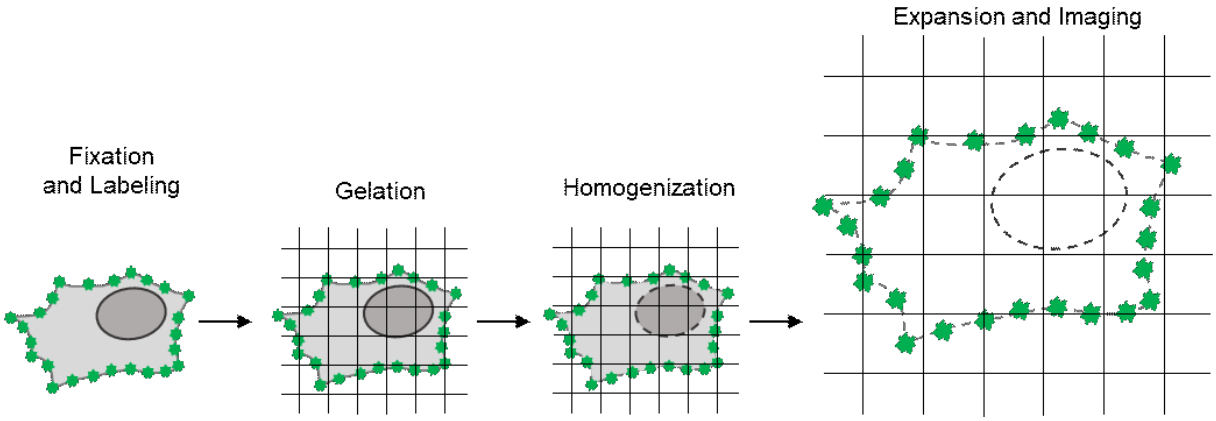

Figure 6: General Process of ExM. At first, the sample is labelled and fixated, then embedded in the gel matrix. After homogenization with Proteinase K, the gel with the anchored fluorophores is isotropically expanded and can be imaged on a conventional fluorescence microscope.

Expansion of fungi is challenging and the protocol has to be adapted, since fungal cells are surrounded by a rigid cell wall containing different components like chitin, glucans and glycoproteins (Bowman and Free, 2006; Gow, Latge and Munro, 2017), which have to be digested for a sufficient isotropical expansion. However, ExM is a suitable possibility to image fungi at super-resolution since fungi are very tiny organisms and many cellular components cannot be observed in a sufficient way using diffraction limited methods. Moreover, in many cases fungi show huge autofluorescence (Knaus *et al.*, 2013), what can be circumvented by the application of ExM.

CLEM

CLEM combines the advantages of fluorescence-based microscopy with the very high resolution of electron microscopy. In general, firstly, fluorescence images are taken, here one can use widefield techniques but using super-resolution methods like SMLM or SIM yield more detailed information. The sample then is prepared for and imaged with EM; after that, both, EM and fluorescence images are correlated (Markert *et al.*, 2016). Hereby it obviously is very important to image the same spot of the sample. The aim of this work was to gain information about the localization of fungal rhodopsins in the subcellular context. Therefore, *U. maydis* sporidia as well as *F fujikuroi* hyphae (Sputh, 2020) were embedded in LR-White resin. From this resin block, thin sections were cut, which were treated with an antibody labelling against GFP to yield sufficient fluorescence signals. For imaging the fluorescence, in this work only SIM was used. After SIM imaging, the samples were prepared for EM. The sections were contrasted, fixated and coated; images were taken using scanning electron microscopy (SEM) and finally the correlation with the fluorescence recordings was done.

In the following, the principle of electron microscopy with its subtypes SEM and Transmission electron microscopy (TEM) will be described in short.

Electron microscopy generates resolutions lower than 1 nm. This can be done by using an electron beam generated by a tungsten cathode, that is transported to the sample via electromagnetic lenses.

The resolution limit is not reached due to diffraction limit like in widefield techniques; here the resolution is limited by the aberration of the electromagnetic lenses. However, EM needs an extensive sample preparation because the whole imaging process takes place in vacuum. There are two main types of EM: SEM and TEM (Goodhew and Humphreys, 2000; Nguyen and Harbison, 2017).

With SEM, mainly surface structures can be observed. The electron beam scans the sample surface and removes electrons from it, the so-called secondary electrons. The accelerating voltage hast to be adjusted depending on the sample: When the sample contains only few elements with high ordinal number, the voltage should be low, otherwise the beam would just pass the sample. Moreover, the sample has to be covered with a metal layer via sputtering and all liquids have to be removed by critical-point-drying. Two detectors can be used for catching the electrons from the sample. The in-lens-SE-detector (SEI) lies inside the SEM and produces images on which the samples look flatter but offer depth information. The outer SE-detector (LEI) is fixed near the sample and creates plastic and sharp images. Among surface structures, also tissue sections can be imaged with SEM via backscattered electrons (Ohta *et al.*, 2012; Koga *et al.*, 2015).

With TEM, thin sections (50-200 nm) of a sample embedded in resin and contrasted with uranylacetate and lead citrate can be imaged. Here, not the secondary electrons, but the elastically scattered electrons are detected. Before contrasting, the samples have to be fixated. When using potassium permanganate, especially membranes will be visible, when using GA and osmiumtetroxide, other cellular structures can also be left in a good condition.

It is possible to apply CLEM on serial sections of a block and with the help of that image set create a 3D model of the sample. This process is called electron tomography. More detailed information about CLEM and its application in fungi can be found in the master thesis of Sebastian Sputh (Sputh, 2020).

2.4 Electrophysiology and Optogenetics

2.4.1 The Patch-Clamp Technique

The patch-clamp technique is, besides the two-electrode voltage clamp (TEVC) method, a common tool in electrophysiology for studying ion currents flowing over cellular membranes. While the latter one often is applied on *Xenopus* oocyte expression system, the patch-clamp method is mainly used for experimenting with mammalian cells. The basic principle is the integration of the cellular plasma membrane into a current circuit and thus being able to measure potential changes caused by ion fluxes over it. Advantage is taken from the electrical properties exhibited by cellular membranes (Figure 7 Red box). The lipid double layer acts as an insulator with very high resistance and a conductivity of about zero because there are no motile charges available in it and only hydrophobic or small uncharged polar molecules can pass it via diffusion. Moreover, the cellular membrane can store charges by acting as a plate capacitor which is connected in parallel with the membrane resistance. Passage of ions through the membrane can only be achieved via specialized transport proteins like for example ion channels or pumps which are embedded in the

lipid double layer. These proteins react to very different stimuli like voltage or pH changes or in the case of rhodopsins to light.

Already in the 1930s, the foundation of electrophysiological techniques was laid by experiments on isolated giant squid axons by the help of a voltage clamp (Cole and Curtis, 1939; Cole, 1979). Later, squid axons as well as muscle fibers were used to carry out experiments with the emerging patch-clamp technique and in 1976, Erwin Neher and Bert Sakmann presented an improved version that was sensitive enough to measure currents evoked by single channels in a frog muscle fiber (Strickholm, 1961; Fishman, 1973; Neher and Sakmann, 1976). For this advance, they received the Nobel Prize for Physiology/Medicine in 1991.

The general principle of the patch-clamp technique for measuring currents transported via rhodopsins is as follows: The rhodopsins are expressed heterologously in mammalian cells. These cells are placed in a perfusion chamber containing a defined electrolyte solution (the bath solution). The cell is then sucked with a micropipette, that is also filled with a defined electrolyte solution (the pipette solution) and that is connected via an electrode to the head stage (preamplifier), the amplifier, an analog-digital (AD)-converter and the computer. It is very important to reach the so-called Gigaseal, that is a very tight connection between pipette tip and plasma membrane so that the leak currents are as weak as possible (resistance should be in the Giga-Ohm range). Only then the background noise is small enough to yield sufficient current traces from the transport proteins.

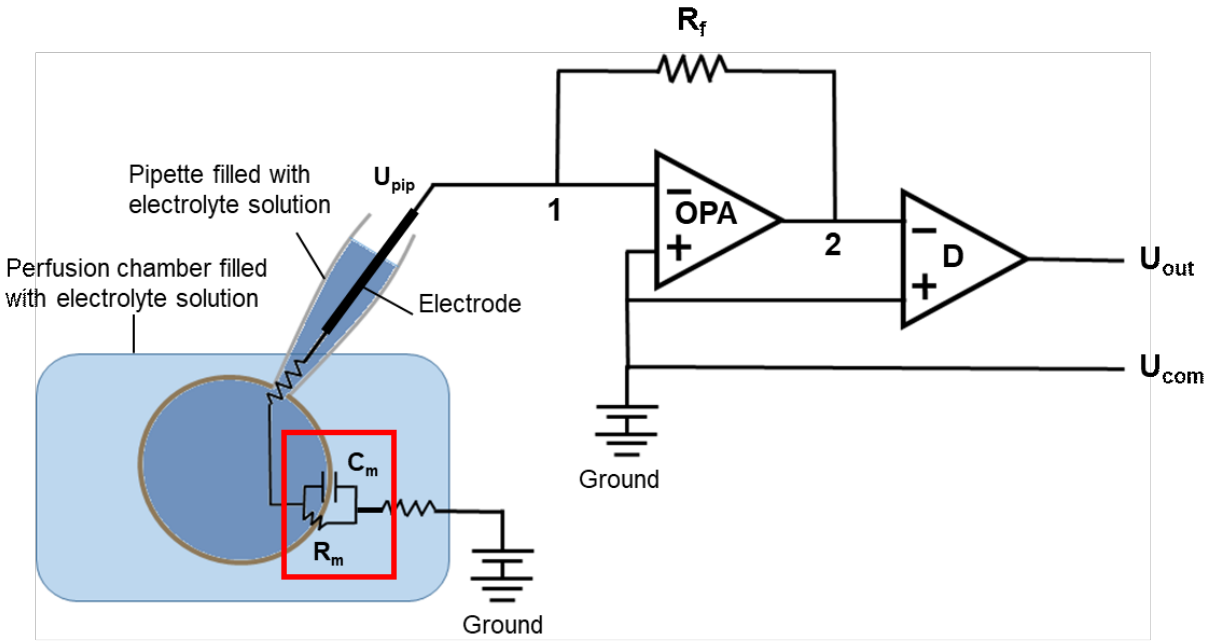

Figure 7: Circuit Diagram of a Current-to-voltage Converter Implemented in the Head Stage of Common Patch-clamp Setups. Two OPAs work together for maintaining the clamp-voltage and thus being able to detect potential changes – hence current flows – at the plasma membrane (for detailed explanation see text). **Red box:** The plasma membrane acts as a plate capacitor and shows high resistance and a conductivity of almost zero. Ions are only able to pass the membrane via specialized transport proteins. The pipette resistance is connected in series to the cellular membrane. Adapted from (Panzer, 2017)

Via a reference electrode the current circuit is closed. The pipette tip has a very small opening and exhibits a serial resistance that is connected in series to the cellular membrane. Now illumination can be applied to the cell, the rhodopsins are then activated, generate a current flowing over the cellular membrane what is recognized by the electronics and output as a current curve on the computer. For a more detailed explanation of the components of the patch-clamp setup see chapter 3.3.1 . The centerpiece that is indispensable for the measuring process is a current-to-voltage converter (Figure 7). This component is required for the application of a defined command voltage (clamp-voltage) to the cellular membrane as well as for the actual measuring process. The central part here is an operational amplifier (OPA) with an inverting and a non-inverting input. Input resistances of OPAs are ideally infinite, what means that no current flows into the OPA. To the inverting input, the microelectrode from the micropipette is connected revealing the membrane potential (U_{pip}). The command voltage (U_{com}) is connected to the non-inverting input. These two input voltages are compared by the OPA and an amplified output potential is given that is proportional to the potential difference. Since U_{pip} and U_{com} are not equal, a potential difference occurs between 1 and 2. Therefore, a current flow occurs over the feedback resistor (R_f) until U_{pip} equals U_{com}. At this point, the voltage of the cellular membrane is clamped. Since this process of establishing the clamp-voltage takes only a few µs, one can assume that U_{pip} always corresponds to U_{com}. When the rhodopsins are now activated by light and transport ions, this is recognized by a second (differential) OPA, that is also connected with U_{com}. These analog signals are converted into digital signals, are again calculated to current values and are visible in the software as current traces over time. Per convention, positive current signals derive either from anions being transported into the cytosol or from cations being transported out of it (vice versa for negative current signals).

Patch-clamp measurements can be performed using different modes concerning the circuit integration of the cell, namely cell-attached, whole-cell, outside-out and inside-out configuration (Figure 8). When the cell is sucked with the micropipette, the cell-attached configuration is reached. In this mode, the interior of the cell cannot be controlled in terms of ion composition since there

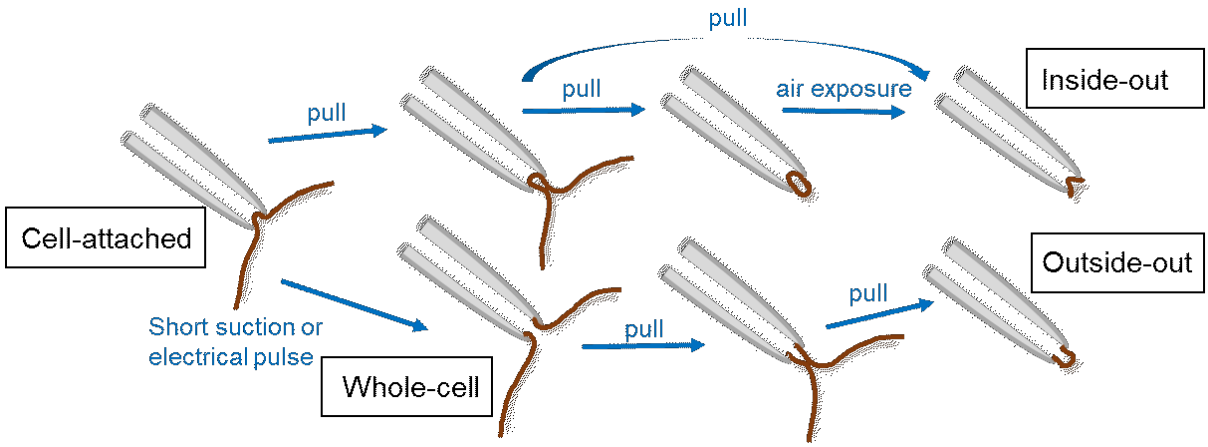

Figure 8: Patch-clamp Configurations. From cell-attached mode, whole-cell mode can be obtained via sucking or an electrical pulse. Inside-out configuration is reached by pulling away the membrane patch. Outside-out mode is achieved by pulling the patch from whole-cell configuration.

is no connection to the cytosol. By pulling away the pipette, the inside-out configuration is obtained. If the patch closes, it is possible to expose the vesicle to the air very shortly to rupture it and regain inside-out mode. The whole-cell mode can also be achieved from cell-attached by rupturing the membrane under the pipette tip ("breakthrough") by the help of a short strong negative pressure or a short electrical pulse. From the whole-cell mode, the outside-out configuration can be obtained by pulling away the micropipette from the cell (Sakmann and Neher, 1984).

In cell-attached, inside-out and outside-out mode, only signals deriving from the small patch inside the pipette tip are accessible for measuring. In contrast, the whole-cell mode offers the possibility to measure transporters of the whole cellular membrane. The cell-attached mode is the only mode where only the extracellular electrolyte composition can be controlled whereas in all three other modes in addition the intracellular ion composition can be defined.

2.4.2 Optogenetics

The research field of optogenetics aims to control neuronal cells via light application, that is the activation and inhibition of neuronal activity with the help of currents deriving from rhodopsins upon illumination (Figure 9). The overall goal of this technique is on the one hand gaining insights into the pathology of neuronal diseases or diseases concerning vision, on the other hand to find possibilities to treat those medical conditions. Two years after the first description of ChR2 (Nagel *et al.*, 2003), this rhodopsin was the first one being used as an optogenetic tool by being able to evoke voltage spikes in hippocampal neurons (Boyden *et al.*, 2005). After this first breakthrough, optogenetics emerged as a very popular research field, huge progress was made and in 2010, optogenetics was chosen as "method of the year" by Nature Methods. The nematode *Caenorhabditis elegans* was the first animal that was manipulated in its behavior by controlling muscle contraction via light application with the help of ChR2. In addition, ChR2 was modified to yield better depolarization results. (Nagel *et al.*, 2005) In the following years, with the discovery and modification of many other rhodopsins besides ChR2, the optogenetic toolbar was enlarged. For the activation of neurons, besides ChR2, for example in *C. noctigama*, the red light-activated channel

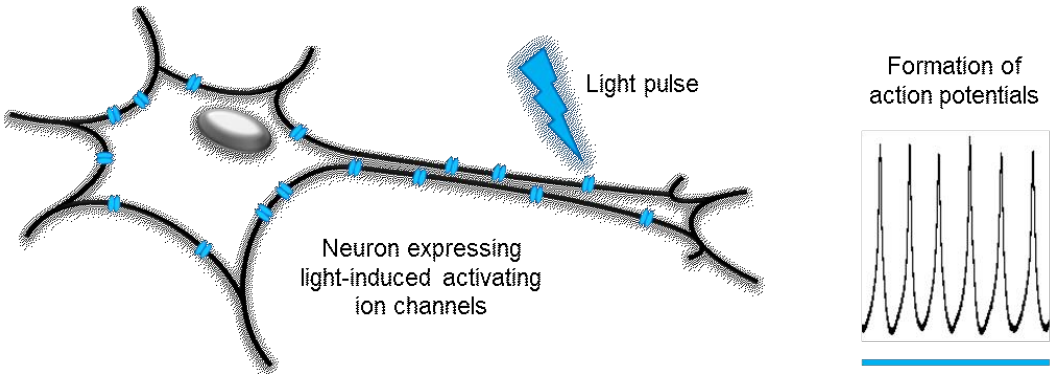

Figure 9: Basic Principle of Optogenetics. Ion channels (here activating ion channels, e.g., inward rectifying proton transporters) are expressed in neurons. They are illuminated with light of their specific excitation wavelength and evoke action potentials due to the depolarizing photo currents.

Chrimson was found which was further improved to ChrimsonR in order to gain enhanced photocurrents (Klapoetke *et al.*, 2014). For inhibition of neuronal activity, among others, NpHR, Arch-3 or LR are used (Han and Boyden, 2007; Chow *et al.*, 2010; Flytzanis *et al.*, 2014). Improved versions here are for example eArch3.0 or eMac3.0 yielding higher photocurrent amplitudes. With this broad range of photoactivatable ion transporters showing different characteristics, for example the silencing or activation of two specific neuronal populations by using light of different wavelengths became possible (Chow *et al.*, 2010; Klapoetke *et al.*, 2014) and over the years, more and more complex experiments and issues could be addressed. Only recently, as mentioned already in the introduction, a major milestone was led by the research team around Botond Roska by being able to restore vision in a blind patient who suffered from Retinitis pigmentosa (inherited disease showing degeneration of photoreceptors) with the help of ChrimsonR (Sahel *et al.*, 2021). For the delivery of the rhodopsin to the retinal ganglion cells, they used an adeno-associated virus-based system, that was established previously in other optogenetic investigations, e.g., for the delivery of an ion channel in cochlear neurons (Duarte *et al.*, 2018). After optogenetic treatment, the blind patient was able to perceive objects with the help of special goggles. (Sahel *et al.*, 2021). This breakthrough shows the huge power of the optogenetic research field. It is furthermore worth mentioning, that optogenetics nowadays is much more than the classical definition of neuronal controlling via light. It is also possible to switch promoters or control protein interactions and cAMP levels by illumination, while the light itself may even be produced via bioluminescent molecules (Sureda-Vives and Sarkisyan, 2020). It is important to investigate more proteins that could find application in optogenetics in the future and the fungal kingdom offers promising candidates. Thus, in this work, ApOps2 from *A. pullulans* was tested for the functional expression in differentiated NG108-15 cells and, moreover, a channel mutant was tested for its characteristics regarding pH- and voltage dependency.

3 Materials and Methods

All steps concerning work with mammalian or fungal cells were conducted under sterile conditions (clean benches: HeraSafe Type HS 12, Heraeus Instruments; Gelaire Flow Laboratories, Flow Laboratories GmbH) and with the use of sterile materials/liquids (autoclaving/ sterile-filtration). Purified double distilled water (ddH_2O) was obtained from an ultrapure water supply (Barnstead GenPure Pro System, Thermo Fisher Scientific) and was additionally sterilized by sterile-filtration. Chemicals, media, buffers and reagents were obtained from the following companies: Merck KGaA, (Sigma Aldrich); Carl Roth GmbH + Co. KG; Thermo Fisher Scientific Inc.; Capricorn Scientific GmbH

3.1 Cell Culture

3.1.1 Mammalian Heterologous Expressing Systems

3.1.1.1 Cell lines

For conducting patch-clamp experiments stably expressing human embryonic kidney (HEK) Flp-In™ T-REx2™-293 cell line (Invitrogen, Thermo Fisher Scientific Inc.) was used. Members of our working group prepared this cell line following the Invitrogen Flp-In system instructions. Briefly, in this cell line, zeocin selection is allowed by a stably integrated pFRT/lacZeo vector. Moreover, they consist of a pc desoxyribonucleic acid (DNA)™6/TR vector, that contains Blasticidin resistance and the gene for a Tet repressor (TetR). The cell line was cotransfected with the Flp recombinase vector pOG44 as well as with the expression plasmid pcDNA™5/FRT/TO© that contains a tetracycline (TC)-inducible cytomegalovirus (CMV) promoter upstream of the gene of interest (GOI) and a Hygromycin (Hyg) resistance. This expression vector is stably integrated into the genome of the cells with the help of the Flp recombinase via recombination at the FRT site. This procedure destroys the zeocin resistance gene. For selecting stably transfected cells, T-REx2 selection medium was used. For obtaining this T-REx2 medium, Dulbecco`s Modified Eagle Medium (DMEM)-high glucose (4500 mg/l glucose) was supplemented with 10% fetal calf serum (FCS), 100 U/ml Penicillin, 100 µg/ml Streptomycin, 15 µg/ml Blasticidin, 100 µg/ml Hyg and 1 mM sodium pyruvate. The GOI expression could be activated by adding 3 µg/ml TC and since rhodopsins need their chromophore, which cannot be provided by the cells themselves, 1 µM ATR had to be added in addition.

The hybrid NG108-15 cell line derived from murine neuroblastoma- (N18TG-2) and glioma cells from a rat (C6BU-1) (Klee and Nirenberg, 1974). This cell line was grown in DMEM – high glucose (4500 mg/l glucose) medium supplemented with 10% FCS, 100 U/ml Penicillin, 100 µg/ml Streptomycin and 1 mM sodium pyruvate (in the following termed DMEM+) and was used for transient transfection and performing patch-clamp experiments in this work. Moreover, NG108-15 cells were used for optogenetic experiments here, since these cells can develop neuronal morphology and function under specific circumstances and can replace primary neurons in many experiments. Necessary for the differentiation process are high levels of cyclic adenosine

monophosphate (cAMP) in the cells. This was achieved via the cell-permeable cAMP analogue dibutyryl cAMP (bt_2cAMP) acting as differentiation inducer, Forskolin, which activates the adenylyl cyclase and 3-Isobutyl-1-Methylxanthine (IBMX) that is an inhibitor of cAMP and cyclic guanosine monophosphate (cGMP) phosphodiesterase. (Chad and Wheal, 1991; Bergsbaken, Sommers and Law, 1993; Tojima *et al.*, 2000).

3.1.1.2 Rhodopsin-DNA-Constructs

HEK Flp-In™ T-REx™-293 cell lines stably transfected as well as NG108-15 cells for transient transfection were used for conducting patch-clamp experiments. The GOI investigated in this work are listed in Table 2. The "2.0"-motif was already explained in chapter 2.1.2.

Table 2: Rhodopsin Constructs and their Expression System. The GOI that are used in this work as well as the respective mammalian heterologous expression systems are listed. Note that here,only in the case of lr-eyfp (blue), the rhodopsin LR (Mac) from *L. maculans* is meant, not the lr (lucy rho) motif.

Expression system	Rhodopsin construct (GOI)
Stably transfected HEK Flp-In cell line	Um*ops1*-eYFP
	Um*ops2*-eYFP
	Ap*ops1*-eYFP
	Ap*ops2*-eYFP
	chr2-eYFP
Transient transfection in NG108-15 cell line	Um*ops1*-eYFP
	Um*ops2*-eYFP
	Um*ops1*(D225E)-eYFP
	Um*ops1*(E129D)-eYFP
	Ap*ops1*-eYFP
	Ap*ops2*-eYFP
	Ap*ops1* 2.0-eYFP (lr-ap*ops1*-TT-eYFP-E)
	Ap*ops2* 2.0-eYFP (lr-*apops2*-TT-eYFP-E)
	Ap*ops3* 2.0-eYFP (lr-ap*ops3*-TT-eYFP-E)
	Ap*ops2* 2.0(F79A,R112H)-eYFP (lr-ap*ops2*-TT-eYFP-E)
	lr-eYFP (*mac*-eYFP)
	earch3.0-eYFP

Um*ops1* and Um*ops2* (Brych *et al.*, 2016) as well as Ap*ops1*, Ap*ops2* and Ap*ops3* (Cene Gostinčar, Nina Gunde Cimerman Lab, Biotechnical faculty, Ljubljana) constructs were obtained from cDNA as described before (Panzer *et al.*, 2019, 2021); Um*ops1* mutants were produced via site directed mutagenesis as stated later in this chapter. Improved versions Ap*ops1* 2.0, Ap*ops2* 2.0 and Ap*ops3* 2.0 as well as the Ap*ops2* 2.0 (F79A,R112H) channel mutant were produced as described before (Panzer *et al.*, 2021) and were kindly provided by Chong Zhang and Jing Yu-Strzelczyk.

3.1.1.1 Culture Conditions

Thawing and Freezing, Cell passage

As mentioned above, the following culture media were used: T-REx2 for stably transfected cell lines, DMEM+ for NG 108-15 cell line.

All mammalian cell lines were stored as cryo stocks in liquid nitrogen. For thawing, a cryo vial was placed on ice. 9 ml preheated (37°) DMEM+ were added to a new culture flask (Nunc™ EasYFlask™ 25 cm² Nunclon™ Delta Surface, Thermo Scientific) and the cryogenic vial was placed under the clean bench. 500 µl warm DMEM+ were added from the flask onto the cells to thaw them by slow pipetting. 500 µl thawed suspension were transferred to the flask. These steps were repeated until the complete cell pellet was thawed and transferred to the flask. The flask then was stored in an incubator (HERAcell, Heraeus, Thermo Fisher Scientific; Binder CB210, Binder) at 37 °C with 5 % carbon dioxide (CO_2) and about 96% air humidity. After 2-3 h, the complete medium was exchanged. Cells were grown until a confluence of 70-90%, then they were passaged using appropriate dilutions. In terms of the stable cell lines, the DMEM+ was exchanged to T-REx2 medium after two successful passages. NG108-15 cell line was passaged three times a week (total volume of culture: 10 ml; dilutions: Monday 3 ml cell suspension + 7 ml medium, Wednesday 2 ml cell suspension + 8 ml medium and Friday 0.75 ml cell suspension in 9.25 ml medium); stable HEK cell lines were passaged twice a week (total volume of culture: 5 ml; dilutions: Monday 0.25 ml cell suspension + 4.75 ml medium and Friday 0.5 ml cell suspension + 4.5 ml medium). For passage, cells were washed with 10 ml 1xPhosphate buffered saline (PBS) (37°C) and detached from the flask bottom using 250 µl Accutase (room temperature, RT) (NG 108-15 cell line) or 250 µl Trypsin-ethylenediaminetetraacetic acid (EDTA) solution (0.05 g/l trypsin, 0.02 g/l EDTA in Hank`s Balanced Salt Solution (HBSS), 37°C) (stable HEK cell lines), respectively. The appropriate volume of medium was added to a new culture flask; the cells were separated mechanically by pipetting. The respective volumes of cell suspension were added to the new culture flask, previous flasks were kept as backup. For freezing, cells were seeded into a large flask (Cellstar® Tissue Culture Flasks, non-pyrogenic, 250 ml, 75 cm², Greiner Bio-One) during cell passage (total volume of culture: 15 ml). Cells were grown to a confluence of 70-90%, then the medium was removed and 3 ml DMEM were added. The cells were detached from the bottom manually using a spatula, 2.4 ml FCS and 600 µl dimethyl sulfoxide (DMSO) were added and labelled cryogenic vials (Cryo.s™, 1 ml, Greiner Bio-One) were filled with the cell suspension (1 ml each). The vials were stored at least 12 h at -80°C in a precooled (-20°C) isopropanol rack and then transferred to the liquid nitrogen.

Coating of glass surfaces

Glass surfaces that were used in this work were 1- and 8-well tissue chambers (ibidi µ-slide glass bottom; Lab-Tek®II Chambered #1.5 German Coverglass System, Nunc, Thermo Fisher Scientific; 8-well on cover glass II, Sarstedt; Cellvis C8-1.5H-N 8 chambered coverglass system) and cover slips (Microscope cover glasses 12 mm, Paul Marienfeld GmbH & Co. KG). Poly-D-lysine (PDL)-coating was carried out as follows: The glass surface was treated with 0.5 M NaOH for 3 h or with 1 M KOH for 20 min. Then the surface was washed with ddH_2O or 1xPBS three

times. This step was skipped when using ibidi cell culture chambers. 0.1 mg/ml PDL (dissolved in ddH_2O) was added to the surface for at least 1 h, then the surface was again washed three times with ddH_2O or 1xPBS. Surfaces were stored at 4°C until use.

Site Directed Mutagenesis

UmOps1(D225E)-eYFP and UmOps1(E129D)-eYFP mutants were obtained via site directed mutagenesis. In short, primers (Table 3) were designed with the help of SnapGene® 4.1.9 and Bioedit Sequence Alignment Editor and obtained from Merck KGaA (Darmstadt, Germany). Gradient polymerase chain reaction (PCR) was performed and the product size was checked by agarose gel electrophoresis. When the PCR was successful, the product was Dpn1-digested and competent *E. coli* XL-1 Blue cells (produced by Jan Schlegel and Stephan Deimel of our working group) were transformed. Liquid *E. coli* cultures were inoculated with the appropriate colonies and Mini- or Midiprep was performed (NucleoSpin® Plasmid, NucleoBond® Xtra EF plasmid purification; Macherey Nagel).

Table 3: Primers Used for Site Directed Mutagenesis. Primers are listed which were used to produce UmOps1(D225E) and UmOps1(E129D) mutants. Mutation sites are highlighted in blue.

Rhodopsin	Mutation	Primer (mutation site)
UmOps1-eYFP	E129D	Fwd: cctgctcctcgacatcctgcttg Rev: caagcaggatgtcgaggagcagg
UmOps1-eYFP	D225E	Fwd: ggtctcgccgagggtagcaacacaatttcg Rev: cgaaattgtgttgctacctcggcgagacc

Differentiation of NG108-15 cells

NG108-15 cells were seeded in DMEM+ onto PDL coated 12 mm coverslips (10^4 cells/ml) during cell passage in a 4-well plate (Nunclon™ Delta Surface, Thermo Fisher Scientific) and incubated for 2-12 h. Then, the medium was removed, the cells washed once with preheated (37°C) DMEM and 400-800 µl preequilibrated (at 37°C and 5% CO_2 for 2-4 h) differentiation medium was added. The differentiation medium contained 1:1 Neurobasalmedium and DMEM, supplemented with 0.05x N2 supplements, 50 µM bt_2cAMP, 0.5 µM Forskolin and 25 µM IBMX. The cells were incubated for 7-10 days, the medium was never changed. Then, transient transfection and/or patch-clamp experiments were performed. For microscopic experiments, the cells were differentiated in an ibidi chamber. Here, 400 µl differentiation medium were added, the general procedure was the same.

Transient Transfection

Transient transfection was carried out on NG108-15 cells using Lipofectamine2000 reagent. In short, for a well of a 6-well plate (Nunclon™ Delta Surface, Thermo Fisher Scientific) the

procedure was as follows: Cells were grown in the well until a confluency of 30-40% was reached. 200 µl DMEM were mixed with 4 µl Lipofectamine2000 in an Eppendorf vial, in an additional vial 200 µl DMEM were mixed with 2 µg DNA. The vials were vortexed and spun down. Then the two liquids were pooled, vortexed and spun down. This transfection mix was incubated for 15 min at RT. The medium was removed from the cells, they were washed once with preheated (37°C) DMEM and 900 µl preheated DMEM were added. Then the transfection mix was added to the well dropwise. The cells were incubated at 37°C and 5% CO_2 for 6 h, then 2 ml DMEM+ and 1 µM ATR were added for providing the chromophore. The cells could be used for further experiments (microscopy or patch-clamp) after 12-24 h. For transfection in a Labtek, Sarstedt, Cellvis or ibidi 8-well chamber, all volumes were divided by 5, for transfection in a 4- or 24-well-plate the volumes were divided by 4.

Preparation for Staining and Microscopic Experiments

For staining and microscopic experiments, cells were seeded into PDL-coated 8-well culture chambers at a density of $5x10^4$ – $1x10^5$ cells/ml during cell passage using the appropriate medium. If necessary, the rhodopsin expression was initiated with 3 µg/ml TC, for providing the chromophore, 1 µM ATR was added. After the cells were incubated for 12-24 h at 37°C and 5% CO_2, imaging or staining could be performed.

Preparation for Patch-clamp Experiments

For patch-clamp experiments on stably expressing HEK cell lines, cells were seeded onto PDL-coated coverslips during cell passage using the appropriate medium. Rhodopsin expression was initiated using 3 µg/ml TC, for providing the chromophore, 1 µM ATR was added. Cells were incubated 12-24 h, then patch-clamp experiments could be performed. For measuring transiently expressing NG108-15 cells, cells were seeded into a 6-well plate during cell-passage at a density of $3x10^5$ cells/ml and transient transfection was carried out. After incubation times, the cells were checked for correct expression at the fluorescence microscope. The cells were mechanically detached from the surface by pipetting and placed on 12-mm coverslips (No PDL in this case!) in a 24-well-plate. Patch-clamp experiments could be carried out directly after this step for a timeframe of about 4 h.

3.1.2 Fungal Cell Culture

3.1.2.1 Strains and Culture Conditions

U. maydis

The *U. maydis* strains used in this work derived from the wild type isolate FB1 (Banuett and Herskowitz, 1989). All constitutive rhodopsin-FP expressing strains as well as the arabinose inducible strains with or without deletion of the native genes, respectively were produced and kindly provided by the Alfred-Batschauer working group from the university of Marburg. The procedure is described in detail before (Panzer *et al.*, 2019). In short, rhodopsin-eGFP fusion

constructs were integrated (single or multiple integrations) into the ip-locus either under the control of constitutive expressing petef promoter (via pETEF-GFP-MXN; p1742 plasmid) or under control of the arabinose inducible pCrg promoter (via pCRG-GFP-MXN; p1747 plasmid). The native genes were either intact or deleted resulting in Carboxin (Cbx) or additional Hyg resistance, respectively. For microscopic experiments, the strains listed in Table 4 were used.

All strains were stored as cryo stocks at -80°C. For thawing and establishing a master plate, 5 µl from the cryo stock were plated on potato dextrose agar (PDA, 39 g/l) and sporidia were grown for 1-3 days at 28°C and 0.95 mW/cm² white light (Memmert IPP 110 Plus incubator). Then this plate was used for inoculating working plates for maximum one week. Working plates (also PDA) were inoculated from the master plate, incubated for 12-24 h and then used only one time for inoculation of liquid cultures. For liquid culture, 20-25 ml potato dextrose broth (PDB 24 g/l, brought to pH 5.6 with 5M NaOH) were inoculated from the working plate and incubated for 7-20 h at 28°C, 100 rpm. If necessary, 2 ml from the liquid culture were centrifuged, washed once with ddH_2O, centrifuged again, resuspended in 5 ml yeast nitrogen base (YNB) supplemented with 0.2% ammonium sulfate and 2% arabinose and incubated at 28°C and 100 rpm for 2.5-4.5 h for rhodopsin-eGFP expression. For generating cryo stocks, 19 ml of an uninduced liquid culture were centrifuged, washed once with ddH_2O, centrifuged again and resuspended in 5 ml fresh 0.5xPDB pH 5.6 supplemented with 35% Glycerol 4 g/l peptone; 0.5 g/l yeast extract and 2.5 g/l sucrose. Cryo vials were each filled with 1 ml of the suspension and directly transferred into liquid nitrogen. After 5 min, the cryo stocks were placed to the -80°C freezer.

Table 4: *U. maydis* strains Used in Microscopic Experiments. For investigation UmOps1, only arabinose induced strains with or without deletion of the native gene and with single or multiple integrations were used. For imaging UmOps2, in addition, constitutive expressing strains were available. (Cbx: Carboxin; Hyg: Hygromycin)

Rhodopsin + FP	Expression	Deletion of the native gene	Number of integrations in ip-locus	Promoter	Resistance	Strain denotation
UmOps1-eGFP	Arabinose inducible	no	multiple	pCrg	Cbx	UmOps1-eGFP KA
	Arabinose inducible	yes	single	pCrg	Cbx, Hyg	ΔUmOps1 UmOps1-eGFP K1
UmOps2-eGFP	Arabinose inducible	yes	multiple	pCrg	Cbx, Hyg	ΔUmOps2 UmOps2-eGFP KB
	Arabinose inducible	No	multiple	pCrg	Cbx	UmOps2-eGFP K1
	Arabinose inducible	No	multiple	pCrg	Cbx	UmOps2-eGFP K7
	Constitutive	Yes	multiple	pOtef	Cbx, Hyg	ΔUmOps2 UmOps2-eGFP K1
	Constitutive	yes	single	pOtef	Cbx, Hyg	ΔUmOps2 UmOps2-eGFP K9

F. fujikuroi

The *F. fujikuroi* strain (T3S2 CarS1) used here was produced from the T3S2 (Transformation 3 Strain 2) strain (García-Martínez *et al.*, 2015) by Jorge Garcìa-Martìnez via UV-mutagenesis (Avalos, Casadesús and Cerdá-Olmedo, 1985). It expresses carotenoids as well as the CarO-eYFP fusion

protein independently of light and was used before (Sputh, 2020; Sputh *et al.*, 2021) (strain denotation CarO::eYFP). The cryo stocks were stored at -80°C. For thawing, a vial was transferred on ice and a DG plate was inoculated under sterile conditions with the help of a toothpick (5 inoculation sites per plate). DG medium consists of 16 g/l agar; 4 g/l NH_4Cl, 1 g/l $MgSO_4$*7 H_2O, 1 g/l KCl; 60 g/l D-glucose and 4 ml/l microelement solution (0.005 g/l H_3BO_3; 0.1 g/l $FeCl_3$; 0.05 g/l $CuSO_4$; 1 g/l $ZnSO_4$; 0.01 g/l $MnCl_2$ and 0.01 g/l MoO_4Na in ddH_2O (Avalos, Casadesús and Cerdá-Olmedo, 1985)). For liquid DG the agar was skipped. The fungus was grown for 3-6 days at 28°C and 0.95 mW/cm² white light until conidia were produced. For harvesting conidia, 10 ml ddH_2O were added to the plate and the spores were scraped with the help of a Drigalski spatula. Conidia were separated from hyphae using a Robu™ glass filter (porosity 1) and were collected on ice. The conidia suspension was centrifuged, washed once with ddH_2O and resuspended in either ddH_2O for proceeding with experiments or in 20% Glycerol in ddH_2O for creating new cryo stocks. Cryo vials were each filled with 300-500 ml of the suspension and directly transferred into liquid nitrogen. After 5 min, the cryo stocks were placed to the -80°C freezer.

3.1.2.2 Preparation for Experiments

Protoplastation of U. maydis Sporidia

A liquid culture was prepared and the rhodopsin expression was activated as described in chapter 3.1.2.1. The suspension was centrifuged, the supernatant was discarded and the pellet resuspended in 1 ml 1 M Sorbitol. Then the suspension was again centrifuged, the supernatant was discarded and the pellet was resuspended in 1:5 diluted (in 0.7 M NaCl) LCD-enzyme solution (0.2 g Lysing enzyme from Trichoderma; 0.001 g Chitinase and 0.5 g Driselase in 20 ml 0.7 M NaCl). The sporidia were then incubated for 20-45 min on a pivoting plate at RT. The progress of protoplastation was traced microscopically. When the cell wall was digested in most of the sporidia, protoplastation progress was stopped by adding the sporidia suspension into 10 ml ice-cold 1 M Sorbitol. The suspension was centrifuged, the supernatant was discarded and the pellet resuspended in 1 ml 1 M Sorbitol. 500 µl of the cell suspension were added into an 8-well culture chamber-well and microscopic images were recorded using either the CLSM or the SIM.

Preparation for Staining and Microscopy

For studying *U. maydis* sporidia, a liquid culture was prepared and if necessary, the rhodopsin expression was activated as described in chapter 3.1.2.1. The suspension was centrifuged and the pellet was washed once with ddH_2O. Then, the suspension was centrifuged again, the supernatant was discarded and the pellet resuspended in ddH_2O. For rhodopsin-localization studies, the sporidia were placed in PDL-coated 8-well culture chambers at a density of 6.5×10^5 sporidia/ml; for expansion microscopy, sporidia were placed on PDL-coated coverslips (diameter 12 mm). In both cases, the sporidia adhered on the surface for 30 min, then the staining and microscopic protocol or the expansion protocol was carried out.

Also, for CLEM experiments a liquid culture was prepared and the rhodopsin expression was activated as described in chapter 3.1.2.1. Here the following strains were used: FB1 wild type, FB1 delUmOps1 pCrg::UmOps1-eGFP K1 and FB1 pCrg::UmOps2-eGFP K7. The suspension was

centrifuged and the pellet washed once with ddH_2O. The suspension was centrifuged again, the supernatant was discarded and the pellet resuspended in 50 µl 100% FCS or 20% bovine serum albumin (BSA), respectively. Then the samples were high-pressure frozen. For a detailed description of the high-pressure freezing and freeze substitution process see the master thesis from S. Sputh (establishment and optimization of the process for *F. fujikuroi* hyphae; the steps were equally carried out for *U. maydis* sporidia) (Sputh, 2020). For both, *F. fujikuroi* and *U. maydis* samples, 100% FCS or 20% BSA were used as filler and LR-White or Epon used as resin.

For conventional fluorescence microscopy on *F. fujikuroi*, conidia dissolved in ddH_2O were seeded into a PDL-coated 8-well culture chamber. For imaging conidia, they were seeded at a density of 6.5×10^5 conidia/ml and settled down for 30 min; then staining could be carried out. For imaging hyphae, 5×10^3 – 1 x 10^4 conidia were seeded into one well of the 8-well culture chamber (PDL-coated). The germination time was 18 h at 28°C and 0.95 mW/cm² white light, then staining could be carried out.

3.2 Microscopic Experiments

3.2.1 Staining of Cellular Compartments in Fungal Cells

The following dyes were used for staining compartments in *U. maydis* sporidia as well as in *F. fujikuroi* conidia and hyphae (Table 5). All dyes were obtained from Thermo Fisher Scientific.

Table 5: Dyes Used in Microscopic Experiments with *U. maydis* and *F. fujikuroi*. SYTO 59 labels nucleic acids, pHrodoRED acidic regions, Mitotracker Orange accumulates in mitochondria, ER-Tracker RED stains the endoplasmic reticulum and FM4-64 is used to identify the plasma membrane and later the tonoplasts. EGFP and eYFP are FPs that are fused to the rhodopsins. The excitation (Ex) as well as the emission (Em) wavelengths are listed.

Dye/FP	Max. Ex/Em [nm]	Specification and labelling
SYTO 59	622/645	Cell permeant; live cell imaging; Stains Nucleic acids (Nucleus; in yeasts: Mitochondria)
pHrodoRED	560/585	Cell permeant; live cell imaging; Higher fluorescence in acidic regions
Mitotracker Orange	554/576	Cell permeant; live cell imaging; Stains mitochondria
ER-Tracker Red	587/615	Cell permeant; live cell imaging; Stains endoplasmic reticulum
FM4-64	515/640	Cell permeant; live cell imaging; Stains the plasma membrane, then is internalized and transported to the tonoplasts in yeasts
eGFP	488/509	Fused to UmOps1 or UmOps2 in *U. maydis* sporidia
eYFP	514/527	Fused to CarO in *F. fujikuroi* conidia and hyphae

Nucleic acids were labelled with the help of SYTO™ 59 Red Fluorescent Nucleic Acid Stain (SYTO 59). This dye labels nuclei or – preferentially in yeast cells - mitochondria. For identification

of acidic regions, pHrodo™ Red succinimidyl ester (pHrodoRED, Powerload included) was used. When pH changes from neutral to acidic, the fluorescence of that dye increases, so it can be used to visualize vacuoles in fungal cells. FM™ 4-64 (N-(3-triethylammoniumpropyl)-4-(6-(4-(diethylamino) phenyl) hexatrienyl) pyridinium dibromide) (FM4-64) has a lipophilic moiety and therefore incorporates in lipid membranes, where the fluorescence is increased. First, the plasma membrane is stained, but over time, the dye is internalized and integrated into intracellular membranes (Fischer-Parton *et al.*, 2000). Therefore, this dye can be used to label vacuolar membranes, the tonoplasts in fungi. MitoTracker® Orange CMTMRos (Mitotracker Orange) was used to stain mitochondria. This is achieved by accumulation of the dye in dependence of the membrane potential of these organelles. ER-Tracker™ Red (BODIPY™ TR Glibenclamide) (ER-Tracker) labels the endoplasmic reticulum via the sulfonylurea receptors of potassium channels which are abundant in this cellular component. All dyes are cell permeant and can be used for imaging living cells.

SYTO 59 and pHrodoRED dyes were used simultaneously to label nucleic acids and acidic regions together with the eGFP- or eYFP-labeled rhodopsins in *U. maydis* sporidia and *F. fujikuroi* hyphae. Mitotracker Orange was used together with SYTO 59 to confirm labeling of mitochondria via SYTO 59 in yeast-like cells (*U. maydis* sporidia). The plasma membrane or the tonoplasts, respectively (FM4-64), were stained in *U. maydis* sporidia and *F. fujikuroi* conidia and the endoplasmic reticulum (ER-Tracker) were labeled in *U. maydis* sporidia to confirm accumulation of rhodopsin-eGFP constructs in the endoplasmic reticulum in selected strains. For one well of an 8-well culture chamber, 250 µl staining solution were used. After incubation in the staining solution, the sporidia, conidia or hyphae were washed two times with ddH_2O and imaged in 400 mOsm Sorbitol or ddH_2O, respectively. The staining solutions were prepared and the staining conditions were applied as follows:

- SYTO 59 and pHrodoRED: 5 µl/ml Powerload and 0.5 µl/ml PhrodoRED were added into an Eppendorf cup, then 1 ml ddH_2O was applied. After that, 1.25-2.5 µM SYTO 59 were added and the solution was mixed. The sporidia, conidia or hyphae were incubated in the staining solution at 28°C in the dark for 30 min.

- FM4-64: 8 µM FM4-64 in ddH_2O were used as staining solution. For plasma membrane localization, staining was performed on ice for 10 min in the dark, for tonoplast localization, the staining was carried out at 28°C for 30 min.

- Mitotracker Orange: Sporidia were incubated in 100 nM Mitotracker Orange in ddH_2O for 30 min at 28°C in the dark.

- ER-Tracker: Sporidia were incubated in 10 µM ER-Tracker in ddH_2O for 1 h at 28°C in the dark.

3.2.2 Microscopes and Settings

In this work, all imaging steps were performed at RT if not stated otherwise. All microscopes and optical elements are mounted on vibration cushioned tables to guarantee stable measuring conditions.

3.2.2.1 Confocal Laser Scanning Microscope

The CLSM (Zeiss LSM700; Carl Zeiss AG) contains 3 laser lines (488 nm: 10 mW, 555 nm: 10 mW, 639 nm: 5 mW) and the following objectives: 10x dry (10x/0.3 EC Plan-Neofluar; Carl Zeiss AG), 63x oil objective (Plan-Apochromat 63x/1.40 OilM27; Carl Zeiss AG), 63x water objective (C-Apochromat 63x/1.2 W Korr UV-VIS-IR; Carl Zeiss AG). Furthermore, an X-Cite lamp (X-Cite® 120Q, Excelitas Technologies Corp.) as well as different filters, mirrors, a beam splitter and a variable secondary dichroid are available. An incubator can be applied to the objective table if necessary to adjust temperature and air humidity. The system is controlled by the ZEN 2012 SP1 (black edition, 64 bit) Software. Two photomultiplier tubes function as detectors. With the help of a smart setup, the dye spectra can be chosen (if the appropriate dye was not found in the list, a dye with similar spectrum was chosen and the recording settings were adjusted manually). Moreover, always the setting "Best signal" was used (the channels were recorded not simultaneously, but shortly one after the other).

Before recording, X-Cite lamp was used in combination with the appropriate filter set to choose a convenient location for imaging. For recording fluorescence images of *U. maydis* sporidia and *F. fujikuroi* conidia, the 63x oil objective was used. For taking gel images in terms of ExM, the 63x water objective was chosen. Pixel dwell times ranged from 1.27 to 3.15 µs, laser powers were set to 2-50%. The pinhole was adjusted to 1 airy unit (AU) for each channel. Detector gain was set to 500-700 for all channels, bit depth to 16 bit, averaging number was 2 for fluorescence and 8 for transmission images with the laser scanning unidirectional in all cases. If not stated otherwise, frame size was always 1024x1024 pixels.

Images were further processed using Fiji Version ImageJ 1.50f (Schindelin *et al.*, 2012) and Zen 2012 Software, Zeiss.

3.2.2.2 Structured Illumination Microscope

The SIM setup consists of an inverse microscope (Carl Zeiss AG), which was internally reconstructed to Elyra S.1 SIM by applying an Elyra S.1 super resolution head where the grid illumination pattern is generated and the laser light is coupled in. Four laser lines (405 nm, 488 nm, 561 nm, 642 nm) and an X-Cite fluorescence lamp are available as well as a 10x dry (Plan-Apochromat) and a 63x oil objective (63x/1.4 Oil DIC M27). Different filter sets for the appropriate laser lines are present and in addition a quad band filter ("FSet77HE") to see all 4 channels simultaneously. The Z-position of the objective table is controlled by a Z-Piezo drive, the X- and Y-positions can be adjusted via a joystick (slow and fast mode possible). An incubator box is mounted to protect the user from the laser light, but also to minimize drift. If necessary, an additional small incubator can be applied directly to the objective table to hold temperature more precisely. A sCMOS camera, PCO Edge 5.5 with cooling system functions as detector. The system is controlled by the ZEN 2012 SP1 (black edition, 64 bit) Software. The grating can be switched between 3 and 5 rotations (3 are mostly used for fast bleaching dyes or for time series).

Before recording, X-Cite lamp was used in combination with the FSet77HE filter to choose a convenient location for imaging. For recording fluorescence images of *U. maydis* sporidia and *F. fujikuroi* conidia and hyphae as well as sections for CLEM technology, the 63x oil objective was

used. 5 rotations were recorded in combination with 5 phase shifts of the grid, so that 25 raw images could be processed to one final SIM image. Laser powers were set to 5-25%.

Images were further processed using Fiji Version ImageJ 1.50f (Schindelin *et al.*, 2012) and Zen 2012 Software, Zeiss.

3.2.3 Expansion Microscopy

U. maydis specific procedure

Sporidia were prepared as described in chapter 3.1.2.2. The sporidia were fixated with 2% formaldehyde (FA) + 0.5% GA or 4% FA + 0.25% GA, respectively for 15 min at RT in the dark. They were washed 2 times for 2 min with ddH_2O. Then the cell wall was digested with the help of LCD-enzyme solution, 1:5 diluted in 0.7 M NaCl. Since the sporidia could not be shaken freely in an Eppendorf cup here, different digestion times were tested: undigested, 30 min and 60 min digestion. After cell wall digestion, the fungal cells were washed 2 times with 1xPBS for 1-2 min each. At this time point, control images were taken to see whether the cells are in a sufficient condition to go on with the ExM protocol. For expansion, the sporidia were once more fixated with 0.25% GA in 1xPBS at RT in the dark for 10 min, then washed 2 times with 1xPBS for 1-2 min each. A humidity chamber for gelation was prepared and the monomer solution (10% 1xPBS, 2 M NaCl, 2.5% acrylamide, 0.15% N,N'-methylenebisacrylamide and 8.625% sodium acrylate in ddH_2O) was mixed with ammonium persulfate (APS, polymerization accelerator, 0.2% end concentration) and tetramethylethylenediamine (TEMED, polymerization starter, 0.2% end concentration) on ice. 75 µl of the liquid gel were dropped on parafilm in the humidity chamber and were immediately covered by the coverslip containing the sporidia, so that the sporidia are in the gel. The samples were incubated in the dark at RT overnight. The next day, the gels were cut for orientation and transferred into a 12-well-plate. The cells were homogenized with Proteinase K. Here, also different time points were tested: 30, 45 and 60 min. After that, the samples were expanded in a 15 ml petri dish filled with ddH_2O (the water was changed every 30 min until the gel is not more expanding). The samples were stored in water overnight, then CLSM images were taken with the help of a one-well tissue chamber coated with PDL.

Images were further processed using Fiji Version ImageJ 1.50f (Schindelin *et al.*, 2012) and Zen 2012 Software, Zeiss.

3.2.4 Correlative Light and Electron Microscopy

For *F. fujikuroi*, the procedure was described in detail by S. Sputh in his master thesis (Sputh, 2020). The preparation of the resin blocks containing *U. maydis* sporidia was carried out by reference to the protocol established for *F. fujikuroi*; for preparation of fungal cells see also chapter 3.1.2.2.

For a first check, whether the resin embedding works in general and to see the subcellular context, sporidia of *U. maydis* FB1 wild type were grown, high-pressure frozen in 100% FCS and embedded in Epon- or LR-White-resin. For performing CLEM experiments, strains FB1 ΔUmOps1 pCrg::UmOps1-eGFP K1 and FB1 pCrg::UmOps2-eGFP K7 were used. Briefly, the protocol was

as follows: LR-White blocks were cut into 100-200 nm slices with the help of an ultramicrotome. The sections were placed on objective slides and antibody labelling was performed. Therefore, the slices were surrounded by a PAP pen and 45-50 µl blocking solution (5% BSA, 0.05% Tween20, 50 mM Tris(hydroxymethyl)aminomethan (TRIS) pH 8.0 in ddH_2O) were added for 30 min. Then, the blocking solution was removed, and 45-50 µl primary antibody solution was applied to the sections (mouse anti GFP IgG monoclonal antibody clones 7.1 and 13.1; final concentration 4-5 µg/ml in blocking solution). The sections were incubated at RT for 1 h in the dark, then washed 2-3 times with blocking solution (2-5 min each). Optionally, an additional washing step (2 min with 0.05% Tween20 and 50 mM TRIS pH 8.0 in ddH_2O) was carried out. After that, the secondary antibody was applied (45-50 µl) for 60 min at RT, incubation took place in the dark (secondary antibody: goat anti mouse x Alexa647 IgG (H+L); final concentration 5 µg/ml). The sections were washed 3 times with 0.05% Tween20 and 50 mM TRIS pH8.0 in ddH_2O for 2-5 min each, then the antibodies were fixated with 2% FA + 0.2% GA in 1xPBS or ddH_2O for 15 min at RT in the dark. The sections were washed 1-2 times with HBSS or ddH_2O for 5 min, then the cell walls were stained with Calcofluor (500 µl/ml in HBSS) for 10 min at RT in the dark. The sections were washed 2 times with HBSS or ddH_2O (5 min each) and finally mounted in VectaShield® Antifade Mounting Medium with a 60x24 mm coverslip. Then fluorescence images were taken. As controls, only the secondary antibody was used as well as an isotype (Isotype mouse IgG_1; final concentration 5 µg/ml) that replaced the primary antibody.

After successful fluorescence imaging, contrasting of the samples took place. First, the VectaShield mounting medium was removed with the help of 1xPBS, then the objective slide was cut with a diamond pen to the appropriate size. 2.5% uranyl acetate were added to the sections for 15 min at RT. The slide was washed by dipping 12 times into a vial filled with 100% EtOH. The same procedure (12x dipping) was done in 50% EtOH (in previously boiled ddH_2O) and then in 100% preboiled ddH_2O. Then, the slide was placed near some NaOH tablets on Parafilm, 50% lead citrate (in preboiled ddH_2O) was added to the sections and everything was covered with a petri dish for 10 min. The slide was washed 2 times in 100% preboiled ddH_2O by dipping 12 times in each vial, then the sections were air-dried for 30 min. The slide was sticked to a SEM sample plate and the edges were covered with conduct silver (connection to the sample plate necessary!). Finally, the slide was coated with a 2.5-3 nm carbon film by vaporizing (Safematic CCU-010). After that, SEM images were taken. Images were correlated using Inkscape and GIMP softwares.

3.3 Patch-Clamp Experiments

3.3.1 The Patch-Clamp Setup

An overview of the patch-clamp setup is depicted in Figure 10. On a vibration cushioned table (Micro-g®, TMC Technical Manufacturing Corp.), an inverse microscope (Zeiss Axiovert 200M, Carl Zeiss AG) is mounted. It is equipped with three objectives (LD Plan-Neofluar 63x/0.75 ∞/0-1.5; Plan-Neofluar 10x/0.30; Achrostigmat 40x/0.55; Carl Zeiss AG) and a camera (Zyla sCMOS, Andor Technology Ltd.). Near the objective table, the head stage (CV 203BU Head stage, Axon

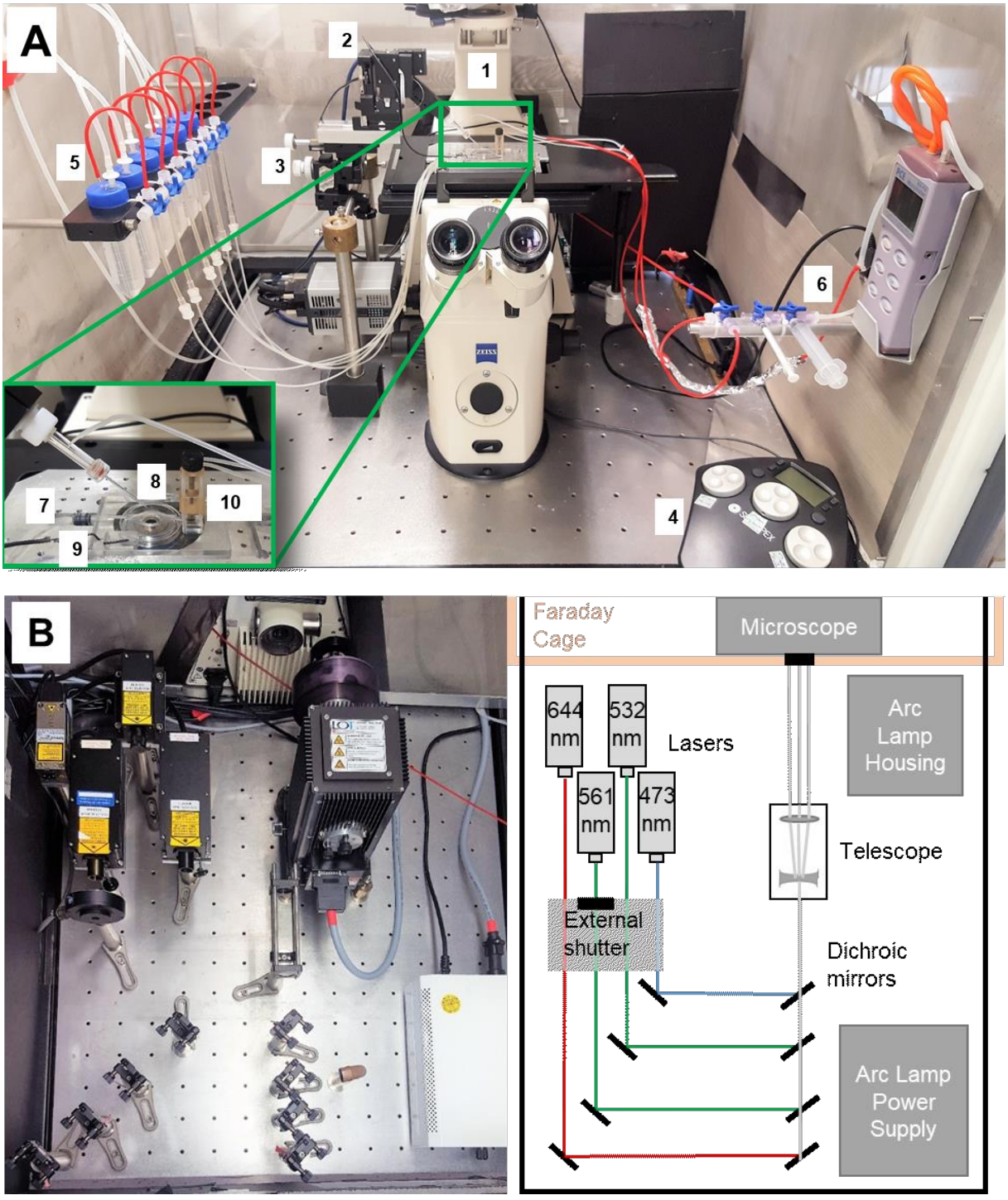

Figure 10: Composition of the Patch-clamp Setup. All components are positioned on a vibration cushioned table. **A:** Inside the Faraday cage, an inverse microscope (1), the head stage (2) with coarse (3) and fine (4) drive as well as the hose (5) and air pressure (6) systems are constructed. Insert: The perfusion chamber consists of a solution input (7) and output (10) as well as a chamber for the reference electrode (9). The micropipette can be positioned in the main chamber (8). **B:** The optical elements can be found behind the Faraday cage. Four laser lines, an external shutter and an arc lamp are available. The laser light is transported via several dichroic mirrors and a telescope. Adapted from (Panzer, 2017)

Instruments, Molecular Devices) is fixed containing the preamplifier, the reference electrode and a port for attaching the pipette holder. A coarse drive or a fine drive (SMX Micromanipulator, Sensapex), the latter via connection to a micromanipulator can move the head stage to adjust the position of the micropipette. At the pipette holder the micropipette which is filled with an electrolyte (pipette solution) can be fixed so that an electrode comes into connection with the pipette solution. Moreover, the pipette holder is connected to an air pressure system, what is necessary for sealing the cell or perform the breakthrough. The cell is sealed using slight negative pressure, that is applied with the help of a 1 ml syringe; the breakthrough can be done by stronger negative pressure using a 10 ml syringe. A manometer (PCE-P50, PCE Group) displays the current pressure. On the objective table, the perfusion chamber can be applied. It consists of a solution input, the main chamber, where the cells are placed, a solution output and a reference chamber. Maximum six 50 ml falcons containing the bath solutions are connected to the solution input via a hose system. The bath solutions can be inserted into the perfusion chamber using an air pressure system. The input is regulated via turncocks. At the chamber output, the bath solutions can be removed by a vacuum pump system (Vacuum gas pump, VWR International GmbH). The reference chamber is always filled with 150 mM KCl solution and the reference electrode coming from the head stage is fixed there. The reference and the main chamber are connected via a 2% agarose (in 150 mM KCl) salt bridge to achieve a closed current circuit. All compounds described so far are surrounded by a Faraday cage and are electrically coupled to it. The Faraday cage itself is grounded, what is necessary to reduce noise or other disturbing signals.

Outside and behind the Faraday cage, but also on the vibration cushioned table, the optical elements are mounted. Four laser lines (473 nm: 100 mW; 532 nm: 150 mW; 561 nm: 150 mW; 644 nm: 200 mW) and an arc lamp (LSH102 Lamp Housing with 50-150 W Universal Arc Lamp Power Supply LSN 150/2, LOT-QuantumDesign GmbH) are available. The laser beams are transported via mirrors (total reflective or dichroic) to the microscope. There they are again reflected by an appropriate dichroic mirror; they then pass the appropriate filter and are passing out through the objective. If necessary, the arc lamp can be placed directly behind the microscope so that the light beam can enter and pass out through the objectives. The 532 nm laser was later connected to an optic fiber (Fiber cable, MM, 400 µm, 0.39NA, SMA to 2.5 mm Ferrule; Fiber end: Fiber Optic Cannula, 400 µm, 0.39NA, 10 mm long; Thorlabs) to carry the light directly to the perfusion chamber (implementation of optic fiber is described in detail in chapter 3.3.2). The measuring settings in terms of laser light transportation that are used in the appropriate experiments are stated directly in the result section.

The patch-clamp setup furthermore consists of an amplifier (Axopatch 200B, Axon Instruments, Molecular Devices) with connection to the preamplifier, an AD converter (Digidata 1440A, Axon CNS, Molecular Devices) and a computer system. The amplifier provides an additional way for generating the breakthrough, that is the "Zap"-function. Here, a short (0.5 ms) electrical pulse is given to the cell, so that the membrane ruptures inside the opening of the micropipette tip. The software used for measuring is Clampex 10.7. With the help of the software, the lasers can be triggered via the digital outputs of the AD converter. Moreover, an external shutter (Uniblitz Model VCM-D1 Shutter Driver, Vincent Associates) is available to control light passing, the arc lamp

contains an integrated shutter (LSZ161/2/450 26C, LOT-QuantumDesign GmbH). Both shutters can also be controlled via the Clampex software.

3.3.2 Implementation of the Optic Fiber

An optic fiber was implemented into the optical system of the patch-clamp setup to transport the laser light directly to the perfusion chamber and hence, to the cell. Therefore, the external shutter was placed in front of the 532 nm laser, additionally a holder for neutral density (ND) filters and then the optic fiber (Figure 11A). The optic fiber goes into the Faraday cage to the microscope where the fiber end was fixed near the perfusion chamber (Figure 11B), equipped with a manipulator for adjusting the position. This array allows the cells being placed directly in front of the optic fiber end (400 µm diameter) what guarantees a homogeneous illumination of the cellular surface (Figure 11C).

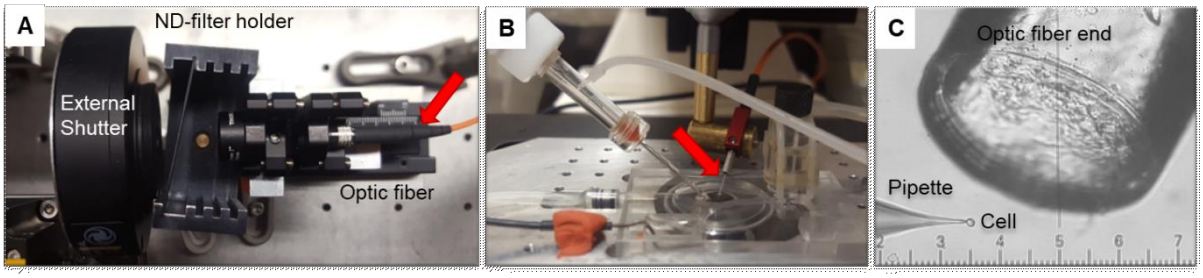

Figure 11: Implementation of the Optic Fiber into the Laser Beam Path of the Patch-clamp Setup. A: The external shutter was placed in front of the 532 nm laser (laser not depicted). Behind the external shutter, a holder for ND filters and then the monopod with the optic fiber (red arrow) was fixed. **B**: The optic fiber goes into the Faraday cage and is fixed near the perfusion chamber (red arrow: fiber end) where it can be positioned manually inside the main chamber. **C**: Inside the main chamber a patched cell can be positioned right in front of the optic fiber end to guarantee homogeneous illumination at the cellular membrane. (1 scale part = 90 µm)

Since the 532 nm laser is diode pumped (diode pumped solid state laser, DPSS laser), the laser output may not be stable in all settings. Thus, the measuring conditions were optimized. The light intensity that is emitted by the laser in comparison with the intensity that is emitted by the coupled optic fiber were measured to find stable laser output ranges and to test the coupling efficiency. It was found that that only by adjusting the output to 35% the laser begins to emit light. Moreover, the emittance is not always linear (Figure 12A). The coupling efficiency is rather high, but also fluctuates (Figure 12B). For stable measuring conditions the laser has to be used in its linear range, while yielding not too high intensities. Therefor again intensity measurements in the output range of 40-60% were performed six times and it could be shown that between 40 and 50% the laser emits linearly and also, the coupling efficiency is relatively stable (Figure 12C, D). The conditions for doing patch-clamp measurements were therefore set to 41% laser output, what resembles an intensity of 84 mW/mm² at the optic fiber end. Since rhodopsin activities are usually measured at lower intensities or only very rarely at higher ones (Nagel *et al.*, 2003; Chow *et al.*, 2010; Fudim *et al.*, 2019), ND filters had to be implemented. The intensities that were reached at the fiber end by using different combinations of ND filters, form a range from 0.02 and 84 mW/mm² output

(Table 6). These filter combinations were used to check the light intensity dependence of different rhodopsins. With the help of this intensity measurements, it was possible to see in which intensity range good current signals from the rhodopsins were reached while they were not yet in a saturation level (see chapter 4.3.1). Thus, other measurements on rhodopsins were taken at an output of around 15 mW/mm² at the optical fiber end (ND filter combination 70.8 + 25). It is stated directly in the result section which measurements were taken using the optical fiber system. Another important point is, that the cell has to lie in the middle directly in front of the optic fiber end to yield homogeneous illumination as well as optimal measuring conditions (Figure 11C).

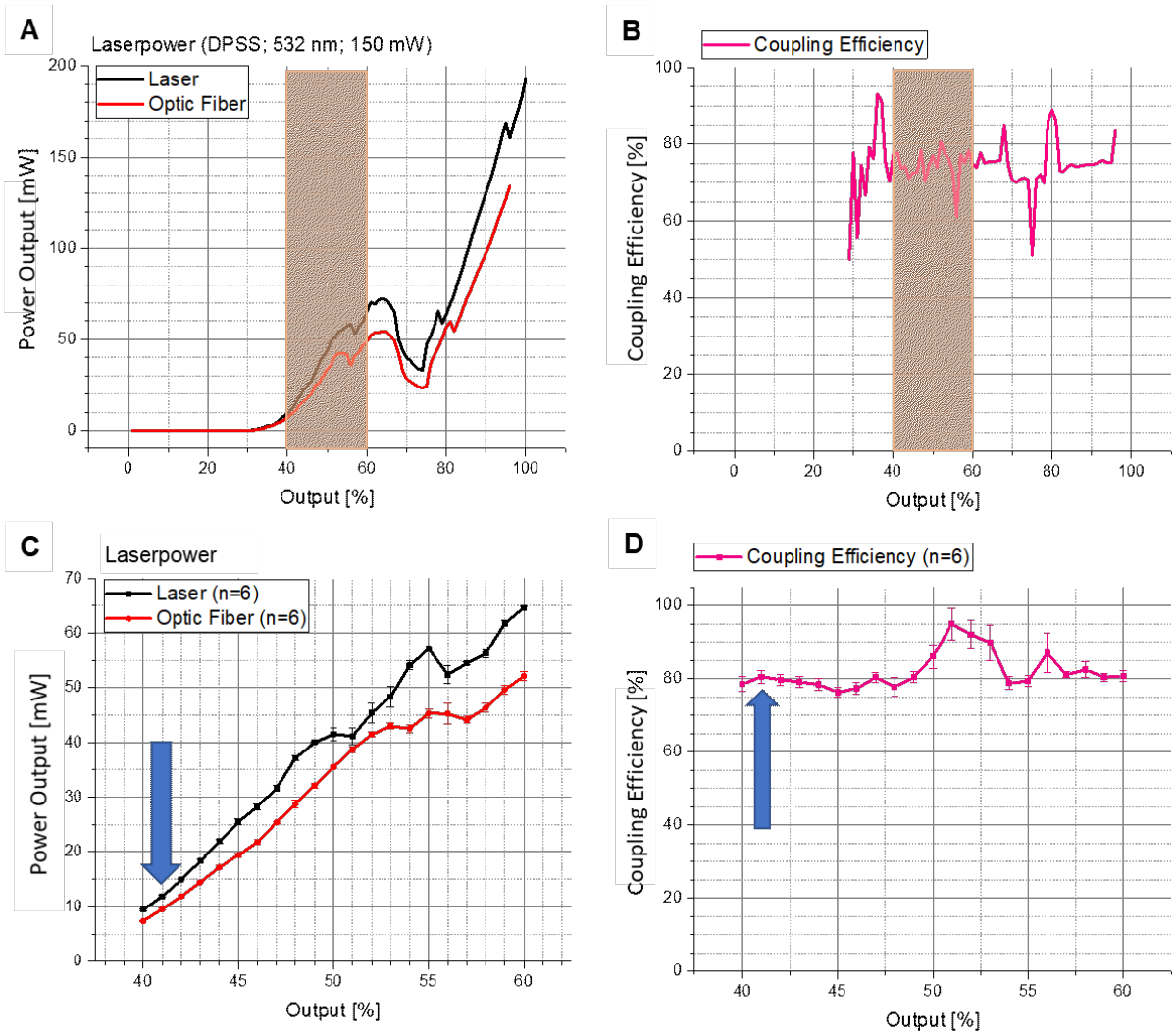

Figure 12: Optimization of Laser Settings for Patch-clamp Measurements Using the Optic Fiber. The 532 nm DPSS laser begins to emit light at 35% output and shows its most stable conditions in a range between 40 and 50% output (**A, C**). The coupling efficiency is in general rather high and shows stable conditions between 40 and 45% output (**B, D**). Therefore, for measuring, the laser output was set to 41% (blue arrows).

Table 6: ND Filter Combinations and the Corresponding Light intensity at the Optic Fiber End. The intensity of the 532 nm laser was decreased to around 15 mW/mm² with the help of ND filters 70.8 and 25. This condition was used to carry out measurements on rhodopsins. Exceptions are the intensity measurements of rhodopsins. Here, the full range of filter combination was used.

ND Filters	Intensity at the optic fiber end [mW/mm^2]	SEM	% Transmission
1+2.5	0.02	0.00	0.02
10+5	0.32	0.00	0.43
1	0.80	0.00	0.88
2.5	1.96	0.03	2.16
70.8+5	2.39	0.00	3.20
5	3.98	0.00	4.39
70.8+10	4.78	0.00	5.59
10	7.96	0.00	8.78
50+25	10.35	0.00	12.12
70.8+25	**14.59**	**0.27**	**17.08**
25	22.55	0.27	24.87
70.8+50	28.13	0.27	32.92
50	44.05	0.27	48.55
70.8	62.35	0.53	68.73
without	83.91	2.43	100.00

3.3.3 Electrodes and Micropipettes

The electrodes of the patch-clamp system (reference and micropipette electrode) are made from silver/silver chloride (Ag/AgCl). They are electrodes of the second type that is here a silver wire covered with silver chloride. These electrodes show a constant electrode potential and do not interact with the bath or pipette solution; they are not polarizable. Both electrodes were chlorinated regularly for 2-5 min using 3 M KCl at 1.7 V. The micropipettes were prepared right before the experiment and were pulled from glass capillaries (GB150F-8P, Science Products) with the help of a vertical puller (Narishige Model PC-10, Narishige Co. Ltd.) in two steps (61.2 °C and 48.3°C). They showed tip resistances of 2-10 MΩ.

3.3.4 Experimental Settings

Except stated otherwise, all experiments on the patch-clamp setup were carried out in a dark room at RT. The output gain at the amplifier was set to 1, low pass Bessel filter to 5 kHz. For measuring, the cells were detached from the cover slip (except differentiated NG108-15 cells) to avoid unstirred layers; the measuring mode was whole-cell in all cases. Depending on the experiment, the appropriate bath solutions were chosen. Table 7 gives an overview of the composition of all bath- and pipette solutions.

Data were analyzed with ClampFit 10.7 software, Excel, Origin Pro 2016 64Bit and Origin 2021b. Mean and standard deviation of the values obtained from different cells were calculated. For investigation of the rhodopsin properties, in all measurements the voltage-clamp mode (V-Clamp)

was used. For doing experiments on differentiated NG108-15 cells in terms of measuring action potentials, the current-clamp mode (I-Clamp Normal) was used. The bath- and pipette solutions that were used for the appropriate experiments are stated in the result section when the appropriate measurements are described. Current densities were calculated with the help of the whole-cell capacitance determined with the ClampFit 10.7 software; significance was analyzed using an unpaired t-test. By using ClampFit, also the current decay kinetics after light-off were analyzed by fitting the current decay after light-off by means of a biexponential fit using Levenberg-Marquardt search method. Detailed information on how time constants were obtained for the single rhodopsins is given directly in the result section.

Table 7: Compositions of Bath- and Pipette Solutions Used in Patch-Clamp Measurements. Amounts of chemicals are listed in mM for all pipette and bath solutions used in this work. NG diff=differentiated NG108-15 cells (For chemicals see list of abbreviations)

Quantities [mM]	NaCl	CsCl	KCl	NaGluc	KGluc	$NaAc*3H_2O$	EGTA	$MgCl_2*6H_2O$	MgGluc	$Mg(Ac)_2*4H_2O$	$CaCl_2*2H_2O$	$Ca(OH)_2$	$Ca(Ac)_2$	MES	HEPES	TRIS	Glucose	pH adjustment
Pipette (263-276 mosm/kg)																		
NaCl pH 5.0	**110**						**10**	**2**						**10**				HCl/NaOH
NaCl pH 7.4	**110**						**10**	**2**							**10**			HCl/NaOH
CsCl pH 5.0		**110**					**10**	**2**						**10**				HCl/TRIS
NaAc pH 7.4						**110**	**10**			**2**					**10**			Acetic acid/ NaOH
NG diff. KGluc pH 7.2					**130**		**10**	**2**							**15**			HCl/KOH
Bath (269-298 mosm/kg)																		
NaCl pH 5.0	**140**							**2**			**2**			**10**				HCl/NaOH
NaCl pH 7.4	**140**							**2**			**2**				**10**			HCl/NaOH
NaCl pH 9.0	**140**							**2**			**2**					**10**		HCl/NaOH
NaGluc pH 5.0				**140**					**2**			**2**		**10**				Gluconic acid/ NaOH
NaGluc pH 7.4				**140**					**2**			**2**			**10**			Gluconic acid/ NaOH
NaGluc pH 9.0				**140**					**2**			**2**				**10**		Gluconic acid/ NaOH
NaAc pH 5.0						**140**				**2**			**2**	**10**				Acetic acid/ NaOH
NaAc pH 7.4						**140**				**2**			**2**		**10**			Acetic acid/ NaOH
NG diff. NaCl pH 7.4	**140**		**3.5**					**2**			**2**				**10**		**10**	HCl/NaOH
Reference			**150**															

3.3.4.1 Action Spectra

Action spectra were recorded using the arc lamp mounted with appropriate filters (LOT Oriel, Andovor Corp.) in combination with neutral density filters (Andover Corp. Optical Filter, LOT-QuantumDesign GmbH) to find the optimal excitation wavelength of the rhodopsins. Photon densitiy was 2×10^{16} photons s^{-1} mm^{-2} (García-Martínez et al., 2015). The applied wavelengths and filters are listed in Table 8. The wavelengths were applied from the blue to the red spectral range and reverse. 3-6 cells were measured for each direction. The cells were illuminated for 100-300 ms at 0 mV clamp-voltage; 3 or 10 runs were averaged for each wavelength. NaCl based solutions were used for bath and pipette. For analysis, the current values were normalized to the value obtained at 532 nm. Mean and standard deviation were plotted over the wavelengths and data were always fitted using the Spline function. Measuring conditions are specified directly in the result section.

Table 8: List of Wavelengths and ND filters used for Action Spectra Measurements. The listed wavelengths were generated using appropriate filters in combination with ND filters which were applied to the arc lamp.

Wavelength [nm]	ND Filters	Wavelength [nm]	ND Filters
400	-	532	0.10/0.15
420	-	560	0.10/0.15
450	0.15	580	0.15/0.20
470	0.10/0.15	600	0.15/0.20
490	0.30	620	0.10/0.15
510	0.10/0.15	640	0.30

3.3.4.2 Intensity Measurements

For investigating the intensity dependence of the different rhodopsins, the light was either applied to the cells via the optic fiber using different sets of ND filters (see Table 6) or – in case of Channelrhodopsin-2 – using the conventional beam path through the objective for the application of 473 nm light. For measuring pump rhodopsins as well as Channelrhodopsin-2, 3 runs were averaged for each light intensity. The pump rhodopsins were illuminated with the 532 nm laser for 100 ms per run and the voltage was clamped to 0 mV. In case of Channelrhodopsin-2, the voltage was clamped to -60 mV, the illumination time was 500 ms using the 473 nm laser. Bath- and pipette solution always was NaCl pH 7.4. The obtained current values were normalized to the value measured at 84 mW/mm^2.

3.3.4.3 Step Protocols

The step protocols were used to perform measurements on the rhodopsins in different environments. Therefor different clamp-voltages reaching, if not stated otherwise, from +40 mV to -120 mV (20 mV steps) were applied to the cells, yielding 9 current traces per run (also termed sweeps). For each condition, 3 runs (consisting of 9 sweeps each) were averaged; the illumination time was 100 ms using the 532 nm laser. If the conventional beam path or the optic fiber was used, will be stated directly in the result section. Measurements always started in NaCl pH 7.4 bath solution. At first, this protocol was used to get information about the voltage dependency of the

rhodopsins; in a second step, the pH dependency was investigated. Therefor NaCl-based bath solutions with different pH values (7.4; 5.0 and 9.0) were applied to the cells. Pipette solutions were NaCl pH 7.4 or NaCl pH 5.0, respectively. To see, which ion species are transported by the rhodopsins, exclusion principle was used. Sodium ions were removed from the pipette solution by replacement of NaCl with CsCl. If the currents are not altered, it is most likely not sodium that is transported. On the extracellular side, chloride was substituted by gluconate to exclude chloride currents. Another topic that was investigated was the WOA-effect. Therefor NaCl-based bath- and pipette solutions with different pH values (pH 5.0 or pH 7.4) were supplemented with NaAc pH 5.0 or pH 7.4, respectively, using different concentrations. Detailed information of the used pipette solutions and the order of bath solutions is given directly in the plots in the result section. The obtained current values were normalized to the value obtained at 0 mV clamp voltage in bath solution NaCl pH 7.4. Current-voltage (I-V)-plots were generated with the clamp-voltage on the x-axis and the normalized current values on the y-axis.

3.3.4.4 Action Potential Protocol

The action potential protocol was used to test whether action potentials could be generated in differentiated NG108-15 cells and whether the ApOps2 rhodopsin can be functionally expressed in this experimental system. For measuring, a current ramp was applied that reaches a maximum level after a given time. During this maximum current-clamped level, the 532 nm laser is switched on for a specific duration. Different values for the maximum current level and the duration of the current ramp were tested. During the current ramp action potentials should occur, the functionality of the rhodopsin is tested by illumination with the laser.

4 Results

4.1 Localization of UmOps1, UmOps2 and CarO – A Microscopic Study

4.1.1 Localization Determination Using Conventional Super-resolution Fluorescence Microscopy

The localization of rhodopsins in fungal cells was investigated using CLSM and SIM. Microscopy was done on *U. maydis* sporidia expressing UmOps1-eGFP or UmOps2-eGFP, respectively; for *F. fujikuroi* imaging, conidia and hyphae expressing CarO-eYFP were imaged. In addition, counterstaining experiments were performed on different *U. maydis* strains as well as on *F. fujikuroi* CarO::eYFP to assign the rhodopsin site to specific cellular structures or compartments. SYTO 59 was used to label nucleic acids; pHrodoRED stains acidic compartments (in fungi the vacuolar lumen), Mitotracker Orange labels mitochondria, ER-Tracker is selective for the endoplasmic reticulum and FM4-64 is embedded in the plasma membrane or the tonoplasts depending on staining conditions. Specific experimental conditions are indicated directly in the figures.

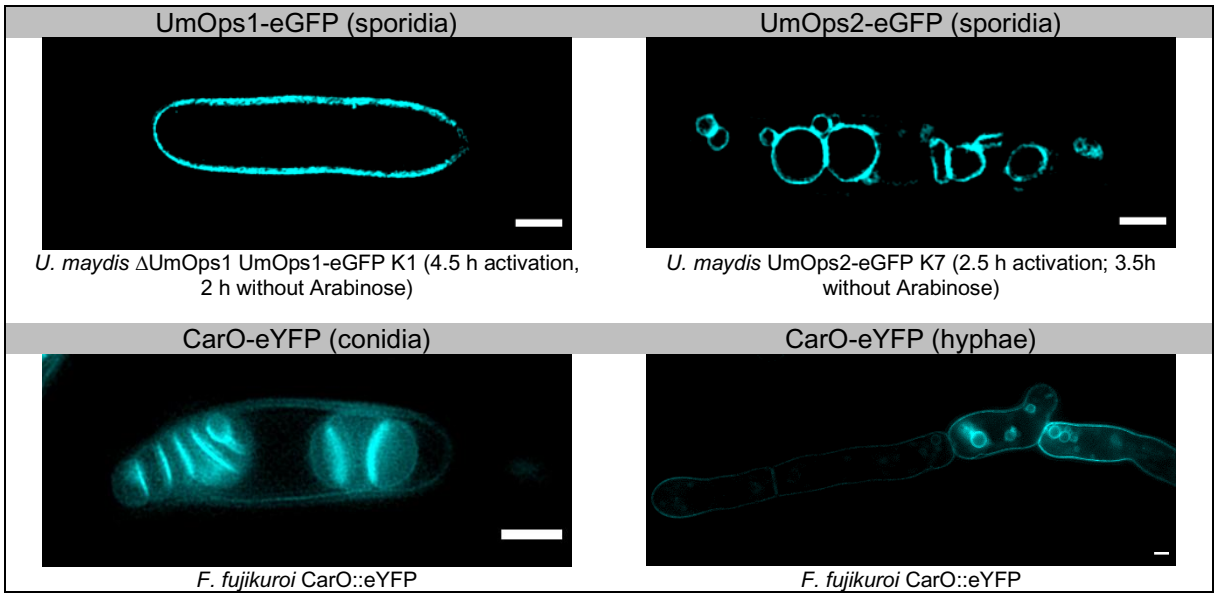

Figure 13: SIM Images of Rhodopsins. UmOps1 was localized in the plasma membrane whereas UmOps2 could be observed in spherical intracellular structures. The localization of CarO described previously (García-Martínez *et al.*, 2015) could be confirmed: This rhodopsin resided in the plasma membrane as well as in intracellular membrane systems in both, conidia and hyphae. CLSM and SIM images; scale bars: 2 µm

SIM images of *F. fujikuroi* conidia and hyphae expressing CarO-eYFP as well as *U. maydis* sporidia expressing UmOps1-eGFP or UmOps2-eGFP, respectively were recorded (Figure 13). UmOps1 was localized in the plasma membrane whereas UmOps2 resided in more or less spherical

structures inside the cell. The localization of CarO was previously described (García-Martínez *et al.*, 2015) and could be confirmed: CarO was present in the plasma membrane of conidia as well as of hyphae, but also fluorescence signals could be observed in intracellular membrane systems. In hyphae, there was a heterogeneous distribution of CarO in the plasma membrane, showing stronger signals at the former conidia region as it was stated before (García-Martínez *et al.*, 2015).

To identify the cellular structures and organelles, where the rhodopsins are located, counterstaining experiments were done. The fungal cells were treated with SYTO 59 and pHrodoRED to stain nucleic acids as well as acidic region (Figure 14 and Supplementary Figure 2). In all strains pHrodoRED could be observed in the vacuoles, since those organelles have a low pH. The vacuoles in *U. maydis* were spherical and different in size. However, in many cases there were two prominent vacuoles that were bigger compared to the others. In *F. fujikuroi* hyphae, a lower number of vacuoles was observed which were mainly big in size, smaller ones were detected not so often.

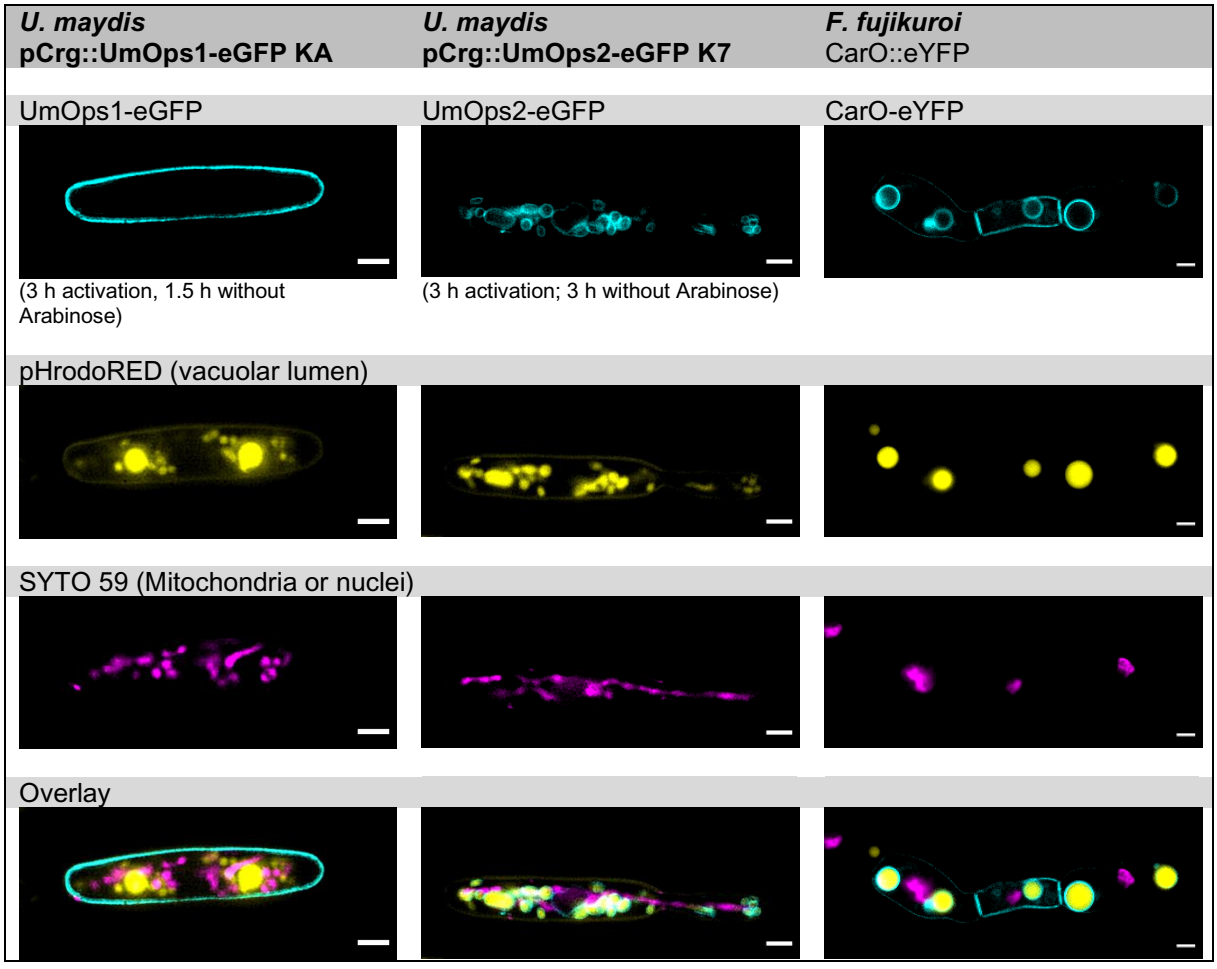

Figure 14: Counterstaining of Rhodopsins with SYTO 59 and pHrodoRED. PHrodoRED was observed in the vacuoles in all strains, SYTO 59 stains the nuclei in *F. fujikuroi* hyphae. In *U. maydis* sporidia, SYTO 59 labeled mitochondria. The intracellular fluorescence signals from UmOps2 as well as from CarO surrounded the vacuoles. SIM images; scale bars: 2 µm

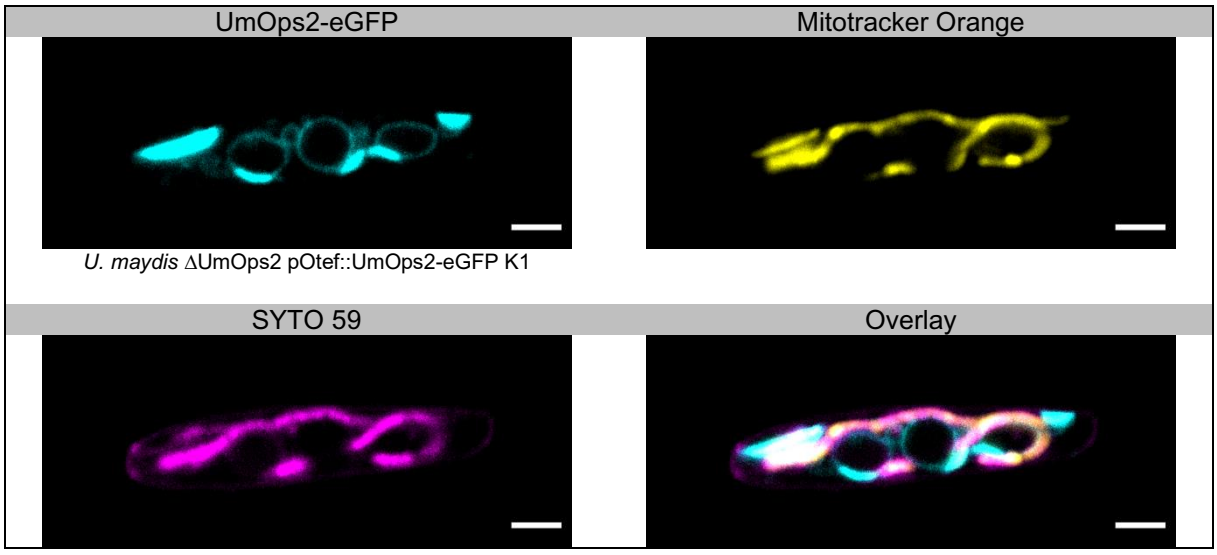

Figure 15: Counterstaining of SYTO 59 with Mitotracker Orange. SYTO 59 colocalized with Mitotracker Orange in *U. maydis* sporidia (here expressing UmOps2) what confirms that SYTO 59 labels preferentially mitochondria in yeast(-like) cells. No colocalization with the rhodopsin signals occurred. CLSM images; scale bars: 2 µm

SYTO 59 stained mitochondria in all *U. maydis* sporidia, what is typical for that dye in yeast cells (Molecular Probes). To confirm that, *U. maydis* sporidia expressing UmOps2-eGFP were counterstained with SYTO 59 and Mitotracker Orange (Figure 15). A clear colocalization for both dyes was observed, no colocalization with the UmOps2-eGFP signals occurred. The mitochondria in *U. maydis* were mostly filamentous structures, in some cases also short and oval. In contrast, in *F. fujikuroi*, the nuclei were stained by SYTO 59 (Figure 14). They showed a heterogenous fluorescence level and an irregular shape. CarO could again be observed in the plasma membrane and in intracellular structures. The intracellular fluorescence signals surrounded the vacuoles so that there is an indication for CarO to be localized in the tonoplast. No colocalization for CarO and the nuclei could be shown. In *U. maydis*, as stated before, UmOps1 was localized only in the plasma membrane and showed no colocalization with both dyes. UmOps2 surrounded the vacuoles, what may indicate a tonoplast localization like for CarO. In all cases, no colocalization with mitochondria was observed. However, in many strains which are expressing UmOps2-eGFP, the rhodopsin showed additional strong fluorescence signals inside the cell (Supplementary Figure 2). These could derive from extensive expression of the rhodopsin, so that the proteins get stuck in the endoplasmic reticulum and fluoresce there. This issue was checked with the help of ER-Tracker dye (Figure 16). The staining was done using *U. maydis* sporidia expressing UmOps2-eGFP and it was observed that the strongly fluorescent regions inside the cell deriving from eGFP colocalized with the ER-Tracker signals. That means, that the rhodopsins were overexpressed and could not be transported to the target region yet. The expression could be fine-tuned by adjusting the activation time with Arabinose when using the pCrg promoter as well as the time point of imaging after removing this sugar in a sufficient manner. To verify the vacuolar membrane localization of UmOps2 and CarO, staining was performed using FM4-64 dye as a tonoplast labelling dye (Figure 17). FM4-64 at first integrates in the plasma membrane when staining was performed on ice for 10 min. With time, the dye gets internalized and is trafficked to the tonoplasts.

This trafficking could be achieved faster by staining the fungal cells at 28°C for 30 min. Colocalization was observed for UmOps1-eGFP and FM4-64 in *U. maydis* sporidia when staining was performed on ice and the dye still resided in the plasma membrane. When FM4-64 was internalized and trafficked to the tonoplasts, no colocalization occurred. This result shows that UmOps1 is a rhodopsin that resides only in the plasma membrane. In contrast, UmOps2-eGFP showed colocalization with the dye when internalization was finished, so that it can be stated, that the final localization of UmOps2 is the vacuolar membrane system. For UmOps2-eGFP, no plasma membrane localization was observed. In *F.fujikuroi* conidia, also a colocalization of internalized FM4-64 with the intracellular structures exhibiting CarO-eYFP fluorescence could be shown. When stained on ice, fluorescence signals of FM4-64 as well as of CarO-eYFP in the plasma membrane were visible. These results confirm that the target structures of CarO are the tonoplasts as well as the plasma membrane as it was already assumed before (García-Martínez *et al.*, 2015).

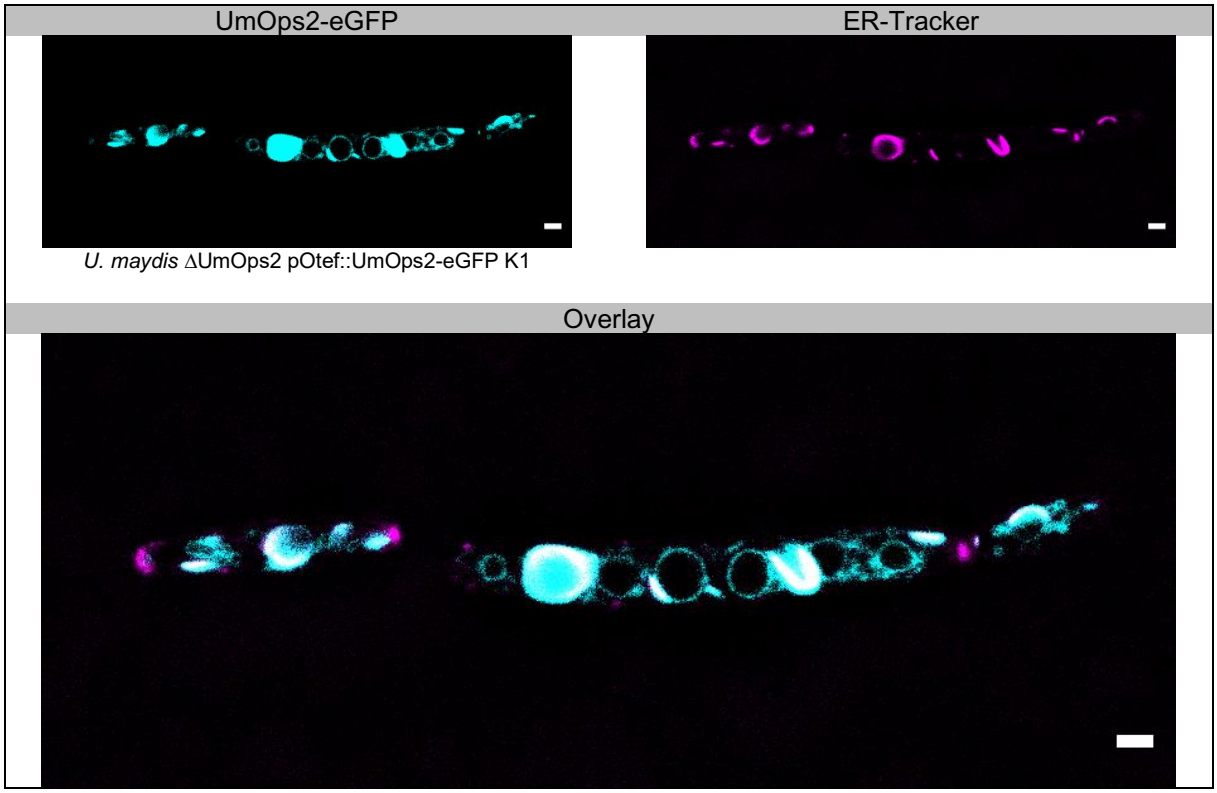

Figure 16: Counterstaining of UmOps2-eGFP with ER-Tracker. The strongly green fluorescent regions inside the cell colocalized with ER-Tracker signals what indicates a huge amount of UmOps2-eGFP still stuck in the endoplasmic reticulum. CLSM images; scale bars: 2 µm

As a next step, it was tested, whether novel super-resolution techniques like ExM or CLEM could be performed on fungi. Therefore, ExM and CLEM were tested on *U. maydis* sporidia. Regarding ExM, a protocol for the application in fungi was established; for doing CLEM, a protocol already established for *F. fujikuroi* hyphae expressing CarO-eYFP was used (Sputh, 2020). The results obtained for UmOps1- or UmOps2-eGFP expressing sporidia will be shown in comparison to the results from experiments using *F. fujikuroi* (Sputh, 2020).

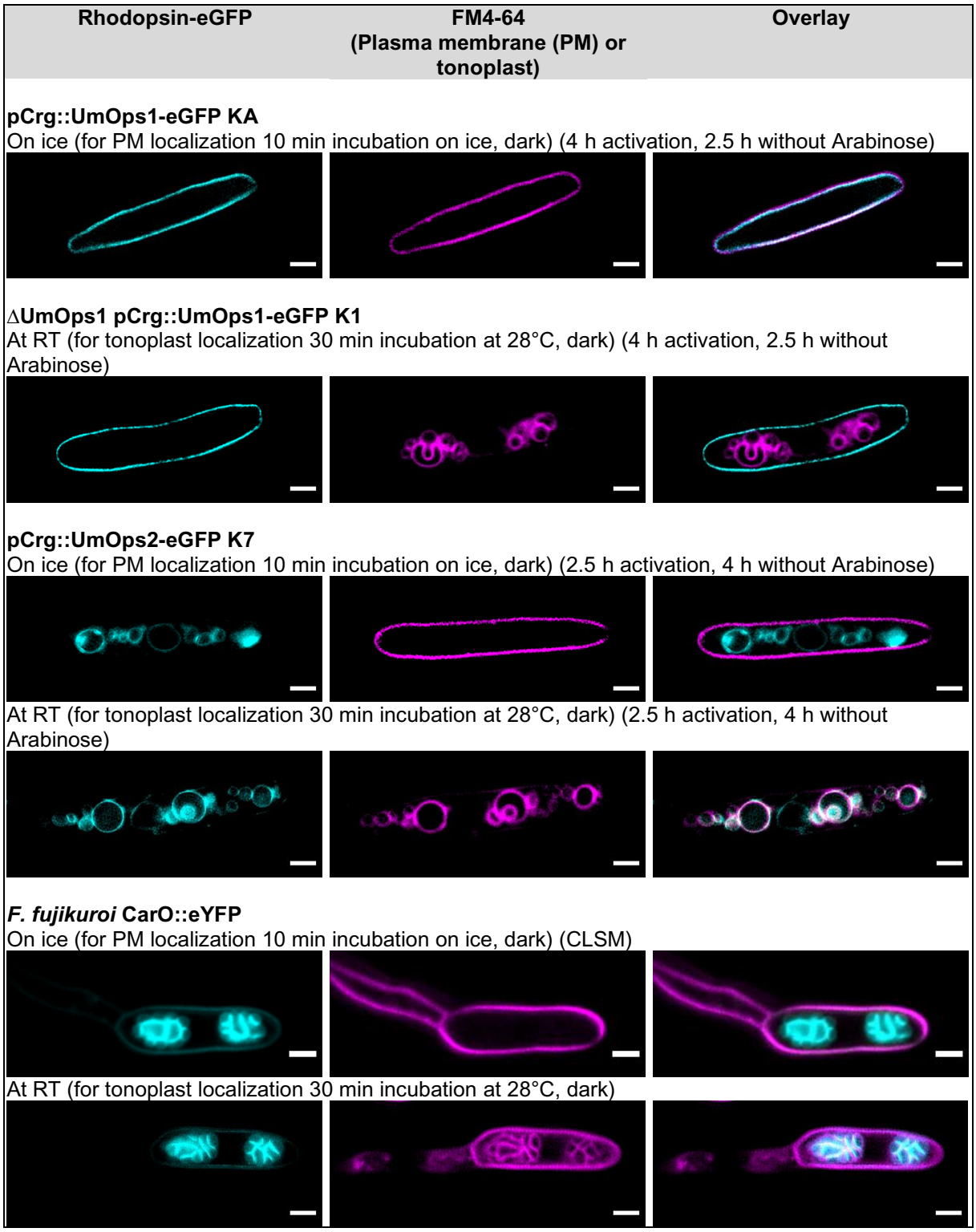

Figure 17: Counterstaining of Rhodopsins with FM4-64. When staining was performed on ice, FM4-64 labeled the plasma membrane and showed colocalization with UmOps1 and partially CarO. When stained at RT, FM4-64 was trafficked to the tonoplasts. There it colocalized with UmOps2 as well as partially CarO. If not stated otherwise: SIM images; scale bars: 2 µm

4.1.2 Depiction of Fluorescence-labeled Rhodopsins with the Help of Novel Microscopic Techniques

4.1.2.1 Expansion Microscopy

ExM was developed as a rather facile, but strikingly effective method to extend the range of techniques that allow for super resolution microscopy. The basic principle is the embedding of a fixated labelled sample in a polyacrylamide gel followed by homogenization of cellular components with Proteinase K. Then the gel is isotropically expanded and the cellular debris is washed out while the labels stay at their places due to crosslinking with the gel. Thus, the labels are expanded together with the gel and depict a larger image of the structure of interest. In this work, ExM was applied on *U. maydis* sporidia expressing UmOps1-eGFP.

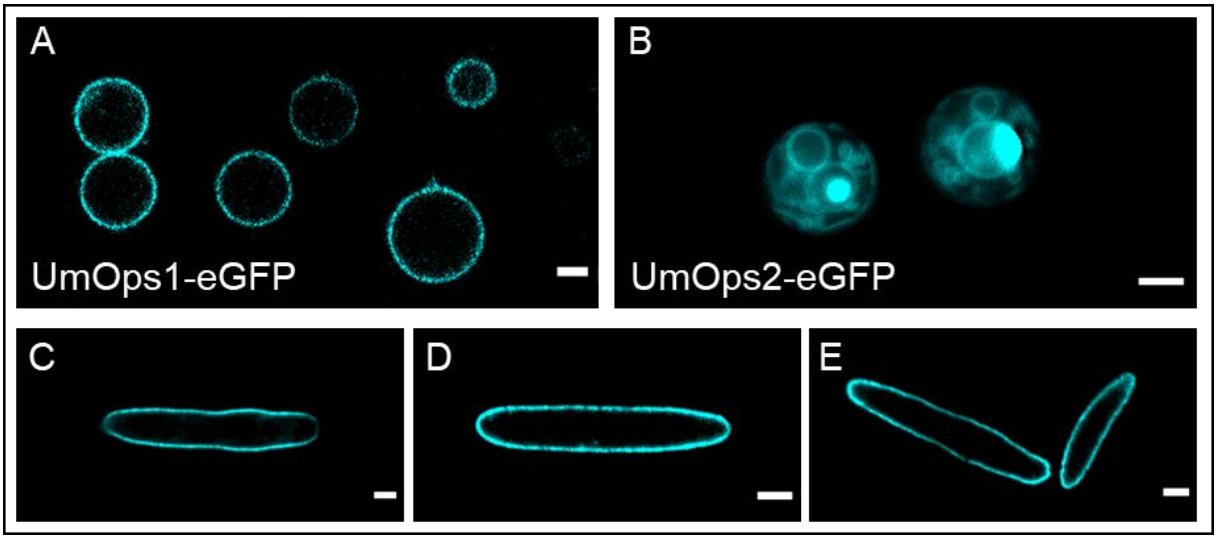

Figure 18: Protoplastation and Fixation of Rhodopsin-eGFP Expressing *U. maydis* sporidia. The cell wall of the sporidia was digested with the LCD-enzyme solution and resulted in spherical protoplasts. Fluorescence signals deriving from UmOps1-eGFP or UmOps2-eGFP, respectively, were not impaired. UmOps1 still resided in the plasma membrane (**A**, CLSM), whereas UmOps2 was visible in the tonoplasts (**B**, SIM). In comparison to living cells (**C**, CLSM), fixation of the sporidia (**D**, CLSM) did not alter the fluorescence (here: UmOps1-eGFP). Additional cell wall digestion for 30 min had no negative effect on the shape or fluorescence signal (**E**, CLSM). Image D was published (Götz *et al.*, 2020). Scale bars: 2 µm

For applying ExM on fungi, it is very important to completely digest the cell wall before application of the ExM protocol to enable a sufficient isotropical expansion of the cells and cellular components after homogenization with Proteinase K. Thus, in a first step the protoplastation of live *U. maydis* sporidia was tested using an enzyme mix containing different enzymes for digesting cell wall components. The sporidia were shaken in the LCD enzyme mix for 20-45 min at RT and protoplastation was observed microscopically. The cell wall was first digested in the tip region, thus allowing the protoplast to emerge from the remaining wall components (Supplementary Figure 3A). In almost all sporidia the cell wall could be digested during this time, while the fluorescence of the rhodopsin-eGFP fusion constructs was not impaired (Figure 18A, B). Most of

the sporidia showed spherical shapes what means, that the plasma membrane was still intact, but the cell wall that usually determines the cigar-like shape of the sporidia, was digested and removed in a sufficient manner. When performing CLSM or SIM, UmOps1-eGFP still resided in the plasma membrane, whereas UmOps2 was located in the vacuolar membranes.

For further testing ExM on *U. maydis*, the UmOps1-eGFP expressing strain pCrg::UmOps1-eGFP KA was used. To retain the original shape of the sporidia, it was necessary to fixate the fungal cells before digesting the cell wall. Fixation as well as 30 min digestion after fixation did not alter the fluorescence of UmOps1-eGFP (Figure 18C, D, E). Next, on fixated sporidia, the LCD enzyme mix was used to test different duration times of cell wall digestion in terms of homogeneous expansion of the sporidia. Undigested sporidia as well as digested sporidia (30 min or 1 h) were gelated, homogenized and expanded. The undigested sample (Figure 19A) did not increase in size, indicating that the cell wall impairs the isotropical expansion of the cell. Moreover, intense autofluorescence is visible due to glutaraldehyde fixation. The 30 min digested sample showed non-autofluorescent expanded sporidia (Figure 19B) as well as unexpanded or partially expanded cells. When the cell wall was digested for 1 h, almost exclusively expanded sporidia could be observed. That means, that an incompletely digested cell wall impairs the isotropical expansion of fungal cells. For *U. maydis* sporidia, 1 h cell wall digestion was set to be sufficient to obtain good expansion results.

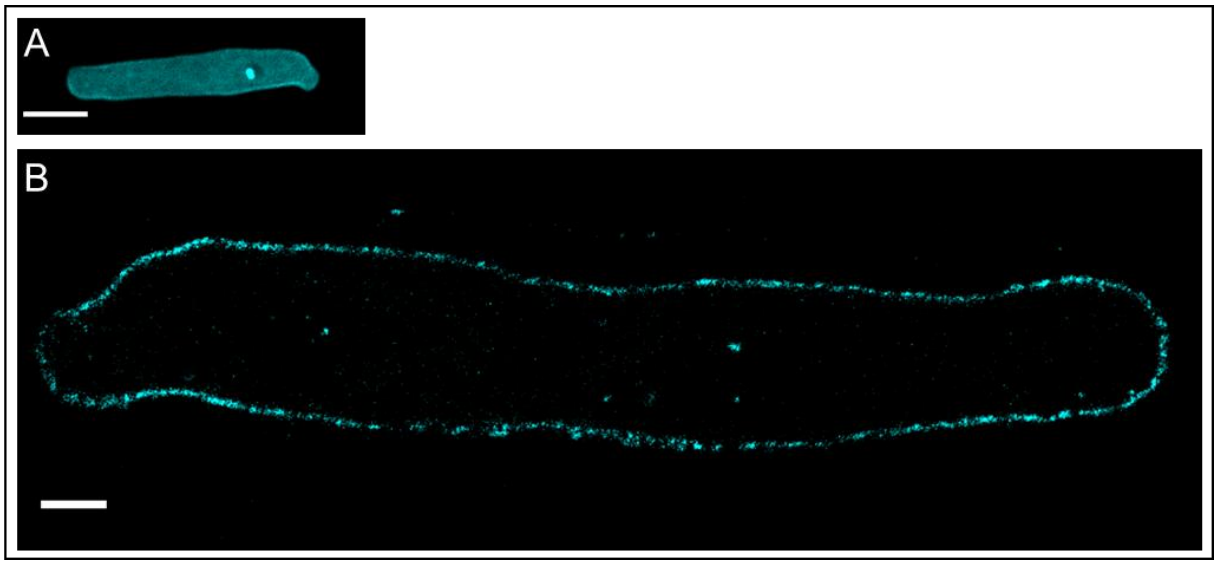

Figure 19: Expansion of UmOps1-eGFP Expressing *U. maydis* Sporidia. A: Sporidia did not expand when the cell wall was not digested. Moreover, huge autofluorescence deriving from glutaraldehyde fixation could be observed. **B:** Sufficient cell wall digestion and Proteinase K homogenization resulted in expansion of the fungal cells showing a more detailed view of the plasma membrane localized UmOps1. CLSM; scale bars: 5µm

Another critical step in the expansion protocol is the homogenization of the cellular components with Proteinase K. In this step, the fixated proteins of the cells are loosened in their cohesion while the fluorophores and some components are anchored in the polymer gel, so that during expansion, the remaining fluorophores are isotropically increasing their distance from one another. In the

U. maydis strain used here, the UmOps1 was labelled with an eGFP, what itself may be affected by Proteinase K. Thus, long exposure to this enzyme could reduce the fluorescence level in the expanded sample. For testing the cell wall digestion durations, the homogenization was carried out for 1 h. It was now examined whether increased fluorescence signal levels could be yielded, when lowering the homogenization duration from 1 h to 45 min or 30 min, respectively. At all durations similar fluorescence signals could be obtained (Supplementary Figure 3B, C, D) and since expansion worked well in all cases, 1 h was chosen as good duration for Proteinase K treatment in *U. maydis* sporidia. Furthermore, it could be clearly seen, that UmOps1 is present in the plasma membrane region, however the fluorescence signals show a spotty distribution.

The expansion factor was determined by measuring the diameter of unexpanded and expanded sporidia. Expanded cells showed a mean diameter of 12±1.8 µm (n=15) in comparison to 2.6±0.45 µm (n=46) in unexpanded sporidia, so that an expansion factor of 4.6 could be reached. This is in accordance with the values obtained with a lower number of measured sporidia published before (Götz *et al.*, 2020).

In general, it could be shown that by precise adjustment of the protocol, ExM could be successfully applied to fungal cells, here *U. maydis* sporidia expressing UmOps1-eGFP. Moreover, it could be shown that ExM is also applicable for imaging FPs, however, the homogenization time with Proteinase K must be carefully adapted and it has to be checked whether the FPs themselves are affected by this step. The most important difference to ExM standard protocols is the digestion of the fungal cell wall, that has to be implemented in the protocol after the fixation (and if necessary, labelling) steps to retain the native shape of the fungal cells (Figure 20).

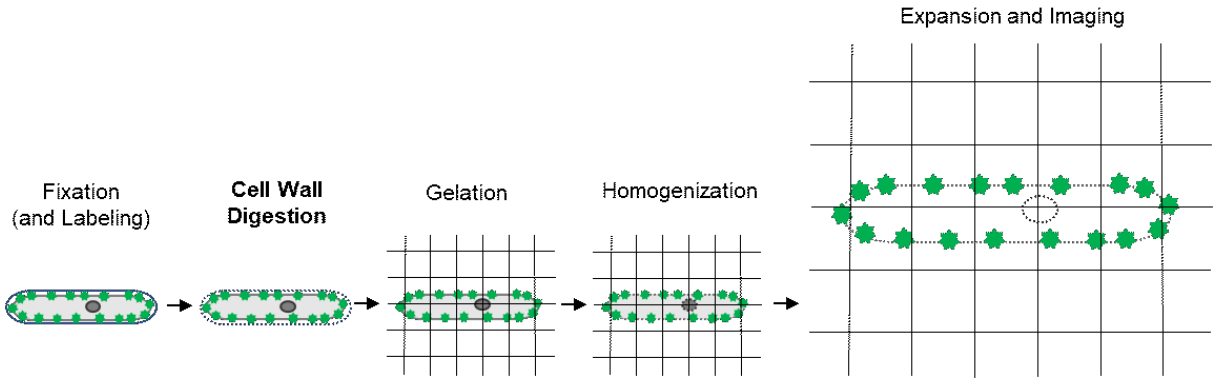

Figure 20: General Process of ExM in Fungi. The most important step that has to be implemented into the ExM standard protocol is the cell wall digestion which is necessary to obtain successful expansion. To maintain the original shape of fungal cells, they have to be fixated before the digestion step since the cell wall is the structure that determines the shape of fungi.

4.1.2.2 CLEM

Another super resolution technique that gained importance during the last decades is CLEM. This technique requires extensive preparation steps but allows for observing fluorescently labelled structures in the subcellular context. Concerning CLEM in fungi, this technique was successfully

applied in *F. fujikuroi* by S. Sputh by imaging the rhodopsin-FP construct CarO-eYFP in the subcellular environment of hyphae (Sputh, 2020). The attempt to apply CLEM to *U. maydis* sporidia will be briefly depicted here, partially in comparison to the results yielded for CarO (the image concerning CLEM in *F. fujikuroi* was recorded by S. Sputh and was kindly provided to be shown here). As a first step, *U. maydis* FB1 wild type sporidia as well as sporidia expressing UmOps1-eGFP (strain FB1 delUmOps1 pCrg::UmOps1-eGFP K1) or UmOps2-eGFP (strain FB1 pCrg::UmOps2-eGFP K7), respectively, were grown, high-pressure frozen in 100% FCS or 20% BSA, embedded in Epon or LR-White and cut into 100-200 nm sections. The sections of the FCS- and BSA-FB1 wild type samples (Epon and LR-White) were prepared and imaged on the TEM to see whether the embedding worked in general (Figure 21). In both resins, sporidia were embedded in a sufficient manner and subcellular structures could be observed (cell wall, nucleus, mitochondria, vacuoles, lipid bodies). The cell wall sometimes was not directly connected to the cell itself any more in both resins. In BSA, however, more often artifacts occurred (Figure 21C, red box) compared to FCS, thus, further experiments were carried out using FCS samples.

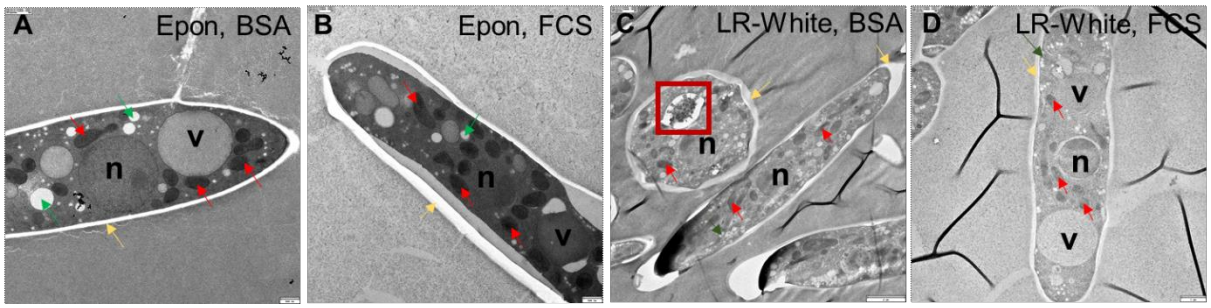

Figure 21: TEM images of *U. maydis* sporidia. FB1 wild type was embedded in Epon (**A, B**) or LR-White resin (**C, D**) using either FCS (**B, D**) or BSA (**A, C**) as filler. In all samples, the sporidia were embedded in the resin in a sufficient manner and subcellular structures like nuclei (n), vacuoles (v), mitochondria (red arrows), lipid bodies (green arrows) and the cell walls (yellow arrows) could be observed. In the BSA samples, however, sometimes artifacts (**C**, red box) occurred.

Sections of sporidia expressing UmOps1-eGFP frozen in 100% FCS and embedded in LR-White were stained with calcofluor to see whether the cell wall can be used as a mark for correlation. Calcofluor staining worked well; the cell walls were visible with no background (Figure 22A, E). When applying high laser powers, the autofluorescence of the sporidia could be observed in the 488 channel so one can see, that in some cases, the cell wall was ripped off the sporidia like it could already be seen in the TEM images (Supplementary Figure 4). In the 561 nm as well as in the 642 nm channel, no fluorescence signals were visible (data not shown). As a next step, in addition to the cell wall staining, sporidia expressing UmOps1-eGFP were treated with antibodies (isotype; primary antibody only; primary + secondary antibody; for details see chapter 3.2.4). When using the isotype or only the primary antibody, no fluorescence signals could be observed in the 642 nm channel (Supplementary Figure 5). When staining was carried out with the primary and secondary antibody, fluorescence signals could be detected in the plasma membrane region of the sporidia in some cases (Figure 22B, C), however, also unspecific labeling between the sporidia occurred on

but not besides the sections. Imaging was also done using the UmOps2-eGFP expressing strain. The signals deriving from the antibody staining were observed mainly inside the cells, what correlates with the tonoplast (and partially endoplasmic reticulum-) localization of UmOps2-eGFP (Figure 22F). Here, also a correlation image could be recorded (Figure 22G, H). Correlation of SIM and REM images could be done using the cell wall as a mark; antibody signals were, as already mentioned, visible inside the cell, but the tonoplast localization was not very clear. However, the antibody signals seemed to be localized near the nucleus what could derive from UmOps2-eGFP still stuck in the endoplasmic reticulum like it was observed before in some cases (Supplementary Figure 2). In summary, it could be shown that it is possible to perform CLEM on *U. maydis* in general; however, the protocol and especially the antibody staining still need optimization to gain sufficient results for explicit statements about the localization of UmOps1 and UmOps2 in the subcellular context. For *F. fujikuroi*, successful CLEM could be performed (Figure 22D) and even a 3D model could be produced from serial imaging of sections (Sputh, 2020; Sputh *et al.*, 2021).

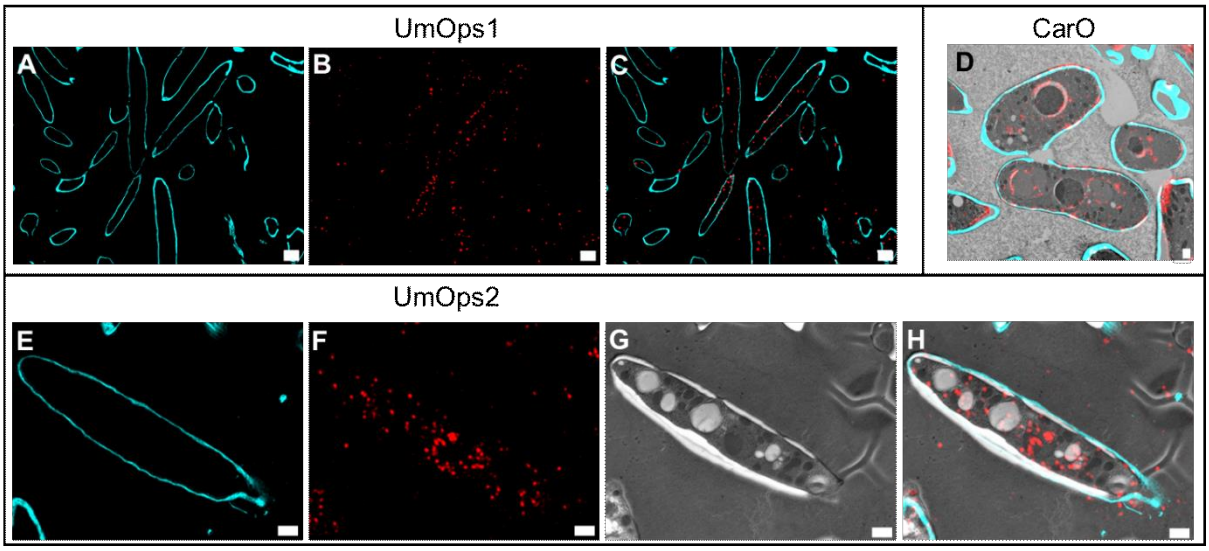

Figure 22: CLEM in *U. maydis* sporidia in comparison to *F. fujikuroi*. Calcofluor cell wall staining (**A, E**) was used as a mark to correlate fluorescence and EM images. Sporidia expressing UmOps1-eGFP (**A, B, C**) or UmOps2-eGFP (**E, F, G, H**) were antibody-stained against eGFP (**B, F**). For UmOps2-eGFP expressing sporidia, a correlation image could be obtained (**H**) using fluorescence (**E, F**) and EM (**G**) image. The CLEM protocol was successfully established before for *F. fujikuroi* hyphae to image CarO in the subcellular context (**D**). Image D was published (Sputh, 2020; Sputh *et al.*, 2021); scale bars: 1 µm

4.2 Exploring the Function of Fungal Rhodopsins – An Electrophysiological Study

4.2.1 Expression of Fungal Rhodopsins in Heterologous Mammalian Systems

The rhodopsin-eYFP constructs were analyzed either using stably expressing HEK293 cell lines or via transiently transfected NG108-15 cells. For performing patch-clamp measurements, a good plasma membrane localization is indispensable. To check this issue, CLSM images were taken from the different rhodopsin-eYFP constructs.

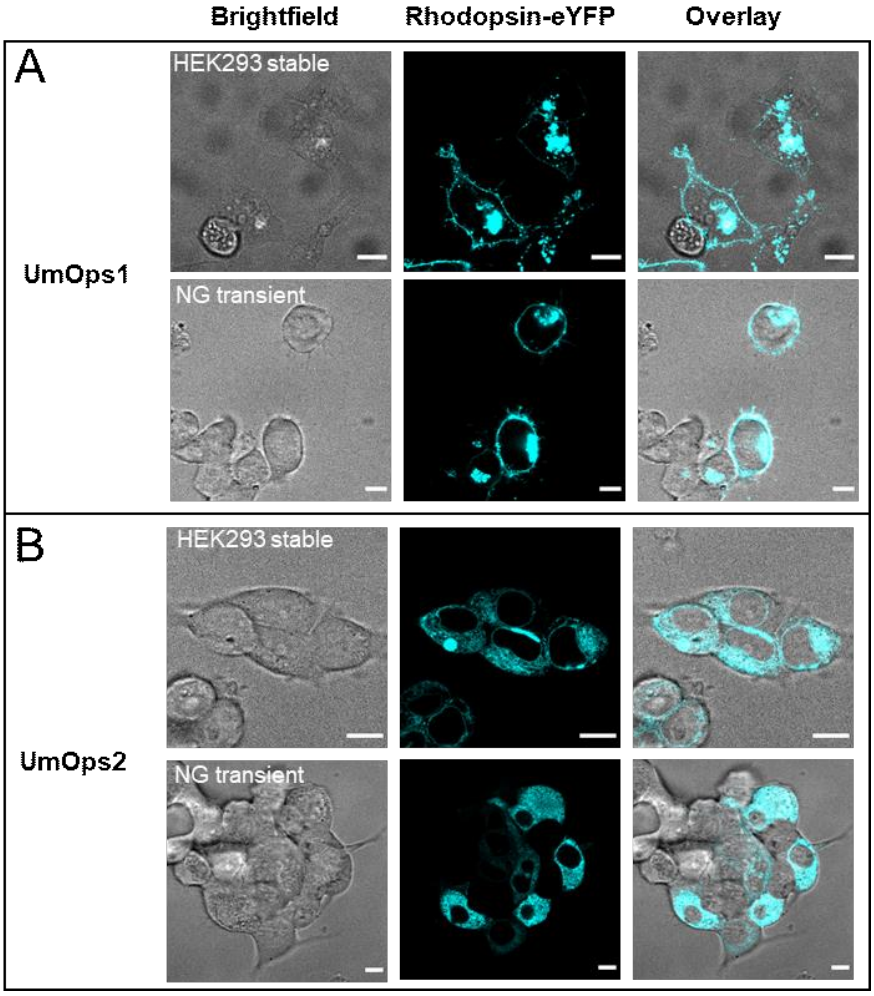

Figure 23: Expression of UmOps1-eYFP or UmOps2-eYFP in Mammalian Cells. UmOps1-eYFP was localized in the plasma membrane in stable HEK293 cells as well as in transiently transfected NG108-15 cell line. In contrast, in both cell lines UmOps2-eYFP resided mainly intracellularly. However, both constructs showed accessibility to patch-clamp measurements. Image of UmOps1-eYFP in stable HEK293 cell line was published (Panzer *et al.*, 2019); scale bars: 10 µm

UmOps1-eYFP showed plasma membrane localization in the stable cell line like it could be already shown previously (Panzer, 2017; Panzer *et al.*, 2019) as well as when transiently transfected resulting in an adequate accessibility for patch-clamp measurements (Figure 23A). However, there are some fluorescence signals inside the cell what might derive from rhodopsin constructs stuck in the ER due to overexpression. UmOps2-eYFP showed only weak plasma membrane localization in stably expressing HEK293 cells what could be shown before (Panzer, 2017; Panzer *et al.*, 2019), but also in transiently transfected NG108-15 cells the plasma membrane localization was only poor (Figure 23B). However, the stably expressing cell line yielded measurable currents when performing patch-clamp experiments.

By site directed mutagenesis, UmOps1(E129D) and UmOps1(D225E) mutants were created. UmOps1(E129D) was localized exclusively in intracellular structures (Figure 24A), what led to poor accessibility to patch-clamp measurements. In contrast, UmOps1(D225E) showed good plasma membrane localization with only little intracellular fluorescence (Figure 24B).

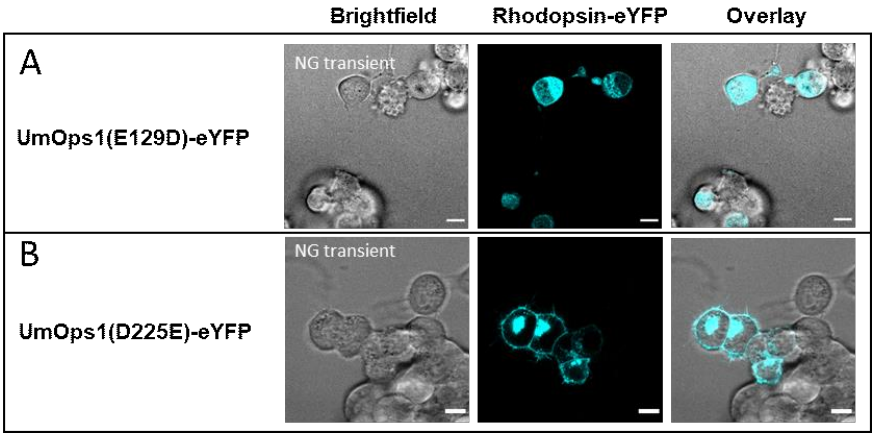

Figure 24: Transient Expression of UmOps1-mutants in NG108-15 Cells. UmOps1(E129D)-eYFP signals could be observed exclusively intracellularly (**A**), whereas UmOps1(D225E)-eYFP showed sufficient plasma membrane expression (**B**). However, in the latter mutant some intracellular fluorescence signals could be observed. Scale bars: 10 µm

Concerning the *A. pullulans* rhodopsins, ApOps1-eYFP was localized mainly intracellularly in the stable cell line, whereas transiently transfected NG108-15 cells yielded a sufficient plasma membrane localization (Figure 25A). ApOps2-eYFP was expressed in the plasma membrane in the stable cell line as well as when transiently transfected (Figure 25B). ApOps3-eYFP was only investigated in the improved 2.0 version: To yield even better prerequisite for good electrophysiological measurements and for application in optogenetics, all ApOps constructs were modified using the lr- and TT-eYFP-E (2.0)-motif for improving plasma membrane trafficking. The modification was carried out and the resulting constructs were kindly provided by members of the Georg Nagel group. All three modified ApOps constructs resided almost exclusively in the plasma membrane (Figure 25C). Furthermore, deriving from ApOps2 2.0 a channel mutant (ApOps2 2.0(F79A, R112H)) was created also by members of the Georg Nagel group. This channel showed perfect plasma membrane localization (Figure 25D).

Concerning the characterization of the *A. pullulans* rhodopsins, the basic measurements to find out whether these proteins are green light-driven proton pumps were carried out using the improved versions of the rhodopsins transiently expressed in NG108-15 cells due to the good plasma membrane localization. However, for comparison, some measurements were also performed using the ApOps2 construct lacking the modifications. With this original ApOps2 construct also the experiments concerning the WOA-effect as well as the expression and functionality in differentiated NG108-15 cells were carried out.

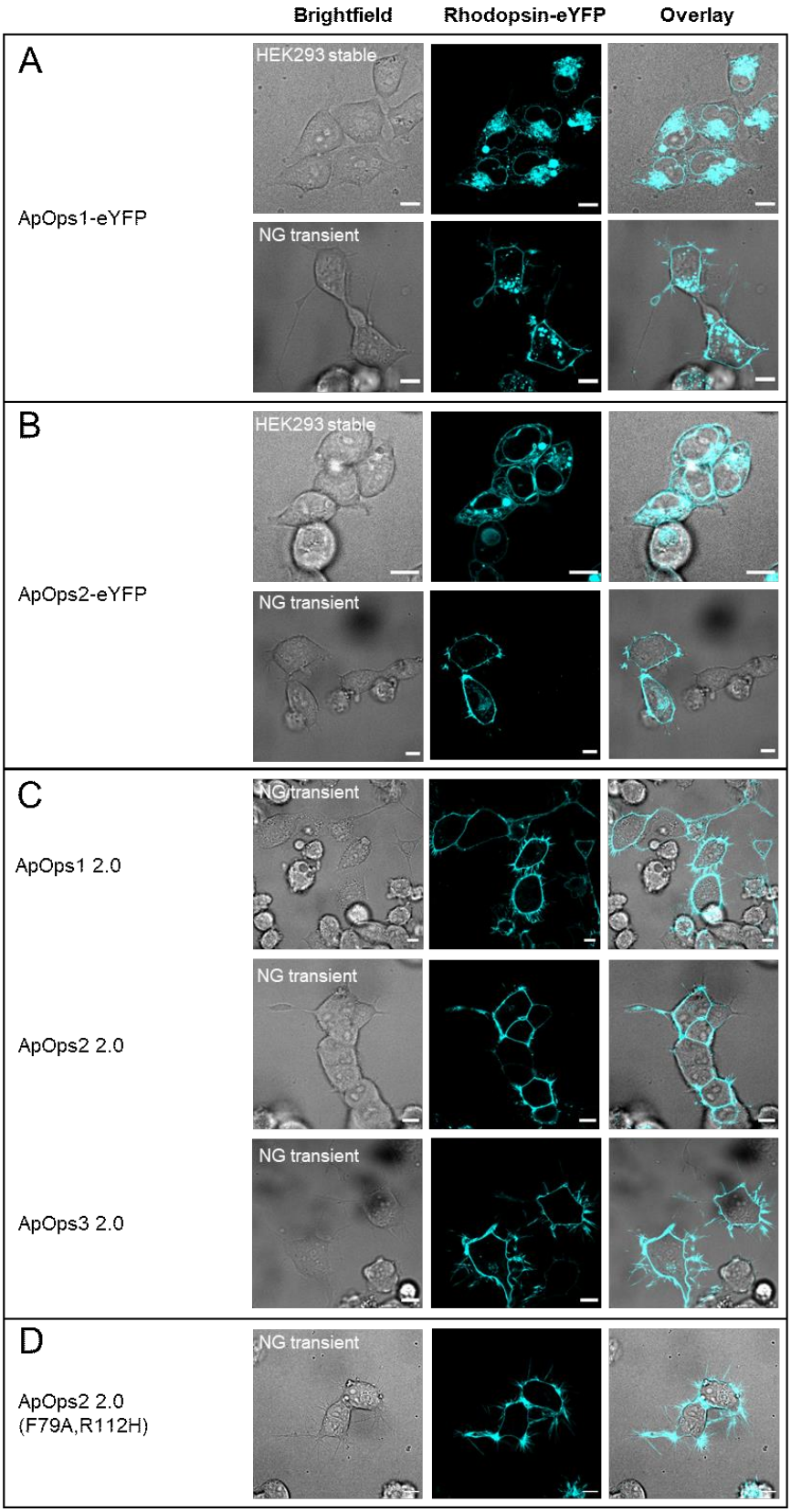

Figure 25: Transient Expression of *A. pullulans* Rhodopsins in NG108-15 Cells. ApOps1-eYFP (**A**) as well as ApOps2-eYFP (**B**) yielded better plasma membrane localization in NG108-15 cells compared to the stable HEK293 cell line. All improved versions, ApOps1 2.0, ApOps2 2.0 and ApOps3 2.0 (**C**) as well as the channel mutant ApOps2 2.0(F79A,R112H) (**D**) resided almost exclusively in the plasma membrane. Fluorescence images of ApOps1 2.0, ApOps2 2.0, ApOps3 2.0 as well as of the channel mutant were published (Panzer *et al.*, 2021); scale bars: 10 µm

4.2.2 Fungal Rhodopsins are Ion Pumps that are Maximally Activated by Green Light

HEK-cells stably expressing UmOps1 or UmOps2 as well as NG108-15-cells transiently transfected with ApOps1 2.0, ApOps2 2.0 or ApOps3 2.0, respectively, were analyzed with the patch clamp-technique.

Due to the occurrence of conserved amino acid residues that are linked to outward proton pump activity in other rhodopsins, it was first analyzed, whether the *U. maydis* and *A. pullulans* rhodopsins also show pump function. Measurements were done under physiological conditions using NaCl pH 7.4 as bath and pipette solution; clamp-voltages ranging from +40 mV to -120 mV (20 mV steps) were applied (step-protocol) and three runs were averaged. The rhodopsins were activated using a DPSS laser emitting 532 nm wavelength. The light was either applied directly via the beam path through the objective of the microscope in case of *U. maydis* rhodopsins (intensity not completely stable) or with the help of an optic fiber when measuring *A. pullulans* rhodopsins by placing the cells right in front of the fiber end to gain homogeneous illumination of the plasma membrane using a light intensity of 15 mW/mm².

Upon illumination, both, UmOps1 as well as UmOps2 exhibited positive photocurrents (Figure 26A, C). Although a voltage dependency with decreasing currents at lower clamp-voltages could be observed, even at negative clamp-voltages the photocurrents remained positive suggesting that both rhodopsins are ion pumps, transporting ions also against the electrochemical gradient. In UmOps1, a prominent transient initial peak current was visible that did not disappear with decreasing clamp-voltages, but also showed slight voltage-dependency getting lower with more negative clamp-voltages. In contrast, UmOps2 only yielded small initial peak currents and the stationary currents dominated especially at positive clamp-voltages. However, at low clamp-voltages, the initial peak is visible more clearly.

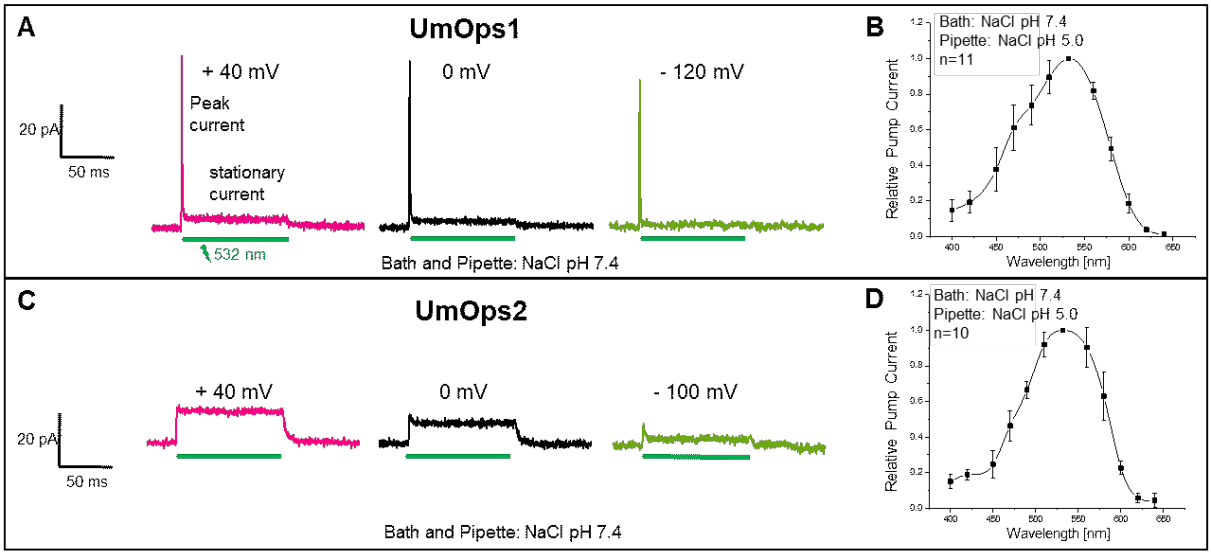

Figure 26: Photocurrents and Action Spectra of UmOps1 and UmOps2. UmOps1 as well as UmOps2 showed positive photocurrents upon 532 nm illumination at different clamp voltages (**A, C**). Both rhodopsins yielded their maximal transport activity when applying green light (**B, D**). Both action spectra and the current trace of UmOps1 at 0 mV were published (Panzer, 2017; Panzer *et al.*, 2019).

In general, UmOps1 and UmOps2 yielded rather low current amplitudes compared to the *A. pullulans* rhodopsins, which exhibited relatively high photocurrents. The current signals of ApOps1 2.0, ApOps2 2.0 and ApOps3 2.0 were positive at all clamp-voltages (Figure 27A, C, E) as it was the case for UmOps1 and UmOps2, so that it could be stated, that the three *A. pullulans* rhodopsins are also ion pumps. All of them yielded a voltage dependency with decreasing photocurrents at decreasing clamp-voltages because the pumps have to work against the electrochemical gradient. ApOps1 2.0 as well as ApOps3 2.0 showed an initial transient peak current at lower clamp-voltages, whereas in ApOps2 2.0 measurements, a peak was never visible. Here, the stationary currents were always dominating. The activating constant (τ_{on}) of ApOps1 2.0 was slower compared to the other two *A. pullulans* rhodopsins, reaching the saturation level of the stationary pump current after about 25 ms. Due to the high photocurrents of the *A. pullulans* rhodopsins, it is possible to clearly observe the current decay kinetics after light-off. All three rhodopsins exhibit a biexponential decay consisting of a fast (τ_{fast}) and a slow time constant (τ_{slow}) which will be analyzed more detailed in chapter 4.2.3.

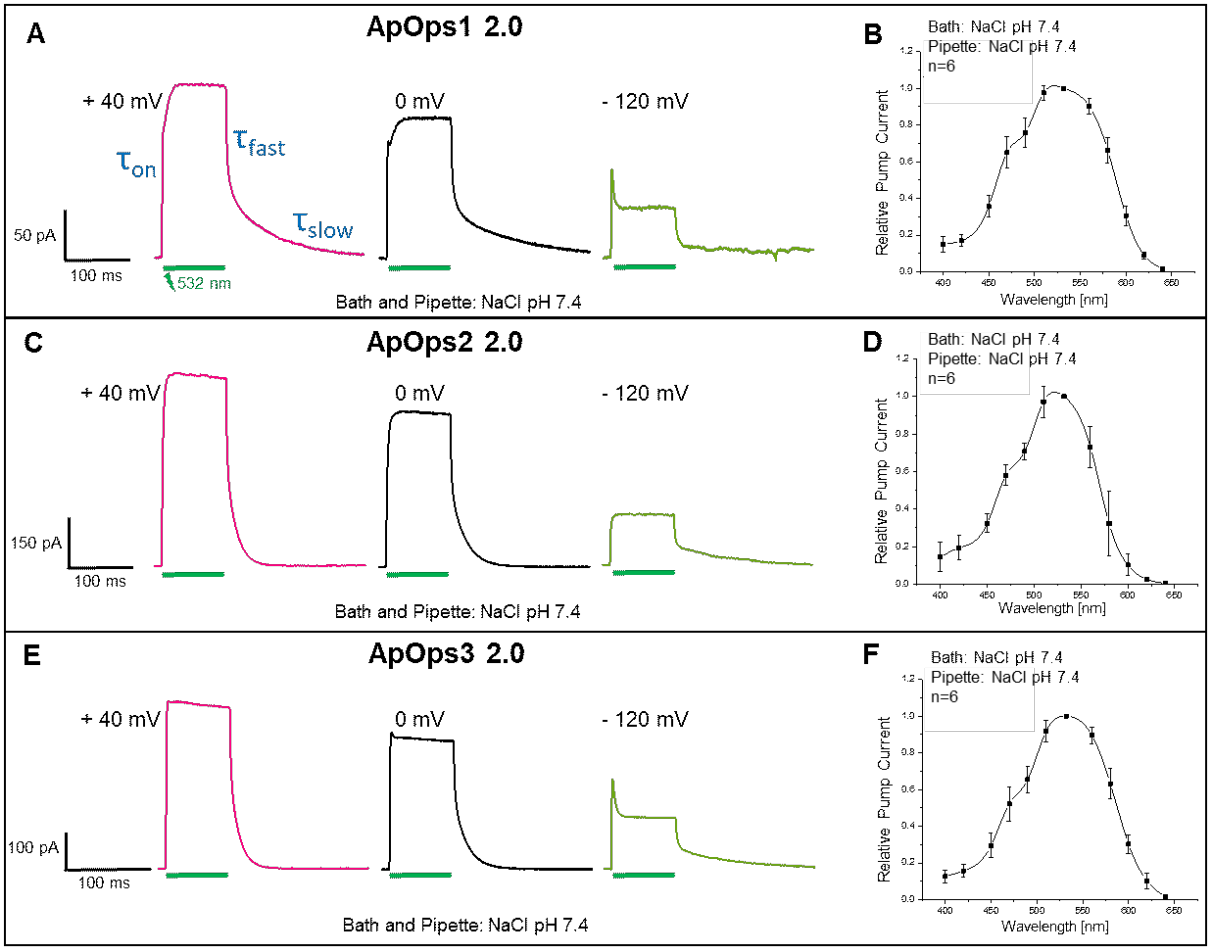

Figure 27: Photocurrents and Action Spectra of ApOps1 2.0, ApOps2 2.0 and ApOps3 2.0. All three rhodopsins showed positive photocurrents upon 532 nm illumination at different clamp voltages (**A, C, E**) and yielded their maximal transport activity when applying green light (**B, D, F**). ApOps1 2.0 showed the slowest time constant for reaching the stationary current level (τ_{on}; **A**). In all three rhodopsins a biexponential decay of the photocurrent after light-off was observed (τ_{fast} and τ_{slow}; **A**). Action spectra and current traces were published (Panzer *et al.*, 2021).

It was further analyzed, at which wavelength the rhodopsins yield their maximum pump activity. Therefore, action spectra were measured using an XBO lamp with narrow bandwidth filters generating wavelengths from 400 nm to 640 nm. The clamp voltage was 0 mV, three runs were averaged for *A. pullulans* rhodopsins, 10 runs for *U. maydis* rhodopsins. Illumination time was 300 ms for UmOps1 and UmOps2; for ApOps1 2.0, ApOps2 2.0 and ApOps3 2.0, the cells were illuminated for 100 ms. In case of the *U. maydis* rhodopsins, NaCl pH 7.4 was chosen as bath solution, but NaCl pH 5.0 as pipette solution because of the assumption that they transport protons and therefore yield higher absolute currents when there is a proton gradient. The *A. pullulans* rhodopsins were analyzed using NaCl pH 7.4 extra- and intracellularly. The values obtained were normalized to the value measured at 532 nm; mean and standard deviation of the normalized currents were calculated.

Bell shaped action spectra with the highest pump activity in the green spectral range were obtained for UmOps1 (Figure 26B), UmOps2 (Figure 26D) and all three *A. pullulans* rhodopsins (Figure 27B, D, F). When applying 640 nm, the activity was always reduced to almost 0, whereas residual activity remained when excited with blue light (400 nm). Measurements were done starting either in the blue or in the red spectral range; moreover, in the case of UmOps1 and UmOps2, different pH values and cellular backgrounds were tested (Supplementary Figure 6 and Supplementary Figure 7). Mostly, 532 nm light evoked the highest pump currents, but in some cases maximum activity was observed when applying 510 nm or 560 nm, respectively. However, the maximum pump activity was always reached under green light illumination. A detailed listing of the observed pump maxima and their respective wavelength can be found in Supplementary Table 1. UmOps1 as well as UmOps2 yielded slightly broader spectra in the presence of intra- and extracellular pH 7.4 compared to intracellular pH 5.0 (Supplementary Figure 7A, B), what might be due to the decreased signal to noise ratio under physiological conditions.

To summarize the findings so far, one can state, that all five rhodopsins, UmOps1, UmOps2, ApOps1 2.0, ApOps2 2.0 as well as ApOps3 2.0 are green-light activated ion pumps, that show voltage-dependent behavior. However, all of them have individual features and show different characteristics concerning the current amplitude or the initial transient peak current. These individual properties will be characterized further in the next chapters. The next step was to investigate the pH dependency of the pump currents and to identify the ion species that is translocated via those proteins even though there are reasons to assume that they all might be proton pumps due to the conserved amino acid residues necessary for this kind of transport.

4.2.3 *Ustilago Maydis* and *Aureobasidium Pullulans* Rhodopsins Show Proton Pump Activity with Different Voltage and pH Dependency

To investigate further the voltage- and pH dependency of the rhodopsins, step protocols (+40 mV to -120 mV; 20 mV steps; average of 3 runs) were applied while illuminating the cells with the DPSS laser (532 nm) via beam path through the microscope (*U. maydis* rhodopsins; light intensity not stable) or optic fiber (*A. pullulans* rhodopsins; light intensity: 15 mW/mm²). NaCl pH 7.4 pipette solution was used in all cases except for UmOps1, here NaCl pH 5.0 was applied for yielding a better signal to noise ratio (in case of an outward proton pump). On the extracellular side (bath solutions), also NaCl based electrolytes were taken exhibiting different pH values (pH 7.4;

5.0 and 9.0). I-V-plots were created showing mean and standard deviation with clamp-voltages on the x-axis and the normalized pump currents on the y-axis. Normalization was done to the value obtained at 0 mV clamp-voltage in bath solution NaCl pH 7.4. Polynomial cubic function was used to fit the data for better visualization. For the absolute current plots, the current traces of one representative cell were transferred from ClampFit 10.7 software directly to Origin; absolute pump currents were plotted over time.

For outward directed proton pumps, one would expect only positive current signals at all clamp-voltages and pH values. However, there should be a pH dependency, that shows increased current signals in pH 9.0 and decreased current signals in pH 5.0 compared to physiological pH 7.4. Moreover, a voltage dependency showing higher pump currents with increasing clamp-voltage should occur. I-V-plots were generated from measurements on UmOps1 and UmOps2 (Figure 28A, B) as well as ApOps1 2.0, ApOps2 2.0 and ApOps3 2.0 (Figure 28C, D, E). Patch-clamp recordings on UmOps1 were recorded using intracellular NaCl pH 7.4 in addition to pH 5.0 yielding similar results, only with decreased signal to noise ratio (Supplementary Figure 8A).

In all cases, the rhodopsins yielded positive current signals. That means, that they exhibited ion pump function independently from clamp-voltage or pH-value. A clear voltage-dependency was visible yielding lower photocurrents with lower clamp-voltages in all cases because of the

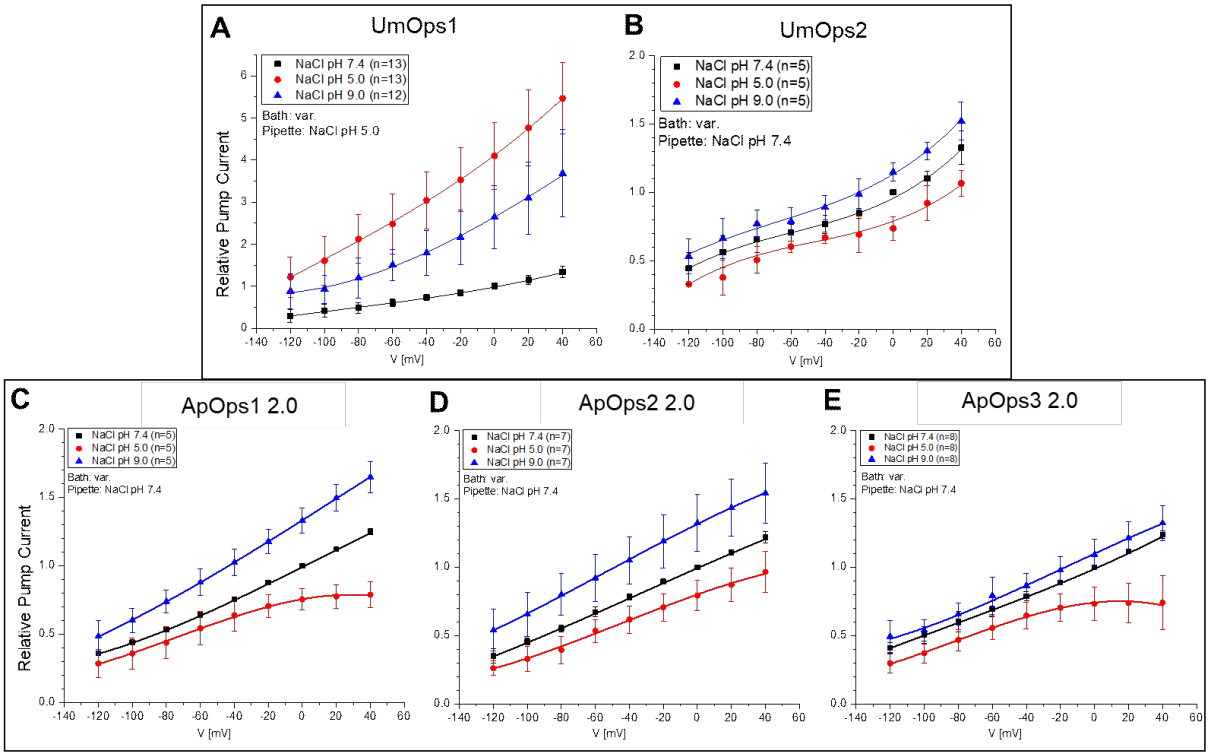

Figure 28: PH- and Voltage Dependency of *U. maydis* and *A. pullulans* Rhodopsins. I-V-plots for the five rhodopsins are shown. Mean and standard deviations are depicted with the current values being normalized to the value measured at 0 mV in NaCl pH 7.4. All rhodopsins showed pump function with decreasing photocurrents at lower clamp-voltages due to the electrochemical gradient. Moreover, four of them showed the (for proton pumps) expected pH dependency with higher currents at extracellular pH 9.0 and lower currents at extracellular pH 5.0 (**B:** UmOps2; **C, D, E**: *A. pullulans* rhodopsins). Only UmOps1 yielded massive enhancement of photocurrents at extracellular acidic pH, even exceeding the values obtained at pH 9.0 (**A**). All plots were published (Panzer *et al.*, 2019, 2021)

heightened electrochemical gradient as mentioned before. However, in ApOps1 2.0 and ApOps3 2.0 this voltage-dependency seems to disappear when applying acidic pH 5.0 and positive clamp-voltages (Figure 28C, E and Figure 30A, C). For ApOps1 2.0, the step-protocol was extended from +40 to +100 mV and the voltage dependency was virtually reversed with lower current signals at higher clamp-voltages (Supplementary Figure 9). When looking at the pH dependency, one can see, that all rhodopsins except UmOps1 showed the expected behavior of an outward proton pump. All three *A. pullulans* rhodopsins as well as UmOps2 yielded increased photocurrents at extracellular pH 9.0 and decreased current signals in pH 5.0 compared to pH 7.4 at all recorded clamp-voltages. In case of UmOps1, the expected behavior only is present when comparing pH 7.4 and pH 9.0 with higher pump currents in pH 9.0. In contrast, when applying extracellular acidic pH 5.0, UmOps1 shows a striking enhancement in pump activity, that exceeds even the current signals obtained in pH 9.0. This finding contradicts the assumption for UmOps1 being an outward directed proton pump at first glance. Changing the direction of pH value application from pH 7.4→5.0→9.0 to pH 7.4 →9.0→5.0 did not alter the characteristics of UmOps1 (Supplementary Figure 8B, C). Moreover, the ratios of the normalized mean current values at pH 7.4 to the ones at pH 5.0 or pH 9.0 were higher in UmOps1 compared to the other four rhodopsins: Here, at 0 mV clamp-voltage, the mean current signal at pH 9.0 was on average 2.64 ± 0.75 times, at pH 5.0 even 4.10 ± 0.80 times as large as the mean current signal at pH 7.4 which is considered to be 1 due to normalization. The other four rhodopsins yielded mean current signals that were for pH 5.0 at 0 mV on average 0.73 to 0.79, for pH 9.0 on average 1.09 to 1.33 the size of the value obtained at pH 7.4 (for exact values see Supplementary Table 2).

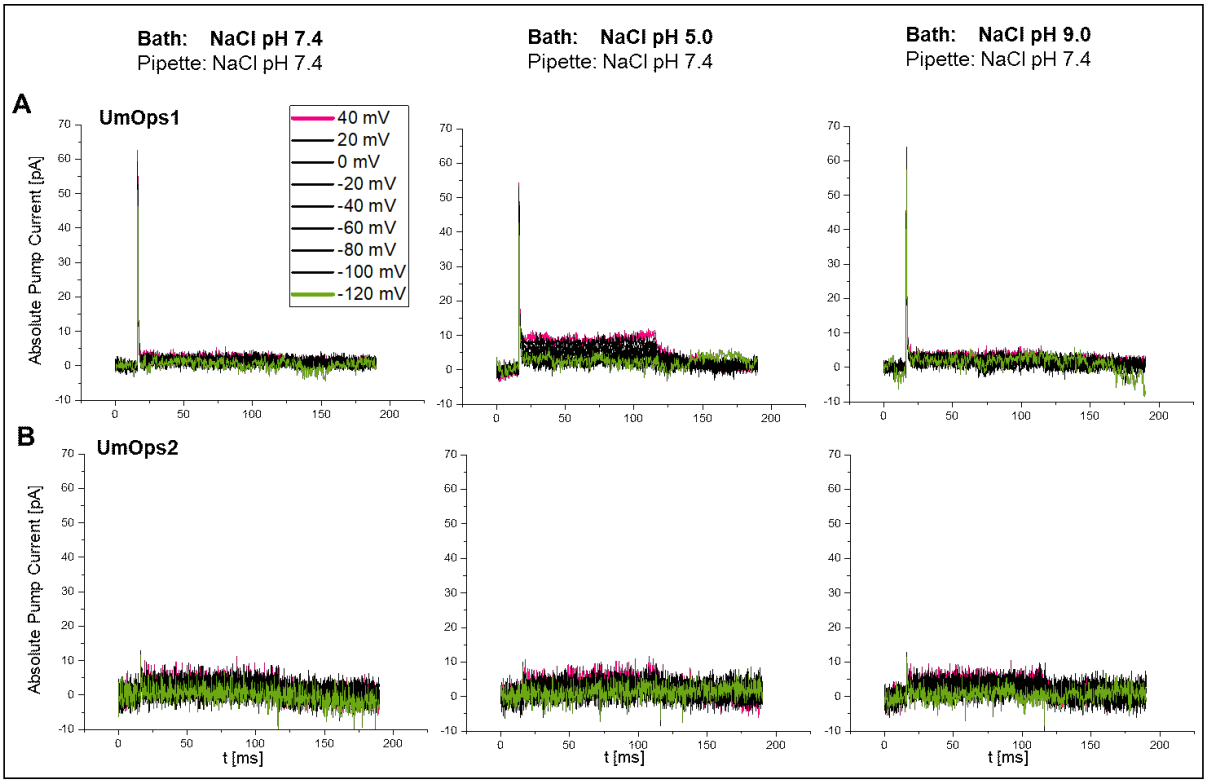

Figure 29: Absolute Photocurrents of UmOps1 and UmOps2 Plotted over Time. The two rhodopsins showed voltage and pH dependency as stated before. UmOps1 showed prominent initial peak currents (**A**) whereas UmOps2 yielded only small initial peaks at all measured conditions (**B**).

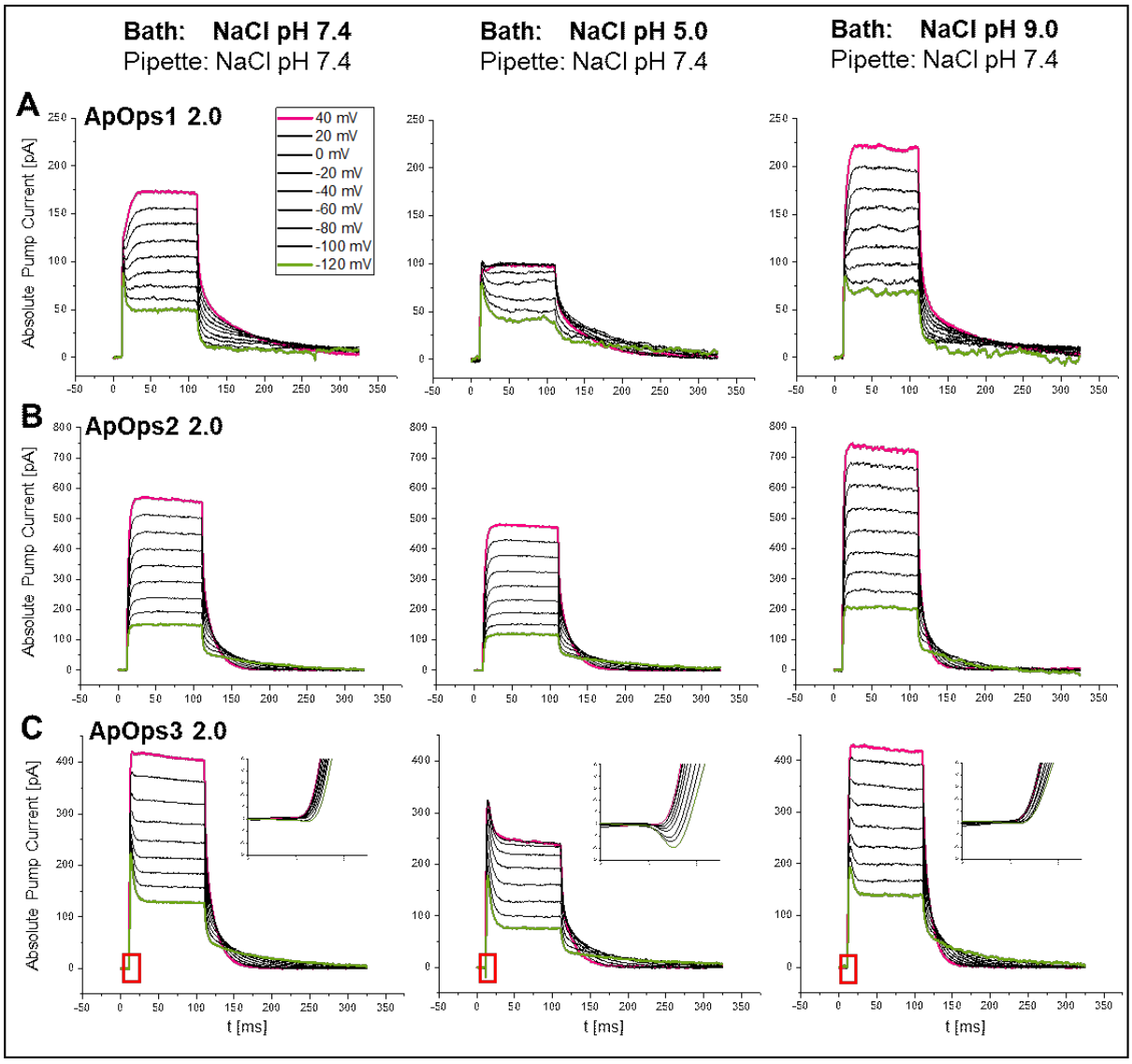

Figure 30: Absolute Photocurrents of ApOps1 2.0, ApOps2 2.0 and ApOps3 2.0 Plotted over Time. All three rhodopsins showed voltage and pH dependency as stated before. ApOps1 2.0 as well as ApOps3 2.0 showed initial peak currents at least at lower clamp-voltages (**A, C**), whereas ApOps2 2.0 showed only dominating stationary photocurrents (**B**). The voltage dependency of ApOps1 2.0 and ApOps3 2.0 disappeared at higher clamp-voltages in extracellular NaCl pH 5.0. **C red boxes and inserts**: ApOps3 2.0 showed negative currents right after light application at extracellular pH 5.0. Current traces at extracellular pH 7.4 were published (Panzer *et al.*, 2021)

Absolute currents, recorded while applying NaCl based bath solutions with different pH values (intracellular NaCl pH 7.4), were plotted over time and with this, one can clearly see as stated before, that all five rhodopsins showed special features and characteristics under the given conditions. As it could be already shown for physiological conditions, also when applying pH 5.0 and pH 9.0, both *U. maydis* rhodopsins (Figure 29) as well as ApOps1 2.0 and ApOps3 2.0 (Figure 30A, C) exhibited initial transient peak currents. In the case of both *A. pullulans* rhodopsins at least at lower clamp-voltages this peak was visible. Only in ApOps3 2.0 and acidic environment (extracellular NaCl pH 5.0) the transient current peak was prominent at all clamp-voltages (Figure 30C). ApOps2 2.0 showed dominant stationary photocurrents at all pH-values that were recorded. Moreover, this was also the one rhodopsin yielding the highest stationary currents with

amplitudes up to 664 pA at 0 mV at extracellular pH 7.4. For comparison, the NaCl-based measurements were performed in addition using the ApOps2 construct without the 2.0-modifications yielding similar results regarding pH- and voltage dependency (Supplementary Figure 10); however, a very small peak current could be observed at lower clamp voltages at all pH conditions because the stationary current is not dominating. Moreover, at extracellular pH 9.0, the photocurrent gets lower over time, but does not decrease under the pH 7.4 level even after 10 min (Supplementary Figure 11). One interesting feature was observed in ApOps3 2.0: At extracellular pH 5.0, right after light application before the transient current peak appears, the signal was lowered to negative values for less than a ms when applying negative clamp-voltages (Figure 30C red boxes and inserts). That implies that for this short time period, ions are transported in the opposite direction before the pump activity comes into effect. In contrast to the *A. pullulans* rhodopsins, UmOps1 as well as UmOps2 yielded only very small stationary photocurrents resulting in a poor signal to noise ratio (Figure 29). For better comparison of current amplitudes and exclusion of impact of cell size, current densities were calculated and will be further analyzed later in this chapter. With the help of I-V plots, it could be shown that all rhodopsins exhibit a pH dependency with UmOps1 strikingly being the only one yielding the largest pump currents at extracellular acidic pH 5.0. This characteristic is also visible in the absolute current plots with the rhodopsin signals changing their amplitudes with changing pH value.

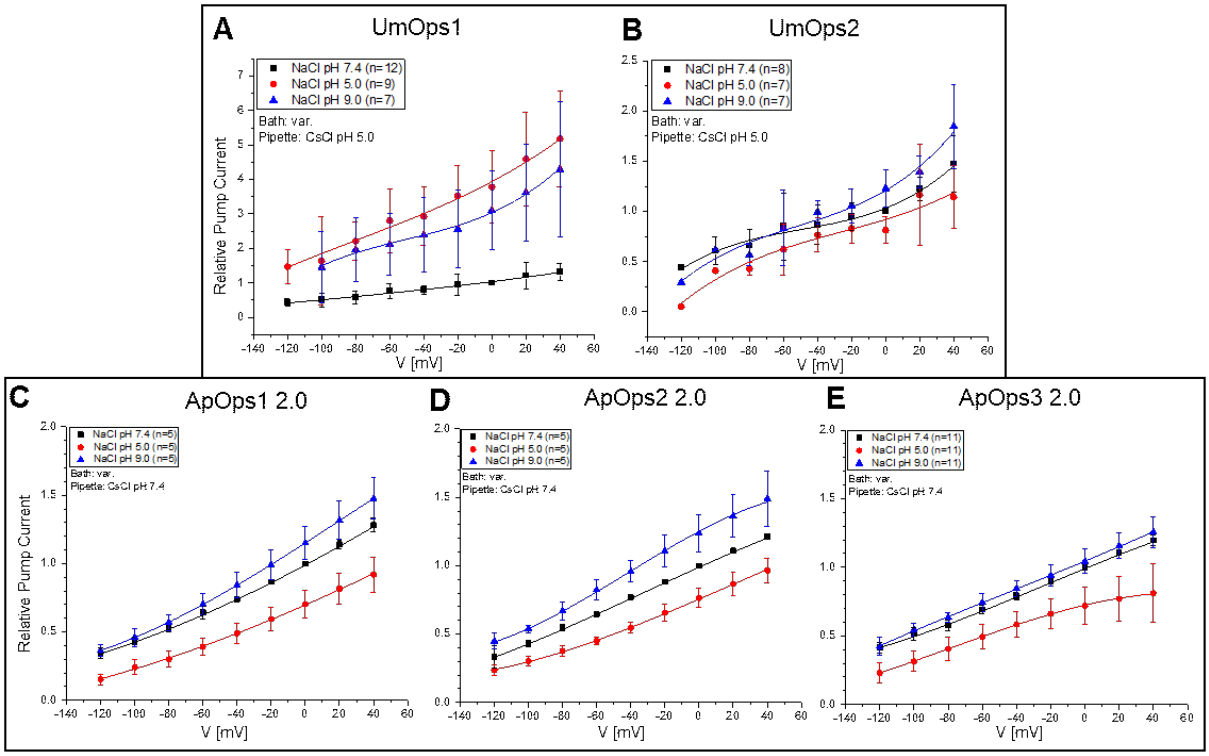

Figure 31: I-V-plots of the Rhodopsins Using Intracellular CsCl. For measuring UmOps1 and UmOps2, intracellular pH 5.0 was used for better signal to noise ratio (**A, B**). For both *U. maydis* rhodopsins, the voltage and pH dependency were similar compared to measurements using intracellular NaCl. UmOps1 still yielded highest pump currents at extracellular pH 5.0. The pH and voltage dependency of ApOps2 2.0 as well as ApOps3 2.0 were not altered by exchanging NaCl to CsCl (**D, E**). However, the saturation of the current amplitudes at positive clamp voltages in extracellular pH 5.0 of ApOps1 2.0 could not be observed (**C**). All I-V-plots were published (Panzer, 2017; Panzer *et al.*, 2019, 2021)

In a next step, the ion species transported by the rhodopsins was identified. As mentioned above, the amino acid sequences encourage the assumption, that UmOps1 and UmOps2 as well as the three *A. pullulans* rhodopsins act as outward directed proton pumps. In the measurements done before, positive photocurrents were observed under various conditions. Per convention, that means, that either positive charges are translocated from the intra- to extracellular side or negative charges vice versa. Since measurements were done using NaCl-based electrolytes, it is also possible, that sodium or chloride ions were pumped in the appropriate direction. To exclude this, sodium was exchanged with cesium, which is a rather big ion, that should not fit through the rhodopsin pore. Chloride was replaced with gluconate, that is also a large molecule not being transported by microbial rhodopsins. Thus, intracellular CsCl or extracellular NaGluc was applied and step protocols were measured. When the current signals do not change compared to measurements in NaCl, one can state, that most likely protons are transported by the rhodopsin. I-V-plots were generated for all rhodopsins, absolute current plots were only done for the *A. pullulans* rhodopsins, since the signals of *U. maydis* rhodopsins were small in general thus yielding only poor signal to noise ratios.

In UmOps1 and UmOps2 measurements, intracellular CsCl pH 5.0 was used for better signal to noise ratio compared to intracellular pH 7.4; for the *A. pullulans* rhodopsins, CsCl solution had a pH of 7.4. Extracellular NaCl solutions with different pH values (7.4; 5.0 or 9.0) were used in all cases. In both *U. maydis* rhodopsins, the same voltage and pH dependency was observed in general compared to sodium-based pipette solution with UmOps1 being again the only rhodopsin yielding highest photocurrents in extracellular pH 5.0 (Figure 31A, B) what could already be shown before (Panzer, 2017). When measuring the *A. pullulans* rhodopsins, the pH and voltage dependency of ApOps2 2.0 and ApOps3 2.0 was also not altered by exchanging intracellular NaCl to CsCl (Figure 31D, E and Supplementary Figure 12B, C). For ApOps2 without the 2.0 modifications, this characteristic could be shown before (Bräuer, 2018). In ApOps1 2.0, the saturation of the photocurrents measured at positive clamp-voltages in extracellular pH 5.0 with intracellular NaCl could not be observed when using CsCl as pipette solution (Figure 31C and Supplementary Figure 12A). The occurrence of the transient peak currents in all three *A. pullulans* rhodopsins as well as the initial reversed currents at extracellular pH 5.0 in ApOps3 2.0 remained very similar compared to the NaCl measurements (Supplementary Figure 12).

When applying NaGluc bath solutions exhibiting different pH values in general, the pH and voltage dependency of the *U. maydis* rhodopsins were not altered with UmOps1 again being the only one reaching highest photocurrents at extracellular pH 5.0 (Figure 32A, B). However, when gluconate was present in the extracellular solution at pH 7.4, the currents were always enhanced compared to currents measured in NaCl pH 7.4 bath solution independently from the clamp-voltage. The reason might be due to gluconate being a weak organic acid, which was shown before being responsible for a boost in current amplitude for CarO, the rhodopsin of *F. fujikuroi* (García-Martínez *et al.*, 2015). These characteristics of UmOps1 and UmOps2 were already shown before (Panzer, 2017). The *A. pullulans* rhodopsins show similar pH and voltage dependency when using extracellular NaGluc or NaCl (Figure 32C, D, E and Supplementary Figure 13). Like in UmOps1 and UmOps2, NaGluc caused a current enhancement in all three rhodopsins. For ApOps2 without 2.0 modifications, this could be shown before (Bräuer, 2018). Initial peak currents were visible only

in ApOps1 2.0 and ApOps3 2.0 at negative clamp-voltages. The saturation of the photocurrents at positive clamp-voltages in extracellular pH 5.0, that was observed in ApOps1 2.0 and ApOps3 2.0 when using NaCl-based bath solutions, was not yielded in NaGluc based bath solutions. The initial reversed currents occurring shortly after light-on in ApOps3 2.0 at extracellular pH 5.0 were present also in NaGluc-based bath solution (Supplementary Figure 13).

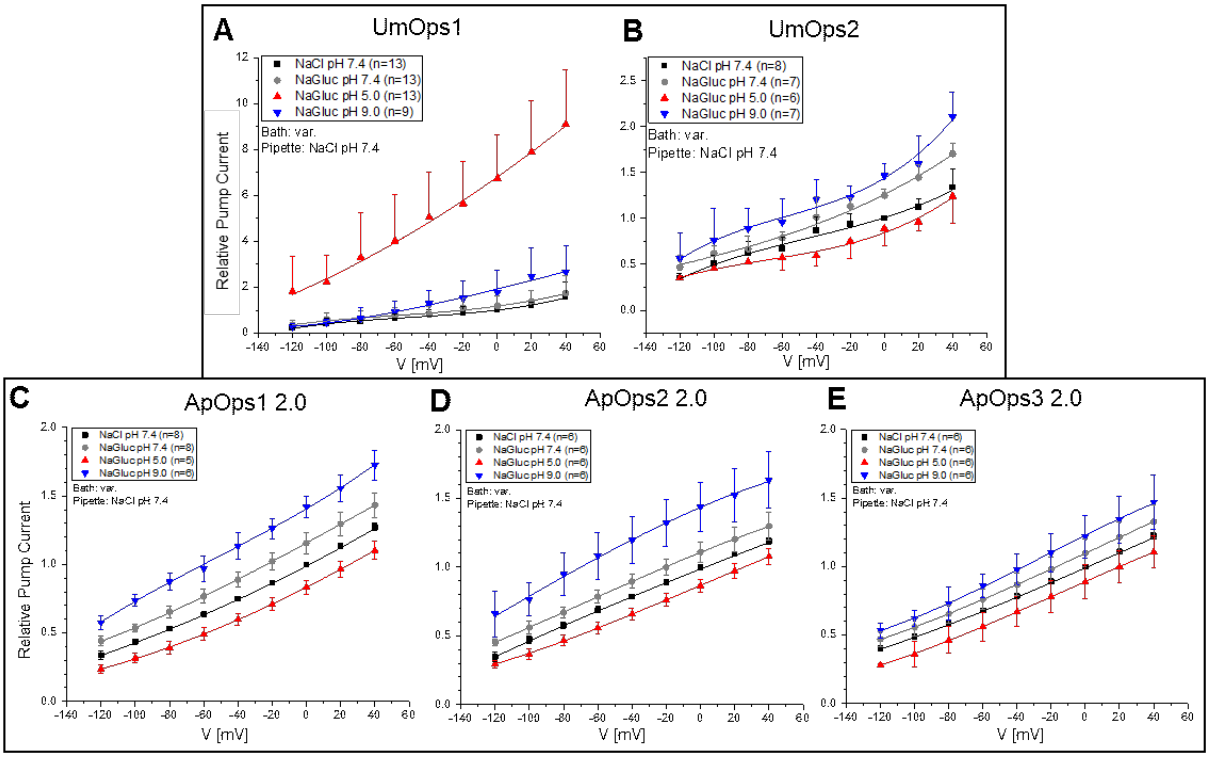

Figure 32: I-V-plots of the Rhodopsins Using Extracellular NaGluc. For both *U. maydis* rhodopsins, the voltage and pH dependency were similar compared to measurements using intracellular NaCl (**A, B**). UmOps1 still yielded highest pump currents at extracellular pH 5.0. The pH and voltage dependency of ApOps2 2.0 were not altered by exchanging NaCl to NaGluc (**D**). However, the saturation of the current amplitudes at positive clamp voltages in extracellular pH 5.0 of ApOps1 2.0 and ApOps3 2.0 could not be observed (**C, E**). All rhodopsins showed an enhancement of the pump current when NaGluc pH 7.4 was present instead of NaCl pH 7.4. All I-V-plots were published (Panzer, 2017; Panzer *et al.*, 2019, 2021)

To summarize the findings so far, one can state that most likely all five rhodopsins are transporting protons from the intra- to the extracellular side of a cell. So UmOps1 and UmOps2 as well as ApOps1 2.0, ApOps2 2.0 and ApOps3 2.0 are green-light-driven outward rectifying proton pumps with UmOps1 exhibiting a striking activity boost in acidic extracellular environment.

Furthermore, current densities were calculated to compare the pump currents of the five rhodopsins independently from cell size. However, different expression levels can occur especially when transfection was performed transiently. Absolute pump currents measured at 0 mV clamp-voltage in bath and pipette solutions as indicated were divided by the whole-cell capacitance obtained for the appropriate cell in the appropriate electrolyte solutions. Mean and standard

deviation were calculated; the data are given as box plots. In Supplementary Table 3, in addition, median values as well as maximum and minimum values are listed for all rhodopsins. Unpaired t-test was performed and significance level is given in the plots.

UmOps1 as well as UmOps2 yielded rather low current densities reaching mean values of only 0.096±0.077 or 0.14±0.066 pA/pF, respectively in physiological pH intra- and extracellular (Figure 33). When changing the intracellular pH to a value of 5.0, the current densities increased in UmOps1 as well as in UmOps2 yielding mean values of 0.28±0.25 or 0.29±0.11 pA/pF, respectively for intracellular NaCl and 0.21±0.16 or 0.21±0.14 pA/pF, respectively for intracellular CsCl. In extracellular NaGluc pH 7.4 and intracellular NaCl pH 7.4 UmOps1 yielded 0.097±0.088 pA/pF, UmOps2 yielded 0.18±0.088 pA/pF. The current densities were not significantly different when exchanging intracellular sodium with cesium or extracellular sodium with gluconate ($p>0.05$) what confirms the assumption that both rhodopsins are outward proton pumps. In addition, the increase of current density upon intracellular pH lowering encourages this assumption. When comparing extracellular NaCl pH 7.4 with extracellular NaGluc pH 7.4 in both rhodopsins a slight enhancement in current density mean values can be observed due to the WOA-effect, however this increase is not significant and also not the case in every single cell (data not shown) most likely due to the poor signal to noise ratio.

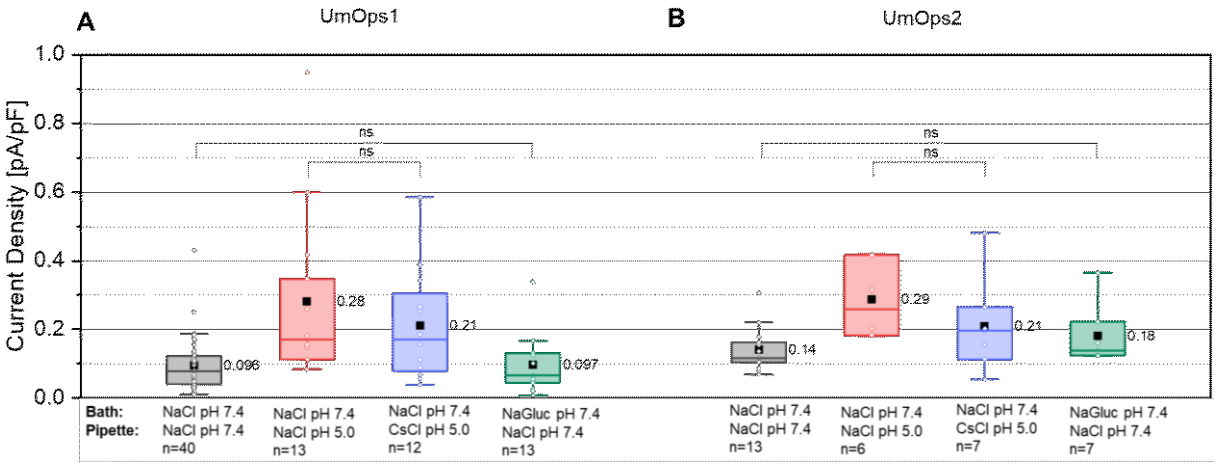

Figure 33: Current Densities of UmOps1 and UmOps2 at 0 mV Clamp-voltage. Both *U. maydis* rhodopsins yield rather low current densities. UmOps1 (**A**) as well as UmOps2 (**B**) yielded higher current densities when changing intracellular pH 7.4 to pH 5.0. Extracellular NaGluc and intracellular CsCl did not alter the current density in a significant manner compared to the appropriate NaCl measurements (not significant (ns): $p>0.05$).

In contrast to the *U. maydis* rhodopsins, the *A. pullulans* rhodopsins showed higher current densities in general (Figure 34). In physiological intra- and extracellular NaCl, ApOps1 2.0 reached a mean value of 4.5±1.2 pA/pF, ApOps2 2.0 5.4±4.8 pA/pF and ApOps3 2.0 7.3±3.2 pA/pF. For ApOps2 without the 2.0 modifications, at 15 mW/mm² (optic fiber) the mean current density was 4.13±1.20 pA/pF what is similar to the 2.0 construct (Supplementary Figure 14). However, when measuring the ApOps2 construct under direct laser illumination through the objective, a mean current density of 9.46±2.18 pA/pF was reached what indicates, that in this case higher and uncontrolled intensities were applied because the emission conditions of the laser were not optimized with the help of the optic fiber.

When exchanging extracellular sodium to gluconate, mean values of 5.00±1.45 pA/pF for ApOps1 2.0, 5.28±2.94 pA/pF for ApOps2 2.0 and 8.97±2.67 pA/pF for ApOps3 2.0 were yielded (Figure 34). Like for the *U. maydis* rhodopsins, the current density difference caused by the WOA-effect was not significant because variations in the expression level predominate. However, the good signal to noise ratio allowed a closer look on the single cell level where all cells showed higher current densities in extracellular NaGluc pH 7.4 compared to extracellular NaCl pH 7.4 due to the WOA-effect (Supplementary Figure 15). When exchanging intracellular sodium to cesium at physiological pH, ApOps1 2.0 reached a mean current density of 4.25±1.09 pA/pF, ApOps2 2.0 5.41±2.82 pA/pF and ApOps3 2.0 3.09±2.25 pA/pF. For ApOps1 2.0 and ApOp2 2.0, the difference when measuring in extracellular NaGluc pH 7.4 or with intracellular CsCl pH 7.4 compared to extra- or intracellular NaCl pH 7.4 was not statistically significant ($p>0.05$), what confirms the assumption, that ApOps1 2.0 as well as ApOps2 2.0, like UmOps1 and UmOps2, are outward proton pumps. In contrast, the values obtained from CsCl-measurements of ApOps3 2.0 were statistically extremely different ($p<0.001$) to the values measured in NaGluc and very different to the values obtained in NaCl ($p<0.01$). That could be a hint, that not only protons are transported, but also sodium or that some modulation of pump activity occurs in the presence/absence of sodium or cesium.

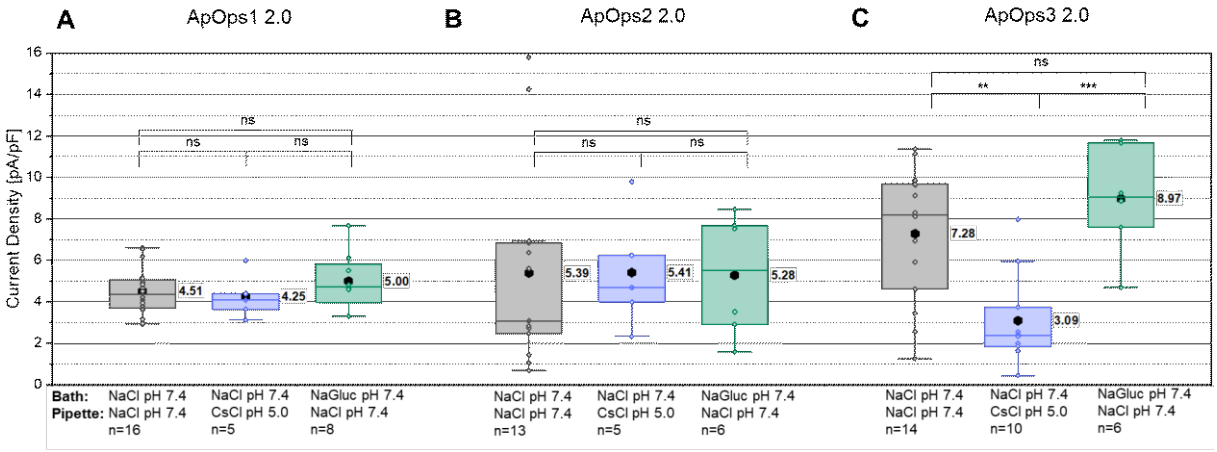

Figure 34: Current Densities of ApOps1 2.0, ApOps2 2.0 and ApOps3 2.0 at 0 mV Clamp-voltage.. All *A. pullulans* rhodopsins yielded rather high current densities. In ApOps1 2.0 (**A**) and ApOps2 2.0 (**B**) the current densities did not change significantly when exchanging NaCl to NaGluc or CsCl (not significant (ns): $p>0.05$). In ApOps3 2.0 (**C**) the measurements with intracellular CsCl yielded significantly lower current densities compared to the other conditions (** $p<0.01$; *** $p<0.001$). Current densities were published (Panzer *et al.*, 2021).

Furthermore, the current decay kinetics of the rhodopsins were analyzed. In case of *A. pullulans* rhodopsins this could be directly done using the measurements carried out in NaCl pH 7.4 bath and pipette solutions at different clamp voltages. For UmOps1 and UmOps2, this was not possible due to the very small photocurrents. Therefore, a very short light pulse (1.5 ms) was applied at 0 mV clamp-voltage in NaCl based solutions (pH 7.4) on transiently expressing NG108-15 cells resulting in a higher current signal due to the initial peak current.

The photocurrents of all rhodopsins decayed in a biexponential manner; fast and slow time constants were acquired. Figure 35 shows the time constants of all five rhodopsins obtained at 0 mV clamp-voltage. At 0 mV clamp voltage, all rhodopsins yielded similar fast time constants exhibiting values smaller than 2.2 ms (Figure 35A). UmOps1 showed the smallest fast time constant with 0.91±0.22 ms; the fast time constant of UmOps2 was 1.5±0.63 ms, for ApOps1 2.0 it was 2.2±0.10 ms, for ApOps2 2.0 1.3±0.096 ms and for ApOps3 2.0 2.0±0.36 ms. In contrast, the slow time constants differed among the rhodopsins (Figure 35B): UmOps1 as well as ApOps1 2.0 yielded rather high slow time constants with 90±23 ms or 72±16 ms, respectively, whereas UmOps2 yielded the lowest slow time constant with 9.2±1.4 ms, followed by ApOp2 2.0 with 19±2.9 and ApOps3 2.0 with 20±2.6 ms. For the *A. pullulans* rhodopsins, it was possible to obtain time constant values along the whole measured clamp-voltage range from +40 mV down to -120 mV in 20 mV steps (Supplementary Figure 16). Like it was the case at 0 mV clamp-voltage, ApOps2 2.0 yielded lower fast time constants compared to ApOps1 2.0 and ApOps3 2.0 at all other clamp-voltages. However, almost no or only a very slight voltage dependency could be observed for the fast time constant (Supplementary Figure 16A). In contrast, the slow time constants of all three *A. pullulans* rhodopsins showed a strong voltage dependency yielding decreasing values with increasing clamp-voltage (Supplementary Figure 16B). At all clamp-voltages, ApOps1 2.0 reached the highest slow time constants like it was observed yet for 0 mV.

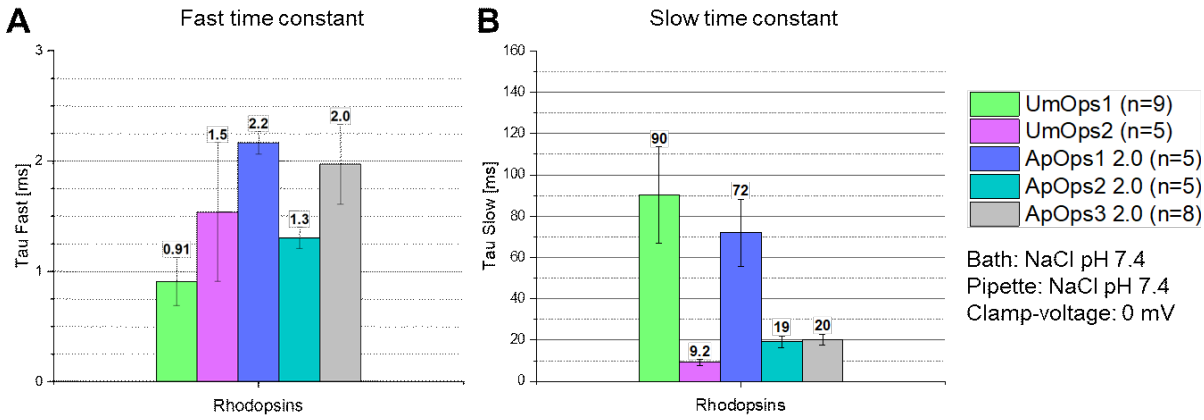

Figure 35: Current Decay Kinetics of the Rhodopsins After Light-Off. All rhodopsins showed a biexponential current decay after illumination end revealing a fast (**A**) and a slow (**B**) time constant. The fast time constants were in a similar range for all rhodopsins with UmOps1 yielding the lowest and ApOps1 2.0 yielding the highest value. In contrast, the slow time constant showed different ranges among the rhodopsins. Whereas UmOps1 as well as ApOps1 2.0 yielded rather high values, the other three rhodopsin showed lower time constants.

4.2.4 Reaction of Rhodopsins to Extracellular Stimuli – The Acetate Effect

As mentioned before, it could already be shown, that some rhodopsins react to extracellular WOAs. CarO from *F. fujikuroi* as well as UmOps1 from *U. maydis* showed enhanced pump activity in the presence of extracellular gluconate, acetate or IAA in a dose-dependent manner (García-Martínez *et al.*, 2015; Panzer, 2017; Adam *et al.*, 2018; Wilczek, 2018). For UmOps1 also IPA was tested yielding photocurrents that were increased; however, with longer carbon-chain length the increase in the current amplitude was decreasing (Panzer, 2017). Moreover, since for UmOps1 a current increase in acidic environment was observed, the pump currents could be heightened up to 64-fold by combining extracellular pH 5.0 with the supplementation with different concentrations of acetate (Panzer, 2017).

Here, this WOA-effect was investigated for UmOps1 and 2 as well as for ApOps2 and ApOps2 2.0 under physiological conditions (NaCl pH 7.4 based bath and pipette solutions, supplemented with different concentrations of NaAc pH 7.4). The measurements on UmOps1 and UmOps2 were recorded under direct laser illumination through the objective; ApOps2 as well as ApOps2 2.0 were illuminated via the optic fiber with laser output of 54% without ND filters, what does not resemble the optimal measuring conditions (see chapter 3.3.2).

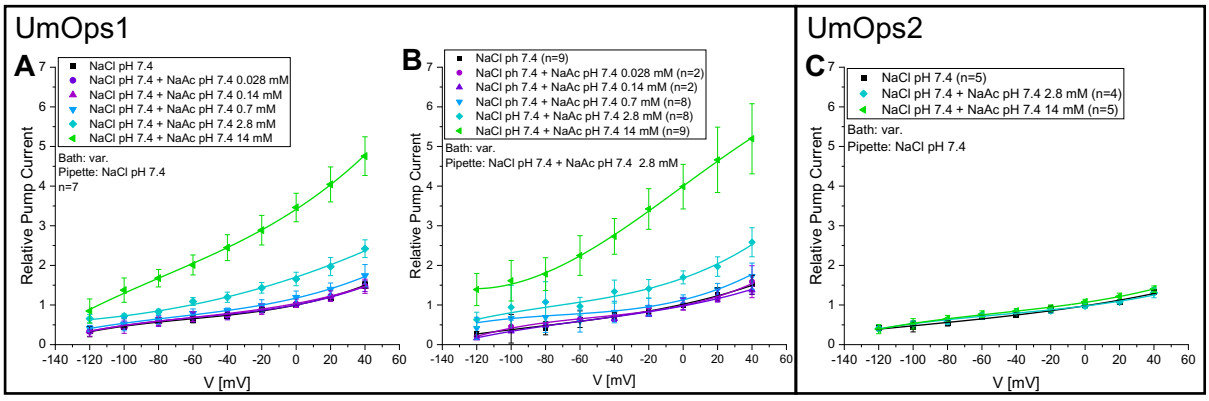

Figure 36: WOA-effect in UmOps1 and UmOps2 Caused by Acetate. UmOps1 showed increased pump currents in the presence of extracellular acetate (**A**); intracellular acetate (2.8 mM) did not alter this characteristic (**B**). In contrast, UmOps2 did not show a current enhancement when applying extracellular acetate (**C**). Plots A and B were published (Panzer *et al.*, 2019)

Despite of the different settings, one can clearly see, that UmOps1 (Figure 36A) as well as ApOps2 (without (Figure 37A) and with (Figure 37C) 2.0 modification) showed increasing photocurrents with increasing concentrations of acetate in the extracellular medium. In contrast, UmOps2 did not show this effect under the applied conditions (Figure 36C). At 0 mV clamp-voltage, UmOps1 showed a current enhancement factor of 3.5±0.36 at an extracellular acetate concentration of 14 mM compared to 0 mM; in ApOps2 the current increase reached 1.5±0.16-fold and in ApOps2 2.0 1.5±0.12-fold values at an extracellular acetate concentration of 14 mM. Due to the

different laser settings, one cannot compare the UmOps1 measurements with the ApOps2 and ApOps2 2.0 measurements directly; however, one can see that the 2.0 modified and the ApOps2 construct without modification show similar characteristics. In UmOps2, almost no enhancement (factor 1.1±0.069) was visible in presence of 14 mM of extracellular acetate. Higher acetate concentrations were tested for ApOps2 and ApOps2 2.0. In ApOps2, the pump current at 0 mV was enhanced 2.5±0.45-fold when applying 140 mM NaAc on the extracellular side, in ApOps2 2.0 a factor of 2.6±0.36 was reached.

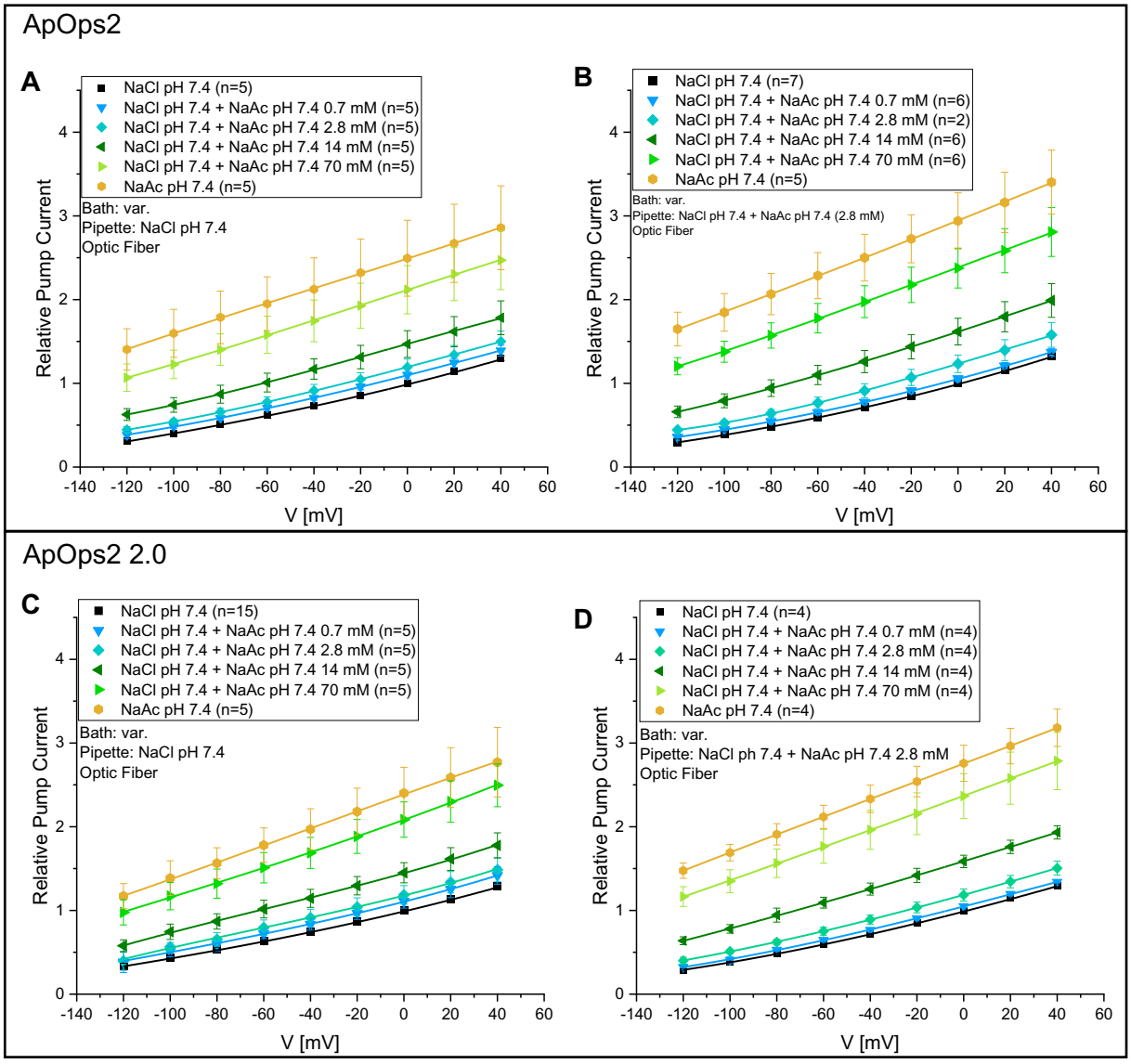

Figure 37: WOA-effect in ApOps2 or ApOps2 2.0 Caused by Acetate. Different concentrations of extracellular acetate increased the photocurrents in ApOps2 (**A**). The presence of 2.8 mM intracellular acetate did not change this characteristic (**B**). The modified construct ApOps2 2.0 showed similar characteristics yielding enhanced pump currents upon extracellular acetate application independent from the absence (**C**) or presence (**D**) of intracellular acetate.

Acetate has a pK_a value of 4.76, so most molecules should be deprotonated at pH 7.4 and cannot pass the plasma membrane in this ionized state. However, the microenvironment directly at the plasma membrane can only hardly be controlled or be observed, so it could be possible that extracellular acetate gets protonated near the membrane, enters the cell, gets again deprotonated and thus causes a current increase through the rhodopsins by lowering the intracellular pH. Therefore, it was furthermore tested, whether intracellular acetate at a concentration of 2.8 mM has an effect of the current enhancement upon extracellular acetate supplementation. This issue was investigated before on CarO and it was found that the acetate effect was still present even when applying intracellular NaAc (Wilczek, 2018). At 0 mV, the photocurrent of UmOps1 was enhanced 4.0±0.56-fold at an extracellular acetate concentration of 14 mM and even at equimolar extracellular concentration of 2.8 mM, the pump current was enhanced 1.7±0.16-fold (Figure 36B), yielding almost the same enhancement factor compared to the measurements without intracellular acetate (1.7±0.17-fold at extracellular 2.8 mM NaAc; Figure 36A). For ApOps2 the following enhancement factors were observed with intracellular NaAc pH 7.4 2.8 mM at 0 mV clamp-voltage (Figure 37B): extracellular NaAc pH 7.4 2.8 mM: 1.2±0.10; 14 mM: 1.6±0.16; 140 mM: 2.9±0.34. For ApOps2 2.0 the factors under the same conditions are the following (Figure 37D): extracellular 2.8 mM: 1.2±0.071; 14 mM: 1.6±0.074; 140 mM: 2.8±0.22. For a better overview, all values obtained are listed in Supplementary Table 4 and the values measured at 0 mV clamp-voltage were plotted with a Hill-fit in Supplementary Figure 17. Since ApOps2 and ApOps2 2.0 show almost the same behavior, the 2.0 modification doesn`t seem to have an impact on the rhodopsin function in these experiments. The current enhancement factors of UmOps1, ApOps2 and ApOps2 2.0 slightly increased in most of the cases when extracellular acetate concentration exceeds the intracellular one at physiological pH. That means that some molecules of acetate may enter the cell in their protonated state and therefore cause a further current enhancement. However, there is a current increase visible even at equimolar range or in the presence of a lower amount of extracellular NaAc compared to intracellular so that acetate should not enter the cell under these conditions due to the chemical gradient.

4.2.5 Identification of Key Amino Acids with Rhodopsin Mutants

Amino acid sequences of the tested rhodopsins in general show features necessary for proton pumping and indeed this function could be observed in electrophysiological measurements. Site directed mutagenesis was used to change specific amino acid residues to identify key moieties involved in the transport process. Especially the amino acid residues that could be connected with the WOA-effect of the rhodopsins or with the striking pH characteristic in UmOps1 are interesting. Moreover, turning a pump into a channel could be of interest when application in optogenetics is an option what is the case for ApOps2.

One important residue in a rhodopsin is the proton donor site, which is an aspartate in BR, LR, CsR and CarO. The *A. pullulans* rhodopsins and also UmOps2 show this moiety at the respective position, whereas UmOps1 contains a glutamate. Another key region is the proton releasing group that is slightly differently structured among the tested rhodopsins. ApOps1, ApOps2 and UmOps2 contain two glutamates and one aspartate like BR; UmOps1 and ApOps3 contain two aspartates and only one glutamate. (See Table 1 and Supplementary Figure 1).

The UmOps1(E129D) and the UmOps1(D225E) mutants were created to investigate possible variations in functionality and changing characteristics. In ApOps2 2.0 the R112 position was mutated that could be shown previously in other rhodopsins to turn a pump into a channel (Vogt *et al.*, 2015; Wilczek, 2018). In addition, position F79 was mutated because this site together with Y78 are the corresponding positions of Y58 and Y57 in CsR, where at least the latter one participates in proton transport (Vogt *et al.*, 2015). Indeed, the F79A mutant yielded higher currents in ApOps2 2.0 (Panzer *et al.*, 2021).

At a first glance, UmOps1(E129D) showed almost no membrane localization (Figure 24). However, this was also the case for UmOps2 wild type, but in this case, still electrophysiological measurements could be conducted and photocurrents occurred. In almost all cases measurements on UmOps1(E129D) expressing cells did not yield visible or measurable photocurrents. Only in one cell current amplitudes with suitable but still very poor signal to noise ratio could be observed. In contrast to the wild type, no prominent peak current occurred; 0.7 mM acetate only slightly increased the current amplitude (Supplementary Figure 18). It is difficult to figure out whether these observations are a result of the poor plasma membrane trafficking and therefore poor accessibility to patch-clamp measurements or if the function of the protein is impaired by the donor site mutation.

UmOps1(D225E) was transported to the plasma membrane in a sufficient manner so that patch-clamp measurements could be carried out resulting in photo currents with sufficient signal to noise ratios. At first, an action spectrum was measured at 0 mV clamp-voltage and like in the wild type, the D225E mutant exhibited maximum pump currents under green light illumination (Figure 38A). The spectrum was bell-shaped and comparable to the spectrum of UmOps1 wild type yielded from measurements in transiently transfected NG108-15 cells (Supplementary Figure 7A). Especially when starting with red light, the maximum was slightly shifted to lower wavelengths in the D225E mutant (hypsochromic shift) (Supplementary Figure 19). As a next step, different pH-values and clamp-voltages were applied to the mutant using NaCl-based bath- and pipette solutions (Figure 38 B). The voltage-dependency of the D225E mutant resembles that of the wild type yielding higher photo currents at higher clamp-voltages. In contrast, the pH-dependency shows a considerable difference to the wild type. Whereas at extracellular pH 9 the current amplitudes were higher compared to pH 7.4 like it was the case in the wild type, at extracellular acidic pH 5.0 the photocurrents in the D225E mutant decreased compared to physiological pH what strongly contrasts the characteristics of wild type UmOps1 (see also Figure 28A). In addition, the reaction to extracellular acetate in pH 5.0 based environment is not so strong compared to the wild type maybe due to the lacking current boost caused by extracellular pH 5.0 (Figure 38C). However, in general the WOA-effect occurred also in physiological pH independently of the presence of intracellular acetate (Figure 38D, E; Supplementary Table 4). Interestingly, after light-off, an additional current peak occurred under conditions that prompted the wild type to the exhibition of enhanced stationary currents (i.e., extracellular pH 5.0 or presence of acetate) (Figure 38F). It seems that even the slight change from an aspartate to a glutamate in the proton releasing group can lead to strong changes in the pump characteristics of a rhodopsin and that a very fine-tuned interaction of defined moieties is necessary for the respective transport properties.

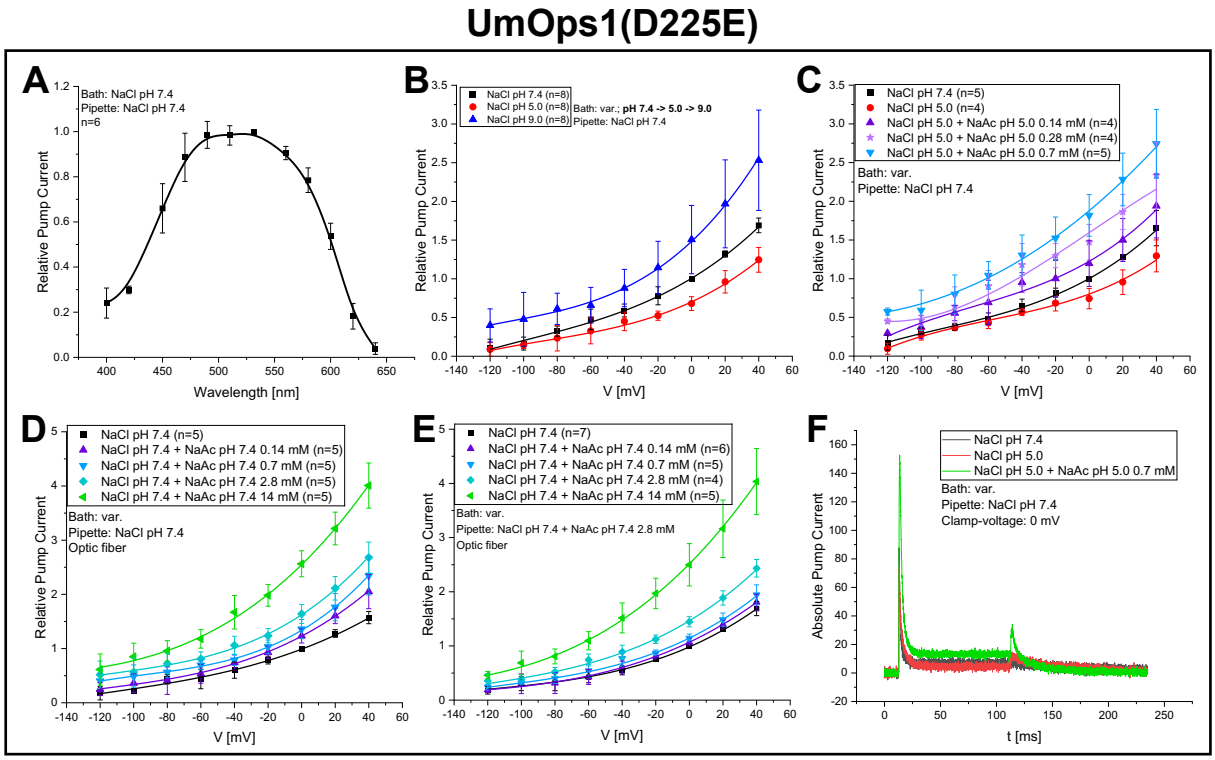

Figure 38: Electrophysiological Characteristics of UmOps1(D225E) Mutant. A: UmOps1 yielded a bell-shaped action spectrum with maximum pump currents occurring under green light illumination. **B:** Voltage- and pH-dependency of UmOps1(D225E): The voltage dependency is comparable to the wild type showing higher photocurrents when applying higher clamp-voltages. In contrast, the pH-dependency was different to the wild type yielding higher pump currents in extracellular pH 9.0, but lower currents in extracellular pH 5.0 (compared to pH 7.4). **C:** The WOA-effect was still present under acidic conditions, however yielding lower rations compared to the wild type. **D, E**: Also under physiological conditions, the WOA-effect was observed yielding higher pump currents with increasing extracellular acetate concentrations independently from intracellular acetate application (2.8 mM). **F**: When looking at the absolute currents, one can see, that after light-off, an additional current peak occurred when applying conditions, that would increase the photocurrents in the wild type. Absolute current traces were published (Panzer *et al.*, 2019)

Especially in the field of optogenetics, rhodopsin mutants were created to obtain optimized tools for controlling neuronal firing. ApOps2 2.0(F79A,R112H) mutant (Figure 39A) was created by members of the Georg Nagel group to produce a proton channel with intense photocurrents. The R112H mutation only already yielded a proton channel, but the additional mutation of the conserved F79 to an A further increased the channel currents (Panzer *et al.*, 2021). Here, patch-clamp measurements were performed using different pH- and clamp-voltage conditions. Illumination was achieved via the optic fiber (15 mW/mm²); the light exposure time was set to 1 s. The I-V plot showing a clear pH-dependency obtained from all eight cells depicts here the mean absolute currents (Figure 39B). Furthermore, the photocurrents were voltage-dependent what could be observed best when looking at the current traces of a single cell (Figure 39C). In general, higher currents were obtained with increasing pH or voltage, respectively. Reversal potentials were obtained for extracellular pH 7.4 and pH 5.0. Therefore, absolute current traces were analyzed in Clampfit 10.7 software, the I-V plots were generated and the curves fitted with a straight line fit.

Mean and standard deviation from 8 cells were calculated. At extra- and intracellular NaCl pH 7.4 the ApOps2 2.0(F79A,R112H) construct showed channel characteristics with a reversal potential of -6.3±5.4 mV. At extracellular pH 5.0, no positive current signals occurred in the applied clamp-voltage range, the extrapolated reversal potential was 62±6.9 mV. At extracellular pH 9.0 a reversal potential of -95±12 mV was yielded.

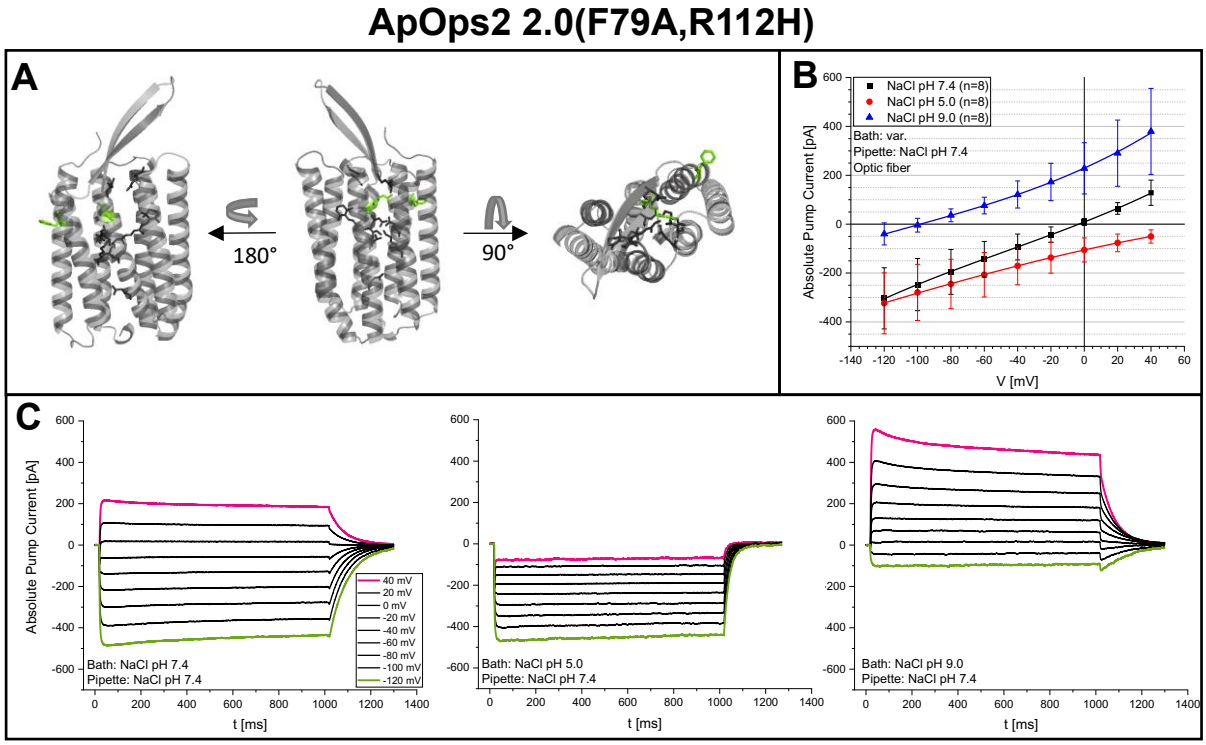

Figure 39: Voltage- and pH-dependency of ApOps2 2.0(F79A,R112H). A: Rhodopsin Model depicting the mutated amino acids F79 and R112 (green). **B:** I-V plot showing means and standard deviations of the absolute photocurrents measured at different clamp-voltages and pH values. The rhodopsin mutant showed channel characteristics yielding positive and negative currents at extracellular pH 7.4 and pH 9.0. In extracellular pH 5.0 only negative currents were obtained in the applied clamp-voltage range. **C:** Absolute photocurrents of one cell. The voltage-dependency was clearly visible yielding lower currents with decreasing clamp-voltage. Plots were published (Panzer *et al.*, 2021)

4.3 *Aureobasidium pullulans* Rhodopsins for Application as Optogenetic Tools

4.3.1 Exploring the Ion Transport Capacity of *A. pullulans* rhodopsins in Comparison to Established Optogenetic Tools ChR2, LR and eArch3.0

Since all *A. pullulans* rhodopsins show rather high pump currents, especially ApOps2 in the improved version 2.0 as well as the ApOps2 2.0 (F79A,R112H) channel mutant, a potential application as an optogenetic tool was obvious since many other rhodopsins are used in this field yet. For example, ChR2, LR or eArch3.0 are important representatives. Many rhodopsins were used as basis for creating improved mutants with enhanced properties for controlling neuronal activities by light. It is also common to color-tune the proteins for yielding pairs of activating and inhibiting rhodopsins.

In this study, as a first step, the intensity dependence of the *A. pullulans* rhodopsins was tested in comparison to well-studied rhodopsins ChR2, LR and eArch3.0. Light intensities (532 nm) ranging from 0.02 to 84 mW/mm² were applied via the optic fiber and with the help of neutral density filters (Table 6) in NaCl-based bath- and pipette solutions at physiological pH 7.4. ChR2 was measured at a clamp-voltage of -60 mV, eArch3.0 and the *A. pullulans* rhodopsins at 0 mV. None of the measured rhodopsins was saturated at 84 mW/mm². Almost all rhodopsins showed an initial current peak at high light intensities, except ApOps2 2.0 with a dominating stationary current at all tested intensities.

Rhodopsins are usually measured at lower intensities (e.g.: CsR, HEK cells: 2.47 mW/mm²; Oocytes: 10 mW/mm² (Fudim *et al.*, 2019); CsR, Oocytes: 0.1-0.3 mW/mm² (Vogt, 2016); Halo/LR: 2.1-5.3 mW/mm² (Chow *et al.*, 2010)); however, also higher intensities were applied (e.g.: ChR2, HEK cells: up to 100 mW/mm²; Oocytes: 3-10 mW/mm² (Nagel *et al.*, 2003)). For further characterization of the *A. pullulans* rhodopsins, 15 mW/mm² were chosen because all three show a sufficient current signal at this intensity (Figure 40D, E, F). Assuming the current value at 84 mW/mm² being 100%, at 15 mW/mm² ChR2 reaches 63±4.9 % of the maximum pump activity (Figure 40A), eArch3.0 reaches 40±6.5 % (Figure 40B), LR 68±6.2 % (Figure 40C), ApOps1 2.0 63±4.2 % (Figure 40D), ApOps2 2.0 50±2.5 % (Figure 40E) and ApOps3 2.0 63±5.4 % (Figure 40F). However, one has to take into account that 532 nm is not the optimal wavelength for exciting ChR2 (ca. 460 nm, (Nagel *et al.*, 2003)), eArch3.0 (550 nm (Okazaki *et al.*, 2014)) and LR (550 nm (Chow *et al.*, 2010)). Therefore, only the three rhodopsins from *A. pullulans* can be compared directly. Here, ApOps2 2.0 showed the highest pump capacity while reaching only about 50% from the maximal value at 15 mW/mm². The current amplitude of this rhodopsin was not impaired after being excited with 84 mW/mm² (data not shown). However, all rhodopsins withstand very high light intensities reaching no saturation level at 84 mW/mm². Since all three *A. pullulans* rhodopsins show relatively high pump currents, they are all potential proteins that could be lined up in the optogenetic toolbar with ApOps2 being the most promising candidate because of its highest pump capacity. As a next step, ApOps2 was tested whether it can be (functionally) expressed in differentiated NG108-15 cells.

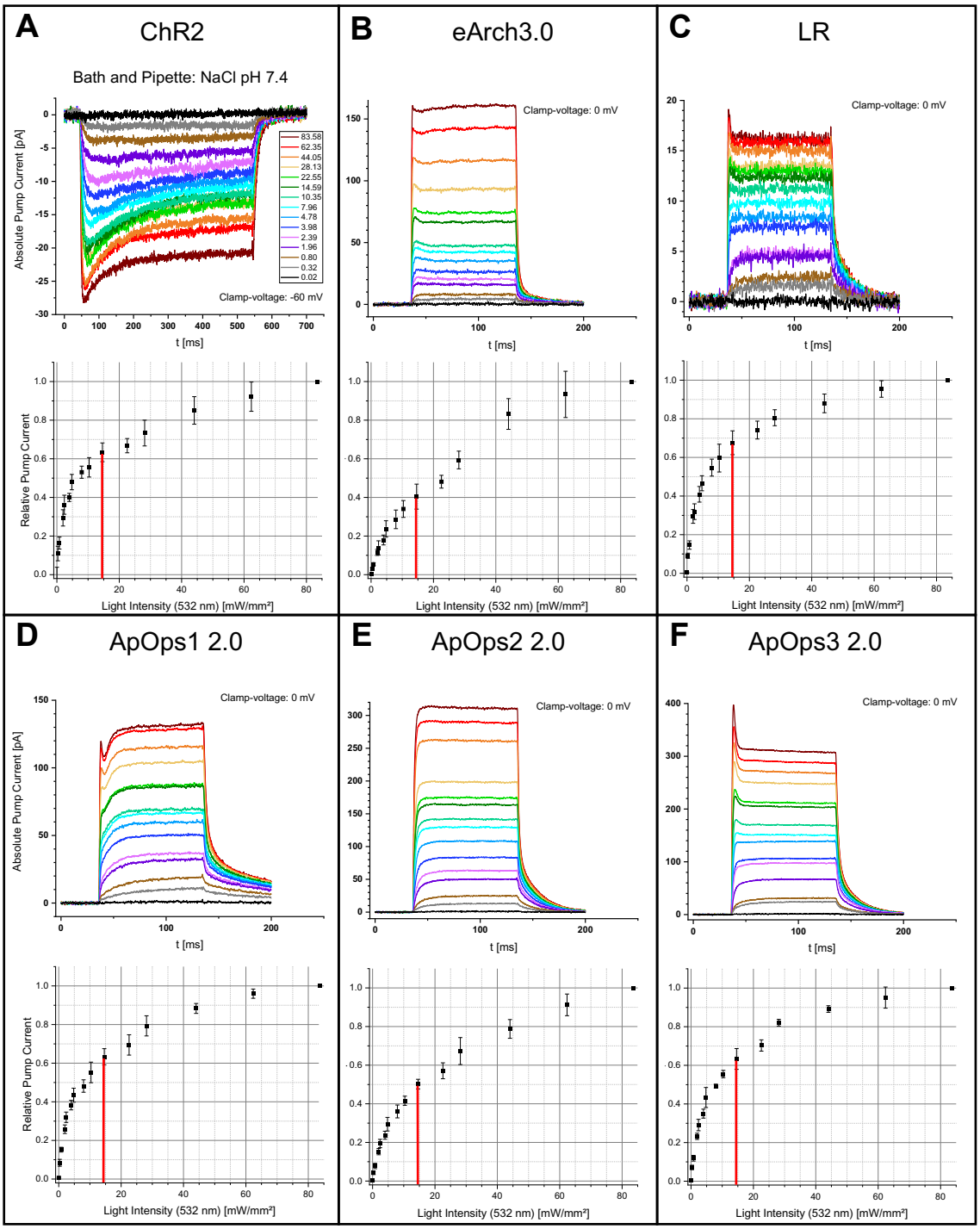

Figure 40: Light Intensity Measurements on Different Rhodopsins. Different light intensities were applied (wavelength 532 nm) via the optic fiber with the help of ND filters under physiological pH conditions. Absolute current traces of one cell of each rhodopsin are depicted as well as the relative current (mean and standard deviation of 5 cells) in dependence of the light intensity assuming the value measured at 84 mW/mm² being 100% (=1.0). The red bars illustrate the mW number (ca. 15 mW/mm²) which was chosen for other patch-clamp experiments. For ChR2 (**A**), eArch3.0 (**B**) and LR (**C**), 532 nm is not the optimal excitation wavelength; therefore, only ApOps1 2.0 (**D**); ApOps2 2.0 (**E**) and ApOps3 2.0 (**F**) can be compared directly. Here, ApOps2 2.0 showed the highest pump capacity, since it reached only around 50% of its maximum pump current at 15 mW/mm² whereas the other two *A. pullulans* rhodopsins reach about 63%. Relative current plots of the *A. pullulans* rhodopsins were published (Panzer *et al.*, 2021)

4.3.2 ApOps2 is Functionally Expressed in Differentiated NG108-15 Cells

For investigating the expression of ApOps2 in neuronal cells, NG108-15 cells were differentiated with the help of bt_2cAMP, Forskolin and IBMX (see chapter 3.1.1.1). After initiating the differentiation process, morphological differentiation was already visible after two days with the cells developing dendrites which were growing further during the following days (Supplementary Figure 20). Functional differentiation was lagging behind the morphological changes and could be observed after 7-10 days by showing the capability to create action potentials (Figure 41A) upon application of a current-clamp (Figure 41B). Cells were preferentially patched in the axon hillock region of the cells (Figure 41D). At the time point of functional differentiation, transient transfection was performed. ApOps2 was expressed in the plasma membrane, only few fluorescence signals were observed intracellularly (Figure 41E). With ApOps2 expressing differentiated NG108-15 cells, patch-clamp experiments were carried out. No action potentials could be observed in transfected cells. However, one could observe a huge repolarization when 532 nm light was applied (Figure 41C). That means, that ApOps2 pumps protons out of the cell and therefor repolarizes the plasma membrane. This was not observed in differentiated cells which do not express the rhodopsin (Figure 41A).

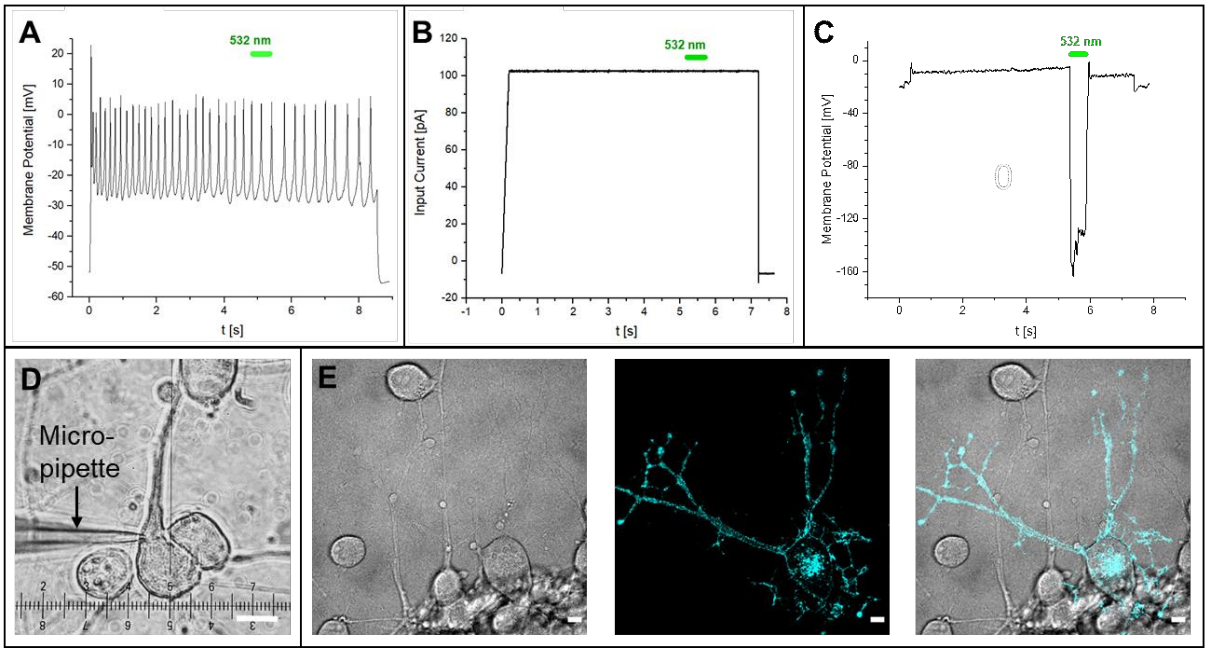

Figure 41: Functional Expression of ApOps2 in Differentiated NG108-15 Cells. 7 to 10 days after differentiation initiation, action potentials could be generated in differentiated NG108-15 cells (**A**) when applying a current-clamp (**B**). Cells were preferentially patched in the axon hillock region (**D**). Transient transfection of differentiated cells yielded plasma membrane localization of ApOps2 (**E**) as well as a strong repolarization event upon green light illumination (**C**). That means that ApOps2 was functionally expressed in differentiated NG108-15 cells.

5 Discussion and Outlook

Electrophysiological as well as microscopic experiments were carried out on fungal rhodopsins in this work. These proteins are very interesting research objects, since they are very abundant among fungi, especially in plant-associated fungi (Adam *et al.*, 2018), but the reason why they are so conserved is not fully elucidated yet. To understand the impact of rhodopsins on fungal biology might be of interest when it comes for example to the fight against plant-pathogenic fungi which cause huge losses in crop harvests. Photoreceptors are key players in the life of fungi and act as regulators of many processes like reproduction, changes in lifestyle or spore germination to just name a few and all of them are connected in a complex regulatory network (Yu and Fischer, 2019). While blue- as well as red-light receptors are well studied, only few information is available about rhodopsins which are designated as green-light receptors due to their ability to bind retinal as chromophore (Ernst *et al.*, 2014). As representatives of microbial rhodopsins, fungal rhodopsins could also be of interest for technical applications like bioelectronics, since these type 1 rhodopsins are capable of ion transport, act more or less as photo diodes and may be more stable in specific detergent environments (Ji *et al.*, 2017). Among the microbial rhodopsins, that are membrane bound proteins consisting of 7 alpha-helices, divers transport properties could be elucidated yet. Many of them are able to transport protons, but also chloride, sodium or cat- or anions in general can be transferred over cellular membranes upon light illumination depending on the amino acid sequence. This transfer can occur unidirectionally depicting a pump rhodopsin or bidirectionally representing an ion channel. (Ernst *et al.*, 2014) In the huge research field of optogenetics, that aims to control neuronal activity by light and that passed a milestone this year by recovering vision at least partially in a blind patient, microbial - and also fungal - rhodopsins are the key players. To optimize their function, mutations are inserted in these proteins to gain even higher photocurrent or to perform color-tuning to yield batho- or hypsochromic shifts concerning the excitation wavelength. (Ernst *et al.*, 2014; Deisseroth, 2015; Sahel *et al.*, 2021; Yawo *et al.*, 2021)

Here, UmOps1 and UmOps2 from *U. maydis* as well as ApOps1, ApOps2 and ApOps3 from *A. pullulans* were characterized electrophysiologically to get information about their ion transport properties. Rhodopsin mutants were created to identify amino acid residues that are key players in this transport process. Current enhancement in the presence of WOA, that was already described in other fungal rhodopsins (García-Martínez *et al.*, 2015; Panzer, 2017; Adam *et al.*, 2018; Bräuer, 2018; Wilczek, 2018), was investigated for the *U. maydis* rhodopsins as well as for ApOps2 by supplementing acetate in the patch-clamp electrolyte solutions under pH 7.4 conditions. ApOps2 was used for the expression in differentiated NG108-15 cells to test the functionality of this fungal rhodopsin in neuronal cells addressing the question whether it is a promising candidate that can be used as an optogenetic tool. Furthermore, microscopic studies were done to elucidate the localization of fungal rhodopsins in the native system, that is in fungal cells. This was done on *U. maydis* sporidia, the yeast-like form of this fungus, via eGFP-tagged UmOps1 or UmOps2, respectively expressing strains. Moreover, an already characterized fungal rhodopsin, CarO from *F. fujikuroi*, was imaged microscopically in addition to confirm the already published localization with the help of counterstaining experiments.

Electrophysiological experiments were performed using the patch-clamp technique on mammalian cells expressing the fungal rhodopsins. For achieving good results in whole-cell mode, it is very important to have the rhodopsins expressed in the plasma membrane. For UmOps1 as well as ApOps1 and ApOps2, the plasma membrane localization in mammalian cells was rather good (Figure 23A and Figure 25A, B). In contrast, UmOps2 was mainly localized intracellularly, however, sufficient photocurrents could be measured (Figure 23B and Figure 26C). This was not the case for the proton donor mutant UmOps1(E129D) which was exclusively located intracellularly and no photocurrents could be observed except in one case (Figure 24A and Supplementary Figure 18B). Since the UmOps1(D225E) proton releasing site mutant, by contrast, showed good membrane localization with only few intracellular fluorescence signals and yielded sufficient current signals (Figure 24B and Figure 38F), it may be, that inserting mutations could have impact on the protein folding process and therefore enhance or impair the trafficking process or functionality. However, glutamate as well as aspartate, both are polar amino acids and therefore the protein core should not be destabilized in a huge manner (Baruah and Biswas, 2014; Kumar and Biswas, 2019). Maybe, the overall secondary structure of UmOps1(E129D) is slightly shifted and trafficking signals may be somehow impaired or do not fulfill the appropriate function correctly. According to spectroscopic data it was even speculated that E129 may not be the proton donor in UmOps1 (La Greca *et al.*, under review). The corresponding mutation of the proton releasing site in CarO(E224D) also showed sufficient accessibility to patch-clamp experiments while being localized intracellularly as well as partly in the plasma membrane (Wilczek, 2018). The 2.0 membrane trafficking cassette was tested for the *A. pullulans* rhodopsins to improve the membrane localization and indeed the three rhodopsins and additionally the ApOps2 2.0(F79A,R112H) channel mutant were almost exclusively expressed in the plasma membrane (Figure 25C, D).

As already mentioned, fungal rhodopsins belong to the huge group of microbial rhodopsins. Rhodopsins of the bacterial and archaeal subgroup are well studied in terms of electrophysiology as well as structural information. For fungal rhodopsins, only few data are available concerning ion transport functions of the representatives of this subgroup and only recently the first crystal structure of a fungal rhodopsin, LR, was resolved (Adam *et al.*, 2018; Bergo *et al.*, 2002; García-Martínez *et al.*, 2015; Waschuk *et al.*, 2005; Fan *et al.*, 2011). From this structure, an interaction between ECL1 and the N-terminus was assumed that might be involved at least in stabilization and membrane orientation of this protein. The rhodopsins analyzed in this work were modelled using the LR- as well as the CsR crystal structure (Figure 3) (Fudim *et al.*, 2019; Zabelskii *et al.*, 2021). Both templates yielded slightly different models with different QMEANDisCo values. However, all of those quality parameters were in a good range and together with the conserved amino acid regions that were identified to be necessary for proton transport in BR (Table 1 and Supplemetary Figure 1), the predicted function of UmOps1 and UmOps2 as well as ApOps1, ApOps2 and ApOps3 is the unidirectional transport of protons (out of the cytosol). Furthermore, in all five studied rhodopsin, the very conserved lysine residue in helix 7 is present, that was shown to bind the retinal chromophore via Schiff base (Ernst *et al.*, 2014). On the basis of the models one can see that the retinal chromophore would fit into the protein pocket of all five rhodopsins. These observations give an indication for the tested rhodopsins to be green-light-driven proteins. Fungal rhodopsins, that were electrophysiologically characterized so far, are exclusively outward proton

pumps that are activated by green light, however showing different characteristics when it comes to the photocycle, e.g., fast or slow cycling (Bieszke, Spudich, *et al.*, 1999; Waschuk *et al.*, 2005; Fan *et al.*, 2011; García-Martínez *et al.*, 2015; Panzer, 2017; Bräuer, 2018).

Patch-clamp experiments done on UmOps1, UmOps2 and the three *A. pullulans* rhodopsins indeed identified all five rhodopsins to be ion pumps that are driven by green light and transport protons out of the cytosol with the 2.0 cassette not altering the transport characteristics in a visible or measurable manner (Figure 26-28, Figure 30, 31, Supplementary Figure 6-8, Supplementary Figure 11; Supplementary Table 1). However, with respect to the LR crystal structure, one should consider that the N-terminus could also be of importance in regulation of the protein function and thus altering this region should be considered carefully. The maximal pump activity for all five rhodopsins was achieved under green light illumination yielding bell-shaped action spectra like it was the case for previously characterized fungal rhodopsins (Chow *et al.*, 2010; Fan *et al.*, 2011; García-Martínez *et al.*, 2015, 2015; Panzer, 2017; Bräuer, 2018). Perceiving green light makes sense especially for plant-associated fungi since those wavelengths are not exploited for photosynthesis and therefore dominate in the phyllosphere. However, in a recent study, the authors claim that light can be modulated by the fungal cell wall. The structure of the components may alter and define the light that reaches intracellular structures (Baró *et al.*, 2021). Therefore, also the wavelengths that fall onto fungal cells may change during transmission of the cell wall and – e.g., exhibit a different wavelength when hitting the plasma or inner membranes and therefore the rhodopsins. This is a further hint, that photobiology in fungi is a very complex issue, also since fungi exhibit different cell wall compositions among the species and even in one species the structure can change depending on the developmental stage or environment (Gow, Latge and Munro, 2017).

All five rhodopsins showed outward pump currents with current densities that were similar at 0 mV clamp-voltage under different pH- and clamp-voltage conditions (intracellular pH 7.4 or 5.0 and extracellular pH 7.4, 5.0 or 9.0) in presence of NaCl as well as when supplementing intracellular sodium with cesium (except for ApOps3, discussed later) or extracellular chloride with gluconate (Figure 33, 34). That means, per exclusion principle, that most likely only protons are transported. Also, the voltage- and the pH-dependency in most cases indicated proton transport with higher pump currents at higher clamp-voltages or pH-value due to the electrochemical gradient. The proton transport was further confirmed by using different extracellular ion compositions in TEVC measurements (Panzer *et al.*, 2021). In general, the *U. maydis* rhodopsins yielded rather small photocurrents with mean current densities lower than 0.1 pA/pF for UmOps1 and lower than 0.2 pA/pF for UmOps2 under NaCl-based physiological conditions at 0 mV clamp-voltage, whereas the *A. pullulans* rhodopsins showed relatively high ones (mean 4.5 pA/pF and above) with ApOps2 reaching the highest single cell value up to 15.8 pA/pF in one cell (Supplementary Table 3). The current density of CarO from *F. fujikuroi* under comparable conditions was 2.2±0.63 pA/pF (García-Martínez *et al.*, 2015). However, direct comparison of the current densities between the *A. pullulans* rhodopsins and CarO, UmOps1 and UmOps2 is not possible, because for the latter three, no optic fiber illumination with a defined light intensity of 15 mW/mm² was used. This issue was addressed as an example for ApOps2 (Supplementary Figure 14): When measuring HEK cells stably expressing ApOps2 in comparison to transiently with ApOps2 2.0 transfected NG108-15 cells, the current density was not significantly different when measured with the optic fiber, but

showed a huge increase when measuring the HEK cell line with direct laser illumination with most likely higher and maybe unstable light intensities. Unstable light intensities can occur, when the laser settings were not optimized via intensity measurements because diode pumped lasers show fluctuating emission and only in a small power output range, the emission is linear and stable (see chapter 3.3.2). Thus, one can assume, that *U. maydis* rhodopsins as well as CarO would yield even lower current densities when being measured with the optic fiber and therefore also in comparison with the *A. pullulans* rhodopsins.

Regarding the current decay after light-off, a biexponential function was used to fit the data yielding a fast and a slow time constant with the slow one showing a clear voltage-dependency (Figure 35, Supplementary Figure 16). This is in accordance with previous results obtained for BR (Geibel *et al.*, 2001). Whereas the fast time constants were in a similar range, also in comparison to CarO, that showed a fast time constant of 1.4±0.26 ms at 0 mV clamp-voltage (García-Martínez *et al.*, 2015), the slow time constants differed among the rhodopsins yielding higher ones for UmOps1 and ApOps1. UmOps2, ApOps2 and ApOps3 lie in a similar range compared to CarO (20±3.8 ms at 0 mV clamp-voltage) (García-Martínez *et al.*, 2015) and also to BR. In the case of BR, it was also stated, that this voltage-dependent decay determines the voltage-dependency of the stationary currents (Geibel *et al.*, 2001). This relation can be transferred to the *A. pullulans* rhodopsins, since the proteins can be activated only when the photocycle was passed completely and the rhodopsin is again in the ground state. The longer it takes to regain the ground state for the single proteins (i.e., higher slow time constant at lower clamp-voltage), the lower is the stationary current because less proteins already gained the ability to be reactivated. To gain more insights into features of the rhodopsin photocycles, one could perform spectroscopic measurements, also with respect to the different characteristics of the single rhodopsins. However, since one can assume a higher pump activity when yielding smaller time constants in general, ApOps2 and ApOps3 as well as UmOps2 are more potent pumps compared to ApOps1 or UmOps1, respectively.

For the *A. pullulans* rhodopsins, the number of activated pumps in the cellular membrane was calculated (not depicted in the Result section). This was done by calculating the product of the stationary pump current and the slow time constant of the current decay after light-off divided by the elementary charge and the cell surface area. The cell surface area was obtained from the membrane capacitance divided by the specific membrane capacitance of NG108-15 cells (1,72±0.14 µF/cm²) (Feldbauer *et al.*, 2016). 10.8±7.2 * 10^3 pumps/µm² (n=5) were calculated for ApOps1 2.0, whereas ApOps2 2.0 and ApOps3 2.0 yielded lower values of 7.4±5.7 * 10^3 pumps/µm² (n=5) and 4.9±2.9 * 10^3 pumps/µm² (n=8), respectively, what means a higher pump power at lower expression rate. This result is in accordance with the current density as well as the kinetics measurements. Moreover, the number of activated pumps is in a similar range compared to previous results performed on HEK-cells expressing ChR2-eYFP (Zimmermann *et al.*, 2008). A further experimental setting confirmed the higher pump activity of ApOps2 compared to ApOps1: Each of the two rhodopsins was combined with another rhodopsin (ChR2) in one tandem cassette, to directly compare the pump currents independent from the expression as it was described previously (Kleinlogel *et al.*, 2011; Diemar, 2016; Feldbauer *et al.*, 2016; Yogendran, 2018; Vierock *et al.*, 2020). Indeed, ApOps2 showed a 4-fold pump activity in comparison to ApOps1 and even a

higher activity than LR under the given conditions (Diemar, 2016; Yogendran, 2018; Panzer *et al.*, 2021).

Having a closer look on the current traces and I-V-plots in general, every rhodopsin showed special characteristics that are unique. This issue was also taken up by Arend Vogt, who characterized a bunch of rhodopsins yielding different voltage- and pH-dependent as well as different current and kinetic characteristics throughout the analyzed proteins (Vogt, 2016). Also, among the *U. maydis* and the *A. pullulans* rhodopsins, different characteristics were visible. At first, it has to be mentioned, that one rhodopsin of *U. maydis*, namely UmOps3, is not even expressed under laboratory conditions, but only *in planta*, where it might act as a stress sensor as it was described among the small heat shock proteins (Estrada *et al.*, 2009; Ghosh, 2014; Brych *et al.*, 2016). The other two *U. maydis* rhodopsins, UmOps1 and UmOps2, by contrast, are expressed in axenic cultures. For the *A. pullulans* rhodopsins, this issue still remains to be elucidated. The five rhodopsins that were electrophysiologically analyzed here, also showed special features that are individual for the respective rhodopsin. ApOps3, as already indicated above, showed significantly decreased current densities when measured with intracellular cesium (Figure 34C) what could be an indication for an additional sodium transport or, what is more likely with respect to the amino acid sequence, a regulatory effect of the ion species that is present. Either cesium impairs the function or sodium boosts the function of this rhodopsin. The latter case is more plausible since *A. pullulans* is a halotolerant fungus which inhabits (among plant surfaces) also salterns where it has to deal with high salt concentrations (Gunde-Cimerman *et al.*, 2000; Kogej *et al.*, 2005; Zajc *et al.*, 2012). Therefore, sodium could enter the cell due to the chemical gradient and cause increased proton currents over the plasma membrane via ApOps3 which in turn forges a proton gradient over the membrane that could be used as energy source for outward sodium transporters. To address this hypothesis, the subcellular localization of ApOps3 could be investigated via fluorescence microscopy and if ApOps3 localizes to the plasma membrane, this would be a further hint for the rhodopsin being involved in sensing the environmental ion composition. Another feature that was only observed in ApOps3 was the leakage current right after light-on in extracellular pH 5.0 independently of the present ion species (NaCl, CsCl or NaGluc) (Figure 30C, Supplementary Figure 12C, 13C). For a very short time period (less than 1 ms), negative currents occurred what means that the pump needs some time to reach the full activity under conditions where the electrochemical gradient works against the pump direction. A characteristic that was observed in ApOps1 and ApOps3 was the saturation of the pump current under extracellular acidic conditions when applying positive clamp-voltages in intra- and extracellular NaCl (Figure 28C, E). For ApOps1 it could be tested and shown, that this saturation gets stronger and the voltage-dependency was virtually reversed when applying even higher clamp-voltages up to 100 mV (Supplementary Figure 9). This saturation disappeared in both rhodopsins when applying extracellular NaGluc; when applying intracellular CsCl, it disappeared in ApOps1 and was also weaker in ApOps3 (Figure 31C, E, 32C, E). This result, taken together with the ion leakage of ApOps3 indicates a very fine-tuned regulatory effect of the ion species and the surrounding pH that are present on the rhodopsin pump properties. Previous research showed, that it is even possible, that the transported ion species can change depending on the environment, for example, KR2 turns from a sodium to a proton pump in the presence of potassium, rubidium or cesium (Inoue *et al.*, 2013) what illustrates the high sensitivity of those proteins to their surroundings.

According to this, another explanation for the saturation of the pump current in ApOps1 and ApOps3 could be, that at specific conditions, chloride ions are also transported outwards by the rhodopsins. However, this is very unlikely considering the amino acid sequence (Ernst *et al.*, 2014).

When further looking at the absolute current traces, one can see that in all rhodopsins except ApOsp2, initial current peaks occur, at least at lower clamp-voltages (Figure 29, 30). The height of the initial peak current depends strongly on the relay time between the two light pulses. This relay time was for UmOps1 and UmOps2 2 s between the sweeps and 20 s between the single runs that were averaged, for the *A. pullulans* rhodopsins the relay time between the sweeps were 3 s and 30 s between the runs. Since this delay was equal for the three *A. pullulans* rhodopsins, this issue can be excluded as a cause for the lacking current peak in ApOps2, where the stationary currents were always dominating.

A very striking feature was observed in another one of the studied rhodopsins, namely UmOps1, which yielded a massive current enhancement in extracellular pH 5.0 (Figure 28A, 29A and Supplementary Table 2). This unusual characteristic was already described before (Panzer, 2017) and contradicted the assumption of a proton pump at a first glance. However, since the current densities under cesium and gluconate conditions were similar to that in NaCl, it is most likely, that UmOps1 is an outward directed proton pump, also with respect to the conserved amino acid residues. However, some slight variations can be depicted regarding the amino acid sequence when comparing UmOps1 with BR. To address the question, whether these slight variations could lead to this striking characteristic, mutations were done and patch-clamp measurements performed. In the proton donor site, BR and the other fungal rhodopsins tested here have an aspartate (BR D96), but UmOps1 contains a glutamate at the respective position 129. The respective vice versa mutation in LR (D150E) lead to NR-like characteristics meaning less pump activity (Fan *et al.*, 2011). Thus, the E129D mutation in UmOps1 was used to address not only the striking pH dependency, but furthermore the question whether the very low stationary pump currents of this rhodopsin may be caused by this amino acid residue. As already mentioned, the E129D mutation in UmOps1 resulted in almost complete absence of photocurrents (Supplementary Figure 18B). Moreover, the protein was not trafficked to the plasma membrane in a sufficient manner (Figure 24A). To test whether the poor currents were only caused by the internal localization or indeed due to the non- functionality of the rhodopsin mutant, one can consider to modify this mutant with the 2.0 trafficking cassette that enhanced plasma membrane localization of the *A. pullulans* rhodopsins in NG108-15 cells as well as in oocytes (Panzer *et al.*, 2021). In addition, other expression and measuring systems could be tested, for example *Saccharomyces cerevisiae* or giant unilamellar vesicles (Bertl *et al.*, 1998; Terpitz *et al.*, 2008; Garten *et al.*, 2017). This result shows that it is not necessarily possible to expect a specific characteristic only by mutating an amino acid showing a special characteristic in another rhodopsin. A further UmOps1 mutant was created addressing the proton releasing group. UmOps1 carries an aspartate at position 225, whereas BR carries a glutamate at the respective site (BR D194). The UmOps1(D225E) mutant yielded good plasma membrane localization as well as sufficient photocurrents in patch-clamp measurements (Figure 24B and Figure 38). Indeed, a change in pH dependency was observed compared to the wild type whereas the voltage-dependency with higher pump currents at higher clamp-voltages and also the action spectrum remained similar. The massive current enhancement of the wild type in

extracellular pH 5.0 was abolished in UmOps1(D225E) depicting lower pump currents in this condition compared to physiological pH 7.4. This result indicates, that the proton releasing group is a key player for the extraordinary rapid transport of protons in UmOps1 under acidic conditions. It seems to be necessary to release the protons fast so that the photocycle is not impaired and a proton jam occurs. This assumption is supported by the occurrence of a small current peak after light-off in the UmOps1(D225E) mutant. This peak indicates an accumulation of protons inside the rhodopsins which cannot be transported in a sufficient way while the proteins cannot fulfill the whole photocycle under light conditions. After light-off, the proteins relax back to the ground state and the protons are released by all rhodopsins stuck in a specific intermediate. However, ApOps3 and LR wild type each possess also an aspartate at this respective position in the proton releasing group. Neither for ApOps3 this stunning pH dependency was observed here, nor it was reported for LR yet. The latter one was shown to reveal BR-like pH-dependent characteristics concerning its photocycle and BR did not show current enhancements in acidic environments in electrophysiological experiments (Geibel *et al.*, 2001; Waschuk *et al.*, 2005). This again implicates that the specific characteristics of rhodopsins cannot be directly predicted via slight amino acid variations. However, for BR it could be shown that the proton releasing group plays a crucial role in how fast the photocycle can be passed. Proton uptake and release by this group are rate-limiting steps in the proton transport process and dependent on pH and the amino acid moieties that are present. (Misra *et al.*, 1997; Balashov *et al.*, 1999)

It was previously shown that especially fungal CarO-like rhodopsins react to extracellular WOAs. This issue was checked for CarO itself as well as for UmOps1 by supplementing the extracellular medium with different concentrations of acetate at a pH of 5.0. The photocurrents were enhanced in a dose-dependent manner. In both rhodopsins, this boosting effect was also observed when using IAA, and in UmOps1 furthermore when using IPA. However, the boosting effect was smaller with increasing carbon chain length. Preliminary experiments indicated the presence of the WOA-effect caused by acetate also for ApOps2. For UmOps2, an LR-like fungal rhodopsins, as well as for BR, these effects could not be observed in such a great manner. (García-Martínez *et al.*, 2015; Panzer, 2017; Adam *et al.*, 2018; Bräuer, 2018)

In this work, it was firstly checked for UmOps1 whether this acetate effect was visible also under physiological conditions, since previously, the striking boosting effect of pH 5.0 was additionally addressed in the experiments when using pH 5.0 based solutions, yielding up to 64-fold photocurrents compared to pH 7.4 without acetate (Panzer, 2017). When applying extracellular acetate under pH 7.4 conditions, UmOps1 yielded higher photocurrents with higher acetate concentrations, while again, in UmOps2 this current increase was not observed (Figure 36A, C and Supplementary Table 4). However, since the pH 5.0 boost was lacking for UmOps1, the increase ratios were smaller here: When supplementing the extracellular medium with 14 mM acetate at a pH of 7.4, the currents were enhanced 3.5-fold at 0 mV clamp-voltage compared to zero acetate while they were increased 64-fold under pH 5.0 conditions. That shows again, that UmOps1 is highly sensitive to pH changes. Also, for CarO, the acetate effect could be shown under physiological conditions (Wilczek, 2018). Since two of the *A. pullulans* rhodopsins, ApOps1 and ApOps2, are CarO-like rhodopsins, the acetate boosting effect was also expected for them, but not for ApOps3, what belongs, among UmOps2, to the LR-like rhodopsins. Up to now, this issue

could only be checked for ApOps2; for ApOps1 as well as ApOps3, the acetate effect still remains to be investigated. ApOps2 was used without and with the 2.0 modification and like it was the case in the pH dependency measurements, this 2.0 trafficking cassette did not alter the results in a considerable manner (Figure 37A, C; Supplementary Figure 17 and Supplementary Table 4). When applying different concentrations of acetate to the extracellular NaCl-based solution, in ApOps2, a dose-dependent enhancement of the photocurrents occurred. The ratio of the pump currents when applying 0 mM or 14 mM acetate was with 1.5 smaller compared to UmOps1 assuming the latter one being more sensitive to this extracellular stimulus. In terms of the acetate effect, a frequently discussed issue was addressed moreover: Acetate may diffuse over the plasma membrane in its protonated state, deprotonates there, causes an intracellular pH decrease and therefore boosts the proton transport. This mechanism is used frequently to acidify the intracellular space in oocyte experiments. The pK_a of acetate is 4.76; thus, at pH 5.0 about half of the molecules should be protonated and therefore being capable to pass the membrane and cause this acidifying effect. This should not be the case under physiological conditions (pH 7.4), where almost all molecules are deprotonated. However, several studies could show that there are microdomains along the plasma membrane where the pH can drastically change locally caused for example by proton transporters even when the solution is buffered (Zeng and Xu, 2012; De-la-Rosa *et al.*, 2016; Ferenczi *et al.*, 2016). Thus, it is theoretically possible, that also the rhodopsins themselves cause local pH changes to enable acetate diffusing through the plasma membrane. To address this, 2.8 mM intracellular acetate was applied to UmOps1 or ApOps2/ApOps2 2.0 expressing cells and measurements were done using different extracellular acetate concentrations. Similar boosting effects occurred compared to measurements without intracellular acetate, even at equimolar intra- and extracellular acetate concentration (Figure 36B; Figure 37B; Supplementary Figure 17 and Supplementary Table 4). When the extracellular acetate concentration exceeds the intracellular one, one could see slightly enhanced pump currents compared to measurements without intracellular acetate. Similar results were obtained for CarO (Wilczek, 2018). One has to consider further, that the chemical gradient only can be taken into account for deprotonated acetate due to intra- and extracellular pH 7.4 so that it would be theoretically still possible that protonated molecules enter the cell and are deprotonated there. In general, the results lead to the conclusion, that it may indeed be that a small amount of the acetate molecules enters the cell and causes very slightly enhanced pump currents what was also visible in UmOps2 and BR (Figure 36C; Supplementary Table 4; BR: data not shown). However, the enhancement in UmOps1 as well as in ApOps2 and also in CarO when increasing the extracellular acetate concentration was heightened in a considerably larger scale compared to UmOps2 and BR so that there is a clear indication that the supporting effect of acetate in UmOps1, CarO and ApOps2 occurs most likely via an interaction site on the extracellular part of the protein. This interaction with WOAs could be a hint for a plant-fungus interaction since IAA is a common plant hormone involved in many regulation processes and even the fungi themselves are able to produce this auxin (Buckley and Pugh, 1971; Felle *et al.*, 1986; Rück *et al.*, 1993; Woodward and Bartel, 2005; Spaepen, Vanderleyden and Remans, 2007; Reineke *et al.*, 2008; Tsavkelova *et al.*, 2012; Sun *et al.*, 2019). However, the effect of IAA still remains to be elucidated for the *A. pullulans* rhodopsins. The D225E mutation of UmOps1 had only a slight effect on the acetate mediated current enhancement. The photocurrents still were increased with increasing acetate concentration, however with slightly decreased ratios compared to the wild type in higher

acetate concentrations (Figure 38C, D, E, F and Supplementary Table 4). That indicates that the proton releasing group is a key player in the striking pH dependency of UmOps1 but only plays a minor role in acetate signaling. Interestingly, the measurements using intracellular acetate did not yield slightly higher photocurrents compared to measurements without intracellular acetate at higher extracellular acetate concentrations like it was the case for the wild type UmOps1 and also for ApOps2. Moreover, when looking at the measurements with NaGluc as bath solution, a slight current enhancement was observed in wild type UmOps1 and UmOps2 as well as in ApOps1, ApOps2 and ApOps3 since NaGluc is also a WOA. Taken together, the results indeed suggest a general boosting effect of WOAs, however with acetate yielding striking enhancements in photocurrents that in contrast do not occur in all rhodopsins in the same manner but seem to be specific for CarO-like rhodopsins. As already mentioned before, spectroscopic methods could be used to shed more light onto the photocycles of those rhodopsins to gain more information about intermediate states and effects of WOAs on the protein`s photocycles. Researchers of the Ramona Schlesinger Lab (Freie Universität Berlin, Fachbereich Physik) showed that UmOps1 can be purified in a sufficient manner to perform spectroscopy to unveil more details about the photocycle of this rhodopsin. Similar characteristics were yielded in terms of the intermediate states when comparing to the data of the BR photocycle. Strikingly, under acidic conditions the UmOps1 photocycle was faster than in physiological pH, what was not the case for BR. Moreover, the presence of IAA had an accelerating effect on the photocycle. (La Greca *et al.*, under review). These results are consistent with the electrophysiological observations made in this and previous work (Panzer, 2017; Panzer *et al.*, 2019).

ApOps2 was considered as a promising candidate for the application in optogenetics due to its high pump activity. Moreover, this was the rhodopsin yielding the highest pump capacity out of the three *A. pullulans* rhodopsins reaching only about 50% of the maximal pump activity at 15 mW/mm² whereas the other two reached already about 63% (Figure 40). Thus, it was tested, whether this rhodopsin could be functionally expressed in neuronal cells. Therefore, NG108-15 cells were differentiated (Supplementary Figure 20). As expected, the morphological preceded the functional differentiation. Dendrites were already visible on the second day after differentiation initiation, whereas action potentials were yielded not before day 7. When functional differentiation took place, the neuronal cells were transiently transfected with the ApOps2-eYFP construct and indeed the rhodopsin was trafficked to the plasma membrane (Figure 41E). This localization is necessary to repolarize the membrane via ion transport. No action potentials were reached in transfected cells, however, upon green light illumination, a huge drop in the membrane potential was visible that implies the correct function of ApOps2 depicting the potential to repolarize the membrane (Figure 41C). In untransfected cells, no potential changes were visible upon green light illumination and action potentials were not impaired by the light pulses (Figure 41A). One can conclude, that it is possible in general to use ApOps2 as an optogenetic tool for the manipulation of neuronal cells but maybe another expression system should be preferred. First experiments with primary neurons could also show that ApOps2 can be expressed in the plasma membrane of those cells (unpublished data from Christian Werner). Moreover, drosophila experiments are imaginable. Over the course of the optogenetic experiments, channel mutants of the *A. pullulans* rhodopsins were created by mutating a conserved arginine residue that could be shown previously to change a pump into a channel (Panzer *et al.*, 2021). This residue was mutated before in CsR (CsR(R83Q))

and in CarO (CarO(R114Q)) resulting in channel currents (Vogt *et al.*, 2015; Wilczek, 2018). Another residue that was additionally mutated in the *A. pullulans* rhodopsins was a phenylalanine at the corresponding position to CsR Y58. In the latter one, this amino acid is near a position (Y57) that was shown to be involved in the proton transport. In ApOps2, F79 sits on the outside of the protein (Figure 39A) like it is the case for CsR Y58 when looking at the rhodopsin models (Vogt *et al.*, 2015). However, in ApOps2 2.0 and ApOps3 2.0 (but not in ApOps1 2.0) slightly enhanced channel currents occurred in oocyte measurements, when mutation of F79 was done in addition to the arginine mutation (Panzer *et al.*, 2021). Maybe mutation of F79 leads to slight rearrangements in the whole helix or protein so that Y78 (corresponding position to CsR Y57) and therefor the proton transport is influenced. Moreover, one has to take into account, that the ApOps2 model is based on the CsR template and not on structural information deriving from crystallographic experiments. Therefore, it might be that F79 in reality does not sit on the outside of the protein pocket but might be tilted to the inside and is somehow involved in the proton transport process. From all three *A. pullulans* rhodopsins, ApOps2 2.0(F79A,R112H) yielded the highest relative currents in TEVC measurements in oocytes (Panzer *et al.*, 2021). Thus, this construct was also measured on the patch-clamp setup in NaCl-based intra- extracellular solutions depicting intracellular pH 7.4 and extracellular pH 5.0, pH 7.4 or pH 9.0 (Figure 39B, C). The Nernst potential of protons should be 0 mV for equal intra- and extracellular pH, 141.6 mV for intracellular pH 7.4 and extracellular pH 5.0 and -94.4 mV for extracellular pH 9.0 and intracellular pH 7.4. The mutant showed clear characteristics of a proton channel with a reversal potential of -6.3±5.4 mV at intra- and extracellular pH 7.4 and a reversal potential of -95±12 mV at extracellular pH 9.0 and intracellular pH 7.4. At extracellular pH 5.0 (intracellular pH 7.4) no reversal potential could be observed directly in the measurements. Linear extrapolation suggests a reversal potential of 62±6.9 mV, what is lower than the expected one. However, the linear fit may distort the extrapolated value since obviously the curve is not exactly linear. Moreover, maybe regulatory effects are present at extracellular acidic pH that modify the characteristics of the channel mutant under these conditions. Nevertheless, taking together, ApOps2 can be considered as a promising candidate for further experimenting in terms on optogenetic research.

To summarize the results so far, five rhodopsins were identified as green-light-driven outward proton pumps with each rhodopsin showing specific characteristics depending on the environment. It is furthermore interesting to find out more about the rhodopsins regarding their function in the native system, the fungi themselves. The first step was to localize selected rhodopsins in fungal cells with the help of fluorescence microscopy. For CarO from *F. fujikuroi*, it could be shown before, that the rhodopsin is localized in the plasma membrane and in intracellular structures (García-Martínez *et al.*, 2015). The assumption, that those intracellular structures are the vacuolar membranes, could be confirmed here with the help of counterstaining experiments using pHrodo Red as a vacuole marker as well as FM4-64 as a plasma membrane and tonoplast marker (Figure 14 and Figure 17). CarO-eYFP showed colocalization with the latter dye in the plasma membrane region of *F. fujikuroi* conidia when staining was performed on ice what prevents FM4-64 being internalized. When performing the staining at RT, FM4-64 is internalized and transported to the tonoplasts where it also colocalized with CarO-eYFP. When staining *F. fujikuroi* hyphae with pHrodo Red, the CarO-eYFP signals were found to surround the pHrodo Red marked vacuoles. This kind of counterstaining experiments was also carried out using *U. maydis* sporidia expressing

either UmOps1-eGFP or UmOps2-eGFP (Figure 14 and Figure 17). UmOps1 was exclusively found in the plasma membrane whereas UmOps2 signals could only be observed in the tonoplasts or in the ER, in the latter one due to extensive expression. ER-localization was confirmed by using the ER-Tracker dye (Supplementary Figure 2 and Figure 16). None of the three rhodopsins showed colocalization to the SYTO 59 dye that labels the nuclei in *F. fujikuroi* hyphae and mitochondria in *U. maydis* sporidia. With the help of Mitotracker Orange, the labelling of mitochondria in sporidia was confirmed (Figure 15). The differing localization of UmOps1 and UmOps2 in *U. maydis* is in line with the different characteristics of the two rhodopsins in electrophysiological experiments. UmOps1 reacted to extracellular stimuli like pH-changes or acetate in a much greater manner compared to UmOps2, what makes sense since UmOps1 in the plasma membrane is closer connected to the environment than UmOps2 in the vacuoles. This distribution of rhodopsins inside fungal cells could also be shown recently for two rhodopsins of *A. alternata* with OpsA localizing to the tonoplasts and OpsB residing in the plasma membrane (Pinecker, 2020). Both of them also show ion transport activity (unpublished data from Ulrich Terpitz) that still remains to be further analyzed and characterized. Another rhodopsin, however not closely related to the fungal rhodopsins since it is a gene fusion product of rhodopsin and guanylyl cyclase, BeGC1 from *B. emersonii*, was found to be located in the plasma membrane near the eyespot (Avelar *et al.*, 2014).

Since the localization of CarO, UmOps1 and UmOps2 could be depicted well using conventional super-resolution fluorescence microscopic techniques, the application of novel methods like ExM and CLEM was tested. ExM could be successfully performed on sporidia expressing UmOps1-eGFP (Figure 19) yielding an expansion factor of 4.6 what is typical for the applied protocol, since the expansion factor depends on the crosslinker concentration in the gel (Wassie, Zhao and Boyden, 2019). One challenge that had to be solved in advance was the digestion of the fungal cell wall since complete removal of it is a premise for expansion. Since fungal cell walls differ in their structure depending of the fungal species and even in one fungus differences can occur depending on the developmental stage or environmental conditions, an enzyme cocktail containing lysing enzyme from *Trichoderma*, chitinase and driselase and was used, termed LCD enzyme mix. Indeed, this LCD enzyme mix application resulted in complete protoplastation after 1 h (Figure 18A, B) and therefore sufficient expansion of sporidia. One has to take into account, that the cells have to be fixated before digesting the cell wall to preserve the original shape of the sporidia (Figure 18E). When first digesting the cell wall, then fixation of the fungal cells takes place and the ExM protocol is applied, spherical expanded protoplasts are obtained (Götz *et al.*, 2020). Another critical step is the homogenization of all cellular components with Proteinase K that is also required for sufficient expansion. Usually when using organic dyes, one can easily homogenize the cells over night, but since the chromophore in the experiments here was eGFP, this FP would may also be affected by the homogenization process, however not in such a great manner like other proteins, because eGFP shows greater stability in the presence of Proteinase K (Aoki *et al.*, 2008; Faulkner, Thomas and Neely, 2020). Sufficient expansion was already obtained when performing homogenization for 30 min. Also, after 45 or 60 min of homogenization sufficient fluorescence signals were obtained as expected so that 1 h of homogenization was set to be the chosen homogenization time. In the expanded images, UmOps1 reveals a somehow spotty distribution along the plasma membrane. It would be of interest to test, whether the native distribution is altered by the fixation method and a different picture could be obtained by using for example glyoxal for an initial fixation step since it

is difficult to reach appropriate fixation when it comes to membrane proteins and glyoxal was shown to preserve the native structure better compared to FA or GA (Stanly *et al.*, 2016; Richter *et al.*, 2018).

Among UmOps1, in *U. maydis* also α-tubulin marked with an antibody (label ATTO647) could be expanded. ExM was furthermore successfully applied on other fungi by using the LCD enzyme mix for digestion of the cell wall. In *Fusarium oxysporum*, the expanded plasma membrane could be depicted with the help of the lipid membrane integrating dye mCling resulting in an expansion factor of about 4.4. Moreover, expanded nuclei were shown via a histone-H1-mCherry construct. In *Aspergillus nidulans*, mitochondria labeled via mRFP tagged to the N-terminus of citrate synthase as well as again the plasma membrane via mCling could be visualized in an expanded manner revealing an expansion factor of 4.4. (Götz *et al.*, 2020)

Thus, it could be shown, that ExM provides a relatively easy application for the use of super-resolved microscopy in fungi what is necessary since fungi are very tiny organisms and many subcellular structures are below the diffraction limit. Moreover, this technique can be applied in a normal wet-lab containing a conventional fluorescence microscope, what makes this method available and affordable for a broad range of research laboratories.

Another novel super-resolution technique is CLEM, that was successfully applied in *F. fujikuroi* hyphae before (Sputh, 2020; Sputh *et al.*, 2021). This technique needs a more extensive sample preparation compared to ExM but it is capable to identify the localization of specific structures in the subcellular context via the correlation of the fluorescence image with the electron micrograph. In *F. fujikuroi* samples, the subcellular tonoplast and plasma membrane localization of CarO-eYFP, here labeled with an antibody against GFP, could be confirmed and even a 3D-model of a hyphae depicting CarO, the cell wall, the nucleus, vacuoles and mitochondria was made (Sputh, 2020). In general, the process also works for *U. maydis* sporidia and an image depicting fluorescence signals from Calcofluor (cell wall) as well as antibody-labeled UmOps2-eGFP was yielded in combination with the corresponding electron micrograph. However, the specificity of the antibody staining, that is necessary for the process, has to be optimized since for UmOps2-eGFP as well as for UmOps1-eGFP no satisfying results were obtained. Another possibility would be the use of mEosEM, that was shown to yield good fluorescence results even after being fixated and embedded in resin (Fu *et al.*, 2020), so that the fungi could be stained before the CLEM procedure.

As one can see, there are many ways to investigate rhodopsins in terms of their localization in native cells and their electrophysiological characteristics. However, more research is necessary to reveal the biological role that play those abundant proteins in the fungi themselves. For *F. fujikuroi*, it was found that CarO activity slows down the spore germination (García-Martínez *et al.*, 2015). Moreover, this rhodopsin seems to be involved in the rice infection process, since rice plants that were infected with a CarO-deficient strain, had stronger symptoms of the Bakanae disease (Adam *et al.*, 2018). In addition, other fungal rhodopsins could be shown to be involved in different cellular processes concerning the virulence and pathogenicity of the respective fungus like Sop-1 in *S. sclerotium* or Nop-1 in *N. crassa* (Lyu *et al.*, 2016; Wang *et al.*, 2018). Also, the rhodopsins of *A. alternata* were shown to be involved in growth, spore production regulation or pH signaling (Pinecker, 2020). However, it is difficult to assign a special process or signaling pathway to the

rhodopsins alone, since the photobiology of fungi is very complex and different photoreceptors work together in terms of gene expression regulation, also regarding their own expression pattern. For example, the proton pump function of UmOps1 is activated by green light and experiences a boost under extracellular acidic pH; however, the expression of the rhodopsin itself is highly dependent on Wco1 and massively upregulated under blue light conditions (Brych *et al.*, 2016; Panzer *et al.*, 2019). Moreover, latest research could show that Um*ops1* as well as Um*ops2* were upregulated by the transcription factor NRG1 under acidic conditions. In addition, Wco1 was affected by this upregulation by NRG1. (Sánchez-Arreguin *et al.*, 2021) Taken together, this research depicts the complex interplay between different environmental clues (pH, light quality) and cellular processes (gene expression pattern, proton transport over membranes). PH is an important factor that influences fungal life in general (Peñalva *et al.*, 2008; Orij, Brul and Smits, 2011; Fernandes *et al.*, 2017; Vylkova, 2017) and here, rhodopsins may be further involved since they are able to alter the pH of cellular compartments or the cellular environment by proton pumping. Since pH regulation plays crucial roles not only concerning the environment of the fungal cell, but is also important regarding intracellular compartments, it makes sense for rhodopsins to localize also to inner membrane systems, e.g., the tonoplasts. Moreover, it could be possible, that fungal rhodopsins exhibit light-independent functions like it could be shown for BR, that depicts also a scramblase activity by facilitating traverse diffusion of phospholipids over cellular membranes. For another photoreceptor, WcoA of *F. fujikuroi*, a light independent role in terms of transcription regulation was depicted recently (Estrada and Avalos, 2008; Castrillo and Avalos, 2015). In *U. maydis*, it could be shown that under monochromatic blue light conditions, Phy1 affects the action of Wco1 and vice versa under red light conditions what implicated light-independent functions in both photoreceptors (Brych *et al.*, 2021). Furthermore, taking into account that there are many opsins lacking the conserved lysine residue necessary for retinal binding and that it is possible to convert them into a functional proton pump via engineering, it is likely that there must be more functions than the light-dependent ones (Yamauchi *et al.*, 2019). Concerning the impact of UmOps1 or UmOps2 on *U. maydis*, colony growth experiments were done using the solopathogenic strain SG200 as well as the haploid strain FB1, but neither significant change in growth was observed when knocking out UmOps1, UmOps2 or both, nor acidification of the surrounding medium could be related to UmOps1 or UmOps2 (Castro Márquez, 2016). Maybe the reason, why it is so difficult to see clear phenotypes in *U. maydis* UmOps1 or UmOps2 knock-out strains could be, that there may be back-up systems that the fungus can fall back on. For example, UmOps1 can be hypothesized to generate a proton gradient over the membrane that is used to drive other transporters involved in nutrient uptake. If this process is maintained via light, other energy sources like ATP could be saved. But, when the UmOps1 rhodopsin cannot fulfill its proton transport function, e.g., due to light depletion at night – or because of the UmOps1 knockout – the fungus has other proteins as backup to regain the proton motive force over the membrane by using the previously saved energy source ATP via for example the plasma membrane ATPase. However, since there are many possible processes going on in the fungal cells in which rhodopsins may be involved, one could consider to experiment further with rhodopsin knock-out mutants in terms of appressoria formation, because this is an important structure necessary for entering the plant and fulfill the infection process. Preliminary microscopic experiments showed that it is possible to visualize those infection structures in a

sufficient way either using SIM to get more detailed images or using conventional fluorescence microscopes to get overviews (data not shown).

In conclusion, this study gained more insights into the electrophysiological characteristics of five fungal rhodopsins as well as further information about the subcellular localization of these proteins, also, by the successful application of novel super-resolution microscopic techniques. This work paves the way for further research on the interesting features and functions of fungal rhodopsins regarding fungal biology as well as technical or optogenetic applications.

6 References

Abbe, E. (1873) 'Beiträge zur Theorie des Mikroskops und der mikroskopischen Wahrnehmung', *Archiv für mikroskopische Anatomie*, 9(1), pp. 413–468.

Adam, A. *et al.* (2018) 'Protein Activity of the *Fusarium fujikuroi* Rhodopsins CarO and OpsA and Their Relation to Fungus–Plant Interaction', *International Journal of Molecular Sciences*, 19(1), p. 215. doi:10.3390/ijms19010215.

Adamantidis, A. *et al.* (2015) 'Optogenetics: 10 years after ChR2 in neurons—views from the community', *Nature Neuroscience*, 18(9), pp. 1202–1212. doi:10.1038/nn.4106.

Andrews, J.H., Spear, R.N. and Nordheim, E.V. (2002) 'Population biology of *Aureobasidium pullulans* on apple leaf surfaces', *Canadian Journal of Microbiology*, 48(6), pp. 500–513. doi:10.1139/w02-044.

Aoki, T. *et al.* (2008) 'Novel assays for proteases using green fluorescent protein-tagged substrate immobilized on a membrane disk', *Analytical Biochemistry*, 378(2), pp. 132–137. doi:10.1016/j.ab.2008.04.022.

Avalos, J. *et al.* (2017) 'Carotenoid Biosynthesis in *Fusarium*', *Journal of Fungi*, 3(3), p. 39. doi:10.3390/jof3030039.

Avalos, J., Casadesús, J. and Cerdá-Olmedo, E. (1985) '*Gibberella fujikuroi* Mutants Obtained with UV Radiation and *N*-Methyl-*N'*-Nitro-*N*-Nitrosoguanidine', *Applied and Environmental Microbiology*, 49(1), pp. 187–191. doi:10.1128/aem.49.1.187-191.1985.

Avelar, G.M. *et al.* (2014) 'A Rhodopsin-Guanylyl Cyclase Gene Fusion Functions in Visual Perception in a Fungus', *Current Biology*, 24(11), pp. 1234–1240. doi:10.1016/j.cub.2014.04.009.

Balashov, S.P. *et al.* (1999) 'The Proton Release Group of Bacteriorhodopsin Controls the Rate of the Final Step of Its Photocycle at Low pH', *Biochemistry*, 38(7), pp. 2026–2039. doi:10.1021/bi981926a.

Balashov, S.P. *et al.* (2005) 'Xanthorhodopsin: A Proton Pump with a Light-Harvesting Carotenoid Antenna', *Science*, 309(5743), pp. 2061–2064. doi:10.1126/science.1118046.

Ballario, P. *et al.* (1996) 'White collar-1, a central regulator of blue light responses in *Neurospora*, is a zinc finger protein.', *The EMBO Journal*, 15(7), pp. 1650–1657. doi:10.1002/j.1460-2075.1996.tb00510.x.

Banuett, F. (1992) '*Ustilago maydis*, the delightful blight', *Trends in Genetics*, 8(5), pp. 174–180. doi:10.1016/0168-9525(92)90220-X.

Banuett, F. and Herskowitz, I. (1989) 'Different a alleles of Ustilago maydis are necessary for maintenance of filamentous growth but not for meiosis', *Proceedings of the National Academy of Sciences*, 86(15), pp. 5878–5882. doi:10.1073/pnas.86.15.5878.

Banuett, F. and Herskowitz, I. (1996) 'Discrete developmental stages during teliospore formation in the corn smut fungus, *Ustilago maydis*', *Development*, 122(10), pp. 2965–2976. doi:10.1242/dev.122.10.2965.

Baró, L. *et al.* (2021) 'Photonics of fungal cell wall', *arXiv:2104.10848 [physics]* [Preprint]. Available at: http://arxiv.org/abs/2104.10848 (Accessed: 19 September 2021).

Baruah, A. and Biswas, P. (2014) 'The role of site-directed point mutations in protein misfolding', *Physical Chemistry Chemical Physics*, 16(27), pp. 13964–13973. doi:10.1039/C3CP55367A.

Baxter, M. and Illston, G.M. (1980) 'Temperature relationships of fungi isolated at low temperatures from soils and other substrates | SpringerLink', *Mycopathologia*, 72(1), pp. 21–25. doi:10.1007/BF00443047.

Béjà, O. and Lanyi, J.K. (2014) 'Nature's toolkit for microbial rhodopsin ion pumps', *Proceedings of the National Academy of Sciences*, 111(18), pp. 6538–6539. doi:10.1073/pnas.1405093111.

Bergo, V. *et al.* (2002) 'A Fourier Transform Infrared Study of *Neurospora* Rhodopsin: Similarities with Archaeal Rhodopsins¶†', *Photochemistry and Photobiology*, 76(3), pp. 341–349. doi:10.1562/0031-8655(2002)0760341AFTISO2.0.CO2.

Bergsbaken, C.L., Sommers, S.L. and Law, P.Y. (1993) 'Effect of forskolin and isobutylmethylxanthine on delta-opioid receptor activity in neuroblastoma x glioma NG108-15 cells.', *Journal of Pharmacology and Experimental Therapeutics*, 264(3), pp. 1474–1483.

Bertl, A. *et al.* (1998) 'Electrophysiology in the eukaryotic model cell *Saccharomyces cerevisiae*', *Pflugers Archiv: European Journal of Physiology*, 436(6), pp. 999–1013. doi:10.1007/s004240050735.

Betzig, E. *et al.* (2006) 'Imaging Intracellular Fluorescent Proteins at Nanometer Resolution', *Science*, 313(5793), pp. 1642–1645. doi:10.1126/science.1127344.

Biasini, M. *et al.* (2014) 'SWISS-MODEL: modelling protein tertiary and quaternary structure using evolutionary information', *Nucleic Acids Research*, 42(W1), pp. W252–W258. doi:10.1093/nar/gku340.

Bieszke, J.A., Spudich, E.N., *et al.* (1999) 'A Eukaryotic Protein, NOP-1, Binds Retinal To Form an Archaeal Rhodopsin-like Photochemically Reactive Pigment', *Biochemistry*, 38(43), pp. 14138–14145. doi:10.1021/bi9916170.

Bieszke, J.A., Braun, E.L., *et al.* (1999) 'The nop-1 gene of *Neurospora crassa* encodes a seven transmembrane helix retinal-binding protein homologous to archaeal rhodopsins', *Proceedings of the National Academy of Sciences*, 96(14), pp. 8034–8039. doi:10.1073/pnas.96.14.8034.

Bogomolni, R.A. and Spudich, J.L. (1982) 'Identification of a third rhodopsin-like pigment in phototactic *Halobacterium halobium*', *Proceedings of the National Academy of Sciences*, 79(20), pp. 6250–6254. doi:10.1073/pnas.79.20.6250.

Bogomolni, R.A., Taylor, M.E. and Stoeckenius, W. (1984) 'Reconstitution of purified halorhodopsin', *Proceedings of the National Academy of Sciences*, 81(17), pp. 5408–5411. doi:10.1073/pnas.81.17.5408.

Bölker, M., Urban, M. and Kahmann, R. (1992) 'The a mating type locus of *U. maydis* specifies cell signaling components', *Cell*, 68(3), pp. 441–450. doi:10.1016/0092-8674(92)90182-C.

Bowman, S.M. and Free, S.J. (2006) 'The structure and synthesis of the fungal cell wall', *BioEssays*, 28(8), pp. 799–808. doi:10.1002/bies.20441.

Boyden, E.S. *et al.* (2005) 'Millisecond-timescale, genetically targeted optical control of neural activity', *Nature Neuroscience*, 8(9), pp. 1263–1268. doi:10.1038/nn1525.

Bräuer, C. (2018) 'Elektrophysiologische Analyse des Rhodopsins ApOps2 aus dem Pilz *Aureobasidium pullulans*'. Bachelor thesis.

Brown, L.S. (2014) 'Eubacterial rhodopsins — Unique photosensors and diverse ion pumps', *Biochimica et Biophysica Acta (BBA) - Bioenergetics*, 1837(5), pp. 553–561. doi:10.1016/j.bbabio.2013.05.006.

Brown, L.S. and Jung, K.-H. (2006) 'Bacteriorhodopsin-like proteins of eubacteria and fungi: the extent of conservation of the haloarchaeal proton-pumping mechanism', *Photochemical & Photobiological Sciences*, 5(6), pp. 538–546. doi:10.1039/B514537F.

Brunk, M. (2014) 'Interdisziplinäre Analyse des pilzlichen Rhodopsins CarO aus *Fusarium fujikuroi*'. Master thesis.

Brych, A. *et al.* (2016) 'White collar 1-induced photolyase expression contributes to UV-tolerance of *Ustilago maydis*', *MicrobiologyOpen*, 5(2), pp. 224–243. doi:10.1002/mbo3.322.

Brych, A. *et al.* (2021) 'Coregulation of gene expression by White collar 1 and phytochrome in *Ustilago maydis*', *Fungal genetics and biology: FG & B*, 152, p. 103570. doi:10.1016/j.fgb.2021.103570.

Buckley, N.G. and Pugh, G.J.F. (1971) 'Auxin Production by Phylloplane Fungi', *Nature*, 231(5301), pp. 332–332. doi:10.1038/231332a0.

Bucur, O. *et al.* (2020) 'Nanoscale imaging of clinical specimens using conventional and rapid-expansion pathology', *Nature Protocols*, 15(5), pp. 1649–1672. doi:10.1038/s41596-020-0300-1.

Castrillo, M. *et al.* (2015) 'Biochemical Characterization of the DASH-Type Cryptochrome CryD From *Fusarium fujikuroi*', *Photochemistry and Photobiology*, 91(6), pp. 1356–1367. doi:10.1111/php.12501.

Castrillo, M. and Avalos, J. (2015) 'The Flavoproteins CryD and VvdA Cooperate with the White Collar Protein WcoA in the Control of Photocarotenogenesis in *Fusarium fujikuroi*', *PLOS ONE*, 10(3), p. e0119785. doi:10.1371/journal.pone.0119785.

Castro Márquez, A. (2016) 'Characterization of Opsins in *Ustilago maydis*'. Bachelor thesis.

Chad, J. and Wheal, H.V. (1991) *Cellular Neurobiology: A Practical Approach*. IRL Press at Oxford University Press.

Chan, G.F. *et al.* (2011) 'Emergence of *Aureobasidium pullulans* as human fungal pathogen and molecular assay for future medical diagnosis', *Folia Microbiologica*, 56(5), p. 459. doi:10.1007/s12223-011-0070-9.

Chang, J.-B. *et al.* (2017) 'Iterative expansion microscopy', *Nature Methods*, 14(6), pp. 593–599. doi:10.1038/nmeth.4261.

Chang, J.-M. *et al.* (2012) 'Accurate multiple sequence alignment of transmembrane proteins with PSI-Coffee', *BMC bioinformatics*, 13 Suppl 4, p. S1. doi:10.1186/1471-2105-13-S4-S1.

Chen, F., Tillberg, P.W. and Boyden, E.S. (2015) 'Expansion microscopy', *Science*, 347(6221), pp. 543–548. doi:10.1126/science.1260088.

Cheng, K.-C., Demirci, A. and Catchmark, J.M. (2011) 'Pullulan: biosynthesis, production, and applications', *Applied Microbiology and Biotechnology*, 92(1), pp. 29–44. doi:10.1007/s00253-011-3477-y.

Chow, B.Y. *et al.* (2010) 'High-performance genetically targetable optical neural silencing by light-driven proton pumps', *Nature*, 463(7277), pp. 98–102. doi:10.1038/nature08652.

Chozinski, T.J. *et al.* (2016) 'Expansion microscopy with conventional antibodies and fluorescent proteins', *Nature Methods*, 13(6), pp. 485–488. doi:10.1038/nmeth.3833.

Cole, K.S. (1979) 'Mostly Membranes', *Annual Review of Physiology*, 41(1), pp. 1–23. doi:10.1146/annurev.ph.41.030179.000245.

Cole, K.S. and Curtis, H.J. (1939) 'Electric Impedance of the Squid Giant Axon During Activity', *Journal of General Physiology*, 22(5), pp. 649–670. doi:10.1085/jgp.22.5.649.

Corrochano, L.M. (2019) 'Light in the Fungal World: From Photoreception to Gene Transcription and Beyond | Annual Review of Genetics', *Annual Review of Genetics*, 53, pp. 149–170. doi:10.1146/annurev-genet-120417-031415.

Cortesão, M. *et al.* (2021) 'MARSBOx: Fungal and Bacterial Endurance From a Balloon-Flown Analog Mission in the Stratosphere', *Frontiers in Microbiology*, 12, p. 177. doi:10.3389/fmicb.2021.601713.

DasSarma, S. and Schwieterman, E.W. (2021) 'Early evolution of purple retinal pigments on Earth and implications for exoplanet biosignatures', *International Journal of Astrobiology*, 20(3), pp. 241–250. doi:10.1017/S1473550418000423.

Deisseroth, K. (2015) 'Optogenetics: 10 years of microbial opsins in neuroscience', *Nature Neuroscience*, 18(9), pp. 1213–1225. doi:10.1038/nn.4091.

De-la-Rosa, V. *et al.* (2016) 'Currents through Hv1 channels deplete protons in their vicinity', *Journal of General Physiology*, 147(2), pp. 127–136. doi:10.1085/jgp.201511496.

Demmerle, J. *et al.* (2017) 'Strategic and practical guidelines for successful structured illumination microscopy', *Nature Protocols*, 12(5), pp. 988–1010. doi:10.1038/nprot.2017.019.

Diemar, A. (2016) 'Elektrophysiologische Untersuchung eines Tandemproteins für den Vergleich von Pumpaktivitäten pilzlicher Rhodopsine'. Bachelor thesis.

Dimakopoulou, M. *et al.* (2008) 'Phyllosphere grapevine yeast *Aureobasidium pullulans* reduces Aspergillus carbonarius (sour rot) incidence in wine-producing vineyards in Greece', *Biological Control*, 46(2), pp. 158–165. doi:10.1016/j.biocontrol.2008.04.015.

Duarte, M.J. *et al.* (2018) 'Ancestral Adeno-Associated Virus Vector Delivery of Opsins to Spiral Ganglion Neurons: Implications for Optogenetic Cochlear Implants', *Molecular Therapy: The Journal of the American Society of Gene Therapy*, 26(8), pp. 1931–1939. doi:10.1016/j.ymthe.2018.05.023.

Duebel, J., Marazova, K. and Sahel, J.-A. (2015) 'Optogenetics', *Current Opinion in Ophthalmology*, 26(3), pp. 226–232. doi:10.1097/ICU.0000000000000140.

Ehrlich, H.G. (1958) 'Nuclear Behavior in Mycelium of a Solopathogenic Line and in a Cross of Two Haploid Lines of *Ustilago Maydis* (DC.) Cda', *Mycologia*, 50(5), pp. 622–627. doi:10.2307/3756169.

Ernst, O.P. *et al.* (2014) 'Microbial and Animal Rhodopsins: Structures, Functions, and Molecular Mechanisms', *Chemical Reviews*, 114(1), pp. 126–163. doi:10.1021/cr4003769.

Estrada, A.F. *et al.* (2009) '*Ustilago maydis* accumulates β-carotene at levels determined by a retinal-forming carotenoid oxygenase', *Fungal Genetics and Biology*, 46(10), pp. 803–813. doi:10.1016/j.fgb.2009.06.011.

Estrada, A.F. and Avalos, J. (2008) 'The White Collar protein WcoA of *Fusarium fujikuroi* is not essential for photocarotenogenesis, but is involved in the regulation of secondary metabolism and conidiation', *Fungal Genetics and Biology*, 45(5), pp. 705–718. doi:10.1016/j.fgb.2007.12.003.

Estrada, A.F. and Avalos, J. (2009) 'Regulation and targeted mutation of opsA, coding for the NOP-1 opsin orthologue in *Fusarium fujikuroi*', *Journal of Molecular Biology*, 387(1), pp. 59–73. doi:10.1016/j.jmb.2009.01.057.

Fan, Y. *et al.* (2011) 'Photochemical characterization of a novel fungal rhodopsin from *Phaeosphaeria nodorum*', *Biochimica et Biophysica Acta (BBA) - Bioenergetics*, 1807(11), pp. 1457–1466. doi:10.1016/j.bbabio.2011.07.005.

Faulkner, E.L., Thomas, S.G. and Neely, R.K. (2020) 'An introduction to the methodology of expansion microscopy', *The International Journal of Biochemistry & Cell Biology*, 124, p. 105764. doi:10.1016/j.biocel.2020.105764.

Feldbauer, K. *et al.* (2016) 'Optochemokine Tandem for Light-Control of Intracellular Ca2+', *PLOS ONE*, 11(10), p. e0165344. doi:10.1371/journal.pone.0165344.

Felle, H. *et al.* (1986) 'Indole-3-acetic acid and fusicoccin cause cytosolic acidification of corn coleoptile cells', *Proceedings of the National Academy of Sciences of the United States of America* [Preprint]. Available at: https://khepri-node.dev.meta-infra.org/papers/indole-3-acetic-acid-and-fusicoccin-cause/16593782 (Accessed: 14 November 2021).

Ferenczi, E.A. *et al.* (2016) 'Optogenetic approaches addressing extracellular modulation of neural excitability', *Scientific Reports*, 6(1), p. 23947. doi:10.1038/srep23947.

Fernandes, T.R. *et al.* (2017) 'How alkalinization drives fungal pathogenicity', *PLOS Pathogens*, 13(11), p. e1006621. doi:10.1371/journal.ppat.1006621.

Fischer-Parton, S. *et al.* (2000) 'Confocal microscopy of FM4-64 as a tool for analysing endocytosis and vesicle trafficking in living fungal hyphae', *Journal of Microscopy*, 198(3), pp. 246–259. doi:10.1046/j.1365-2818.2000.00708.x.

Fishman, H.M. (1973) 'Relaxation Spectra of Potassium Channel Noise from Squid Axon Membranes', *Proceedings of the National Academy of Sciences*, 70(3), pp. 876–879. doi:10.1073/pnas.70.3.876.

Flytzanis, N.C. *et al.* (2014) 'Archaerhodopsin Variants with Enhanced Voltage Sensitive Fluorescence in Mammalian and *Caenorhabditis elegans* Neurons', *Nature communications*, 5, p. 4894. doi:10.1038/ncomms5894.

Franco, D.L. *et al.* (2017) 'Spontaneous circadian rhythms in a cold-adapted natural isolate of <i>Aureobasidium pullulans</I>', *Scientific Reports*, 7(1), p. 13837. doi:10.1038/s41598-017-14085-6.

Fu, Z. *et al.* (2020) 'mEosEM withstands osmium staining and Epon embedding for super-resolution CLEM', *Nature Methods*, 17(1), pp. 55–58. doi:10.1038/s41592-019-0613-6.

Fudim, R. *et al.* (2019) 'Design of a light-gated proton channel based on the crystal structure of Coccomyxa rhodopsin', *Science Signaling*, 12(573), p. eaav4203. doi:10.1126/scisignal.aav4203.

Gambarotto, D. *et al.* (2019) 'Imaging cellular ultrastructures using expansion microscopy (U-ExM)', *Nature Methods*, 16(1), pp. 71–74. doi:10.1038/s41592-018-0238-1.

Gao, S. *et al.* (2015) 'Optogenetic manipulation of cGMP in cells and animals by the tightly light-regulated guanylyl-cyclase opsin CyclOp', *Nature Communications*, 6(1), p. 8046. doi:10.1038/ncomms9046.

García-Martínez, J. *et al.* (2015) 'The CarO rhodopsin of the fungus *Fusarium fujikuroi* is a light-driven proton pump that retards spore germination', *Scientific Reports*, 5(1), p. 7798. doi:10.1038/srep07798.

Garten, M. *et al.* (2017) 'Whole-GUV patch-clamping', *Proceedings of the National Academy of Sciences of the United States of America*, 114(2), pp. 328–333. doi:10.1073/pnas.1609142114.

Geibel, S. *et al.* (2001) 'The voltage-dependent proton pumping in bacteriorhodopsin is characterized by optoelectric behavior.', *Biophysical Journal*, 81(4), pp. 2059–2068.

Ghosh, A. (2014) 'Small heat shock proteins (HSP12, HSP20 and HSP30) play a role in *Ustilago* maydis pathogenesis', *FEMS Microbiology Letters*, 361(1), pp. 17–24. doi:10.1111/1574-6968.12605.

Gillissen, B. *et al.* (1992) 'A two-component regulatory system for self/non-self recognition in *Ustilago maydis*', *Cell*, 68(4), pp. 647–657. doi:10.1016/0092-8674(92)90141-X.

Goodhew, P.J. and Humphreys, J. (2000) *Electron Microscopy and Analysis*. CRC Press.

Gostinčar, C. *et al.* (2014) 'Genome sequencing of four *Aureobasidium pullulans* varieties: biotechnological potential, stress tolerance, and description of new species', *BMC Genomics*, 15(1), p. 549. doi:10.1186/1471-2164-15-549.

Götz, R. *et al.* (2020) 'Expansion Microscopy for Cell Biology Analysis in Fungi', *Frontiers in Microbiology*, 11, p. 574. doi:10.3389/fmicb.2020.00574.

Govorunova, E.G. *et al.* (2015) 'Natural light-gated anion channels: A family of microbial rhodopsins for advanced optogenetics', *Science*, 349(6248), pp. 647–650. doi:10.1126/science.aaa7484.

Govorunova, E.G. and Koppel, L.A. (2016) 'The road to optogenetics: Microbial rhodopsins', *Biochemistry (Moscow)*, 81(9), pp. 928–940. doi:10.1134/S0006297916090029.

Gow, N.A.R., Latge, J.-P. and Munro, C.A. (2017) 'The Fungal Cell Wall: Structure, Biosynthesis, and Function', *Microbiology Spectrum*, 5(3), p. 5.3.01. doi:10.1128/microbiolspec.FUNK-0035-2016.

Gunde-Cimerman, N. *et al.* (2000) 'Hypersaline waters in salterns – natural ecological niches for halophilic black yeasts', *FEMS Microbiology Ecology*, 32(3), pp. 235–240. doi:10.1111/j.1574-6941.2000.tb00716.x.

Gustafsson, M.G.L. (2000) 'Surpassing the lateral resolution limit by a factor of two using structured illumination microscopy', *Journal of Microscopy*, 198(2), pp. 82–87. doi:10.1046/j.1365-2818.2000.00710.x.

Han, X. and Boyden, E.S. (2007) 'Multiple-color optical activation, silencing, and desynchronization of neural activity, with single-spike temporal resolution', *PloS One*, 2(3), p. e299. doi:10.1371/journal.pone.0000299.

He, Q. *et al.* (2002) 'White Collar-1, a DNA Binding Transcription Factor and a Light Sensor', *Science*, 297(5582), pp. 840–843. doi:10.1126/science.1072795.

Heintzmann, R. and Huser, T. (2017) 'Super-Resolution Structured Illumination Microscopy', *Chemical Reviews*, 117(23), pp. 13890–13908. doi:10.1021/acs.chemrev.7b00218.

Hell, S.W. and Wichmann, J. (1994) 'OSA | Breaking the diffraction resolution limit by stimulated emission: stimulated-emission-depletion fluorescence microscopy', *Optics Letters*, 19(11), pp. 780–782. doi:10.1364/OL.19.000780.

Horneck, G., Klaus, D.M. and Mancinelli, R.L. (2010) 'Space Microbiology', *Microbiology and Molecular Biology Reviews*, 74(1), pp. 121–156. doi:10.1128/MMBR.00016-09.

Humphries, Z. *et al.* (2017) 'A new family and genus in Dothideales for *Aureobasidium*-like species isolated from house dust', *IMA Fungus*, 8(2), pp. 299–315. doi:10.5598/imafungus.2017.08.02.05.

Inoue, K. *et al.* (2013) 'A light-driven sodium ion pump in marine bacteria', *Nature Communications*, 4, p. 1678. doi:10.1038/ncomms2689.

Inoue, K. *et al.* (2016) 'A natural light-driven inward proton pump', *Nature Communications*, 7(1), p. 13415. doi:10.1038/ncomms13415.

Inoue, K., Nishihama, R. and Kohchi, T. (2017) 'Evolutionary origin of phytochrome responses and signaling in land plants', *Plant, Cell & Environment*, 40(11), pp. 2502–2508. doi:10.1111/pce.12908.

Ji, L. *et al.* (2017) 'Detergent-resistant oligomeric Leptosphaeria rhodopsin is a promising bio-nanomaterial and an alternative to bacteriorhodopsin', *Biochemical and Biophysical Research Communications*, 493(1), pp. 352–357. doi:10.1016/j.bbrc.2017.09.018.

Kämper, J. *et al.* (2006) 'Insights from the genome of the biotrophic fungal plant pathogen *Ustilago maydis*', *Nature*, 444(7115), pp. 97–101. doi:10.1038/nature05248.

Kao, P. and Nodine, M.D. (2019) 'Transcriptional Activation of *Arabidopsis* Zygotes Is Required for Initial Cell Divisions', *Scientific Reports*, 9(1), p. 17159. doi:10.1038/s41598-019-53704-2.

Kato, H.E. *et al.* (2015) 'Structural basis for Na+ transport mechanism by a light-driven Na+ pump', *Nature*, 521(7550), pp. 48–53. doi:10.1038/nature14322.

Khorana, H.G. *et al.* (1979) 'Amino acid sequence of bacteriorhodopsin.', *Proceedings of the National Academy of Sciences of the United States of America*, 76(10), p. 5046. doi:10.1073/pnas.76.10.5046.

Kikukawa, T. *et al.* (2012) 'Photo-Induced Proton Transfers of Microbial Rhodopsins', in *Molecular Photochemistry - Various Aspects*. InTech, pp. 89–108.

Klapoetke, N.C. *et al.* (2014) 'Independent optical excitation of distinct neural populations', *Nature Methods*, 11(3), pp. 338–346. doi:10.1038/nmeth.2836.

Klare, J.P., Chizhov, I. and Engelhard, M. (2008) 'Microbial Rhodopsins: Scaffolds for Ion Pumps, Channels, and Sensors', in Schäfer, G. and Penefsky, H.S. (eds) *Bioenergetics: Energy Conservation*

and Conversion. Berlin, Heidelberg: Springer (Results and Problems in Cell Differentiation), pp. 73–122. doi:10.1007/400_2007_041.

Klee, W.A. and Nirenberg, M. (1974) 'A Neuroblastoma × Glioma Hybrid Cell Line with Morphine Receptors', *Proceedings of the National Academy of Sciences of the United States of America*, 71(9), pp. 3474–3477.

Kleinlogel, S. *et al.* (2011) 'A gene-fusion strategy for stoichiometric and co-localized expression of light-gated membrane proteins', *Nature Methods*, 8(12), pp. 1083–1088. doi:10.1038/nmeth.1766.

Knaus, H. *et al.* (2013) 'Label-free fluorescence microscopy in fungi', *Fungal Biology Reviews*, 27(2), pp. 60–66. doi:10.1016/j.fbr.2013.05.003.

Kocková-Kratochvílová, A., Černáková, M. and Sláviková, E. (1980) 'Morphological changes during the life cycle of *Aureobasidium pullulans* (de Bary) Arnaud', *Folia Microbiologica*, 25(1), pp. 56–67. doi:10.1007/BF02876398.

Koga, D. *et al.* (2015) 'High-resolution imaging by scanning electron microscopy of semithin sections in correlation with light microscopy', *Microscopy*, 64(6), pp. 387–394. doi:10.1093/jmicro/dfv042.

Kogej, T. *et al.* (2005) 'The Halophilic Fungus *Hortaea werneckii* and the Halotolerant Fungus *Aureobasidium pullulans* Maintain Low Intracellular Cation Concentrations in Hypersaline Environments | Applied and Environmental Microbiology', *Applied and Environmental Microbiology*, 71(11), pp. 6600–6605. doi:10.1128/AEM.71.11.6600-6605.2005.

Kojima, K., Shibukawa, A. and Sudo, Y. (2020) 'The Unlimited Potential of Microbial Rhodopsins as Optical Tools', *Biochemistry*, 59(3), pp. 218–229. doi:10.1021/acs.biochem.9b00768.

Kronstad, J.W. and Leong, S.A. (1989) 'Isolation of two alleles of the b locus of *Ustilago maydis*', *Proceedings of the National Academy of Sciences*, 86(3), pp. 978–982. doi:10.1073/pnas.86.3.978.

Ku, T. *et al.* (2016) 'Multiplexed and scalable super-resolution imaging of three-dimensional protein localization in size-adjustable tissues', *Nature Biotechnology*, 34(9), pp. 973–981. doi:10.1038/nbt.3641.

Kumar, A. and Biswas, P. (2019) 'Effect of site-directed point mutations on protein misfolding: A simulation study', *Proteins: Structure, Function, and Bioinformatics*, 87(9), pp. 760–773. doi:10.1002/prot.25702.

Kunz, T.C. *et al.* (2019) 'Detection of *Chlamydia* Developmental Forms and Secreted Effectors by Expansion Microscopy', *Frontiers in Cellular and Infection Microbiology*, 9, p. 276. doi:10.3389/fcimb.2019.00276.

La Greca, M. *et al.* (under review).

Lanver, D. *et al.* (2018) 'The Biotrophic Development of *Ustilago maydis* Studied by RNA-Seq Analysis', *The Plant Cell*, 30(2), pp. 300–323. doi:10.1105/tpc.17.00764.

Lanyi, J.K. (2006) 'Proton transfers in the bacteriorhodopsin photocycle', *Biochimica et Biophysica Acta (BBA) - Bioenergetics*, 1757(8), pp. 1012–1018. doi:10.1016/j.bbabio.2005.11.003.

Lanyi, J.K. and Luecke, H. (2001) 'Bacteriorhodopsin', *Current Opinion in Structural Biology*, 11(4), pp. 415–419. doi:10.1016/S0959-440X(00)00226-8.

Lanyi, J.K. and Schobert, B. (2003) 'Mechanism of Proton Transport in Bacteriorhodopsin from Crystallographic Structures of the K, L, M1, M2, and M2' Intermediates of the Photocycle', *Journal of Molecular Biology*, 328(2), pp. 439–450. doi:10.1016/S0022-2836(03)00263-8.

Leathers, T.D. (2003) 'Biotechnological production and applications of pullulan', *Applied Microbiology and Biotechnology*, 62(5), pp. 468–473. doi:10.1007/s00253-003-1386-4.

Lehmler, C. *et al.* (1997) 'Identification of a motor protein required for filamentous growth in *Ustilago maydis*', *The EMBO Journal*, 16(12), pp. 3464–3473. doi:10.1093/emboj/16.12.3464.

León-Ramírez, C.G. *et al.* (2004) 'Infection of alternative host plant species by *Ustilago maydis*', *New Phytologist*, 164(2), pp. 337–346. doi:10.1111/j.1469-8137.2004.01171.x.

Li, Y.-T. *et al.* (2018) 'A Review on Bacteriorhodopsin-Based Bioelectronic Devices', *Sensors*, 18(5), p. 1368. doi:10.3390/s18051368.

Lichtman, J.W. and Conchello, J.-A. (2005) 'Fluorescence microscopy | Nature Methods', *Nature Methods*, 2, pp. 910–919. doi:10.1038/nmeth8817.

van de Linde, S. *et al.* (2011) 'Direct stochastic optical reconstruction microscopy with standard fluorescent probes', *Nature Protocols*, 6(7), pp. 991–1009. doi:10.1038/nprot.2011.336.

Linden, H. and Macino, G. (1997) 'White collar 2, a partner in blue-light signal transduction, controlling expression of light–regulated genes in *Neurospora crassa*', *The EMBO Journal*, 16(1), pp. 98–109. doi:10.1093/emboj/16.1.98.

Lingappa, Y., Sussman, A.S. and Bernstein, I.A. (1963) 'Effect of light and media upon growth and melanin formation in aureobasidium pullulans (de By.)Arn. (=pullularia pullulans)', *Mycopathologia et mycologia applicata*, 20(1), pp. 109–128. doi:10.1007/BF02054883.

Lozier, R.H., Bogomolni, R.A. and Stoeckenius, W. (1975) 'Bacteriorhodopsin: a light-driven proton pump in *Halobacterium Halobium*', *Biophysical Journal*, 15(9), pp. 955–962. doi:10.1016/S0006-3495(75)85875-9.

Luecke, H. *et al.* (2008) 'Crystallographic structure of xanthorhodopsin, the light-driven proton pump with a dual chromophore', *Proceedings of the National Academy of Sciences*, 105(43), pp. 16561–16565. doi:10.1073/pnas.0807162105.

Lyu, X. *et al.* (2016) 'The Microbial Opsin Homolog Sop1 is involved in *Sclerotinia sclerotiorum* Development and Environmental Stress Response', *Frontiers in Microbiology*, 6, p. 1504. doi:10.3389/fmicb.2015.01504.

Mahyad, B., Janfaza, S. and Hosseini, E.S. (2015) 'Bio-nano hybrid materials based on bacteriorhodopsin: Potential applications and future strategies', *Advances in Colloid and Interface Science*, 225, pp. 194–202. doi:10.1016/j.cis.2015.09.006.

Markert, S.M. *et al.* (2016) 'Filling the gap: adding super-resolution to array tomography for correlated ultrastructural and molecular identification of electrical synapses at the *C. elegans* connectome', *Neurophotonics*, 3(4), p. 041802. doi:10.1117/1.NPh.3.4.041802.

Martínez-Espinoza, A.D., García-Pedrajas, M.D. and Gold, S.E. (2002) 'The *Ustilaginales* as Plant Pests and Model Systems', *Fungal Genetics and Biology*, 35(1), pp. 1–20. doi:10.1006/fgbi.2001.1301.

Matsuno-Yagi, A. and Mukohata, Y. (1980) 'ATP synthesis linked to light-dependent proton uptake in a red mutant strain of *Halobacterium* lacking bacteriorhodopsin', *Archives of Biochemistry and Biophysics*, 199(1), pp. 297–303. doi:10.1016/0003-9861(80)90284-2.

Mendoza-Mendoza, A. *et al.* (2009) 'Physical-chemical plant-derived signals induce differentiation in *Ustilago maydis*', *Molecular Microbiology*, 71(4), pp. 895–911. doi:10.1111/j.1365-2958.2008.06567.x.

Misra, S. *et al.* (1997) 'Proton uptake and release are rate-limiting steps in the photocycle of the bacteriorhodopsin mutant E204Q', *Biochemistry*, 36(16), pp. 4875–4883. doi:10.1021/bi962673t.

Molecular Probes 'SYTO®Red Fluorescent Nucleic Acid Stains; Product Information'. Available at: https://www.thermofisher.com/document-connect/document-connect.html?url=https%3A%2F%2Fassets.thermofisher.com%2FTFS-Assets%2FLSG%2Fmanuals%2Fmp11340.pdf (Accessed: 13 January 2022).

Müller-Reichert, T. *et al.* (2007) 'Correlative Light and Electron Microscopy of Early Caenorhabditis elegans Embryos in Mitosis', in *Methods in Cell Biology*. Academic Press (Cellular Electron Microscopy), pp. 101–119. doi:10.1016/S0091-679X(06)79004-5.

Muramatsu, D. *et al.* (2012) 'β-Glucan Derived from *Aureobasidium pullulans* Is Effective for the Prevention of Influenza in Mice', *PLOS ONE*, 7(7), p. e41399. doi:10.1271/journal.pone.0041399.

Nagel, G. *et al.* (2002) 'Channelrhodopsin-1: A Light-Gated Proton Channel in Green Algae', *Science*, 296(5577), pp. 2395–2398. doi:10.1126/science.1072068.

Nagel, G. *et al.* (2003) 'Channelrhodopsin-2, a directly light-gated cation-selective membrane channel', *Proceedings of the National Academy of Sciences*, 100(24), pp. 13940–13945. doi:10.1073/pnas.1936192100.

Nagel, G. *et al.* (2005) 'Light Activation of Channelrhodopsin-2 in Excitable Cells of *Caenorhabditis elegans* Triggers Rapid Behavioral Responses', *Current Biology*, 15(24), pp. 2279–2284. doi:10.1016/j.cub.2005.11.032.

Nango, E. *et al.* (2016) 'A three-dimensional movie of structural changes in bacteriorhodopsin', *Science*, 354(6319), pp. 1552–1557. doi:10.1126/science.aah3497.

NCBI Resource Coordinators (2016) 'Database resources of the National Center for Biotechnology Information', *Nucleic Acids Research*, 44(Database issue), pp. D7–D19. doi:10.1093/nar/gkv1290.

Neher, E. and Sakmann, B. (1976) 'Single-channel currents recorded from membrane of denervated frog muscle fibres', *Nature*, 260(5554), pp. 799–802. doi:10.1038/260799a0.

Nguyen, J.N.T. and Harbison, A.M. (2017) 'Scanning Electron Microscopy Sample Preparation and Imaging', in Espina, V. (ed.) *Molecular Profiling: Methods and Protocols*. New York, NY: Springer (Methods in Molecular Biology), pp. 71–84. doi:10.1007/978-1-4939-6990-6_5.

Niehaus, E.-M. *et al.* (2017) 'Comparative genomics of geographically distant *Fusarium fujikuroi* isolates revealed two distinct pathotypes correlating with secondary metabolite profiles', *PLoS pathogens*, 13(10), p. e1006670. doi:10.1371/journal.ppat.1006670.

Odoh, C.K. *et al.* (2021) 'Extremophilic Fungi and Their Role in Control of Pathogenic Microbes', in Yadav, A.N. (ed.) *Recent Trends in Mycological Research: Volume 1: Agricultural and Medical*

Perspective. Cham: Springer International Publishing (Fungal Biology), pp. 219–249. doi:10.1007/978-3-030-60659-6_10.

O'Donnell, K.L. and McLaughlin, D.J. (1984) 'Ultrastructure of Meiosis in *Ustilago Maydis*', *Mycologia*, 76(3), pp. 468–485. doi:10.1080/00275514.1984.12023868.

Oesterhelt, D. and Stoeckenius, W. (1971) 'Rhodopsin-like Protein from the Purple Membrane of *Halobacterium halobium*', *Nature New Biology*, 233(39), pp. 149–152. doi:10.1038/newbio233149a0.

Ohta, K. *et al.* (2012) 'Beam deceleration for block-face scanning electron microscopy of embedded biological tissue', *Micron (Oxford, England: 1993)*, 43(5), pp. 612–620. doi:10.1016/j.micron.2011.11.001.

Okazaki, A. *et al.* (2014) 'Optical silencing of C. elegans cells with light-driven proton pumps', *Methods*, 68(3), pp. 425–430. doi:10.1016/j.ymeth.2014.02.030.

Orij, R., Brul, S. and Smits, G.J. (2011) 'Intracellular pH is a tightly controlled signal in yeast', *Biochimica Et Biophysica Acta*, 1810(10), pp. 933–944. doi:10.1016/j.bbagen.2011.03.011.

Ou, S.H. (1985) *Rice Diseases*. IRRI.

Panzer, S. (2015) 'Elektrophysiologische Analyse des pilzlichen Rhodopsins ApOps2 aus *Aureobasidium pullulans*'. Bachelor thesis.

Panzer, S. (2017) 'Analysis of the Fungal Rhodopsins of the Corn Smut Fungus *Ustilago maydis*'. Master thesis.

Panzer, S. *et al.* (2019) 'Opsin 1 and Opsin 2 of the Corn Smut Fungus *Ustilago maydis* Are Green Light-Driven Proton Pumps', *Frontiers in Microbiology*, 10, p. 735. doi:10.3389/fmicb.2019.00735.

Panzer, S. *et al.* (2021) 'Modified Rhodopsins From *Aureobasidium pullulans* Excel With Very High Proton-Transport Rates', *Frontiers in Molecular Biosciences*, 8, p. 941. doi:10.3389/fmolb.2021.750528.

Pardo-Medina, J. *et al.* (2020) 'Impact of the White Collar photoreceptor WcoA on the *F. fujikuroi* transcriptome', *Frontiers in Microbiology*, 11, p. 3526. doi:10.3389/fmicb.2020619474.

Park, H.-E. *et al.* (2019) 'Scalable and Isotropic Expansion of Tissues with Simply Tunable Expansion Ratio', *Advanced Science*, 6(22), p. 1901673. doi:10.1002/advs.201901673.

Peñalva, M.A. *et al.* (2008) 'Ambient pH gene regulation in fungi: making connections', *Trends in Microbiology*, 16(6), pp. 291–300. doi:10.1016/j.tim.2008.03.006.

Pinecker, C. (2020) 'Untersuchung der Rolle der potentiellen Grünlichtrezeptoren OpsA und OpsB in dem filamentösen Pilz *Alternaria alternata*'.

Prado, M.M. *et al.* (2004) 'A gene of the opsin family in the carotenoid gene cluster of *Fusarium fujikuroi*', *Current Genetics*, 46(1), pp. 47–58. doi:10.1007/s00294-004-0508-6.

Prasongsuk, S. *et al.* (2018) 'The current status of *Aureobasidium pullulans* in biotechnology', *Folia Microbiol*, (63), pp. 129–140. doi:10.1007/s12223-017-0561-4.

Ramos, S. and García Acha, I. (1975) 'A vegetative cycle of *Pullularia pullulans*', *Transactions of the British Mycological Society*, 64(1), pp. 129-IN9. doi:10.1016/S0007-1536(75)80083-0.

Rayleigh, Lord (1903) 'On the Theory of Optical Images, with special reference to the Microscope', *Journal of the Royal Microscopical Society*, 23(4), pp. 474–482. doi:10.1111/j.1365-2818.1903.tb04831.x.

Reineke, G. *et al.* (2008) 'Indole-3-acetic acid (IAA) biosynthesis in the smut fungus Ustilago maydis and its relevance for increased IAA levels in infected tissue and host tumour formation', *Molecular Plant Pathology*, 9(3), pp. 339–355. doi:10.1111/j.1364-3703.2008.00470.x.

Richter, K.N. *et al.* (2018) 'Glyoxal as an alternative fixative to formaldehyde in immunostaining and super-resolution microscopy', *The EMBO Journal*, 37(1), pp. 139–159. doi:10.15252/embj.201695709.

Rockwell, N.C., Su, Y.-S. and Lagarias, J.C. (2006) 'Phytochrome Structure and Signaling Mechanisms', *Annual Review of Plant Biology*, 57(1), pp. 837–858. doi:10.1146/annurev.arplant.56.032604.144208.

Rossberger, S. *et al.* (2013) 'Combination of structured illumination and single molecule localization microscopy in one setup', *Journal of Optics*, 15(9), p. 094003. doi:10.1088/2040-8978/15/9/094003.

Rück, A. *et al.* (1993) 'Patch-clamp analysis establishes a role for an auxin binding protein in the auxin stimulation of plasma membrane current in Zea mays protoplasts', *The Plant Journal*, 4(1), pp. 41–46. doi:10.1046/j.1365-313X.1993.04010041.x.

Rust, M.J., Bates, M. and Zhuang, X. (2006) 'Sub-diffraction-limit imaging by stochastic optical reconstruction microscopy (STORM) | Nature Methods', *Nature Methods*, 3, pp. 793–796. doi:10.1038/nmeth929.

Sahel, J.-A. *et al.* (2021) 'Partial recovery of visual function in a blind patient after optogenetic therapy', *Nature Medicine*, 27(7), pp. 1223–1229. doi:10.1038/s41591-021-01351-4.

Sakmann, B. and Neher, E. (1984) 'Patch Clamp Techniques for Studying Ionic Channels in Excitable Membranes', *Annual Review of Physiology*, 46(1), pp. 455–472. doi:10.1146/annurev.ph.46.030184.002323.

Sánchez-Arreguin, J.A. *et al.* (2020) 'Analysis of the photoreceptors involved in the light-depending basidiocarp formation in *Ustilago maydis*', *Archives of Microbiology*, 202(1), pp. 93–103. doi:10.1007/s00203-019-01725-w.

Sánchez-Arreguin, J.A. *et al.* (2021) 'Acid pH Strategy Adaptation through NRG1 in Ustilago maydis', *Journal of Fungi*, 7(2), p. 91. doi:10.3390/jof7020091.

Sauer, M., Hofkens, J. and Enderlein, J. (2010) *Handbook of Fluorescence Spectroscopy and Imaging: From Ensemble to Single Molecules*. John Wiley & Sons.

Schindelin, J. *et al.* (2012) 'Fiji: an open-source platform for biological-image analysis', *Nature Methods*, 9(7), pp. 676–682. doi:10.1038/nmeth.2019.

Schobert, B. and Lanyi, J.K. (1982) 'Halorhodopsin is a light-driven chloride pump.', *Journal of Biological Chemistry*, 257(17), pp. 10306–10313. doi:10.1016/S0021-9258(18)34020-1.

Sharma, R.R., Singh, D. and Singh, R. (2009) 'Biological control of postharvest diseases of fruits and vegetables by microbial antagonists: A review - ScienceDirect', *Biological Control*, 50(33), pp. 205–221. doi:10.1016/j.biocontrol.2009.05.001.

Smith, H. (2000) 'Phytochromes and light signal perception by plants—an emerging synthesis', *Nature*, 407(6804), pp. 585–591. doi:10.1038/35036500.

Snetselaar, K.M. (1993) 'Microscopic Observation of *Ustilago maydis* Mating Interactions', *Experimental Mycology*, 17(4), pp. 345–355. doi:10.1006/emyc.1993.1033.

Snetselaar, K.M. and Mims, C.W. (1994) 'Light and electron microscopy of *Ustilago maydis* hyphae in maize', *Mycological Research*, 98(3), pp. 347–355. doi:10.1016/S0953-7562(09)80463-2.

Spaepen, S., Vanderleyden, J. and Remans, R. (2007) 'Indole-3-acetic acid in microbial and microorganism-plant signaling', *FEMS Microbiology Reviews*, 31(4), pp. 425–448. doi:10.1111/j.1574-6976.2007.00072.x.

Spudich, E.N. *et al.* (1986) 'Properties of a second sensory receptor protein in *Halobacterium halobium* phototaxis', *Proteins: Structure, Function and Bioinformatics*, 1(3), pp. 239–246. doi:10.1002/prot.340010306.

Spudich, J.L. (2006) 'The multitalented microbial sensory rhodopsins', *Trends in Microbiology*, 14(11), pp. 480–487. doi:10.1016/j.tim.2006.09.005.

Sputh, S. (2020) 'Entwicklung von Protokollen für die Anwendung von korrelativer Fluoreszenz- und Elektronenmikroskopie am Pilz *Fusarium fujikuroi*'.

Sputh, S. *et al.* (2021) 'Superaufgelöste Mikroskopie: Pilze unter Beobachtung', *BIOspektrum*, 27(4), pp. 380–382. doi:10.1007/s12268-021-1592-6.

Stanly, T.A. *et al.* (2016) 'Critical importance of appropriate fixation conditions for faithful imaging of receptor microclusters', *Biology Open*, 5(9), pp. 1343–1350. doi:10.1242/bio.019943.

Steinberg, G. and Perez-Martin, J. (2008) 'Ustilago maydis, a new fungal model system for cell biology', *Trends in Cell Biology*, 18(2), pp. 61–67. doi:10.1016/j.tcb.2007.11.008.

Strickholm, A. (1961) 'Impedance of a Small Electrically Isolated Area of the Muscle Cell Surface', *Journal of General Physiology*, 44(6), pp. 1073–1088. doi:10.1085/jgp.44.6.1073.

Studer, G. *et al.* (2020) 'QMEANDisCo—distance constraints applied on model quality estimation', *Bioinformatics*, 36(6), pp. 1765–1771. doi:10.1093/bioinformatics/btz828.

Sun, P.-F. *et al.* (2019) 'Intraspecific variation in plant growth-promoting traits of *Aureobasidium pullulans*', *Chiang Mai J. Sci.*, 46(1), pp. 15–31.

Sunani, S.K. *et al.* (2020) 'Identification of rice seed infection routes of *Fusarium fujikuroi* inciting bakanae disease of rice', *Journal of Plant Pathology*, 102, pp. 113–121. doi:10.1007/s42161-019-00390-8.

Sureda-Vives, M. and Sarkisyan, K.S. (2020) 'Bioluminescence-Driven Optogenetics', *Life*, 10(12), p. 318. doi:10.3390/life10120318.

Tada, R. *et al.* (2009) 'Involvement of Branched Units at Position 6 in the Reactivity of a Unique Variety of β-D-Glucan from *Aureobasidium pullulans* to Antibodies in Human Sera: Bioscience, Biotechnology, and Biochemistry: Vol 73, No 4', *Bioscience, Biotechnology and Biochemistry*, 73(4), pp. 908–911. doi:10.1271/bbb.80860.

Terpitz, U. *et al.* (2008) 'Electrofused giant protoplasts of *Saccharomyces cerevisiae* as a novel system for electrophysiological studies on membrane proteins', *Biochimica Et Biophysica Acta*, 1778(6), pp. 1493–1500. doi:10.1016/j.bbamem.2008.03.015.

Tojima, T. *et al.* (2000) 'Acquisition of neuronal proteins during differentiation of NG108-15 cells', *Neuroscience Research*, 37(2), pp. 153–161. doi:10.1016/S0168-0102(00)00110-3.

Truckenbrodt, S. *et al.* (2019) 'A practical guide to optimization in X10 expansion microscopy', *Nature Protocols*, 14(3), pp. 832–863. doi:10.1038/s41596-018-0117-3.

Tsavkelova, E. *et al.* (2012) 'Identification and functional characterization of indole-3-acetamide-mediated IAA biosynthesis in plant-associated Fusarium species', *Fungal genetics and biology: FG & B*, 49(1), pp. 48–57. doi:10.1016/j.fgb.2011.10.005.

Urzì, C. *et al.* (1999) 'Intra-specific diversity of *Aureobasidium pullulans* strains isolated from rocks and other habitats assessed by physiological methods and by random amplified polymorphic DNA (RAPD)', *Journal of Microbiological Methods*, 36(1), pp. 95–105. doi:10.1016/S0167-7012(99)00014-7.

Valverde, M.E. *et al.* (1995) 'Huitlacoche (*Ustilago maydis*) as a food source — biology, composition, and production', *Crit Rev Food Sci Nutr*, 35(3), pp. 191–229. doi:10.1080/10408399509527699.

Verhoeff, A.P. *et al.* (1992) 'Presence of viable mould propagules in indoor air in relation to house damp and outdoor air', *Allergy*, 47(2PART1), pp. 83–91. doi:10.1111/j.1398-9995.1992.tb05093.x.

Vierock, J. *et al.* (2020) *BiPOLES: a tool for bidirectional dual-color optogenetic control of neurons*, p. 2020.07.15.204347. doi:10.1101/2020.07.15.204347.

Vogt, A. *et al.* (2015) 'Conversion of a light-driven proton pump into a light-gated ion channel', *Scientific Reports*, 5(1), p. 16450. doi:10.1038/srep16450.

Vogt, A. (2016) 'Elektrophysiologische Untersuchung des gerichteten Protonentransportes in mikrobiellen Untersuchungen'.

Vollmeister, E. *et al.* (2012) 'Fungal development of the plant pathogen *Ustilago maydis*', *FEMS Microbiology Reviews*, 36(1), pp. 59–77. doi:10.1111/j.1574-6976.2011.00296.x.

Vylkova, S. (2017) 'Environmental pH modulation by pathogenic fungi as a strategy to conquer the host', *PLOS Pathogens*, 13(2), p. e1006149. doi:10.1371/journal.ppat.1006149.

Wang, Z. *et al.* (2018) 'Light sensing by opsins and fungal ecology: NOP-1 modulates entry into sexual reproduction in response to environmental cues', *Molecular Ecology*, 27(1), pp. 216–232. doi:10.1111/mec.14425.

Waschuk, S.A. *et al.* (2005) '*Leptosphaeria* rhodopsin: Bacteriorhodopsin-like proton pump from a eukaryote', *Proceedings of the National Academy of Sciences*, 102(19), pp. 6879–6883. doi:10.1073/pnas.0409659102.

Wassie, A.T., Zhao, Y. and Boyden, E.S. (2019) 'Expansion microscopy: principles and uses in biological research', *Nature Methods*, 16(1), pp. 33–41. doi:10.1038/s41592-018-0219-4.

Webb, T.A. and Mundt, J.O. (1978) 'Molds on vegetables at the time of harvest', *Applied and Environmental Microbiology*, 35(4), pp. 655–658. doi:10.1128/aem.35.4.655-658.1978.

Wilczek, J. (2018) 'Electrophysiological studies on the cause of activity increase in the fungal rhodopsin CarO induced by weak organic acids'. Master thesis.

Woodward, A.W. and Bartel, B. (2005) 'Auxin: regulation, action, and interaction', *Annals of Botany*, 95(5), pp. 707–735. doi:10.1093/aob/mci083.

Yamauchi, Y. *et al.* (2019) 'Engineered Functional Recovery of Microbial Rhodopsin Without Retinal-Binding Lysine', *Photochemistry and Photobiology*, 95(5), pp. 1116–1121. doi:10.1111/php.13114.

Yawo, H. *et al.* (2021) *Optogenetics: Light-Sensing Proteins and Their Applications in Neuroscience and Beyond*. Springer Nature.

Yogendran, P. (2018) 'Elektrophysiologische Analyse der pilzlichen Rhodopsine ApOps1 und ApOps2 des *Aureobasidium pullulans*'. Bachelor thesis.

Yu, Z. and Fischer, R. (2019) 'Light sensing and responses in fungi', *Nature Reviews Microbiology*, 17(1), pp. 25–36. doi:10.1038/s41579-018-0109-x.

Zabelskii, D. *et al.* (2021) 'Structure-based insights into evolution of rhodopsins', *Communications Biology*, 4(1), pp. 1–12. doi:10.1038/s42003-021-02326-4.

Zajc, J. *et al.* (2012) 'The Mycobiota of the Salterns', in Raghukumar, C. (ed.) *Biology of Marine Fungi*. Berlin, Heidelberg: Springer (Progress in Molecular and Subcellular Biology), pp. 133–158. doi:10.1007/978-3-642-23342-5_7.

Zajc, J., Džeroski, S., *et al.* (2014) 'Chaophilic or chaotolerant fungi: a new category of extremophiles?', *Frontiers in Microbiology*, 5, p. 708. doi:10.3389/fmicb.2014.00708.

Zajc, J., Kogej, T., *et al.* (2014) 'Osmoadaptation Strategy of the Most Halophilic Fungus, *Wallemia ichthyophaga*, Growing Optimally at Salinities above 15% NaCl', *Applied and Environmental Microbiology*, 80(1), pp. 247–256. doi:10.1128/AEM.02702-13.

Zalar, P. *et al.* (2005) 'Halophilic black yeasts colonize wood immersed in hypersaline water', 48(4), pp. 323–326. doi:10.1515/BOT.2005.042.

Zalar, P. *et al.* (2008) 'Redefinition of *Aureobasidium pullulans* and its varieties', *Studies in Mycology*, 61, pp. 21–38. doi:10.3114/sim.2008.61.02.

Zalar, P. *et al.* (2011) 'Dishwashers – A man-made ecological niche accommodating human opportunistic fungal pathogens', *Fungal Biology*, 115(10), pp. 997–1007. doi:10.1016/j.funbio.2011.04.007.

Zeng, W.-Z. and Xu, T.-L. (2012) 'Proton production, regulation and pathophysiological roles in the mammalian brain', *Neuroscience Bulletin*, 28(1), pp. 1–13. doi:10.1007/s12264-012-1068-2.

Zhdanova, N. *et al.* (2000) 'Fungi from Chernobyl: Mycobiota of the inner regions of the containment structures of the damaged nuclear reactor', *Mycological Research*, 104, pp. 1421–1426. doi:10.1017/S0953756200002756.

Zhou, Y. *et al.* (2021) 'Optogenetic control of plant growth by a microbial rhodopsin', *Nature Plants*, 7(2), pp. 144–151. doi:10.1038/s41477-021-00853-w.

Zimmermann, D. *et al.* (2008) 'Effects on capacitance by overexpression of membrane proteins', *Biochemical and Biophysical Research Communications*, 369(4), pp. 1022–1026. doi:10.1016/j.bbrc.2008.02.153.

Zwettler, F.U. *et al.* (2020) 'Molecular resolution imaging by post-labeling expansion single-molecule localization microscopy (Ex-SMLM)', *Nature Communications*, 11(1), p. 3388. doi:10.1038/s41467-020-17086-8.

Abbreviations

AD	Analog-digital
Ag/AgCl	Silver/silver chloride
ApOps1	*Aureobasidium pullulans* rhodopsin 1
ApOps2	*Aureobasidium pullulans* rhodopsin 2
ApOps3	*Aureobasidium pullulans* rhodopsin 3
APS	Ammonium persulfate
ATP	Adenosine triphosphate
ATR	All-*trans* retinal
AU	Airy unit
BeGC1	*Blastocladiella emersonii* guanylyl cyclase 1
BLUF	Blue Light Using Flavin
BR	Bacteriorhodopsin
BSA	Bovine serum albumine
bt_2cAMP	Dibuturyl cAMP
$Ca(Ac)_2$	Calcium acetate
$CaCl_2$	Calcium chloride
cAMP	Cyclic adenosine monophosphate
$Ca(OH)_2$	Calcium hydroxide
Cbx	Carboxin
Cco1	Carotene cleavage oxygenase 1
cGMP	Cyclic guanosine monophosphate
ChR1	Channelrhodopsin 1
ChR2	Channelrhodopsin 2
CLEM	Correlative light and electron microscopy
CLSM	Confocal laser scanning microscopy/microscope
CMV	Cytomegalovirus
CO_2	Carbon dioxide
CPF	Cryptochrome/photolyase family
CsCl	Caesium chloride
CsR	*Coccomyxa subellipsoidea* rhodopsin
$CuSO_4$	Copper sulfate
ddH_2O	Double distilled (purified) water
DMEM	Dulbecco`s Modified Eagle Medium
DMSO	Dimethyl sulfoxide
DNA	Desoxyribonucleic acid
DPSS	Diode pumped solid state laser
dSTORM	Direct stochastic optical reconstruction microscopy
E	Kir2.1 endoplasmic reticulum export signal
ECL	Extracellular loop
EDTA	Ethylenediaminetetraacetic acid

eGFP	Enhanced green fluorescent protein
EGTA	ethylene glycol-bis(β-aminoethyl ether)-*N*,*N*,*N*',*N*'-tetraacetic acid
EM	Electron microscopy
ER-Tracker	ER-Tracker™ Red (BODIPY™ TR Glibenclamide)
ExM	Expansion microscopy
eYFP	Enhanced yellow fluorescent protein
FA	Formaldehyde
FAD	Flavin adenine dinucleotide
FCS	Fetal calf serum
$FeCl_3$	Iron chloride
FM4-64	FM™4-64 (N-(3-triethylammoniumpropyl)-4-(6-(4-(diethylamino) phenyl) hexatrienyl) pyridinium dibromide)
FP	Fluorescent protein
GA	Glutaraldehyde
GOI	Gene of interest
GPCR	G-protein coupled receptor
H_3BO_3	Boric acid
HBSS	Hank`s Balanced Salt Solution
HCl	Hydrochloric acid
HEK	Human embryonic kidney
HEPES	4-(2-hydroxyethyl)-1-piperazineethanesulfonic acid
HR	Halorhodopsin
Hyg	Hygromycin
IAA	Indole acetic acid
IBMX	3-Isobutyl-1-Methylxanthine
ICL	Intracellular loop
IPA	Indole propionic acid
KCl	Potassium chloride
KGluc	Potassium gluconate
KOH	Potassium hydroxide
KR2	*Krokinobacter eikastus* rhodopsin 2
LEI	Outer SE-detector
LOV domain	Light-Oxygen-Voltage domain
LR	*Leptosphaeria maculans* rhodopsin
lr	Lucy rho signal peptide
MAP	Magnified analysis of the proteome
MES	2-(N-Morpholino)ethane sulphonic acid
$Mg(Ac)_2$	Magnesium acetate
$MgCl_2$	Magnesium chloride
MgGluc	Magnesium gluconate
$MgSO_4$	Magnesium sulfate

Mitotracker Orange	MitoTracker® Orange CMTMRos
$MnCl_2$	Manganese chloride
MoO_4Na	Molybdenum tetroxide sodium
NA	Numeric aperture
NaAc	Sodium acetate
NaCl	Sodium chloride
NaGluc	Sodium gluconate
NaOH	Sodium hydroxide
ND filter	Neutral density filter
NG108-15	Neuroblastoma/glioma 108-15
NH_4Cl	Ammonium chloride
Nop-1	*Neurospora crassa* opsin 1
NpHR	*Natronomonas pharaonis* halorhodopsin
NR-like	*Neurospora crassa* rhodopsin nop-1-like
LCD-enzyme solution	Lysing enzyme chitinase driselase-enzyme solution
OPA	Operational amplifier
PALM	Photoactivated localization microscopy
PBS	Phosphate Buffered Saline
PCR	Polymerase chain reaction
PDA	Potato dextrose agar
PDB	Potato dextrose broth
PDL	Poly-D-lysine
PhaeoRD1	*Phaeosphaeria* rhodopsin 1
PhaeoRD2	*Phaeosphaeria* rhodopsin 2
pHrodoRED	pHrodo™ Red succinimidyl ester
PoXeR	*Parvularcula oceani* xenorhodopsin
RT	Room temperature
SEM	Scanning electron microscopy/microscope
SEI	In-lens-SE-detector
SIM	Structured illumination microscopy/microscope
SMLM	Single molecule localization microscopy
Sop-1	*Sclerotia sclerotion* rhodopsin 1
SRI	Sensory rhodopsin I
SRII	Sensory rhodopsin II
STED	Stimulated emission depletion
STORM	Stochastic optical reconstruction microscopy
SYTO 59	SYTO™ 59 Red Fluorescent Nucleic Acid Stain
T	Kir2.1 Golgi apparatus trafficking signal
TC	Tetracycline
TEM	Transmission electron microscopy/microscope

TEMED	Tetramethylethylenediamine
TetR	Tet repressor
TEVC	Two-electrode voltage clamp
TRIS	Tris(hydroxymethyl)aminomethan
UmOps1	*Ustilago maydis* rhodopsin 1
UmOps2	*Ustilago maydis* rhodopsin 2
UmOps3	*Ustilago maydis* rhodopsin 3
VVD	Vivid
WCC	White Collar Complex
WC-1	White Collar-1
WC-2	White Collar-2
WOA	Weak organic acid
XR	Xanthorhodopsin
YNB	Yeast nitrogen base
$ZnSO_4$	Zinc sulfate

List of Figures

List of Tables

Supplement

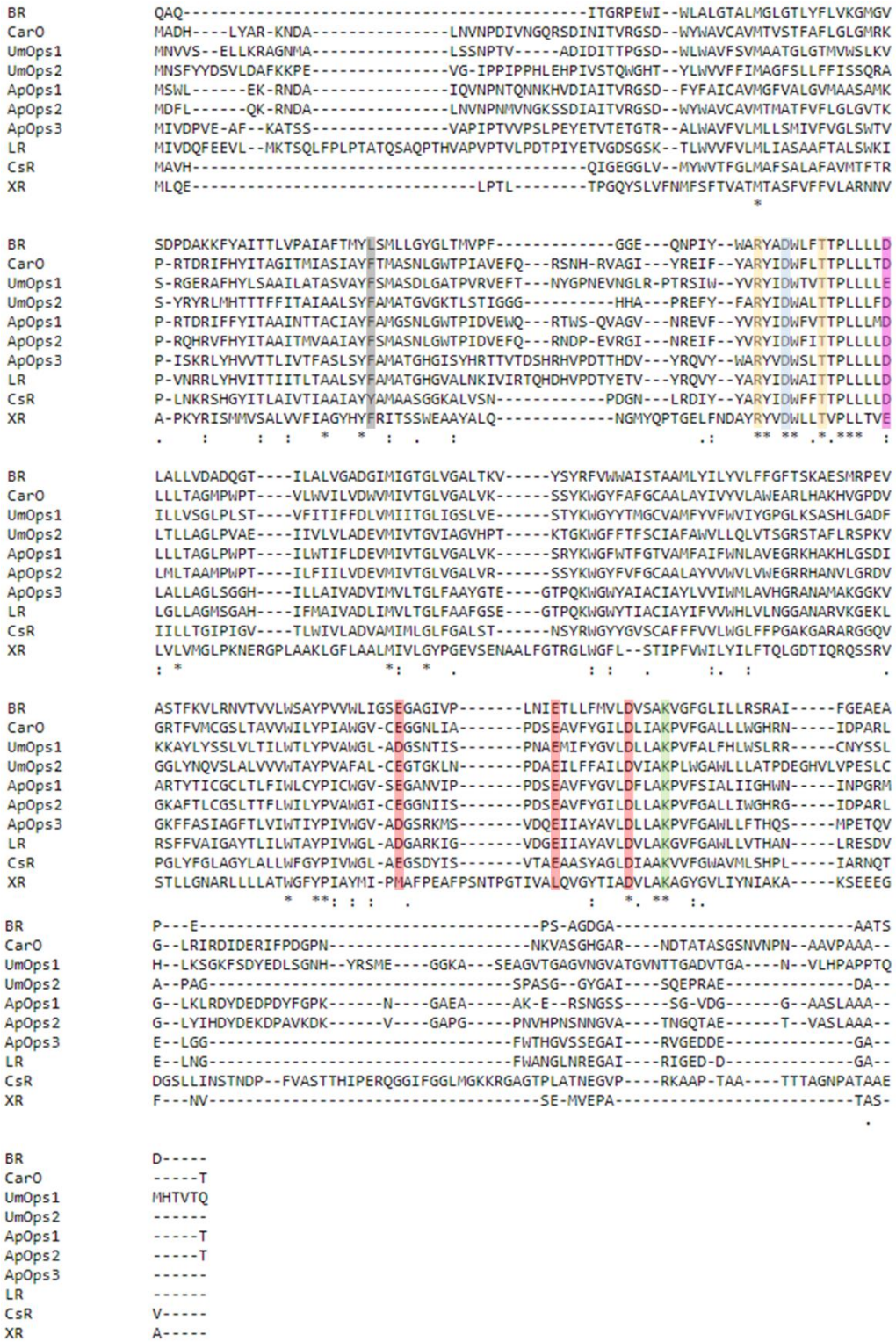

Supplementary Figure 1: Multiple Sequence Alignment of BR and selected rhodopsins. Fungal rhodopsins: CarO (*F. fujikuroi*), UmOps1, UmOps2 (*U. maydis*), ApOps1, ApOps2 and ApOps3 (*A. pullulans*), LR (*L. maculans*), algal rhodopsin CsR (*C. subellipsoidea*); bacterial rhodopsin XR (*S. ruber*). Key residues necessary for proton transport in BR and their counterparts in the other rhodopsins are highlighted (green: retinal binding site BR K216, blue: primary proton acceptor BR D85, purple: proton donor BR D96, yellow: mediators BR R82 and BR T89, red: proton releasing group BR E194, BR E204 and BR D212, grey: F conserved mainly in fungal rhodopsins).

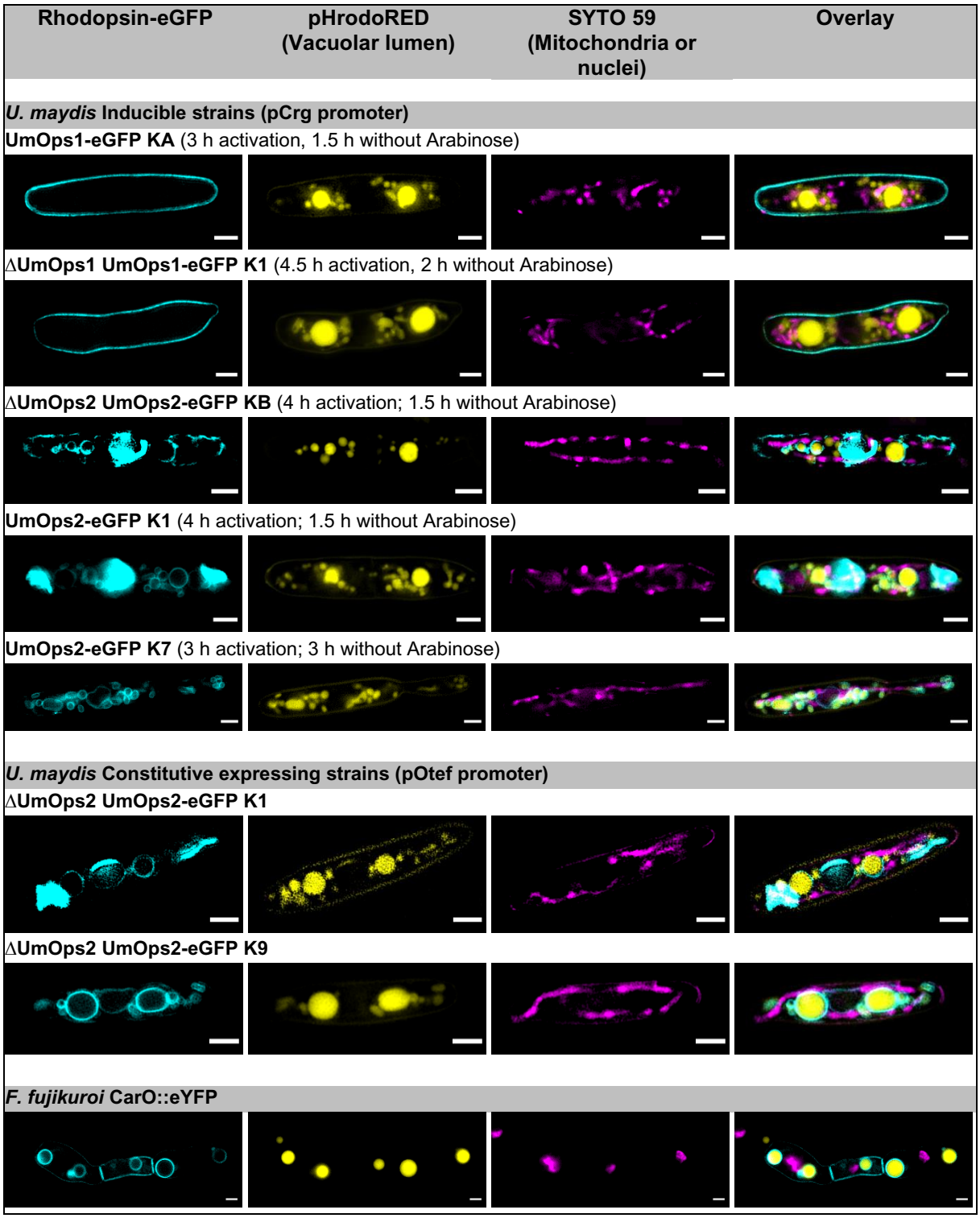

Supplementary Figure 2: Overview of Counterstaining of Rhodopsins with SYTO 59 and pHrodoRED in all Fungal Strains. pHrodoRED was observed in the vacuoles in all strains, SYTO 59 stains the nuclei in *F. fujikuroi* hyphae. In *U. maydis* sporidia, SYTO 59 labeled mitochondria. The intracellular fluorescence signals from UmOps2 as well as from CarO surrounded the vacuoles. Images of ΔUmOps1 UmOps1-eGFP K1 were published (Panzer *et al.*, 2019). SIM images; scale bars: 2 µm

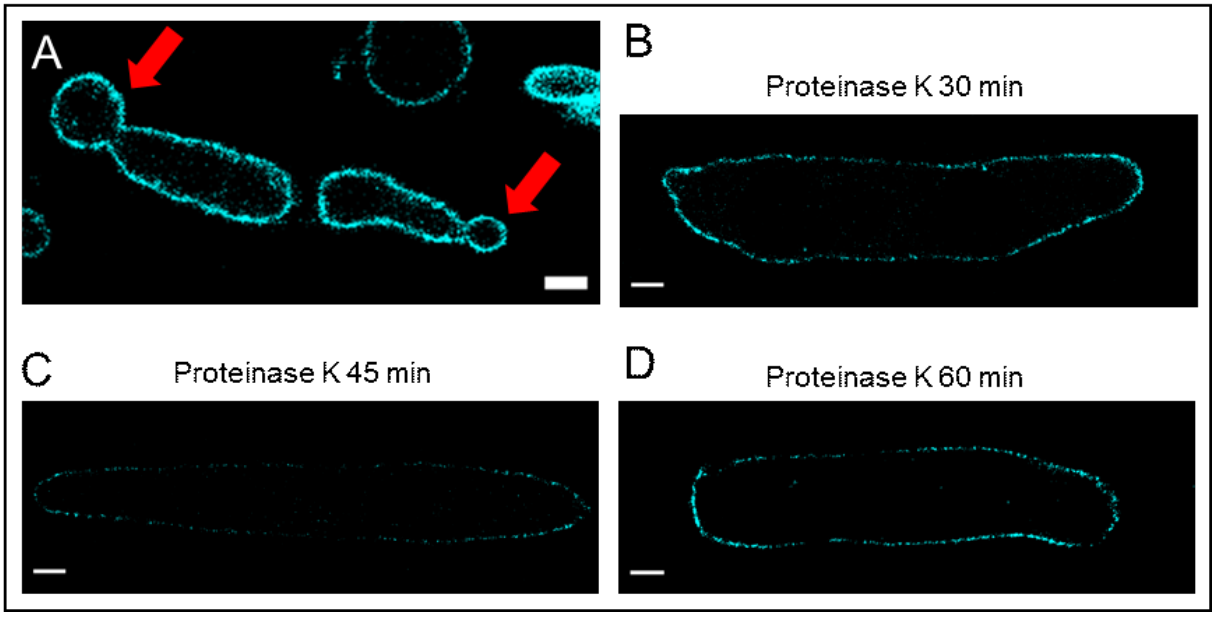

Supplementary Figure 3: Protoplastation and Homogenization of UmOps1-eGFP Expressing Sporidia. When digesting the cell wall with the LCD-enzyme solution, the process started at the tip region of the sporidia allowing the protoplast being released from the remaining cell wall components (**A, red arrows**). Different durations of homogenization with Proteinase K (30, 45 or 60 min) did not alter the fluorescence signals deriving from eGFP (**B, C, D**). Scale bars: A: 2 µm; B, C, D: 5 µm

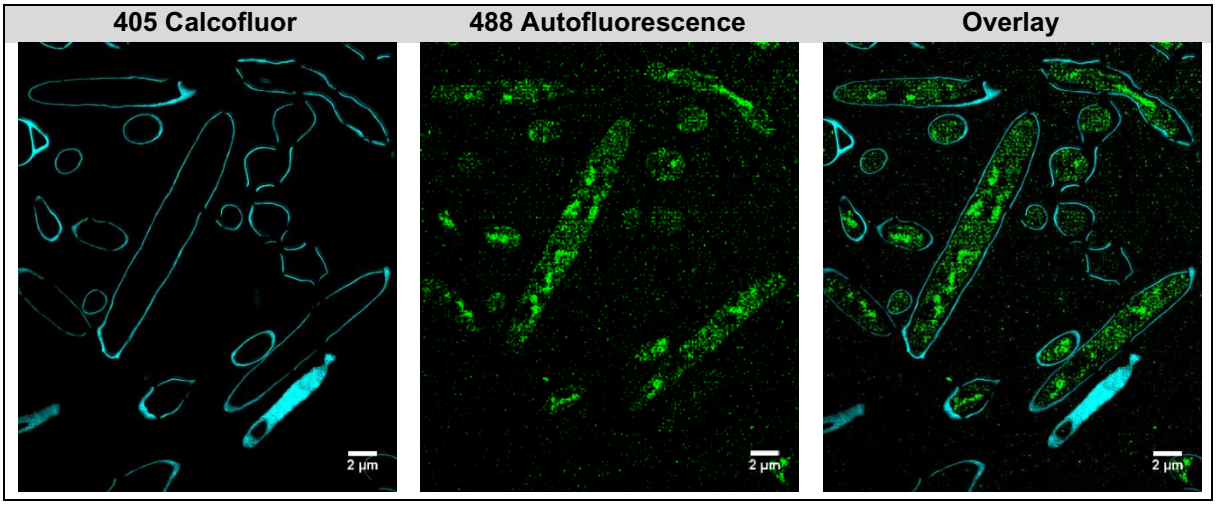

Supplementary Figure 4: Calcofluor staining of *U. maydis* sporidia for CLEM. Calcofluor stained the cell wall of the sporidia in a sufficient manner. High laser powers in the 488 nm channel yielded autofluorescence images of sporidia and one can see in the overlay image, that the cell wall was ripped off the sporidia in some cases during freezing and embedding. However, cell wall staining could be used as a mark for correlation of fluorescence and EM images.

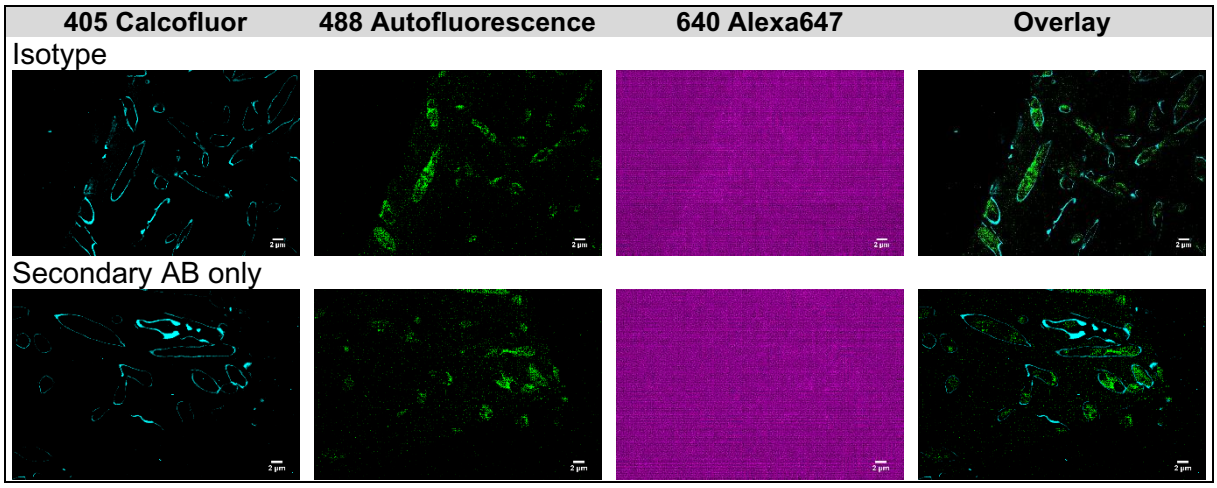

Supplementary Figure 5: Antibody staining of UmOps1-eGFP expressing *U. maydis* sporidia. When using an isotype or only the secondary antibody, no labelling of eGFP occurred and no fluorescence signals could be obtained.

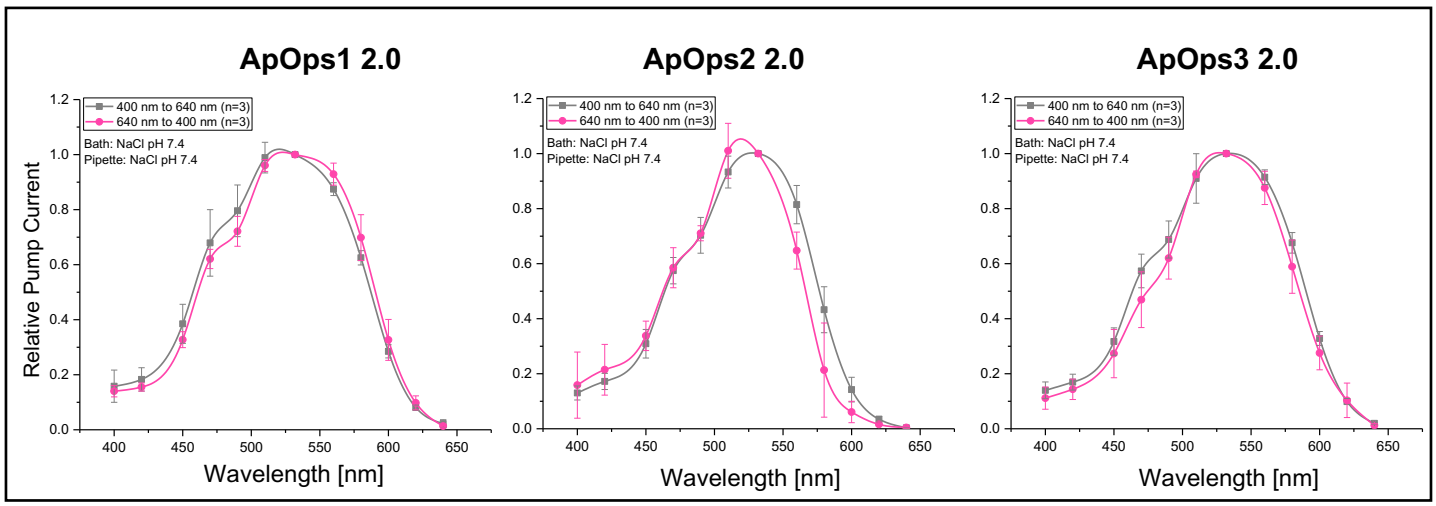

Supplementary Figure 6: Detailed Action Spectra of ApOps1 2.0, ApOps2 2.0 and ApOps3 2.0. Action spectra were recorded either starting in the blue or in the red spectral range. Mean and standard deviations are depicted. In all cases, the order of the applied wavelengths (starting from blue or from red) did not alter the results much. All *A. pullulans* rhodopsins showed their maximum pump activity in the green spectral range.

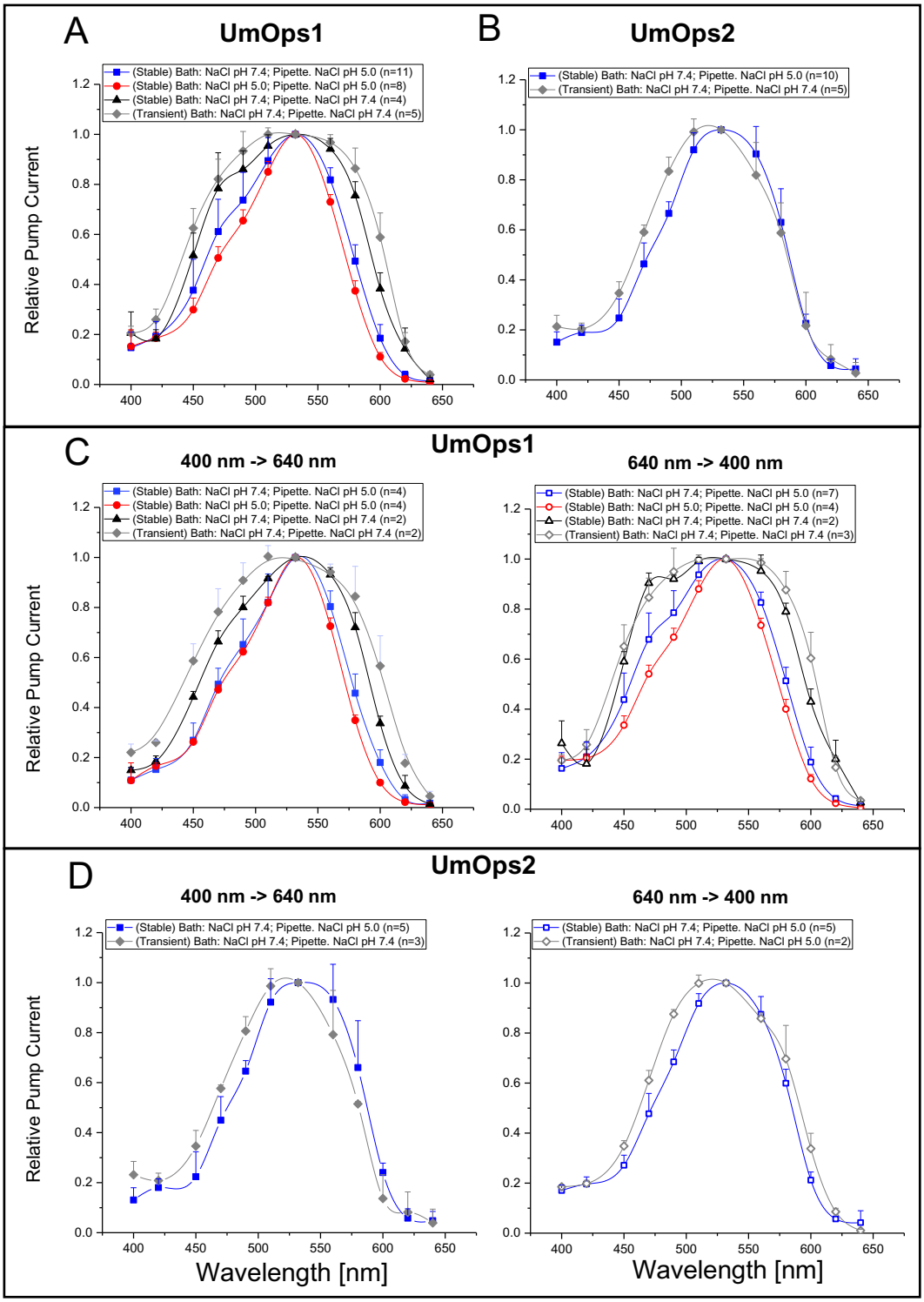

Supplementary Figure 7: Detailed Action Spectra of UmOps1 and UmOps2. Action spectra were recorded in different cellular backgrounds and different pH values of the pipette solution. Transiently transfected NG108-15 cells (grey lines) showed similar results compared to the stable HEK293 cell line. However, using pH 7.4 in the pipette resulted in broader spectra due to the higher signal-to-noise ratio (**A, B**). Action spectra were recorded either starting in the blue or in the red spectral range (**C, D**). Mean and standard deviations are depicted. In all cases, the order of the applied wavelengths (starting from blue or from red) did not alter the results much. UmOps1 as well as UmOps2 show their maximum pump activity in the green spectral range. Action spectra of stably expressing HEK293 cell line using pipette solution NaCl pH 5.0 were published (Panzer, 2017; Panzer *et al.*, 2019).

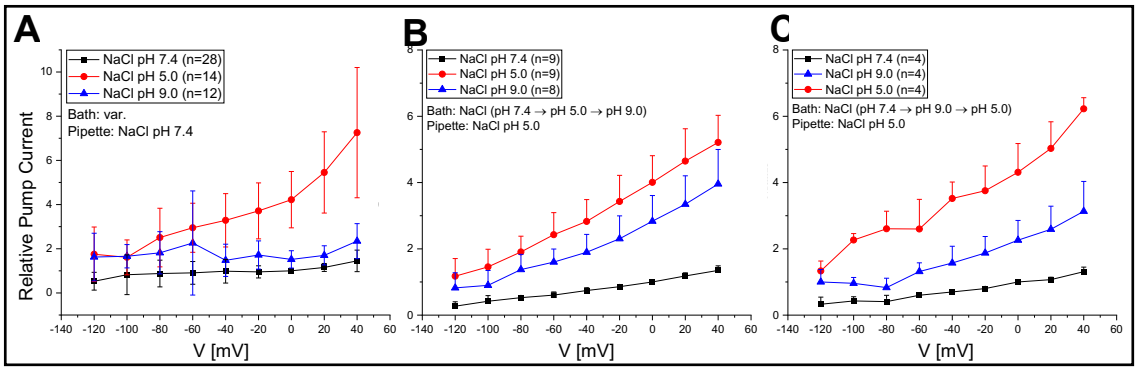

Supplementary Figure 8: I-V-plots of patch-clamp measurements on UmOps1. Using NaCl pH 7.4 as pipette solution (**A**) or changing the order of the applied pH-values from pH 7.4→pH 5.0→pH 9.0 (**B**) to pH 7.4→pH 9.0→pH 5.0 (**C**) did not alter the characteristics of UmOps1.

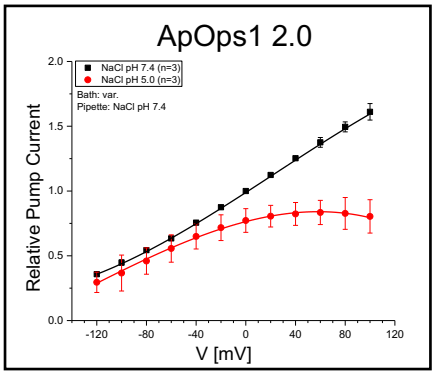

Supplementary Figure 9: Voltage Dependency of ApOps1 2.0 at Extracellular pH 5.0. The photocurrents of ApOps1 2.0 at extracellular pH 5.0 (red line) increased with increasing clamp-voltage from -120 mV to about -20 mV. Then the currents saturated and the voltage dependency was virtually reversed when extending the step protocol from +40 mV to +100 mV.

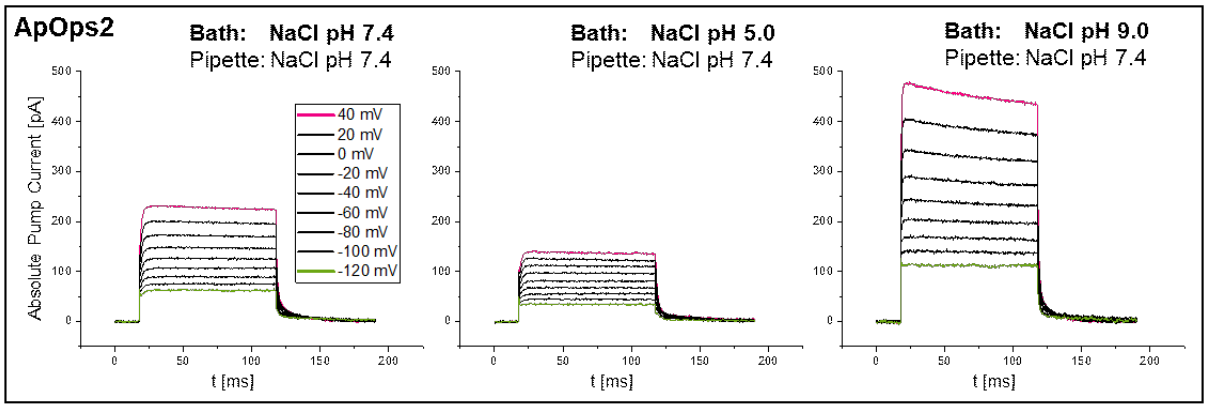

Supplementary Figure 10: Absolute Photocurrents of ApOps2 without 2.0 Modifications Plotted over Time. The pH and the voltage dependency were not altered when measuring without the 2.0 modifications in stably expressing HEK293 cell line. At lower clamp voltages, initial peak currents were visible. Current traces measured at extracellular pH 7.4 were published (Panzer *et al.*, 2021)

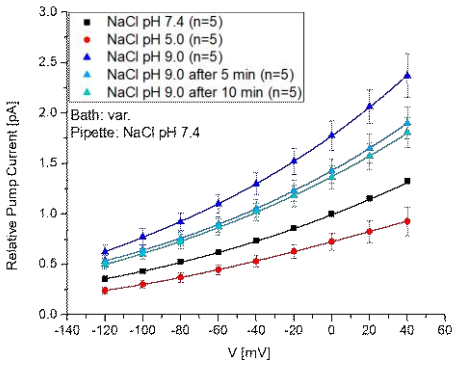

Supplementary Figure 11: PH Dependency of ApOps2 (stable HEK293 cell line). The pH dependency was not altered when measuring without the 2.0 modification. The photocurrents measured at extracellular pH 9.0 get lower over time but do not decrease to the pH 7.4 level even within 10 min.

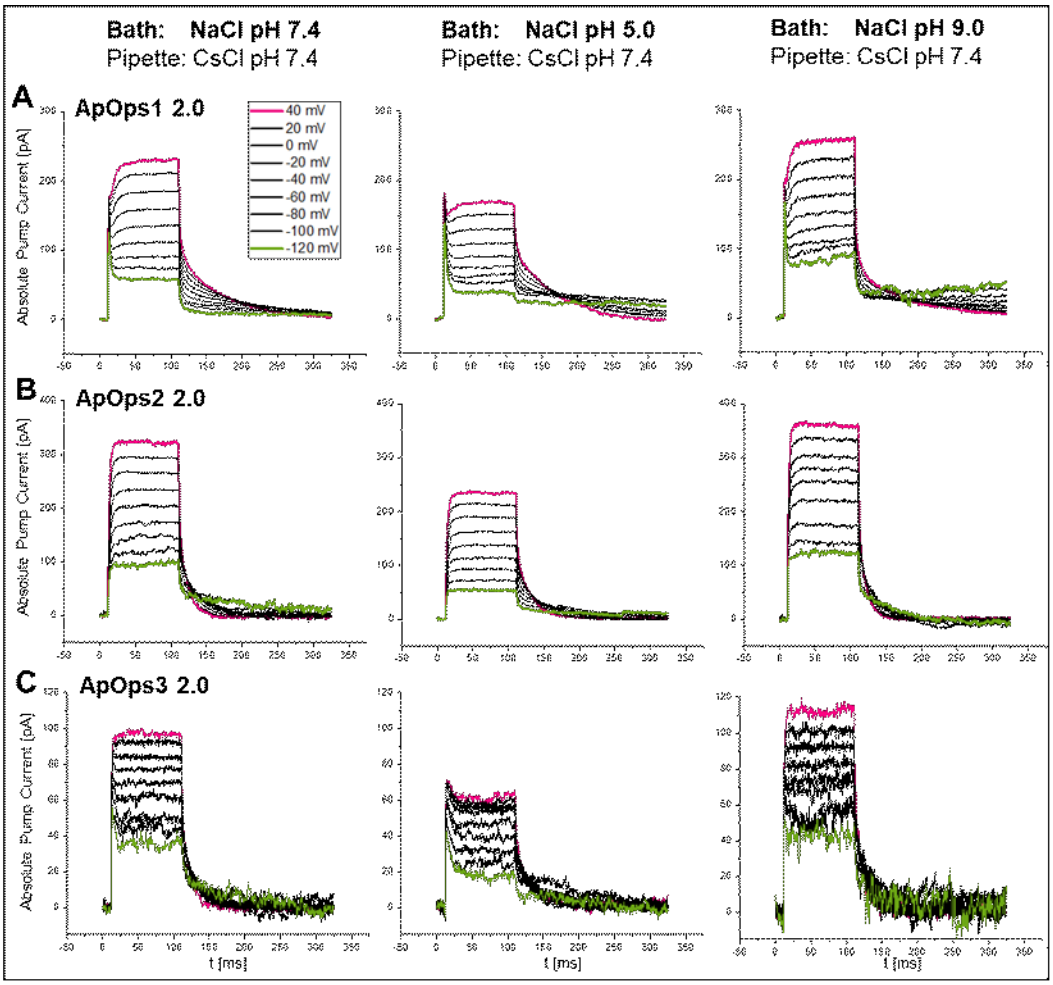

Supplementary Figure 12: Absolute Photocurrents of ApOps1 2.0, ApOps2 2.0 and ApOps3 2.0 Plotted over Time Using Intracellular CsCl. All three rhodopsins showed voltage and pH dependency similar to those using intracellular NaCl. Only ApOps1 2.0 as well as ApOps3 2.0 showed initial peak currents at least at lower clamp-voltages (**A, C**), whereas ApOps2 2.0 showed only dominating stationary photocurrents (**B**). The negative current short after light-on in ApOps3 2.0 at extracellular pH 5.0 was observed again, however, the signal to noise ratio was not so good compared to intracellular NaCl (**C**). The saturation of the photocurrents at positive clamp-voltages in extracellular NaCl pH 5.0 short after light-on disappeared in ApOps1 2.0 (**A**).

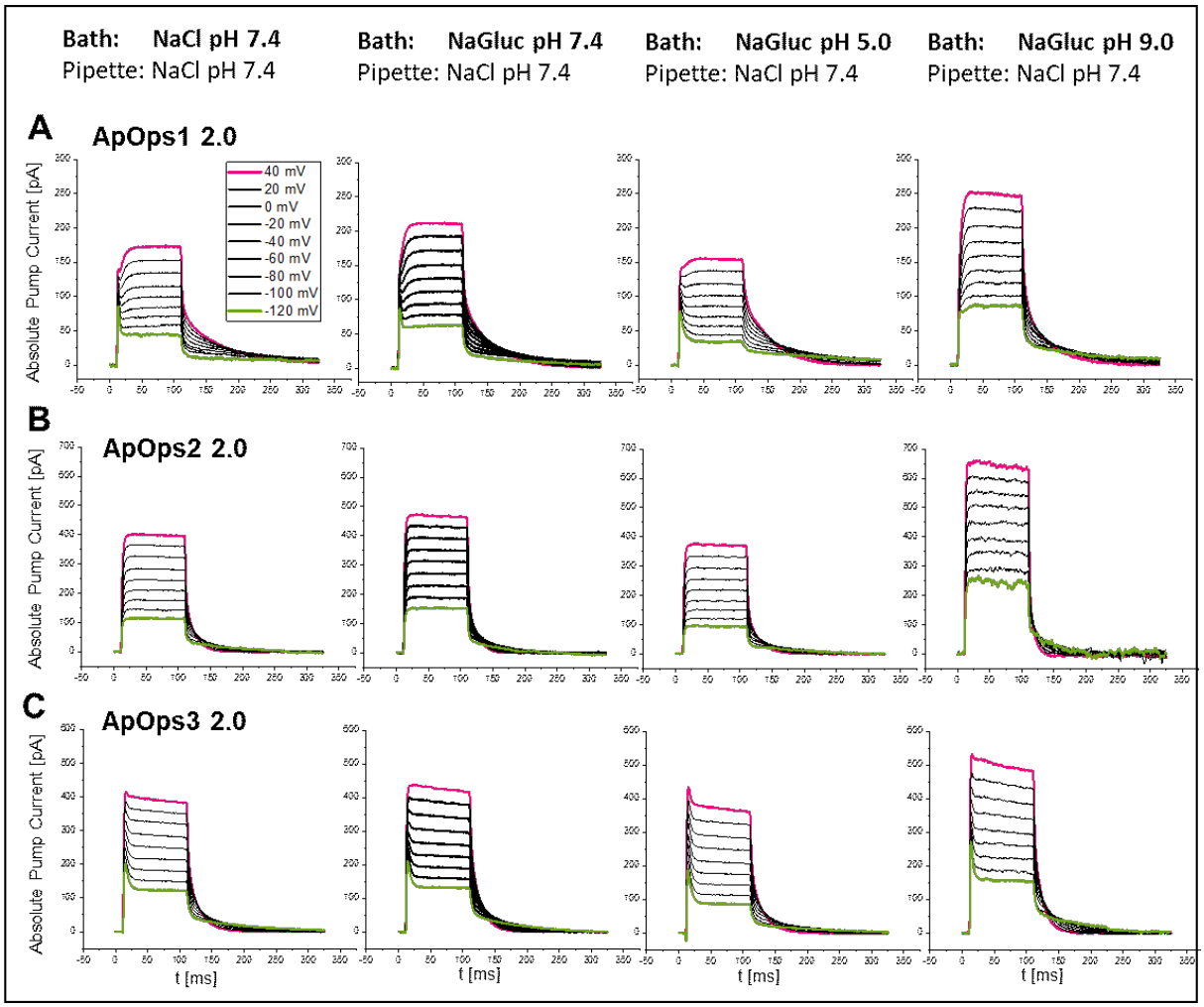

Supplementary Figure 13: Absolute Photocurrents of ApOps1 2.0, ApOps2 2.0 and ApOps3 2.0 Plotted over Time Using Extracellular NaGluc. All three rhodopsins showed voltage and pH dependency similar to those using extracellular NaCl. Only ApOps1 2.0 as well as ApOps3 2.0 showed initial peak currents at least at lower clamp-voltages (**A, C**), whereas ApOps2 2.0 showed only dominating stationary photocurrents (**B**). The negative current short after light-on in ApOps3 2.0 at extracellular pH 5.0 was observed again (**C**). In all three rhodopsins, the presence of NaGluc yielded slightly higher photocurrents compared to extracellular NaCl. The saturation of the photocurrents that was observed at positive clamp-voltages in extracellular NaCl pH 5.0 for ApOps1 2.0 and ApOps3 2.0 disappeared in both rhodopsins in extracellular NaGluc pH5.0.

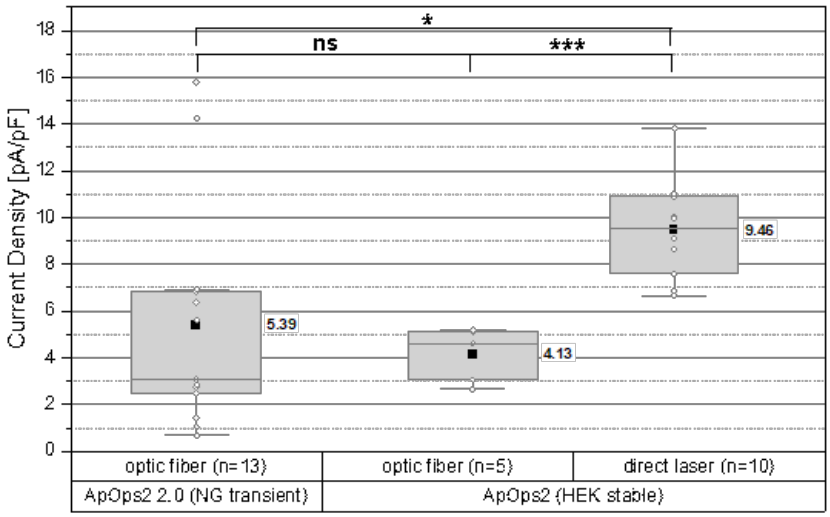

Supplementary Figure 14: Current Densities of ApOps2 Using Different Measuring Conditions. ApOps2 with (transiently transfected NG108-15 cells) or without the 2.0 modification (stably expressing HEK293 cell line) yielded similar current densities (not significant (ns): $p>0.05$) when using the optic fiber for light transportation (stable 15 mW/mm^2). The direct laser caused significantly increased current densities (* $p<0.05$; *** $p<0.001$) what implicates, that higher light intensities occurred or even unstable illumination conditions were applied. Measurements were conducted in intra- and extracellular NaCl pH 7.4.

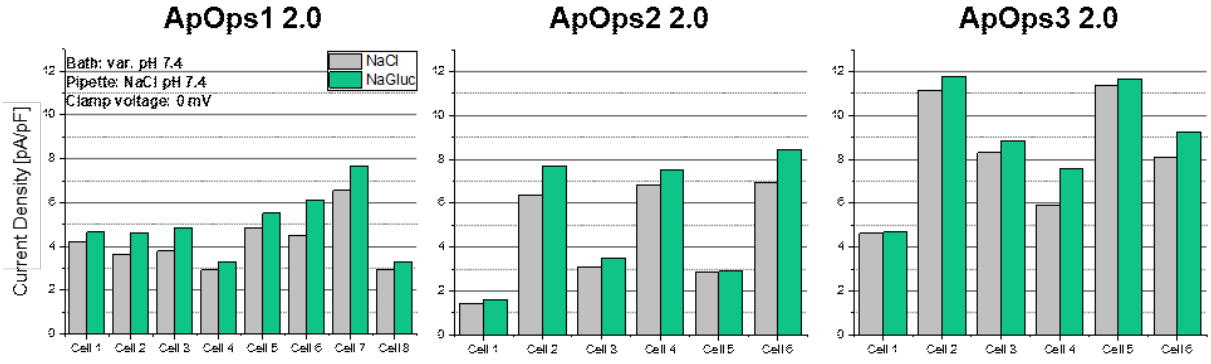

Supplementary Figure 15: Comparison of Current Densities of *A. pullulans* Rhodopsins in Extracellular NaCl or NaGluc. Despite the current densities measured in NaCl and NaGluc are not significantly different, at the single cell level, one can observe, that the current density is always slightly enhanced in extracellular NaGluc due to the WOA-effect.

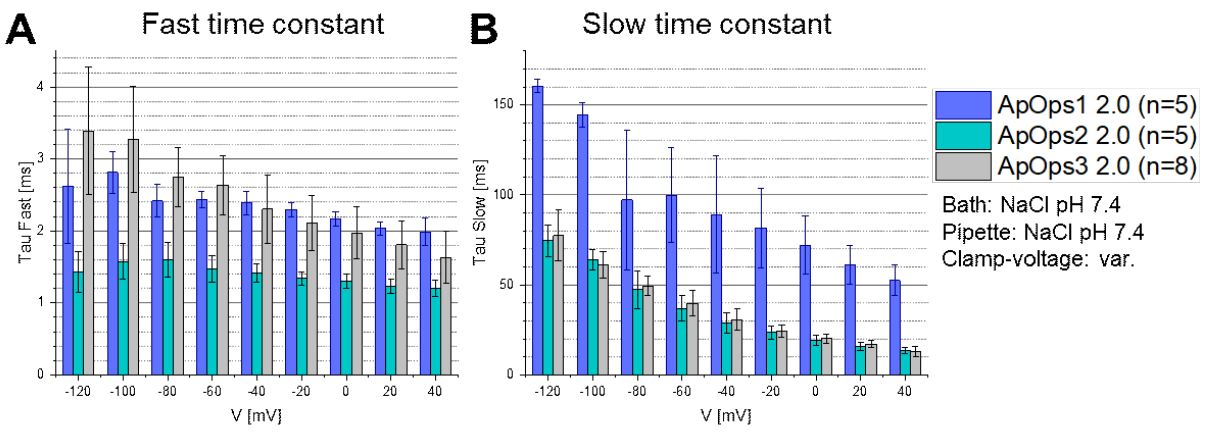

Supplementary Figure 16: Current Decay Kinetics of the *A. pullulans* Rhodopsins After Light-off at Different Clamp-Voltages. The current decays in a biexponential manner yielding a fast (**A**) and a slow (**B**) time constant. The slow time constant was voltage dependent yielding lower time constants at higher clamp-voltages, whereas the fast time constant showed almost no voltage dependency. The lowest fast time constants could be observed for ApOps2 2.0 at all clamp-voltages, ApOps1 2.0 showed the highest slow time constant at all clamp-voltages. Plots were published (Panzer *et al.*, 2021)

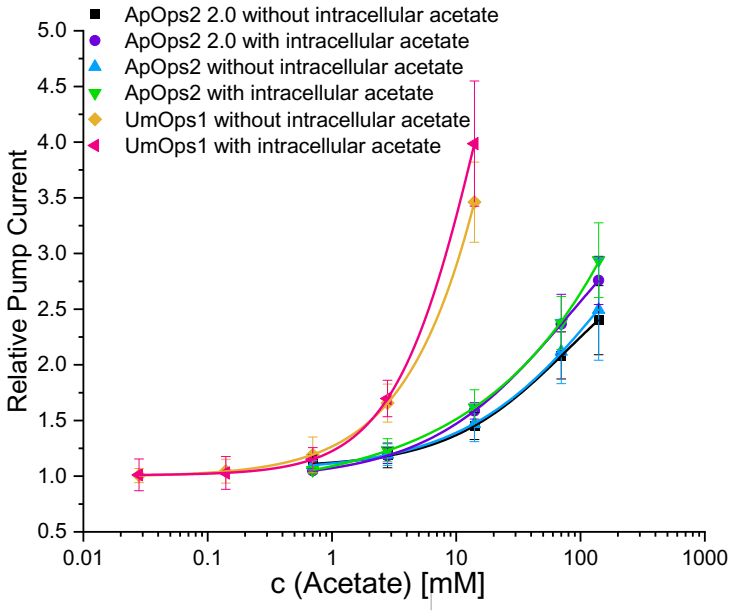

Supplementary Figure 17: Dose-Dependent Current Enhancement in the Presence of Extra- and Intracellular Acetate. All five rhodopsins showed an increase of the photocurrents upon supplementation with acetate on the extracellular side. Intracellular acetate (2.8 mM) was added and even at an equimolar extracellular acetate concentration, a current enhancement occurred. When enhancing further the extracellular acetate dose, the values obtained with intracellular acetate slightly exceeded the ones without intracellular acetate. The reaction of ApOps2 to acetate is not altered by the 2.0 modification.

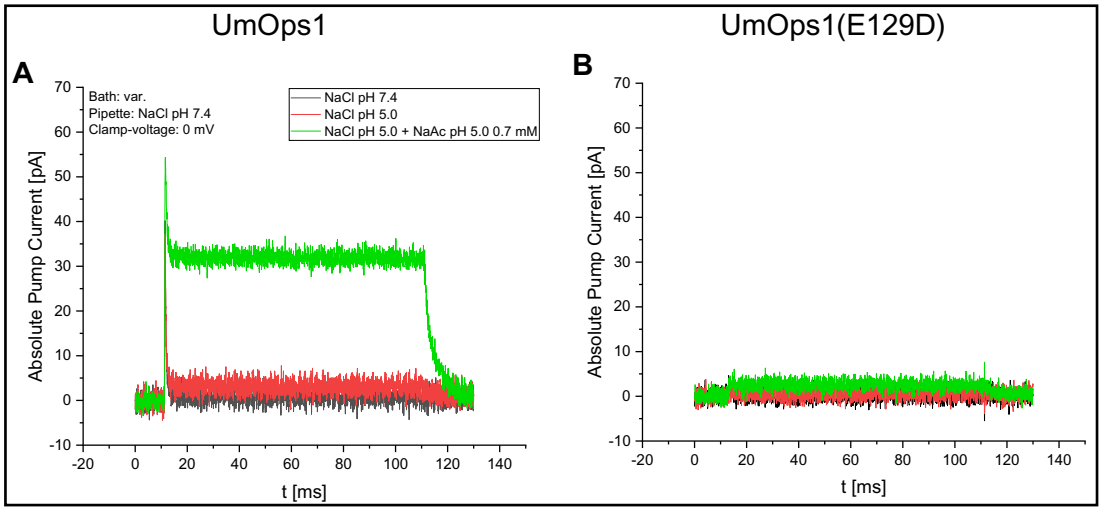

Supplementary Figure 18: Patch-Clamp Measurement in UmOps1 and UmOps1(E129D). UmOps1 showed massive enhancement of the pump current in presence of extracellular acidic environment (pH 5.0) in combination with 0.7 mM acetate (**A**), whereas UmOps1(E129D) mutant did not yield increased photocurrents under the given conditions (**B**).

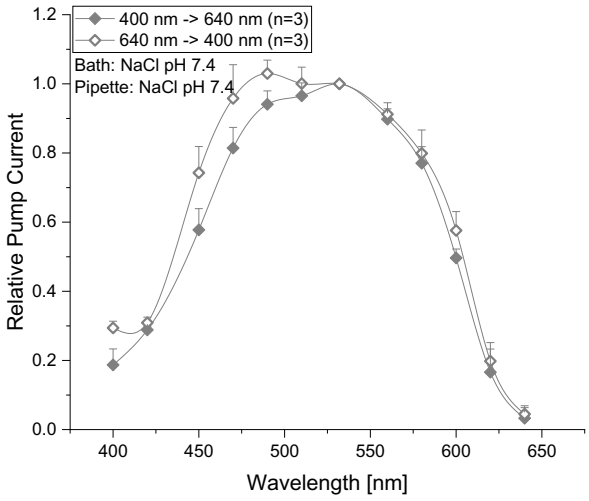

Supplementary Figure 19: Detailed Action Spectrum of UmOps1(D225E). When starting with higher wavelengths, a hypsochromic shift of the maximum could be observed. However, the highest pump activity was always reached when illuminating the rhodopsin mutant with green light.

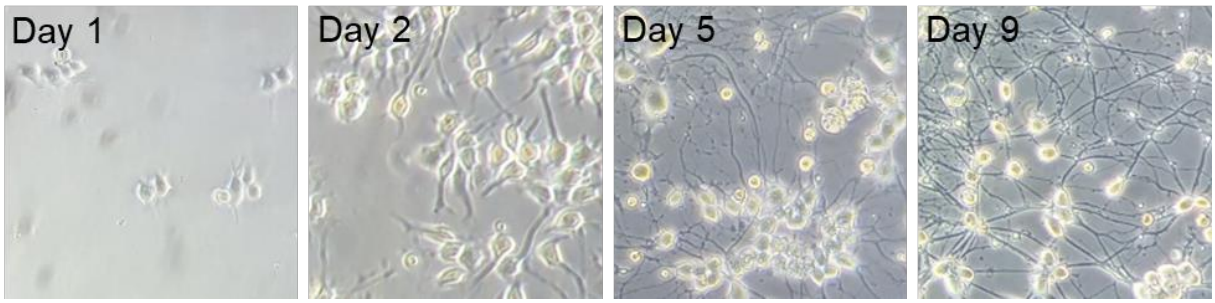

Supplementary Figure 20: Differentiation of NG108-15 Cells. NG108-15 cell line was differentiated with the help of defined chemicals so that the cells develop dendrites and axons.

Supplementary Table 1: Listing of Observed Pump Maxima of the Rhodopsins and the Respective Wavelengths. All tested rhodopsins showed their pump maxima in the green spectral range, however, there were slight deviations. In some cases, the rhodopsins were maximally activated at 510 nm or 560 nm, respectively, in one case even at 490 nm.

			λ [mn]						
			400 -> 640			640 -> 400			
		Total no. of cells	510	**532**	560	490	510	**532**	560
UmOps1			Number of cells yielding the highest activation using the respective λ						
stable	Bs: NaCl pH 7.4; Ps: NaCl pH 5.0	11		4			1	6	
stable	Bs/Ps: NaCl pH 7.4	4		2			1	1	
stable	Bs/Ps: NaCl pH 5.0	8		4				4	
transient	Bs/Ps: NaCl pH 7.4	5	1	1		1	1	1	
UmOps2									
stable	Bs: NaCl pH 7.4; Ps: NaCl pH 5.0	10		4	1			4	1
transient	Bs/Ps: NaCl pH 7.4	5	1	2			1	1	
ApOps1 2.0									
transient	Bs/Ps: NaCl pH 7.4	6	2	1				3	
ApOps2 2.0									
transient	Bs/Ps: NaCl pH 7.4	6		3			1	2	
ApOps3 2.0									
transient	Bs/Ps: NaCl pH 7.4	6	1	2				3	

Supplementary Table 2: Ratios of the Mean Current Values obtained at 0 mV Clamp-voltage at Extracellular pH 7.4 to the mean values Obtained at the Different pH values. UmOps1 yielded larger current ratios compared to the other rhodopsins. The most striking issue is the massive current enhancement at extracellular pH 5.0.

Rhodopsin	Normalized Current Values (at 0 mV)		
	pH 5.0	**pH 7.4**	**pH 9.0**
UmOps1	4.10 ± 0.80	1	2.64 ± 0.75
UmOps2	0.74 ± 0.09	1	1.15 ± 0.07
ApOps1 2.0	0.75 ± 0.08	1	1.33 ± 0.09
ApOps2 2.0	0.79 ± 0.11	1	1.32 ± 0.21
ApOps3 2.0	0.73 ± 0.12	1	1.09 ± 0.11

Supplementary Table 3: Current Densities of UmOps1, UmOps2, ApOps1 2.0, ApOps2 2.0 and ApOps3 2.0. The mean current densities with standard deviation (SD) as well as median, minimum and maximum values of the rhodopsin measurements at 0 mV clamp-voltage in different electrolytes are listed. UmOps1 and UmOps2 yielded higher current densities when intracellular pH 5.0 was applied (compared to intracellular pH 7.4). Extracellular NaGluc enhanced the current densities in all cases except for ApOps2 2.0. In general, the two rhodopsins of *U. maydis* yielded lower current densities compared to all *A. pullulans* rhodopsins. In all rhodopsins except ApOps3 2.0, the values obtained with NaCl- or CsCl-based pipette solutions were comparable. In ApOps3 2.0 the current density decreased when CsCl was applied intracellularly. The highest maximum value was measured in ApOps2 2.0 (green).

Bath	Pipette	Mean	SD	Median	Minimum	Maximum
		[pA/pF]				
UmOps1						
NaCl pH 7.4	NaCl pH 7.4	0.09581	0.07716	0.07913	0.01017	0.43073
NaCl pH 7.4	NaCl pH 5.0	0.28082	0.25002	0.17149	0.08382	0.94827
NaCl pH 7.4	CsCl pH 5.0	0.21206	0.16419	0.171400	0.03861	0.58571
NaGluc pH 7.4	NaCl pH 7.4	0.09740	0.08806	0.06576	0.00747	0.33858
UmOps2						
NaCl pH 7.4	NaCl pH 7.4	0.14091	0.06571	0.11781	0.06872	0.30616
NaCl pH 7.4	NaCl pH 5.0	0.28668	0.11303	0.25997	0.18141	0.41840
NaCl pH 7.4	CsCl pH 5.0	0.20981	0.13715	0.19597	0.05470	0.48033
NaGluc pH 7.4	NaCl pH 7.4	0.18192	0.08757	0.13885	0.12331	0.36451
ApOps1 2.0						
NaCl pH 7.4	NaCl pH 7.4	4.51060	1.17308	4.37276	2.92367	6.59576
NaCl pH 7.4	CsCl pH 5.0	4.24913	1.08555	4.08117	3.12852	5.99464
NaGluc pH 7.4	NaCl pH 7.4	4.99897	1.45076	4.73713	3.30449	7.67910
ApOps2 2.0						
NaCl pH 7.4	NaCl pH 7.4	5.39272	4.79688	3.08161	0.68320	15.79068
NaCl pH 7.4	CsCl pH 5.0	5.40974	2.82005	4.69234	2.33562	9.78571
NaGluc pH 7.4	NaCl pH 7.4	5.28133	2.94045	5.51921	1.58921	8.46247
ApOps3 2.0						
NaCl pH 7.4	NaCl pH 7.4	7.28342	3.24525	8.20900	1.25725	11.37120
NaCl pH 7.4	CsCl pH 5.0	3.09276	2.25219	2.38658	0.43719	7.97829
NaGluc pH 7.4	NaCl pH 7.4	8.97424	2.66662	9.06251	4.68236	11.79275

Supplementary Table 4: Pump Current Ratios of Bath Solutions Without to Bath Solutions With Acetate in Presence or Absence of Intracellular Acetate at 0 mV Clamp-voltage. Due to the normalization, the pump currents in bath solution NaCl pH 7.4 without supplemented acetate (0 mM NaAc) are defined as 1±0. The table shows the ratio of this value to the normalized current values obtained at defined concentrations of extracellular acetate (0.028 to 140 mM) in the different rhodopsins. Moreover, these measurements were done in absence and presence of intracellular acetate (pipette solution without or with 0.28 mM NaAc). All measurements were done under physiological pH conditions (pH 7.4).

	UmOps1		UmOps1(D225E)		UmOps2	ApOps2		ApOps2 2.0	
Pipette solution	**NaCl pH 7.4**	**NaCl pH 7.4 + NaAc pH 7.4 2.8 mM**	**NaCl pH 7.4**	**NaCl pH 7.4 + NaAc pH 7.4 2.8 mM**	**NaCl pH 7.4**	**NaCl pH 7.4**	**NaCl pH 7.4 + NaAc pH 7.4 2.8 mM**	**NaCl pH 7.4**	**NaCl pH 7.4 + NaAc pH 7.4 2.8 mM**
c [NaAc] in bath solution [mM]									
0	**1**±0 (n=7)	**1**±0 (n=9)	**1**±0 (n=5)	**1**±0 (n=7)	**1**±0 (n=5)	**1**±0 (n=5)	**1**±0 (n=7)	**1**±0 (n=15)	**1**±0 (n=4)
0.028	**1.01**±0.064 (n=7)	**1.01**±0.14 (n=2)							
0.14	**1.05**±0.11 (n=7)	**1.03**±0.15 (n=2)	**1.2**±0.13 (n=5)	**1.07**±0.073 (n=6)					
0.7	**1.2**±0.16 (n=7)	**1.2**±0.10 (n=8)	**1.4**±0.18 (n=5)	**1.14**±0.076 (n=5)		**1.1**±0.043 (n=5)	**1.1**±0.032 (n=6)	**1.1**±0.081 (n=5)	**1.05**±0.017 (n=4)
2.8	**1.7**±0.17 (n=7)	**1.7**±0.16 (n=8)	**1.6**±0.17 (n=5)	**1.4**±0.093 (n=4)	**0.98**±0.066 (n=4)	**1.2**±0.097 (n=5)	**1.2**±0.10 (n=2)	**1.2**±0.11 (n=5)	**1.2**±0.071 (n=4)
14	**3.5**±0.36 (n=7)	**4.0**±0.56 (n=9)	**2.6**±0.24 (n=5)	**2.5**±0.39 (n=5)	**1.08**±0.069 (n=5)	**1.5**±0.16 (n=5)	**1.6**±0.16 (n=6)	**1.5**±0.12 (n=5)	**1.6**±0.074 (n=4)
70						**2.1**±0.29 (n=5)	**2.4**±0.24 (n=6)	**2.1**±0.21 (n=5)	**2.4**±0.27 (n=4)
140						**2.5**±0.45 (n=5)	**2.9**±0.34 (n=5)	**2.4**±0.31 (n=5)	**2.8**±0.22 (n=4)

Acknowledgements

I would like to thank…

…PD Dr. Ulrich Terpitz, Prof. Dr. Alfred Batschauer and Prof. Dr. Markus Sauer for being my supervisors, for fruitful discussions and helpful advices.

…again PD Dr. Ulrich Terpitz for the possibility to work further on the interesting fungal rhodopsin topic after finishing my master thesis.

…again Prof. Dr. Markus Sauer for the opportunity to work at the Department for Biotechnology and Biophysics and providing excellent equipment and utensils.

…again Prof. Dr. Alfred Batschauer for the fruitful collaboration, for providing all *Ustilago maydis* strains, the introduction to the photobiology of this interesting fungus and of course for the warm and friendly welcome in Marburg. At this point I want to thank also Annika Brych for the friendly working atmosphere when performing collaborative experiments.

…all collaborators of the Georg Nagel lab: Prof. Dr. Georg Nagel, Chong Zhang, Dr. Shiqiang Gao and Jing Yu-Strzelczyk for the nice and fruitful collaboration on the ApOpsins.

…at this point also Dr. Tilen Konte for providing the first ApOps-constructs and introducing me to halotolerant fungi during my bachelor`s thesis.

…Prof. Dr. Christian Stigloher, Daniela Bunsen and Claudia Gehrig for the possibility to perform CLEM-experiments and for the fruitful collaboration especially together with Sebastian Sputh.

…Dr. Ralph Götz, Janna Eilts, PD Dr. med. Johannes Wagener, Dr. David Turrà and Prof. Dr. Antonio Di Pietro for the fruitful collaboration in terms of ExM on fungi.

…Dr. Jan Schlegel and Nora Trinks for all the patience and helping with any problem.

…again Sebastian Sputh, and furthermore Stephan Deimel, Saskia Haarmann, Jeffrey Wilczek, Parathy Yogendran, Celine Bräuer and Anne Diemar for the friendly working atmosphere.

…Lisa Behringer-Pließ and Petra Geßner for all the helpful advices regarding cell culture, antibodies, dyes (and beyond). …Markus Behringer for helping me with SIM experiments, for answering all questions about microscopy and especially for his help when rebuilding the patch-clamp setup and implementing the optic fiber…Oliver Reichert for any help with PC, software and especially printer problems.

…Stefan Sachs for any help with and discussions and questions about ExM

…all members of the Department of Biotechnology and Biophysics for the great time and the very friendly and inspiring working environment.

…the Joint Practice for Pathology for the possibility to start my job as a part-time member.

…my family and my partner for all the support during really hard times. Without your help that would not have been possible <

…the catnip dealer^^

Curriculum Vitae

Eidesstattliche Erklärungen nach §7 Abs. 2 Satz 3, 4, 5

der Promotionsordnung der Fakultät für Biologie

Eidesstattliche Erklärung

Hiermit erkläre ich an Eides statt, die Dissertation: „**Pilzliche Rhodopsine im Rampenlicht: Eine Mikroskopische und Elektrophysiologische Studie**“, eigenständig, d. h. insbesondere selbständig und ohne Hilfe eines kommerziellen Promotionsberaters, angefertigt und keine anderen, als die von mir angegebenen Quellen und Hilfsmittel verwendet zu haben.

Ich erkläre außerdem, dass die Dissertation weder in gleicher noch in ähnlicher Form bereits in einem anderen Prüfungsverfahren vorgelegen hat.

Weiterhin erkläre ich, dass bei allen Abbildungen und Texten bei denen die Verwertungsrechte (Copyright) nicht bei mir liegen, diese von den Rechtsinhabern eingeholt wurden und die Textstellen bzw. Abbildungen entsprechend den rechtlichen Vorgaben gekennzeichnet sind sowie bei Abbildungen, die dem Internet entnommen wurden, der entsprechende Hypertextlink angegeben wurde.

Affidavit

I hereby declare that my thesis entitled: „**Spotlight on Fungal Rhodopsins: A Microscopic and Electrophysiological Study**” is the result of my own work. I did not receive any help or support from commercial consultants. All sources and / or materials applied are listed and specified in the thesis.

Furthermore I verify that the thesis has not been submitted as part of another examination process neither in identical nor in similar form.

Besides I declare that if I do not hold the copyright for figures and paragraphs, I obtained it from the rights holder and that paragraphs and figures have been marked according to law or for figures taken from the internet the hyperlink has been added accordingly.

Würzburg, den_____

_____

Signature PhD-student